RESEARCH & DEVELOPMENT

Calibration of Structural Layer Coefficients for North Carolina Asphalt Pavements

B. Shane Underwood, Ph.D.
Cassie Castorena, Ph.D.
Narges Matini
Mayzan Isied
Boris Goenaga
Kazuo Kuchiishi
Department of Civil, Construction, and Environmental Engineering
North Carolina State University

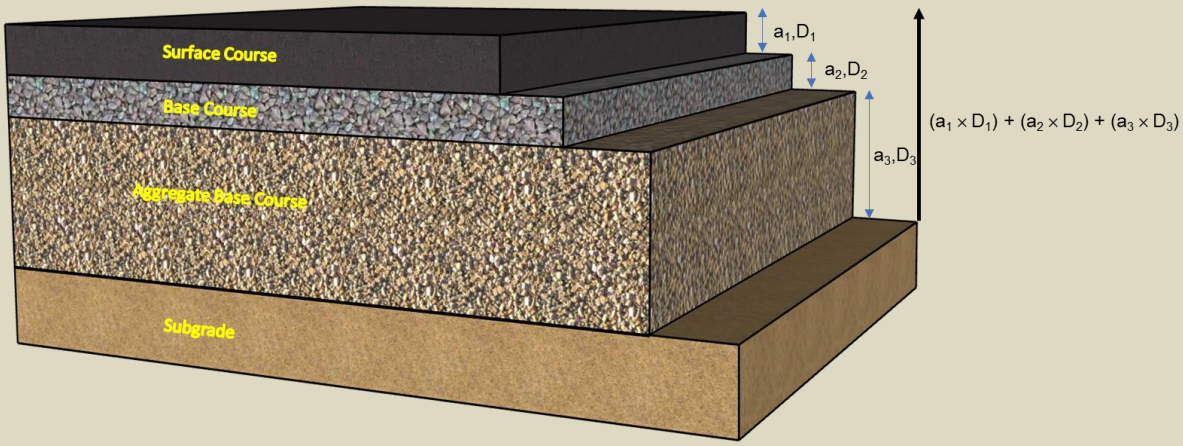

NCDOT Project 2019-20
January 2022

TECHNICAL DOCUMENTATION PAGE

1. Report No. FHWA/NC/2019-20	2. Government Accession No.	3. Recipient's Catalog No.
4. Title and Subtitle Calibration of Structural Layer Coefficients for North Carolina Asphalt Pavements		5. Report Date January 26, 2022
		6. Performing Organization Code
7. Author(s) B. Shane Underwood, Ph.D, Cassie Castorena, Ph.D.,Narges Matini, Mayzan Isied, Boris Goenaga, Kazuo Kuchiishi		8. Performing Organization Report No.
9. Performing Organization Name and Address Civil, Construction, and Environmental Engineering, North Carolina State University 915 Partners Way; Raleigh NC 27606		10. Work Unit No. (TRAIS)
		11. Contract or Grant No.
12. Sponsoring Agency Name and Address North Carolina Department of Transportation Research and Development Unit 104 Fayetteville Street, Raleigh, North Carolina 27601		13. Type of Report and Period Covered Final Report 08/01/2018 – 07/31/2021
		14. Sponsoring Agency Code RP2019-20
Supplementary Notes:		

16. Abstract

The North Carolina Department of Transportation (NCDOT) uses the 1993 AASHTO Guide for Design of Pavement Structures to determine the minimum pavement stiffness that will ensure pavement longevity. For design, the contribution from any given layer is calculated by the product of that layer's thickness and a structural layer coefficient that captures the overall quality and structural benefit of the material. This research has investigated the value of these layer coefficients for North Carolina pavement design. The relevant literature on development of the structural layer coefficients during the AASHO test road project, NCDOT design practices, and the development and identification of structural layer coefficients in other states and agencies was first reviewed and summarized. Then, databases containing pavement performance and material properties were compiled using existing data sources. Next, the structural layer coefficients for paving materials in the pavement performance database were calibrated by using the measured performance data and Excel Solver. These calibrated coefficients were then compared against projected performance using more modern materials.

It was found that the optimal layer coefficients for asphalt concrete base mixtures was 0.2 and that the ABC layer coefficient was 0.14 regardless of traffic levels. For the surface and intermediate mixtures on non-interstate roadways with 20-year cumulative ESALs less than 3 million, the optimal layer coefficient was found to be 0.24. For interstates and roadways with 20-year cumulative ESALs greater than or equal to 3 million, the optimal layer coefficient for surface and intermediate mixtures was found to be 0.43. With respect to current materials, the performance simulations showed inconsistent results between rutting and fatigue performance and thus no systematic changes were identified. The research team has made the following main recommendations regarding layer coefficients in North Carolina.

- The calibrated layer coefficients for non-interstate pavements designed using a 20-year cumulative ESAL less than 3 million, should be changed from 0.44 to 0.24 for asphalt concrete surface and intermediate mixtures and from 0.3 to 0.2 for asphalt concrete base mixtures. It is recommended to retain the current value of 0.14 for the ABC layer.
- The calibrated layer coefficients for interstate pavements at all traffic levels and all other roadways designed using a 20-year design ESAL equal to or greater than 3 million, should be kept at 0.44 for asphalt concrete surface and intermediate mixtures and changed from 0.3 to 0.2 for asphalt concrete base mixtures. It is recommended to retain the current value of 0.14 for the ABC layer.

Other recommendations are made as part of this research project as well as a guideline for monitoring and cataloging the long-term performance of North Carolina roadways are also provided.

17. Key Words AASHTO pavement design, layer coefficients, asphalt concrete, flexible pavements	18. Distribution Statement		
19. Security Classif. (of this report) Unclassified	20. Security Classif. (of this page) Unclassified	21. No. of Pages 224	22. Price

Form DOT F 1700.7 (8-72) **Reproduction of completed page authorized**

Disclaimer

The contents of this report reflect the views of the author who is responsible for the facts and the accuracy of the data presented herein. The contents of the report do not reflect the official views or policies of the North Carolina Department of Transportation. This report does not constitute a standard, specification or regulation."

Acknowledgments

The research team would like to express their gratitude and appreciation to the North Carolina Department of Transportation (NCDOT) for the provided funding needed to conclude this research study.

TABLE OF CONTENTS

LIST OF FIGURES

LIST OF TABLES

EXECUTIVE SUMMARY

The North Carolina Department of Transportation (NCDOT) uses the *AASHTO 1993 Guide for Design of Pavement Structures* to determine the minimum pavement stiffness to ensure pavement longevity. During design, this stiffness is first determined using an iterative design process, charts, or software. Then, the engineer selects materials and layer thicknesses that provide the required stiffness by summing the contributions of individual layers. The contribution from any given layer is calculated by the product of that layer's thickness and a structural layer coefficient that captures the overall quality and structural benefit of the material. In the NCDOT procedure, the structural layer coefficient for asphalt concrete (AC) is 0.44 (surface and intermediate mixtures) or 0.30 (base mixtures), while other material types are lower, e.g., the structural layer coefficient for unbound aggregate base course (ABC) materials is 0.14.

While the NCDOT has had success with these structural layer coefficient values, they are based on a test road constructed and evaluated in one climate zone and with one set of materials. Modern material selection and design have resulted in substantial changes in AC and aggregate base materials since this time. These improvements have likely resulted in different structural contributions from these materials, which means the structural layer coefficients should be reviewed and possibly changed. Proper characterization of these layer coefficients could result in substantial cost savings to the NCDOT by reducing the required pavement thickness and/or leading to pavements that require less frequent rehabilitation and reconstruction.

With respect to this need, this study has achieved two objectives; 1) calibrate the structural layer coefficients for different North Carolina asphalt mixture types using a pavement performance database, NCDOT materials database, and targeted testing; and 2) developed a plan to monitor pavement performance over a long-term period to refine and improve pavement design further.

The method followed in this research consisted of the following steps.

1. The relevant literature on development of the structural layer coefficients during the AASHO test road project, NCDOT design practices, and the development and identification of structural layer coefficients in other states and agencies was reviewed and summarized.
2. Pavement performance and material properties databases were compiled from existing data sources.
3. The structural layer coefficients for paving materials in the pavement performance database were calibrated in four steps; (a) a relationship between the AASHTO present serviceability index (*PSI*) and the NCDOT pavement condition rating (*PCR*) was established, (b) the *PSI* was calculated as a function of traffic levels for each section in the pavement performance database, (c) truck factors were calibrated, and (d) the structural layer coefficients for different layers was calibrated by adjusting the layer coefficient values until the measured/projected and predicted performance at the *PSI* equivalent to the NCDOT's Pavement Condition Rating (*PCR*) of 60 matched.
4. Task 3 was conducted using pavements that were 13-years-old on average and therefore, largely reflect the materials commonly used in the early 2000's. Coefficients for materials currently used were estimated by conducting and comparing pavement performance simulations with material properties from materials produced an average of 13 years ago with material properties with common materials today.

5. A plan was developed for a long-term pavement performance database, which can be used in future calibration efforts.

In Step 3, the major finding was that the basic performance equation that currently underlies the AASHTO 1993 design equation ill fits the observed performance of North Carolina roadways. This finding necessitated that the team adhere to some basic guidelines, established through fitting trials, to achieve the research objectives. These trials suggested that calibration results would be best achieved using the following guidelines:

- adopt universal coefficients for asphalt base and aggregate base layers,
- optimize the fitting on the basis of the *PSI* corresponding to a *PCR* value of 60 instead of trying to match the entire performance degradation curve,
- categorize sections based on the 20-year cumulative ESALs from the original contracts, and
- include interstate pavements into the highest traffic category regardless of their actual traffic levels.

After following these guidelines, the research team found that the optimized layer coefficients for asphalt concrete base mixtures was 0.2 and that the ABC layer coefficient was 0.14 regardless of traffic level. For the surface and intermediate mixtures on non-interstate roadways with 20-year cumulative ESALs less than 3 million, the optimal layer coefficient was found to be 0.24. For interstates and roadways with 20-year cumulative ESALs greater than or equal to 3 million, the optimal layer coefficient for surface and intermediate mixtures was found to be 0.43. With respect to relative performance of reference and current materials, the performance simulations showed inconsistent results between rutting and fatigue performance. On average, the simulations using AASHTO Pavement ME Design suggest that the layer coefficients should further decrease for current materials by approximately 10 percent. The FlexPAVE™ results suggest that the coefficients should increase by approximately 17 percent based on fatigue performance, but should decrease by approximately two percent based on rutting performance.

Based on these conclusions, the research team has made the following recommendations regarding layer coefficients.

- The calibrated layer coefficients for non-interstate pavements designed using a 20-year cumulative ESAL less than 3 million, should be changed from 0.44 to 0.24 for asphalt concrete surface and intermediate mixtures and from 0.3 to 0.2 for asphalt concrete base mixtures. It is recommended to retain the current value of 0.14 for the ABC layer.
- The calibrated layer coefficients for interstate pavements at all traffic levels and all other roadways designed using a 20-year design ESAL equal to or greater than 3 million, should be kept at 0.44 for asphalt concrete surface and intermediate mixtures and changed from 0.3 to 0.2 for asphalt concrete base mixtures. It is recommended to retain the current value of 0.14 for the ABC layer.

The research team does not currently recommend adjusting the layer coefficients from the recommendations above based on the performance comparisons of the reference and current mixtures because of the uncertainty and variation in the performance model predictions from AASHTO Pavement ME Design and FlexPAVE™. However, the team does recommend further

study to identify ways to design and/or produce asphalt mixtures from the same traffic category that will exhibit more consistent performance.

Also, it is noted that this project investigated only new construction sites and it is unknown at this time whether the layer coefficients recommended above are applicable to overlay conditions. The research team found no evidence in the literature as to whether layer coefficients used for new design are equally applicable to overlays and the sites studied in this project did not permit the team to answer this question. Thus, the research team recommends that the NCDOT consider evaluating the efficacy of layer coefficients calibrated here for overlay pavements.

The project also identified some potential issues with respect to the NCDOT truck factors. The origin of the current truck factors used by the NCDOT could not be identified, but analysis in this project suggests that the NCDOT's current truck factors are different than adjacent states (systematically lower). Thus, it is recommended that the NCDOT conduct detailed analysis of their current weigh in motion (WIM) data to confirm that the truck factors it uses still represents the expected truck loading. The research team was unable to do such calibration given the information provided in the available WIM data; however, such analysis is feasible. It may also be possible for the NCDOT to better leverage the traffic clustering analysis performed in FHWA/NC 2008-11 for the purpose of estimating truck loadings.

The above conclusions and recommendations rely on a two-step conversion process to relate measured *PCR* to *PSI*. This conversion carries an inherent uncertainty that limits the ability of this project, and potentially other projects, to reliably calibrate design equations for North Carolina. Thus, the research team recommends that the NCDOT allocate resources to either monitor a subset of pavements over several years in order to better facilitate calibration efforts or consider developing pavement design methods that are amenable to the current data collection efforts, i.e., compatible with *PCR*.

This page is intentionally blank

1. INTRODUCTION

1.1. Overview

Flexible pavement design in North Carolina utilizes the AASHTO 1993 Pavement Design equation. This equation, and associated design guidance, are based on an underlying theory that pavements must be sufficiently stiff to provide long-term performance. Pavement stiffness is designed for by individually and collectively accounting for the structural contributions from each layer in the pavement system. The contributions from each layer are calculated by multiplying the thickness of the individual layer by an associated layer coefficient, which reflects the overall material quality and has been linked directly to the modulus of those layers. Since these layer coefficients are multiplied directly to the layer thickness, the values of the coefficients have a substantial and direct effect on the overall cost of new and rehabilitated pavements.

The North Carolina Department of Transportation (NCDOT) currently uses values, derived largely from the original AASHO road test, which was carried out in Ottawa, Illinois between 1956 and 1962 using mixtures with Illinois limestone aggregate, a relatively soft asphalt, and Marshall based mixtures. While the test road itself used only a single mixture type, the AASHTO design guidelines provides a method to estimate layer coefficients for other materials based on the resilient modulus. Using this relationship suggests that NCDOT mixtures may yield greater structural contribution than the test road mixture (Figure 1) and that the layer coefficient of NCDOT mixtures should be increased. However, relying strictly on the AASHTO relationship is likely not appropriate since there has been little to no calibration that demonstrates its applicability. The relationship also implies that increasing the modulus of asphalt concrete alone will result in better performance, but ignores other factors (e.g., asphalt binder content, etc.) that may also affect long-term durability.

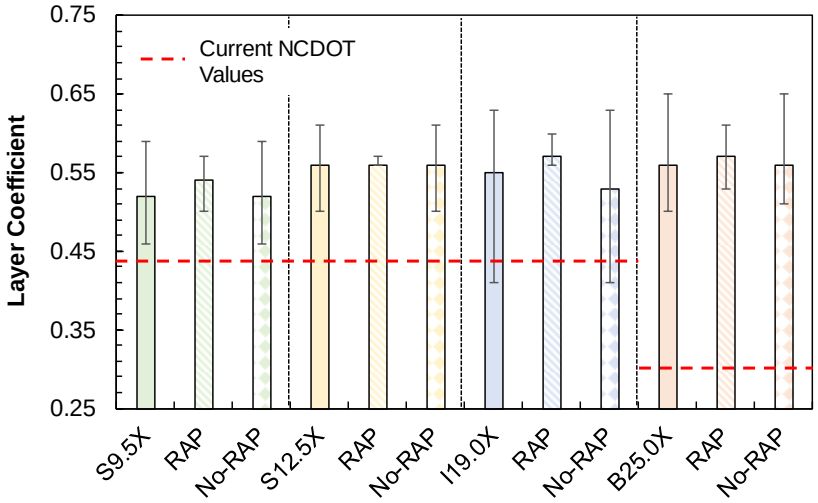

Figure 1. Structural layer coefficient values estimated from existing modulus based relationship in AASHTO 1993 design guide.

Although there are shortcomings in the AASHTO layer coefficient relationship, the data in Figure 1 suggest that NCDOT specifications may not currently reflect modern paving materials and that as a result pavement designs in the state may not be optimal. The research results reported in this report address the need to understand this knowledge gap and develop scientifically supported guidelines for layer coefficient selection.

1.2. Status of the Literature

A comprehensive review of the literature pertaining to this project is presented in Appendix A, while a summary of most relevant components of this review is presented below.

1.2.1. Pavement Condition Index and their Relationships

The pavement condition index that NCDOT uses to evaluate the performance of the pavement is the Pavement Condition Rating (*PCR*), while the basis of the AASHTO design equation is the Present Serviceability Index (*PSI*). A review of the literature found that no relationship between *PCR* and *PSI* exists. However, the literature does contain details on the development of *PCR*, *PSI*, and other pavement indices including Ride Quality Index (RQI), Mean Pavement Rating (MPR), Ride Number (RN), Pavement Condition Index (PCI), and International Roughness Index (*IRI*) were reviewed (Carey and Irick 1960; Loprencipe and Zoccali 2017; Janoff et al. 1985; Janoff 1988; Sayers and Karamihas 1998; ASTM E1489-08 (Reapproved) 2013; Aultman-Hall et al. 2004; Paterson 1987; USACE 1982). This literature also indicated that *IRI* is used by most agencies as one of the indices to trigger a rehabilitation action. As a result, different relationships have been developed to correlate *IRI* with parameters such as Present Serviceability Rating (PSR), *PSI*, Slope Variation (SV), RQI, pavement distresses, and PCI (Zamora 2016; Gillespie et al. 1980; Paterson 1987; Al-Omari and Darter 1994; Gulen et al. 1994; Hall and Munoz 1999; Mactutis et al. 2000; Dewan and Smith 2002; Lin et al. 2003; Chandra et al. 2013; Aultman-hall et al. 2004; Carey and Irick 1960). Since the NCDOT does maintain a record of *IRI* values for many pavement sections, it was concluded that *IRI* could be used as the intermediate parameter to correlate *PCR* and *PSI*.

1.2.2. Calibration of Layer Coefficients

Layer coefficients were first developed through statistical analysis of the AASHO test road results (HRB 1962). However, it was found early on that there were some limitations associated with these original layer coefficients, particularly with respect to generalizability. Thus, there have been many studies to calibrate location specific layer coefficients. The first effort to improve layer coefficient was conducted by Van Til et al. (1972) The Van Til approach to layer coefficient characterization was largely analytical, although the final recommendations involved some experimental observations. The relationships that resulted from the Van Til study first appeared in the 1972 AASHTO design guide and still appear in the 1993 guidelines. Others have also examined this issue and developed different conclusions based on their own local conditions (see Table A.9 and Table A.10 in Appendix A). The methods to arrive at these coefficients generally vary between two approaches; 1) those that rely on in-service experiments with Falling Weight Deflectometers (FWDs) or similar and 2) those that rely on analytical study using in-service performance and/or mechanistic or mechanistic empirical predictions. While many of these efforts were carried out several years ago, there have been two recent efforts to re-evaluate the layer coefficients. Details of these studies are provided in Appendix A, but in short both found that layer coefficients should increase above what is currently in use in the locations of the respective studies. Timm et al. (2014) found that the layer coefficient should be increased to 0.55 and Dave et al. (2019) suggested that the layer coefficient should be recalibrated to 0.58.

1.2.3. Calibration of Truck Factors

All aspects of the AASHTO design calculations, including truck traffic considerations, stem from the basic performance model identified and calibrated from the AASHO test road results. The AASHTO method utilizes the damage equivalency concept to find equivalency factors and ultimately the ESAL contribution for different axle types and loads. Since damage is inferred from the performance model, which is itself dependent upon the layer coefficients, the truck factors are

also dependent upon the values of the layer coefficients. Thus, the literature review evaluated how different researchers and agencies estimate truck factors. The basic finding from this review is that there are different approaches to defining truck factors and thus the values used for the calculation of ESALs in different agencies (ADOT 2017; PennDOT 2015; ODOT 2015; IDOT 2013; GDOT 2005; SCDOT 2008; VDOT 2018; NYDOT 2002, CTDOT 2021; FDOT 2018; CODOT 2008; MNDOT 2021). The most accepted method of defining truck factors is to leverage weigh-in-motion (WIM) experiments and the AASHTO performance equation.

1.2.4. Knowledge Gaps and Applications

The literature review prepared for this research confirmed that the current layer coefficients are the result of statistical analysis of the sections in the 1956-1962 AASHO test road. Despite looking through numerous studies pertaining to pavement evaluation and design at NCDOT, no mention of the origin of the current NCDOT layer coefficients were found. Multiple studies from different agencies have been conducted to evaluate whether these original coefficients are universally applicable and to identify possible modifications to the values. Methodologies have ranged from purely empirical and involve in-situ evaluation of pavement stiffness to purely theoretical using layered elastic analysis. The most successful and long-lasting approaches have relied on combined experimental and analytical study. However, the general applicability of these approaches across agencies has not been demonstrated likely due to differences in performance measurement, construction, mixture design, and management practices (i.e., maintenance, rehabilitation, reconstruction timings and their relationship to design practices). Current asphalts used by the NCDOT are stiffer than the binder used in the AASHO road test and mixtures are designed using the Superpave system. Thus, it is important in the calibration efforts to recognize this condition and not only develop calibrated structural layer coefficients, but also develop relationships or a methodology to determine layer coefficients for future materials.

1.3. Report Organization

This report is organized into 7 primary sections and 5 appendices. Section 1 (this section) describes the overall project, need, state of the literature, and report organization. Section 2 provides an overview of the basic methodology followed in this project to characterize the layer coefficients based on PMS data. Section 3 describes how layer coefficients were estimated for currently used asphalt mixtures. Section 4 presents an introduction to the long-range performance monitoring plan. Section 5 summarizes the conclusions of this project along with some specific recommendations. Section 6 provides an overview of the implementation and technology transfer plan for the project results. Finally, Section 7 lists the references cited in this report. Appendix A includes the detailed literature review, while appendices B-E provide the detailed analysis results related to Sections 2-4. Appendix F provides a detailed guideline for a long-term performance monitoring plan.

This page is intentionally blank

2. CALIBRATING LAYER COEFFICIENTS BASED ON EXISTING PAVEMENT PERFORMANCE

2.1. Calibration Overview

The overall goal of the calibration process is to minimize the error between the predicted performance and that observed from in-service pavements. Figure 2 summarizes the process followed to achieve this goal. The inputs required to perform the calibration included the measured *PCR* values at different points in time for the study sites as well as any information needed for the AASHTO equation (cumulative ESALs at all relevant times when *PCR* was measured, soil modulus, the structural design, and the material types used in the structure). The *PCR* values were obtained for each site from the NCDOT PMS database and converted to *PSI* using equations developed during the research project (see Section 2.3.1). The traffic levels used for calibration were obtained from NCDOT reported traffic counts and converted to ESALs based on WIM data (see Section 2.3.2) and the traffic clustering methodology developed during the FHWA/NC2008-11 project. The soil modulus, structural configuration, and material types were obtained from the original project contracts.

The details of the calibration process itself are given in Section 2.3 and Appendix B. In short, an iterative process was carried out on either individual pavements or groups of pavements to find the layer coefficients that yielded the smallest error possible between the *PSI* predicted from the design equation and the one estimated using the *PCR*-to-*PSI* equations described earlier. An initial set of layer coefficients, (a_i), were first estimated and used to calculate the pavement Structural Number (SN). These were then iteratively updated until the error was minimized. This process was performed using the Microsoft EXCEL Solver tool.

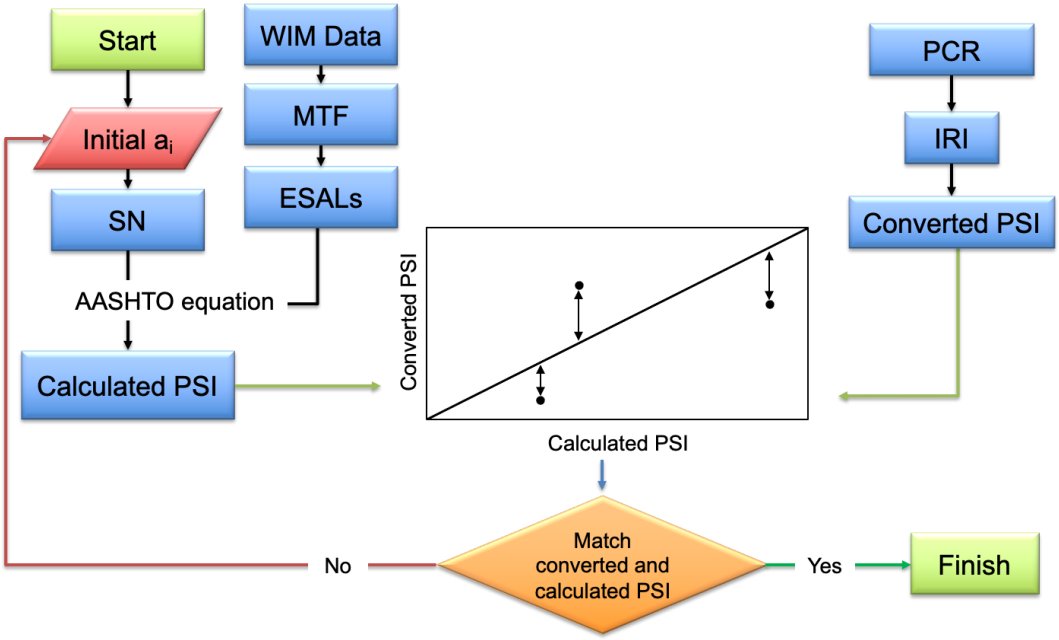

Figure 2. Calibration process flowchart.

2.2. Performance Databases

Two separate performance databases were used in this research. The first database (referred to as the Support Model Database) consisted of *PCR* and *IRI* data from more than 76 pavement sites

and was used to develop the support models to predict *PSI* from *PCR*. The second database (referred to as the Calibration Database) consisted of 33 separate pavement sites and was used to calibrate the layer coefficients. The properties of pavement sites are summarized in Appendix C.

2.2.1. Data used for Support Model Development

The Support Model Database included pavement sections with two types of data. The first type of data was windshield survey data with historical observations of the *PCR* and the *IRI* dating from 1982 up to 2012. The second type of data in the database was the automated distress survey, which contained annual measurements for 2013 to 2018, of the different distresses (such as alligator cracking, raveling, etc.), the *IRI*, and the *PCR*. The number of observations pulled from each database is summarized in Table 1. In this dataset, the age of each road section was set based on the time since the last rehabilitation reported in the PMS database. All sections with an age greater than 20 years were excluded from the analysis. The *PCR* records were also used to verify and correct the pavement age. An age reset was defined when the *PCR* returned to 100, but a difference between two consecutive values equal to 10 *PCR* units was considered non-significant and a result of measurement inconsistencies between years. A detailed explanation of this process is presented in Appendix B.

Table 1. Number of Observations Used from Each Database.

Road Class	Windshield Survey	Automated Survey	Total
Interstates	33,480	6,480	39,960
US Routes	205,964	39,864	245,828
NC Routes	198,679	38,454	237,133

2.2.2. Data used for Layer Coefficient Calibration

At the project outset, 53 pavement sections from the FHWA/NC 2015-02 project (Kim et al. 2018) were identified as candidate analysis sites. An additional 23 sites were added to this list after re-reviewing the NCDOT PMS database. These pavement sections consisted of 61 aggregate base course (ABC) and 15 full depth asphalt (FDA) pavements located on 6 Interstates, 20 US routes, 12 NC routes, and 38 secondary roads. Traffic volumes for each site were estimated from the NCDOT traffic volume clearinghouse, the pavement structures were obtained from the PMS database, and soil properties were estimated using the NCHRP 9-23A (Zapata 2010) soil maps.

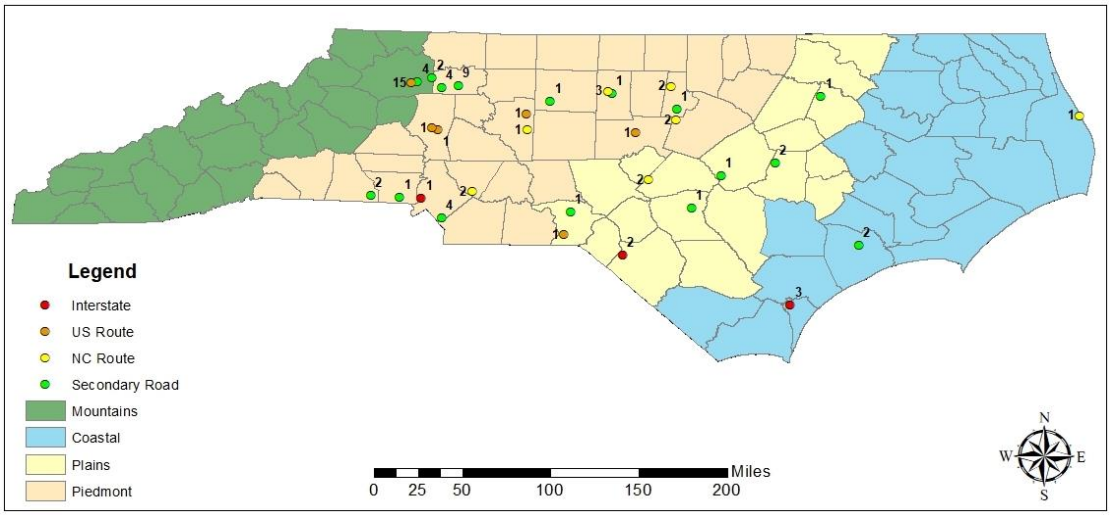

Figure 3. Location of the initial set of analysis pavement sections.

All 76 sites were used at various times to conduct analyses in support of the calibration, but ultimately a final set of 33 pavement sections were selected for performing the final calibration. These 33 sites were selected because of the availability of the original design contract where the structure, soil properties, and also importantly the expected traffic volumes were known. These final set of pavement sections consisted of 22 ABC and 12 FDA pavement types located on 6 Interstates, 3 US routes, 11 NC routes, and 13 secondary roads. The location of the 76 and 33 sections were mapped and are presented in Figure 3 and Figure 4, respectively. In these figures, the functional class is color-coded and the number beside the markers indicates the number of sections closely located either on the same road or different roads.

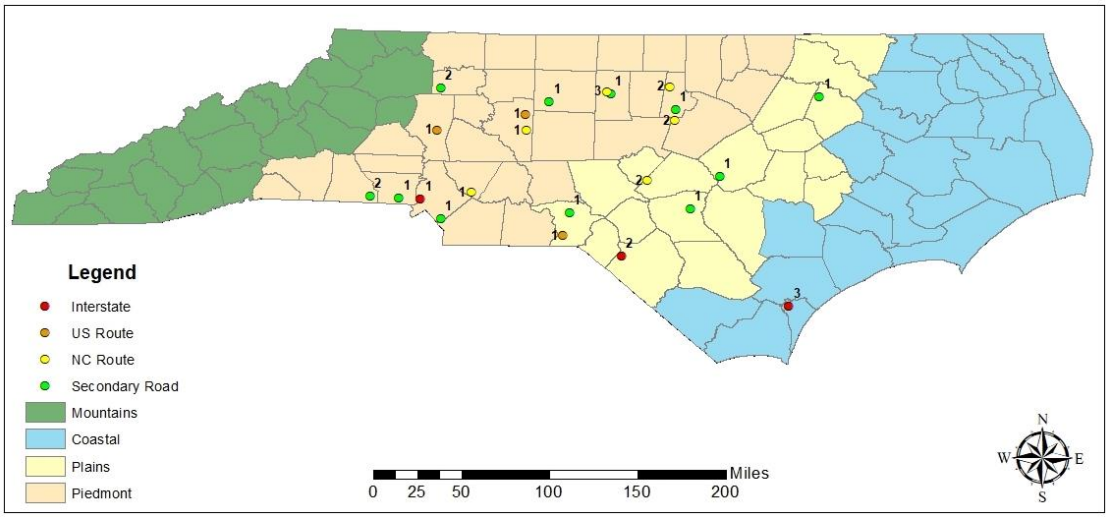

Figure 4. Location of the final set of analysis pavement sections.

2.3. Calibrating Layer Coefficients

2.3.1. Support Model for PCR to PSI conversion

Individual performance models for the *PCR* and the *IRI* were obtained. A detailed description of the procedure followed to derive these models is provided in the Appendix B. For the *PCR*, a sigmoidal curve was used to describe the deterioration process, whereas for the *IRI* an exponential model was selected. Afterwards, both deterioration models were used to develop a relationship between the two outcomes and convert *PCR* values to *IRI* values. These equations are summarized in Equation (1) for Interstates, Equation (2) for US routes, and Equation (3) for NC Routes and Secondary Routes.

$$IRI = -12.71\ln(PCR) + 130 \tag{1}$$

$$IRI = 179.43e^{-0.007\,PCR} \tag{2}$$

$$IRI = 151.55e^{-0.007\,PCR} \tag{3}$$

Next, these *IRI* and *PCR* relationship were used in conjunction with Equation (4), proposed by Gulen et al. (1994), to convert the *IRI* to *PSI*. The final combined relationships to estimate the *PSI* from *PCR* are shown in Equation (5) to (7) for each functional classification.

$$PSI = 9e^{-0.008784\times IRI} \tag{4}$$

$$PSI = 9e^{-0.008784\times\left(-12.71\times Ln(PCR)+130\right)} \tag{5}$$

$$PSI = 9e^{-0.008784\times\left(179.43e^{-0.007\times PCR}\right)} \quad (6)$$

$$PSI = 9e^{-0.008784\times\left(151.55e^{-0.007\times PCR}\right)} \quad (7)$$

2.3.2. Calculating ESAL Values

To calculate the cumulative ESAL values for the calibration, the research team leveraged the data and method developed in FHWA/NC 2008-11 (Stone et al. 2010) to create mixed-traffic inputs for AASHTO Pavement ME Design. The data included traffic and load counts from 12 WIM stations across North Carolina. The data from these stations was segregated by axle type and load level. The details of ESAL calculation process are outlined in Appendix C. In brief, the process began by grouping each site according to the FHWA/NC 2008-11 traffic cluster category (1-4) based on the traffic counts of single-unit (SU) and multi-unit (MU) trucks at each site from the traffic survey data. In parallel, the research team calculated what it termed the mixed-truck factor, *MTF*, for each WIM station and averaged them across all WIM stations in each cluster to obtain cluster specific *MTF* values (see Table 2).

Table 2. Summary of Mixed Truck Factors (*MTF*s) for Calibration Pavement Sections.

Section ID	*MTF*	Section ID	*MTF*	Section ID	*MTF*
40003632060 (4)	0.578	30000087043 (2)	1.107	40001546041	0.577
40001211051	0.602	30000054001 (1)	0.577	30000157032 (1)	0.578
40001125099	0.593	30000054001 (2)	0.577	30000157032 (2)	0.578
40001412033	0.597	30000054001 (3)	0.577	30000109029	0.578
40001452077	0.594	40001765099	0.578	20000070041 (3)	0.579
40001933026	0.601	10000140065	1.119	30000055092 (1)	0.578
40002705023 (1)	0.584	10600140065 (1)	1.119	30000055092 (2)	0.578
40002705023 (2)	0.584	10600140065 (2)	1.119	20000070049 (2)	0.580
40002433001	0.578	40001954032	0.580	10800485060	1.108
40002200036	0.579	30000024013	0.585	10000074078	0.581
30000087043 (1)	1.107	20000001077	1.124	10600074078	0.579

The *MTF* is the ratio of total truck traffic to cumulative ESAL values from the axle load spectra, Equation (8). It was calculated by first determining the total average annual daily truck traffic ($AADTT_{wim}$) from each WIM station. Then, the load equivalency factor (LEF) for each axle type and weight group was calculated. Next, each LEF was multiplied with the number of repetitions of the respective axle type and weight group. Finally, these multiplication products were summed across all axle types and weight groups to find the cumulative daily ESALs at the WIM station ($ESALs_{wim}$).

$$MTF = \frac{ESAL_{WIM}}{AADTT_{WIM} \times 365.25} \quad (8)$$

The cumulative ESALs for each calibration site was finally determined by identifying the AADTT at each study site, multiplying by the *MTF*, and the cumulating traffic over time (with growth). The initial AADTT for the calibration sites were determined from contract documents, but for those sites without contract documents it was estimated from NCDOT traffic count data (as described in Appendix C).

2.3.3. Performing Layer Coefficient Calibration

Calibration for the selected pavement sections was performed using the Excel Solver function. The calibration process consisted of three steps: (a) initial calibration trials, (b) supplementary calibration trials, and (c) final calibration. In the initial trials, 45 different attempts to calibrate the layer coefficient were performed by changing various influential elements in the calibration analysis. A set of guidelines were established to better fit the available data and also obtain practically useful results. The guidelines from the initial trials were refined through an additional set of 30 supplementary calibration trials. These guiding principles were further modified and finalized through the final set of calibration.

Initial Calibration Trials

Many different trials have been explored in order to calibrate the layer coefficients that best represent the structures in this study. As described in Appendix C, a total of 45 different trials were performed with the 76 pavement sections. The trials performed with these pavement sections varied first by whether analysis was done on a section-by-section basis (i.e., determining the optimal layer coefficients independently for each section) or universal basis. They also varied by the number of points on the performance curve that were used for optimization, how the roads were categorized (or not categorized), and whether the asphalt concrete base (AC-Base) and ABC layer structural number values were set to constant values or included in the optimization process. In doing these trials, a high level of variation between different calibration results was observed, but some guiding principles regarding the process of calibration were identified. It is noted that for these 76 sites the soil properties were estimated from the NCHRP 9-23 database (Zapata et al. 2010)

The first finding from the trials was that calibration could not be completed on a section-by-section basis because there were uniqueness issues. The team found that while the total optimized structural number would be consistent, the values of the individual layer coefficients could vary substantially depending on the initial values selected for the coefficients. It was also learned from the early simulations that using all of the measured *PCR* values for optimization was problematic because the AASHTO performance equation did not do a good job of capturing the total pavement deterioration function. North Carolina roadways, it seems, demonstrate a slower performance degradation early on, but then a much more rapid deterioration curve than the AASHTO equation suggests. As result, the research team found that it was necessary to use only those points with *PCR* values less than 100. In select trials, the ideal number of points to use for the optimization was investigated by performing two different analyses; (a) using only the last data point and (b) using all points with *PSI* less than certain threshold (0.1 less than maximum *PSI* value). Through these evaluations, it was found that using the last data point resulted in better identification of the design life and therefore, this approach was selected for subsequent analysis.

Multiple trials also showed limitations with using universal coefficients because the resulting average errors were higher than desirable. Thus, pavement sections were categorized according to factors such as road type, overall fitting error, traffic levels, surface type, and pavement type (ABC or FDA). The results suggested that it would be more useful to categorize sections based on the 20-year cumulative ESALs from the project design contracts because systematic differences were noted between relatively high and relatively low ESAL pavements. It was also observed that fixing the coefficient of AC-Base and/or ABC layers to constant values independent of traffic levels would be necessary. It was found that when optimizing the coefficients for these layers, the optimized values were highly variable and also non-intuitive. Notably, the ABC layer coefficients

were considerably higher than the AC-Base layer coefficients. Given the inherent uncertainty that exists when optimizing the layer coefficients, it was believed that this strategy was justified. Therefore, the coefficient of AC-base and ABC layers were fixed to predefined values. The knowledge gained from these trials established that the calibration results are better fitted and more practical if the following guidelines are followed: universal coefficients for categorized sections calibrated based on fitting the last data point.

In order to decide whether to use sections where contract information was not available, traffic information from contracts and PMS or survey data were compared. In addition, the pavement design parameters including AADT, traffic growth rate, truck percentage, and ESALs from survey and contracts were compared. The results of the comparison for cumulative ESALs based on the contract and based on the survey are shown in Figure 5. The figure indicates that, for the most part, the ESALs from the contracts are higher than ESALs from the survey. This finding is problematic because it means that only those sites where contract data is available can be used for the calibration. In order to calibrate the layer coefficients, it is important to account for the data considered at the time of the design and construction. Based on the observed discrepancies between survey and contract ESAL values for many sections, it was decided to continue the calibration process with only data from contracts. It should be noted though, that for calibration purposes the ESAL numbers calculated as described in Section 2.3.2 using the survey traffic counts were used. Contract ESALs were only used for categorizing the pavement sites.

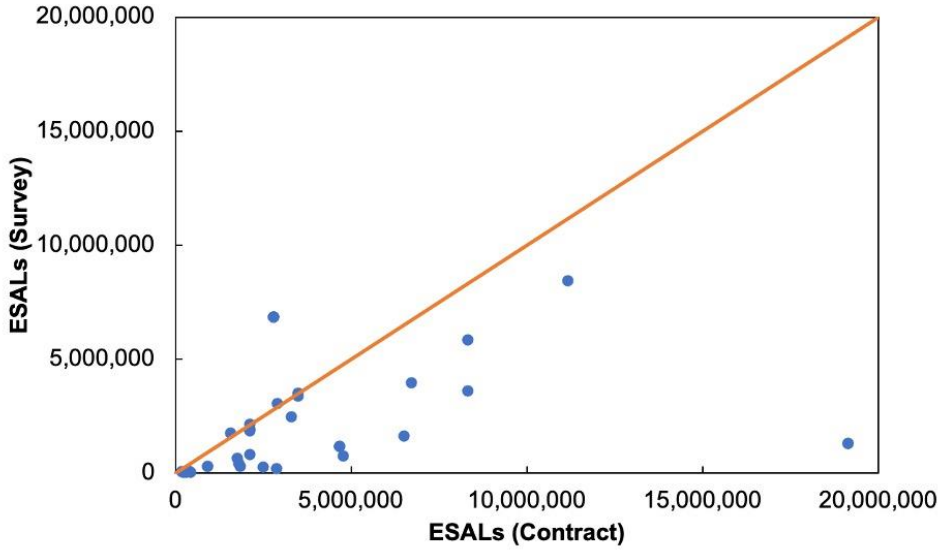

Figure 5. Comparison between contract and survey ESALs.

The knowledge gained from these trials established that the calibration results are better fitted and if the following guidelines are followed: universal coefficients for categorized sections calibrated based on fitting the last data point. It was also decided that categorization should be done in a way that designers would easily be able to identify the category of coefficients for a given design from already available variables. It was decided that the 20-year cumulative ESALs from the original contract yielded better fitted results and more practical from the design standpoint.

Supplementary Calibration Trials

Following the guidelines from initial trials, discussed in previous section, the calibration process was further evaluated and finalized through a total of 33 calibration trials. In this case each of the

33 sites had contract information and relevant details pertaining to soil properties could be extracted from those documents. The knowledge gained from these trials established that the calibration results are better fitted and more consistent with the literature and intuition if the calibration was conducted categorically. In this case, the sections were divided into two categories based on the 20-year cumulative design ESAL estimate from the contracts: less than 2.5 million ESALs and more than or equal to 2.5 million ESALs. The traffic categories were further refined during the final calibration, but the supplementary analysis supported the initial calibration trials that some systematic differences existed in lower volume roadways. The exact cause of this difference was not identified during the research project. However, since most of the roadways are low overall traffic volume secondary roads it was hypothesized that differences in variable certainties (truck traffic volumes and actual loads of the trucks that use the roadway) as well as potential differences in construction oversight and inspections could be the root cause. It was also determined that the AC-base and ABC coefficients need to be fixed to a predefined value of 0.2 and 0.14, respectively. These trials are discussed in detail in Appendix C.

Final Calibration

As discussed in previous section, the supplementary calibration trials suggested dividing roadways into categories based on traffic volume and divided at the 20-year cumulative ESAL volume of 2.5 million. The current NCDOT design guide categorizes the traffic levels into three levels based on the 20-year cumulative ESAL values: less than 3 million, between 3 and 30 million, and more than 30 million. In order to be more consistent with NCDOT guidelines, and to closely follow the guidelines from supplementary calibration trials, it was decided to change the categorization of analysis sections in the final calibration to the following two categories: less than 3 million and greater than or equal to 3 million 20-year cumulative ESALs.

The new division added five more sections to the low volume category, i.e., five sections had 20-year cumulative design ESALs between 2.5 and 3 million. Out of these five sections, three sections were interstates and the other two sections were NC or secondary routes. Close inspection of these five sites showed systematic differences between the interstate and non-interstate sections. Specifically, the interstate sections appeared to behave like the higher volume sections while the NC and secondary routes behaved similar to the other low volume sections. On the basis of this observation it was speculated that some systematic biases exist with low volume roadways that are not present for interstates. These biases may include but are not probably not limited to uncertainty in design inputs, potentially less attention to construction practices, and roadway design factors such as pavement cross section, shoulder types and widths, and drainage considerations. The research team also considered whether US routes might fall under this same condition, but did not have any data on low volume US routes to help determine whether this was the case. Thus, the research team elected to modify the categorization as follows;

- Category 1 – Any non-interstate roadway with cumulative 20-year ESALs less than 3 million
- Category 2 – Any non-interstate roadway with cumulative 20-year ESALs greater than or equal to 3 million and any interstate roadway regardless of traffic level.

The final calibration was conducted by segregating the sites into the two categories just described. The original NCDOT coefficients are presented in Table 3 and the final calibration results based on the finalized categorization method is presented in Table 4. Table 4 also presents the optimized values when all sections are analyzed together without segregating by category for comparison. The calibration results show that the surface layer for Category 1 pavements perform worse than the currently considered layer coefficients suggest that it will; thus, lower coefficients are

recommended for these roadways. The surface and intermediate layer on Category 2 pavements seem to perform as expected with an optimized coefficient of 0.43 for these layers. The consequence of using 0.44 instead of the calibrated value of 0.43 is an increase in the average SSE value from 0.298 to 0.299, which is negligible and will not impact the overall performance. Thus, it is recommended that the NDOT continue using the original coefficient for AC surface and intermediate layers on Category 2 pavements. The AC-base on all types of roads performs worse than design assumption and lower coefficients are recommended. In the case of ABC layer, it performs as expected and it is recommended that the current layer coefficient be retained.

Table 3. Original NCDOT Layer Coefficients.

Pavement Layer	AC-surface/int.	AC-base	ABC
Layer coefficient	0.44	0.30	0.14

Table 4. Final Calibration Results for Categorized Sections.

Type of Calibration	Category	AC-surface/int.	AC-base	ABC	SSE (Avg.)	Number of sections
Universal Calibration	1 and 2 Together	0.41	0.20	0.14	0.45	33
Categorized Calibration	1	0.24	0.20	0.14	0.42	17
	2	0.43	0.20	0.14	0.30	16

The final calibration results are further evaluated by comparing the deterioration of *PSI* to the equivalent *PCR* value of 60 using calibrated and default coefficients. The comparison was conducted for each section and is presented in Appendix C. As shown in Appendix C, the calibration was successful in matching the last data point in some cases and it was not in others. Two representative cases showing a successful match and an unsuccessful match are presented in Figure 6. In Figure 6 (a), the predicted performance curve using the default coefficients does not capture the deterioration pattern of measured and projected performance data and does not match with the last data point. However, using the calibrated coefficients completely matches the deterioration pattern and the last data point. In some cases, the calibrated coefficients did not exactly match the pattern, but they did match the last data point or reduce the difference between the last calculated and projected points.

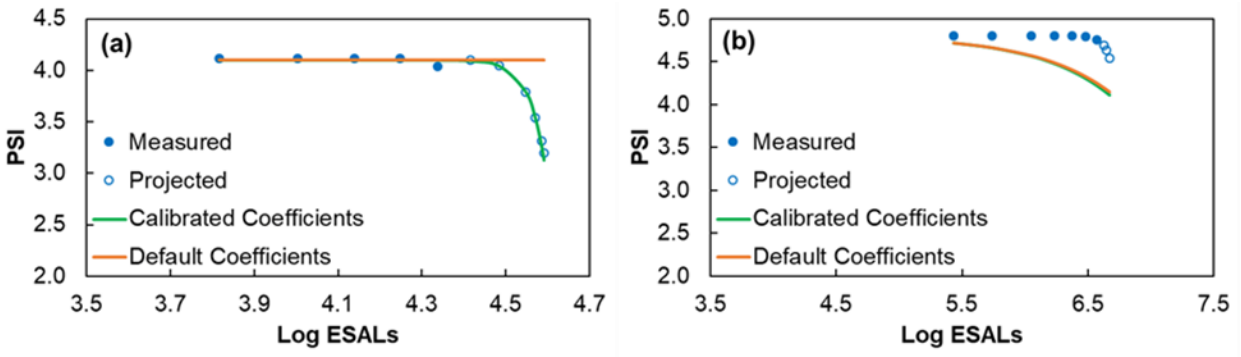

Figure 6. Comparison between default and calibrated coefficients in two cases; (a) successful match (Route ID 40001452077) and (b) unsuccessful match (Route ID 10600140065-1).

In Figure 6 (b), neither the default nor the calibrated coefficients match the pattern nor match the last data point. However, overall, Appendix C shows that the number of cases where the last point is best matched with the calibrated coefficients, is higher than the number of cases that match better with the default coefficients. However, as is also seen in the Appendix C graphs, the uncertainty and variability is quite high. This result is not entirely unexpected as there are many confounding factors (most outside the control of the designer) that collectively affect the long-term pavement performance.

The key findings from this analysis is that there does seem to exist two systematic biases; (1) the underlying AASHTO performance model does not match the overall degradation pattern of NCDOT roadways (especially secondary roads) well and (2) the mixtures, as constructed, on relatively low volume, non-interstate roads systematically underperform relative to the mixtures placed on relatively high volume roads. In the case of the former, the AASHTO equation tends to produce a more gradual decline in performance relative to the performance observed (as converted from *PCR* to *PSI*), which tends to show more rapid decline. It is possible that this effect is due to the conversion from *PCR* to *PSI*. The identification of precise causative factors for this latter effect are beyond the scope of the current effort.

It should also be mentioned that there exists uncertainty with respect to the truck factors that are used to estimate cumulative ESALs. Theoretically, the truck factors are functions of the final layer coefficients since the layer coefficients affect the structural number, which affects the predicted damage accumulation rate. In addition, as described previously, this research has found that North Carolina truck factors are systematically lower than many other states. If the research team's estimate of cumulative ESALs is systematically biased then this affects the final calibration coefficients according to the direction of the bias. If the truck factors used for estimating cumulative ESALs are lower than the true values, then the ESALs are underestimated, which means that the layer coefficients are also underestimated (since the deterioration curves are shorter than they should be). Conversely, if the truck factors used for estimating cumulative ESALs are higher than the true values, then the final layer coefficients are larger than they should be. However, based on the actual values for truck factors used from other states (with the possible exception of the high estimates from Arizona, Connecticut, and Pennsylvania), the range of uncertainty from individual WIM stations (see Appendix C), and the fact that the performance models are calibrated with respect to the logarithm of ESALs, the research team does not feel like the impacts of this uncertainty affect the main conclusion of the study (that layer coefficients should be lowered, and likely substantially, for some cases).

This page is intentionally blank

3. ESTIMATING LAYER COEFFICIENTS FOR NEW MATERIALS

3.1. Overview

The materials used in the previous section to calibrate the layer coefficients do not necessarily represent the materials in common use today by the NCDOT. As described above, many of the pavements in the database were constructed approximately an average 13 years ago, and since this time, materials have changed, especially with the inclusion of higher RAP/RAS contents and polymer modification. Additionally, in the future, it is likely that new materials will be developed that may have different structural layer coefficients from those today, which will need to be estimated. To address this issue, the research study developed a methodology to estimate layer coefficients for materials currently used by the NCDOT and those that it may use in the future. The basis for this analysis is that the structural layer coefficients represent the overall material quality and therefore, the ratio of the layer coefficient for a given material to the layer coefficient of a reference material will be equal to the relative performance of pavements constructed with those two materials. Equation (9) shows how this expected proportionality can be used to relate structural layer coefficients of an unknown material ($a_{material,x}$) when the coefficient for a reference material ($a_{reference}$) and pavement performance of the two materials is known.

$$a_{mterial,x} = \left(\frac{Performance_{material,x}}{Performance_{reference}} \right) \times a_{reference} \tag{9}$$

Experimentally determining the performance of pavements is a multi-decade effort. Therefore, analytical pavement analysis simulations have been performed using material properties from current and past materials to estimate the performance and thereby structural layer coefficients for these new materials.

3.2. Mixture Databases

3.2.1. Historical Mixture Database

At the beginning of the project the research team reviewed data from several past North Carolina DOT research project, see Table 5. After reviewing the specific details of each, the team ultimately decided to select mixtures from the FHWA/NC 2007-07 project to serve as the 'reference' conditions. In that project, twelve hot-mix asphalt (HMA) mixtures were used and selected as the most representative types of asphalt mixtures used in the state of North Carolina at the time (approximately 10 to 15 years ago). The aggregate materials and asphalt binders were collected from multiple quarries and asphalt plants across the state, and their volumetric properties were verified in the laboratory and compared to their respective JMFs. For the current project, five out of these twelve mixes were selected. All five mixes contained RAP (at RBR levels of approximately 15-20%). A summary of the five asphalt mixtures' characteristics is presented in Table 6.

During FHWA/NC 2007-07, each mixture was tested to determine its dynamic modulus (AASHTO T 342), damage characteristics (precursor to AASHTO TP 107), and permanent deformation characteristics (AASHTO T 378). All testing was conducted using a general purpose loading frame; either a MTS-810 (modulus and damage) or UTM-25 (permanent deformation). Differences in the complex modulus testing protocol between reference and current mixtures are observed, but not expected to affect the outcomes presented in this report. The reference mixes were tested under a tension-compression mode, whereas the current mixes were tested under compression mode only. Given that in both cases a small strain level was used (50 to 75 με), the

different modes of loading do not affect the measured viscoelastic properties. This was already shown by Underwood and Kim (2012), where differences in the measured moduli values between tension-compression and compression only tests were found to be statistically insignificant at the 95% confidence level.

Table 5. Summary of NCDOT Materials in NCSU Database.

Project	Mix Types	Material Types	Mixes
2002-07[a]	S9.5C, I19.0C	HMA	2
2003-09[a]	S9.5A-C, S12.5B-D, I19.0B-D, B25.0B&C	HMA, 0-15% RAP	43
2007-07[a]	S9.5B&C, S12.5C, I19.0B&C, B25.0B	HMA, 0-15% RAP	11
2011-04[a]	S9.5B	HMA and WMA	4
2012-01[a]	S9.5B&C, I19C, B25B	HMA and WMA, 20% RAP	12
2012-04[a]	S9.5B	HMA, 8-45% RAP, 15-55% RAS[b]	12
2013-06[a]	S9.5C, S9.5D	HMA, 15-45% RAP, 10-50% RAS[b]	24
2015-02[a]	S9.5B, I19B, and B25B	HMA, 24-30% RAP	6
2015-03[a]	S9.5B	HMA and WMA, 20-40% RAP	10
NCHRP 1-42A	S9.5B	HMA	1
FHWA RA-00108	S12.5B and D, B25.0C	HMA	5
IDEA N-181	S9.5A&D, I19.0B, B25.0B	HMA, 30-40% RAP	5

[a] Numbers refer to FHWA/NC projects, [b] RAS contents are PRAS or MRAS binder replacement %

Table 6. Summary of the Five Reference HMA Mixtures.

Mixture	Binder PG	Asphalt Content (%)	Binder Source	Region
RS9.5B	PG64-22	6.0	Citgo – Wilmington #31	Coastal
RS9.5C	PG70-22	6.4	Citgo – Wilmington #31	Coastal
RI19.0B	PG64-22	4.4	Assoc. Asphalt – Inman #6	Coastal
RI19.0C	PG64-22	4.3	Citgo – Wilmington #3	Piedmont
RB25.0B	PG64-22	4.2	Citgo – Wilmington #31	Coastal

In relation to the fatigue characterization, it is worth noting that the cyclic fatigue test procedure has changed considerably since the FHWA/NC 2007-07 experiments were performed. Notably, the test procedure is currently performed in an AMPT equipment with a user-friendly interface as well as updated setup protocols that minimize the occurrence of end failures and potential specimen damage during the initial setup step. It is believed that these differences, coupled with the fact that the cyclic fatigue tests performed on the reference mixes resulted in a high occurrence of end failures, are an artifact of the testing protocol used in the past. Differences are also noted between the triaxial repeated load permanent deformation (TRLPD) test protocol used in the past and the current Stress Sweep Rutting (SSR) test to characterize the resistance to rutting. The SSR test is conducted in an AMPT machine, which also includes a user-friendly interface, and its embedded shift model analysis approach does not allow to predict TRLPD test results.

Given these uncertainties in damage and permanent deformation, the research team has decided to evaluate the relative differences in performance between the current and reference mixtures by considering only the differences in moduli values and assuming that the inherent fatigue cracking and rutting behaviors of the reference mixtures were the same as the behaviors of the current mixtures. If the results from the reference mixtures are correct, then this strategy will underestimate

the performance improvements that exist in the current mixes and provide a conservative (i.e., underestimated) value of their layer coefficients.

The test specimens for the reference mixes were compacted at a target air void content of 5.5 ± 0.5% and three specimens were used for the complex modulus test for each mix. The complex modulus test was conducted at five temperatures (−10°, 5°, 20°, 40°, and 54°C) and six frequencies (25, 10, 5, 1, 0.5, and 0.1 Hz) according to AASHTO T 342, with the exception that tests were performed in the tension-compression mode of loading. This differs from the test procedure recommendations from AASHTO TP 132 adopted for the current mixtures' characterization, where only three test temperatures (i.e., 4°, 20°, and 40°C) and three frequencies (i.e., 10, 1, and 0.1 Hz) frequencies are used. In order to create a better correspondence between the reference and current dynamic modulus data, the reference mixtures' data was filtered and analyzed through FlexMAT^{TM} V2.1 using a reduced dataset corresponding to 5°, 20°, and 40°C and 10, 1, and 0.1 Hz. Subsequently, the cyclic fatigue test data was then combined and used to generate the parameters for the fatigue cracking damage model. The research team compared the parameters generated from the reduced dataset (three temperatures and three frequencies) and the full dataset (five temperatures and six frequencies) to verify whether a substantial difference would be observed, and the results are presented in Figure 7. In this sense, given that no meaningful difference was observed, the research team does not expect that the pavement performance predictions will be affected by adopting the reduced dynamic modulus dataset over the full dataset.

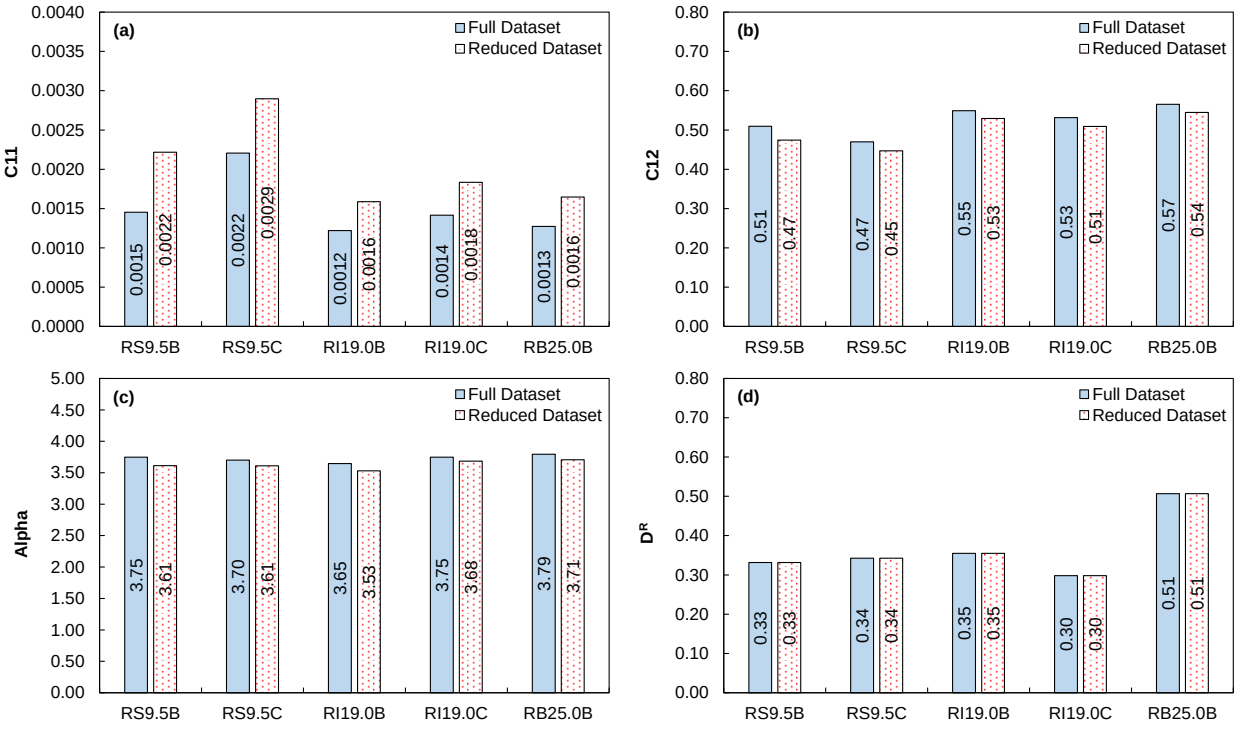

Figure 7. Graph. Comparison between the impact of full and reduced dynamic modulus results dataset for reference mixes on (a) C11, (b) C12, (c) alpha, and (d) D^R parameters.

3.2.2. New Mixture Database

Seven surface, three intermediate, and three base standard mixtures were sampled and tested. These mixtures were collected from the Mountains (MO), Piedmont (PI), and Coastal Plains (CO) regions within the State. While there are regional differences in terms of climate, the mixture

design specifications are applied equally across the regions. In general, the constituent materials are similar across these regions, but each is dominated by different contractors. Each mix in this study was either a post-2018 mix design or a reclassified 2018 mix design. Table 7 summarizes the mixtures tested and their naming convention in this report.

Table 7. Tests Mixtures and Their Naming Convention.

Mixture		Region		
		Mountains	**Piedmont**	**Coastal Plains**
Surface	RS9.5B	MO_RS9.5B	PI_RS9.5B	CO_RS9.5B
	RS9.5C	MO_RS9.5C	PI_RS9.5C	CO_RS9.5C
	RS9.5D	--[1]	PI_RS9.5D	--[1]
Intermediate	RI19.0C	MO_RI19.0C	PI_RI19.0C	CO_RI19.0C
Base	RB25C	MO_RB25C	PI_RB25C	CO_RB25C

[1] The only RS9.5D tested in this project was from the Piedmont

Each mixture was sampled into 5-gallon buckets by NCDOT personnel and collected as loose mix material to be compacted in the lab for testing. All the mixtures were produced by different contractors. The gradation of each mixture is shown in Figure 8. In this graph, the CO_RS9.5B mixture starts as the coarsest mix followed by PI_RS9.5B and MO_RS9.5B. Looking at the smaller sieve sizes, CO_RS9.5B and MO_RS9.5B switch positions. CO_RS9.5C is the finest followed by PI_RS9.5C and MO_RS9.5C. For the intermediate and base mixtures, Figure 8 (c) and (d), CO_RI19.0C is the finest mix of the three followed by MO_RI19.0C and PI_RI19.0C. From Figure 8 (d), PI_RB25C was the coarsest mix of the three tested mixtures.

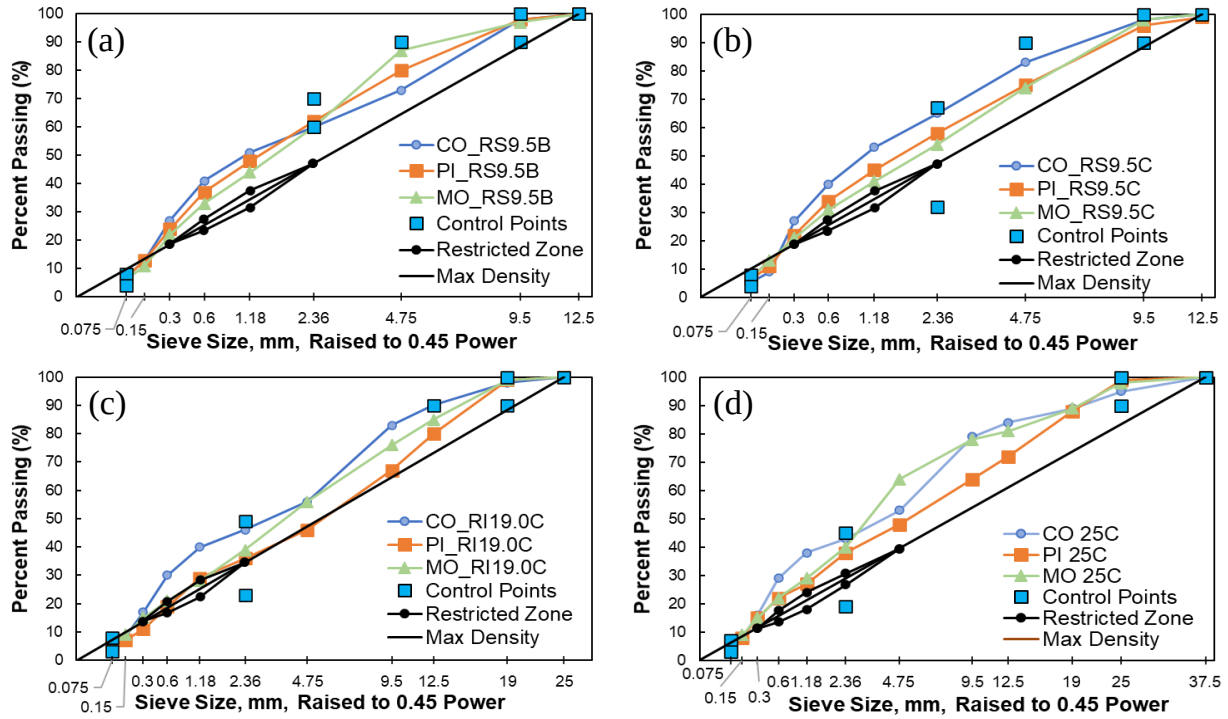

Figure 8. Tested mixtures' gradation charts, (a) RS9.5B mixtures, (b) RS9.5C mixtures, (c) RI19.0C mixtures and (d) RB25C mixtures.

Other mixture design information including NMAS (mm), binder grade, the volume of effective binder (V_{be}), reclaimed asphalt pavement (RAP) percentage, number of design gyrations (N_{des}), voids filled with asphalt (VFA), voids in mineral aggregate (VMA), and theoretical maximum specific gravity (G_{mm}) can be found in Table 8 and Table 9 for surface, and intermediate and base mixtures respectively. In surface "C" mixtures, CO_RS9.5C is distinct from the other two mixtures because of its higher binder content resulting in a higher effective binder content. In fact, that mix had the highest binder content of all the tested mixtures. For surface "B" mixtures, the binder contents of the mixtures were close ranging from 5.8% to 6.5%. In the intermediate mixtures, the RBR% and the effective binder content of the coastal mixture were the highest compared to the other two.

Table 8. Surface Mixtures' Information.

Properties	Mixture						
	RS9.5B			RS9.5C			RS9.5D
	MO	PI	CO	MO	PI	CO	PI
NMAS (mm)	9.5	9.5	9.5	9.5	9.5	9.5	9.5
Binder Grade (Mix Design)	64-22	58-28	64-22	64-22	58-28	64-22	76-22
Binder Grade (Pay Grade)	64-22	64-22	64-22	64-22	64-22	64-22	76-22
Binder Content (%)	6.5	6.3	5.8	5.5	5.8	7	5.6
RBR%	15%	33%	24%	25%	33%	14%	18%
V_{be} (Mix Design)	14.4	13.4	13.2	11.9	12.6	14.6	12.4
RAP Content (%)	20	40	30	30	40	20	20
RAS Content (%)	0	0	0	0	0	0	0
N_{des}	50	50	50	65	65	65	100
VFA (Mix Design)	79	77.2	75.1	75	76.2	77.8	75.6
VMA (Mix Design)	18.4	17.4	17.2	15.9	16.6	18.6	16.4
G_{mm} (Mix Design)	2.475	2.458	2.449	2.46	2.439	2.328	2.496
G_{mm} (NCSU Measured)	2.495	2.422	2.408	2.473	2.452	2.367	2.499

Table 9. Intermediate and Base Mixtures' Information.

Properties	Mixture					
	RI19.0C			RB25C		
	MO	PI	CO	MO	PI	CO
NMAS (mm)	19	19	19	25	25	25
Binder Grade (Mix Design)	64-22	58-28	58-28	64-22	64-22	58-28
Binder Grade (Pay Grade)	64-22	64-22	64-22	64-22	64-22	64-22
Binder Content (%)	5	4.7	4.8	4.5	4.2	4.3
RBR%	18%	30%	42%	27%	26%	42%
V_{be} (Mix Design)	10.4	10.3	14.6	10.3	9.6	9.8
RAP Content (%)	20	12	30	23	30	30
RAS Content (%)	0	4	3	0	0	2
N_{des}	65	65	65	65	65	65
VFA (Mix Design)	72.2	70.5	73.6	71.8	71.5	71
VMA (Mix Design)	14.4	14.3	15.1	14.3	13.6	13.8
G_{mm} (Mix Design)	2.533	2.553	2.489	2.562	2.544	2.513
G_{mm} (NCSU Measured)	2.535	2.536	2.490	2.545	2.508	2.515

3.3. Experimental Results for New Mixtures

3.3.1. Overview

The mechanical characterization of the new mixtures described above was performed using the Asphalt Mixture Performance Tester (AMPT) via dynamic modulus testing (AASHTO TP 132 or AASHTO T 378), cyclic fatigue testing (AASHTO TP 133 or TP 107), and stress-sweep rutting testing (AASHTO TP 134). Included within these test methods are specifications for specimen preparation (AASHTO R 83 and PP 99), determination of theoretical maximum specific gravity (AASHTO T 209), determination of bulk specific gravity (AASHTO T 166), and determination of percent air voids (AASHTO T 269). The target air-void content for all the mixtures was 5 ± 0.5% for all test specimens.

Multiple parameters from each test method were identified and used to statistically compare the mixtures from the same classification. The statistical analysis was carried out as an effort to understand the significance of the observed differences between various test parameters and involved checking the validity of the normality and equal variances assumptions, as well as running analysis of variance (ANOVA) and post-hoc tests. Under the following subsections, a summary of the testing and statistical analysis results for the RS9.5C mixture are presented. The full detailed testing and statistical analysis results for all the tested mixture classifications (including this mixture classification) are presented in Appendix D.

3.3.2. Dynamic Modulus Test Results

The dynamic modulus and phase angle results from the AASHTO TP 132 testing for each of the three RS9.5C mixtures are shown in Figure 9. Overall, the modulus of MO_RS9.5C is on average higher than PI_RS9.5C and CO_RS9.5C. PI_RS9.5C has overall have higher phase angle values than the other two mixtures. MO_RS9.5C has a coarser gradation than the other mixtures and has the lowest effective binder content, which explains why this mixture has the higher modulus values. The phase angle values follow in that PI_RS9.5C has a higher binder content and higher effective binder content. Even though CO_RS9.5C has the highest effective binder content, PI_RS9.5C has the higher RAP percentage by eight percent. Detailed results from the RS9.5B, RI19.0C, and RB25.0C mixtures and are shown in Appendix D. Across all mixtures it is found that regional variations exist. Many of these behaviors can be tracked back to compositional issues (binder content, RAP content, gradation, etc.), but there is no universal compositional factor that governs the observed behaviors. Instead is the unique combination of these factors that dictate the behaviors of the materials.

3.3.3. Cyclic Fatigue Test Results

The test results from AASHTO TP 133/TP 107 are the damage characteristic curves, failure criterion, and apparent damage capacity fatigue performance index, S_{app}, for a given asphalt mixture. Examples of these outcomes are shown for the RS9.5C mixtures in Figure 10. The damage characteristic curve is a functional relationship between the integrity (pseudo stiffness, *C*) of the specimen and the amount of damage, *S*, in the specimen. Figure 10 (a) shows the fitted damage characteristic curves for each mixture. Generally, the damage characteristic curves of higher modulus mixtures tend to be positioned vertically higher than those of other mixtures; however, this outcome does not imply better or worse performance. Although for a given *S* value, a higher modulus material exhibits higher *C* values (higher integrity), the material with a higher modulus material might actually be more brittle and hence more prone to fail at a lower loss in material integrity, i.e., high modulus materials may fail at a higher *C* value. In this case, MO_RS9.5C has

the highest *C* values throughout and the shortest damage curve. It is also worthy to note that MO_RS9.5C had the highest modulus values among the three mixtures.

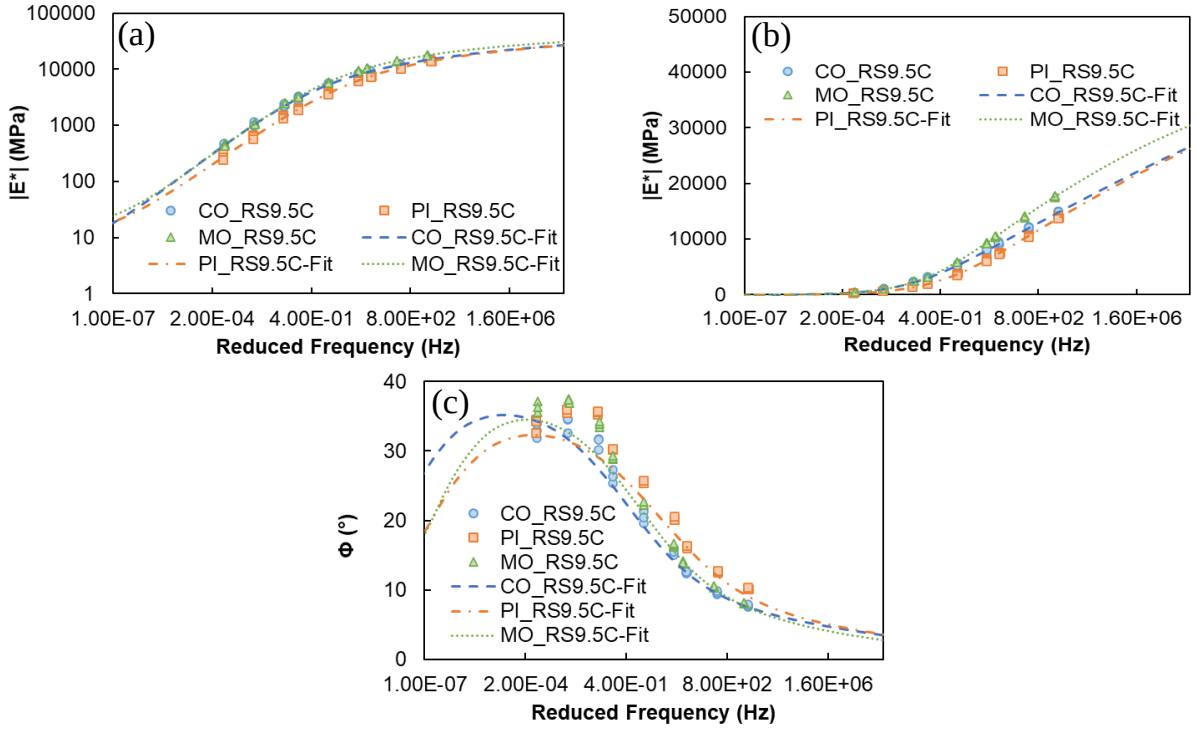

Figure 9. Dynamic modulus and phase angle results for RS9.5C mixtures, (a) dynamic modulus log-log plot, (b) dynamic modulus semi-log plot, and (c) phase angle semi-log plot.

An indicator of the material's fatigue resistance is the D^R value. The D^R failure criterion for a mixture is established by averaging the ratio of average reduction in pseudo stiffness with number of cycles to failure for test specimens used in damage characterization. Figure 10 (b) shows the individual data points that form the relationship that defines D^R. The average D^R values from each data point are shown in Figure 10 (c). A higher D^R value generally indicates better fatigue resistance compared to a lower D^R value. The trend of D^R shows that MO_RS9.5C is the worst performing, followed by CO_RS9.5C and finally PI_RS9.5C.

However, the performance of the mixture cannot be evaluated solely based on the position of the damage characteristic curves or D^R values because both the modulus and inherent fatigue resistance play a role in determining the mixture's fatigue performance within a pavement. If two mixtures have the same fatigue resistance, but one has a higher modulus than the other, the higher modulus mixture will have a longer fatigue life. Similarly, a more fatigue-resistant mixture will have a longer fatigue life than another mixture of similar modulus but less fatigue resistance. S_{app} is an index parameter that was developed to account for these two factors (modulus and fatigue resistance) that affect the cracking potential of a mixture and is based on VECD theory. A higher S_{app} value indicates better fatigue resistance compared to a lower S_{app} value. The S_{app} values are shown Figure 10 (d). PI_RS9.5C has the highest S_{app} values followed by CO_RS9.5C and then MO_RS9.5C. The ranking of S_{app} values shown below make sense because MO_RS9.5C has the lowest effective binder content and coarsest gradation. In this case, the higher modulus mixture translates to lower S_{app} values. As discussed before, PI_RS9.5C has lower dynamic modulus values with a softer binder than the other two mixtures, therefore resulting in better fatigue performance.

It should be noted that Wang et al. (2020) suggest that a S_{app} performance threshold for high traffic volume conditions consistent with the NCDOT usage of RS9.5C mixtures to be higher than 24. Thus, according to this criterion, only PI_RS9.5C passes that threshold with a classification of "Very Heavy". The other two mixtures could be classified as "Standard".

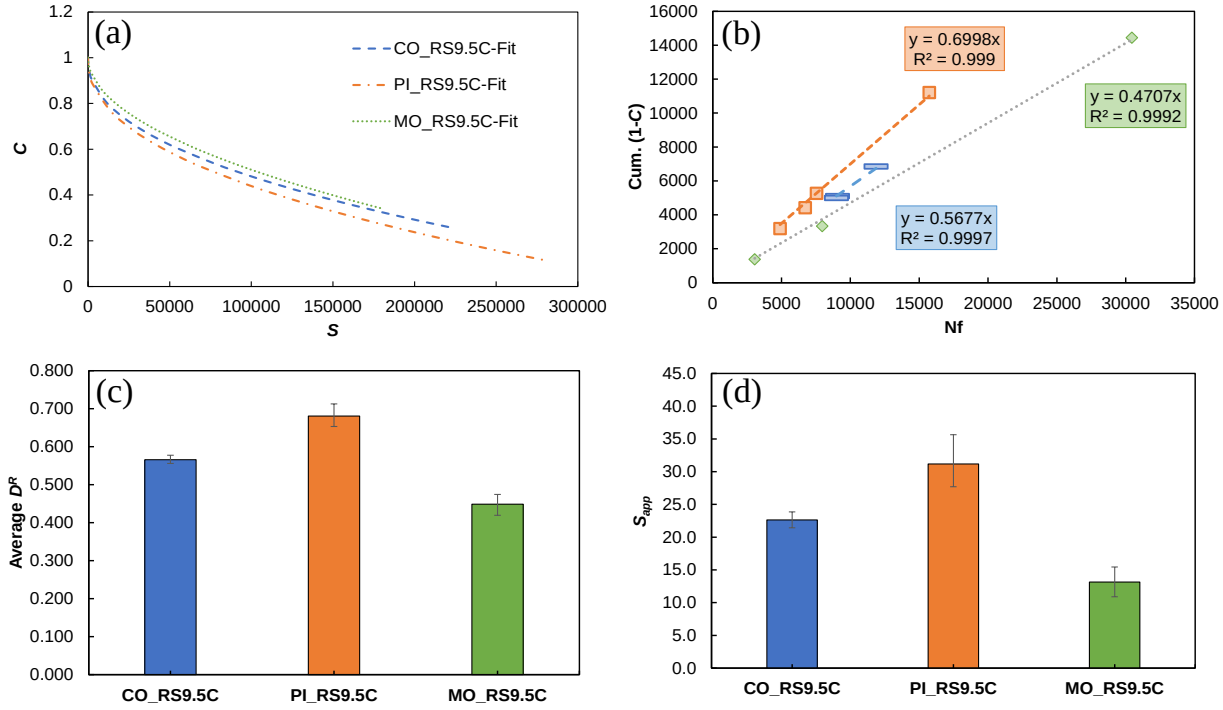

Figure 10. Cyclic fatigue results for RS9.5C mixtures, (a) *C* vs. *S* damage curves, (b) Cum. (1-*C*) vs. N_f, (c) D^R values, and (d) S_{app} values.

Detailed results of the other mix designs are presented in Appendix D. In these mixtures there can also be a substantial variation between mixtures of the same classification. This latter fact is especially true for the RS9.5B mixture which shows S_{app} rankings from approximately 33 (CO_RS9.5B) to approximately 19 (MO_RS9.5B). Of note is the fact that S_{app} values were consistently higher (i.e., better) for the RS9.5B mixtures than the RS9.5C mixtures.

3.3.4. Stress-Sweep Rutting Test Results

The SSR test results are shown in full in Appendix D, but not shown here because each region was tested at a different high temperature in accordance with the AASHTO TP 134 protocol. Thus, direct comparison across regions is not possible. Instead, the results are compiled as the rutting strain index (RSI) values for the RS9.5C mixtures in Figure 11. The RSI is the average permanent strain (in percent) and is defined as the ratio of the permanent deformation in an asphalt layer to the thickness of that layer at the end of a 20-year period. The permanent strain is predicted using a simplified rutting performance model that closely approximates the rut depth predicted from the FlexPAVE™ performance model (Ghanbari et al. 2020). A mixture with a lower RSI value has more rutting resistance than a mixture with a higher RSI value.

The RSI calculation requires users to select a climate region and for this project, the climatic conditions of Wilmington (Coast), NC, Wake Forest (Piedmont), NC, and Asheville (Mountains), NC, have been used. As shown in Figure 11, MO_RS9.5C has the best rutting performance in all locations, followed by CO_RS9.5C and PI_RS9.5C. MO_RS9.5C has the lowest effective binder

content and the coarsest gradation resulting in this performance. Again, like with the other material properties, substantial variation is noted to exist between mixtures of the same designation. With respect to RS9.5B, its performance was worse (i.e., higher RSI) when compared to the RS9.5C mixtures.

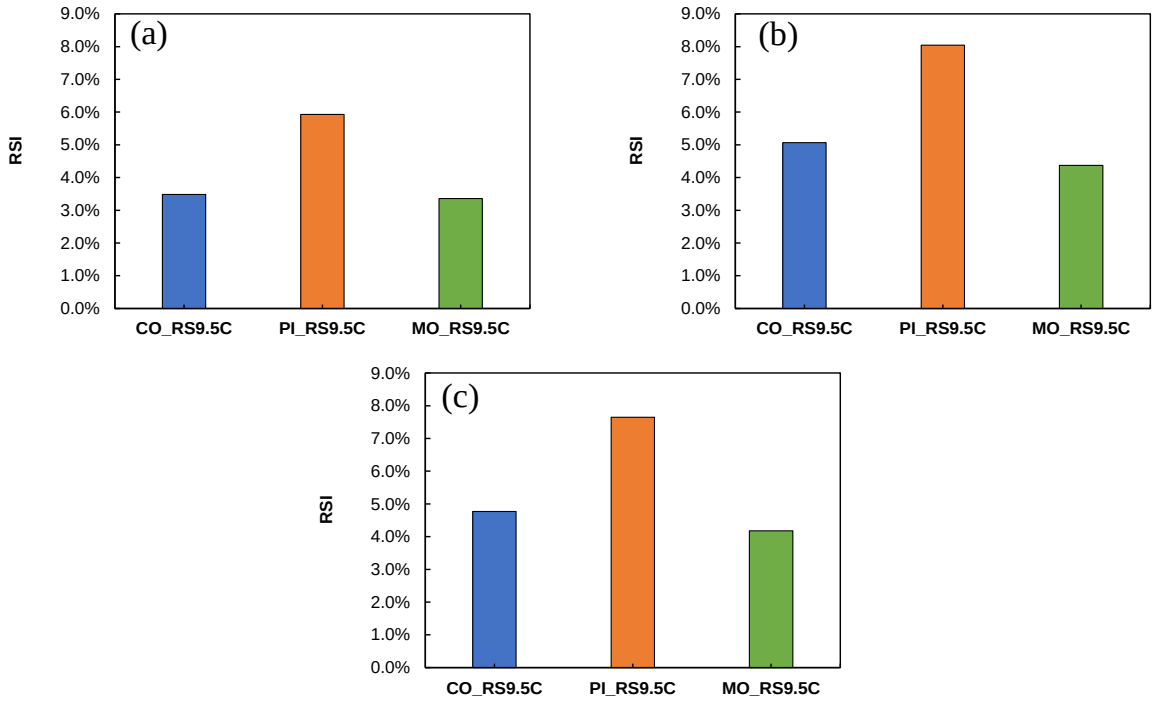

Figure 11. Rutting strain index values for RS9.5C mixtures, (a) Wilmington climatic conditions, (b) Wake Forest climatic conditions, and (c) Asheville climatic conditions.

3.3.5. Summary of Mixture Comparative Analysis

A statistical analysis was performed to assess whether the differences between mixtures of the same designation, but from different regions were significant. This assessment included comparisons of moduli at different temperatures and frequencies as well as comparisons of the *C* vs. *S* curves (specifically the *C* value at *S* values of 20,000 and 120,000), D^R, S_{app}, and RSI. For each comparison, the data was first tested for normality and to determine whether test variances were equal. Depending on the outcome of this analysis either a Welch's ANOVA or one-way ANOVA test was performed to identify whether significant differences existed. A 95% confidence limit was chose as the threshold for statistical significance for all of the parameters. If significant differences were identified then a Games-Howell or Tukey-Kramer analysis was used to characterize the level of difference. The detailed analysis procedures and outcomes are described in Appendix D.

Table 10 to 13 show the overall analysis results for the material parameters for the different mixtures. These tables use letters to signify if the mixtures are statistically different or not. When two conditions have the same letter then they are determined to be statistically similar and when they have different letters they are statistically different. The statistical analysis method used to arrive at these conclusions is also reported in the table. The letters also signify the numerical value of that particular parameter. The lower the letter in the alphabet, the greater the value. Therefore, if a parameter is given "A", it has the higher values for that parameter. For the dynamic modulus

and phase angle, for a given test temperature, if two of the three temperature–frequency combinations were different with respect to two mixtures, then there were assumed different. Also, if a mixture is given two letters, such as "AB", then this mixture is similar to both of the other mixtures. As an example of how to interpret the data in these tables, examine the first row in Table 10. In this row, each mixture has a different letter signifying that all mixtures were significantly different from each other. Since MO_RS9.5C has the letter A it indicates that this mixture has the highest modulus since at 4°C.

From Table 10, for dynamic modulus, PI_RS9.5C is different than the other two mixtures. CO_RS9.5C is different than MO_RS9.5C until the temperature reaches 40°C at which point CO_RS9.5C and MO_RS9.5C become statistically equivalent. For phase angle and cyclic fatigue data, the mixtures are different for all temperatures, while for RSI, CO_RS9.5C is similar to MO_RS9.5C. Table 11 through Table 13 show the detailed results for the remaining mixtures.

The totality of the statistical analysis is that all the tested mixtures of the same classification exhibit differences in respect to index parameters and mechanical properties. Some of the mixtures may be similar in respect to certain index performance parameters, such as S_{app} or RSI, but overall, the mixtures of the same classification exhibit differences. There is not a specific trend when it comes to these differences within each mixture classification. For example, in RI19.0C mixtures, the *C* vs. *S* damage curves show differences, but all S_{app} values are similar. The significance of these differences is highlighted in the next section when the in-service performance is predicted using AASHTO Pavement ME Design and FlexPAVE™ 1.1

Table 10. Summary of Statistical Analysis of Dynamic Modulus, Cyclic Fatigue, and Stress-Sweep Rutting Test Results for RS9.5C Mixtures.

Test	Property/ Temperature	Mixtures			Statistical Analysis Method
		CO	PI	MO	
Dynamic Modulus Parameters	4°C	B	C	A	Tukey-Kramer HSD
	20°C	B	C	A	
	40°C	A	B	A	
Phase Angle Parameters	4°C	C	A	B	
	20°C	C	A	B	
	40°C	C	B	A	
Cyclic Fatigue and Stress Sweep Rutting Parameters	S_{app}	B	A	C	Tukey-Kramer HSD & Games-Howell
	D^R	B	A	C	
	Fingerprint |E*|	B	C	A	
	C at *S* = 20,000	B	C	A	
	C at *S* = 120,000	B	C	A	
	RSI (Asheville, NC)	B	A	B	

Table 11. Summary of Statistical Analysis of Dynamic Modulus, Cyclic Fatigue, and Stress-Sweep Rutting Test Results for RS9.5B Mixtures.

Test	Property/ Temperature	Mixtures			Statistical Analysis Method
		CO	PI	MO	
Dynamic Modulus Parameters	4°C	A	C	B	Tukey-Kramer HSD
	20°C	A	C	B	
	40°C	A	B	B	
Phase Angle Parameters	4°C	C	B	A	
	20°C	C	B	A	
	40°C	B	A	A	
Cyclic Fatigue and Stress Sweep Rutting Parameters	S_{app}	B	A	C	Tukey-Kramer HSD & Games-Howell
	D^R	B	A	C	
	Fingerprint |E*|	A	C	B	
	C at S = 20,000	A	B	B	
	C at S = 120,000	A	B	B	
	RSI (Wilmington, NC)	A	A	B	
	RSI (Wake Forest, NC)	A	B	C	
	RSI (Asheville, NC)	A	B	C	

Table 12. Summary of Statistical Analysis of Dynamic Modulus, Cyclic Fatigue, and Stress-Sweep Rutting Test Results for RI19.0C Mixtures.

Test	Property/ Temperature	Mixtures			Statistical Analysis Method
		CO	PI	MO	
Dynamic Modulus Parameters	4°C	A	B	B	Tukey-Kramer HSD
	20°C	A	C	B	
	40°C	A	C	B	
Phase Angle Parameters	4°C	B	A	AB	
	20°C	C	A	B	
	40°C	B	A	B	
Cyclic Fatigue and Stress Sweep Rutting Parameters	S_{app}	A	B	B	Tukey-Kramer HSD & Games-Howell
	D^R	A	A	B	
	Fingerprint |E*|	A	B	B	
	C at S = 20,000	A	C	B	
	C at S = 90,000	A	C	B	
	RSI (Wake Forest, NC)	B	A	A	

Table 13. Statistical Analysis of Dynamic Modulus, Cyclic Fatigue, and Stress-Sweep Rutting Test Results for RB25C Mixtures.

Test	Property/ Temperature	Mixtures			Statistical Analysis Method
		CO	PI	MO	
Dynamic Modulus Parameters	4°C	B	C	A	Tukey-Kramer HSD
	20°C	A	B	A	
	40°C	A	B	B	
Phase Angle Parameters	4°C	B	A	B	
	20°C	B	A	A	
	40°C	B	B	A	
Cyclic Fatigue and Stress Sweep Rutting Parameters	S_{app}	A	A	A	Tukey-Kramer HSD & Games-Howell
	D^R	B	A	B	
	Fingerprint |E*|	A	B	A	
	C at S = 20,000	A	C	B	
	C at S = 45,000	A	C	B	
	RSI (Asheville, NC)	A	A	A	

3.4. Pavement Performance Simulations

The layer coefficients calibration presented in Section 2 reflect materials in use approximately 13 years ago. To estimate the value of current day materials, these layer coefficients were adjusted based on Equation (9). The pavement performance predictions for the reference case ($Performance_{reference}$) and the current NCDOT mixture case ($Performance_{material,x}$) were determined using the AASHTO Pavement ME Design and FlexPAVE™ since both simulation tools have been used in past NCDOT projects. In both cases, the performance predictions were first performed with respect to rutting and fatigue cracking using material properties consistent with both the reference and current material properties. In these simulations only the dynamic modulus values were changed. It was originally envisioned that the simulations would change the moduli and the material properties related to fatigue cracking and rutting. However, it was found that the historical data was collected using inconsistent testing protocols and could not be used reliably. It is believed that this assumption is reasonably accurate with respect to rutting, since historical and current materials are designed using asphalt pavement analyzer (APA) test results. However, it as also believed that this decision means that the fatigue performance of the reference materials is overestimated especially in the case of the FlexPAVE™ simulations.

Once the simulations were completed, the amount of rutting and fatigue cracking (and fatigue damage in the case of FlexPAVE™) at the end of a 20-year simulation were extracted. Fatigue damage in FlexPAVE is the result of the internal model calculations. The %Cracking calculation uses the initial transfer function (Wang et al. 2021) to convert damage to the percentage of lane area showing fatigue cracking. The *Performance* variables in Equation (9), were then computed by taking the inverse of the predicted distress magnitude (i.e., if a pavement had 0.2 in. of rutting at the end of the 20-year period then the *Performance* value for that case was 1/0.2 = 5). Thus, in the end, the inverse of damage (rut depth, fatigue damage, or fatigue cracking) for the current material divided by the inverse of damage for reference material defines the performance ratio that should be multiplied by the calibrated reference coefficient to determine the current coefficients. The Equation (9) can be rearranged to Equation (10) which is used to adjust the coefficients. For example, suppose a simulation with the reference material yielded 0.15 in of rutting after 20 years

while the same simulation using the current materials yielded 0.13 in of rutting after the same 20-year period. In this case the performance ratio would be 1.15 and when using the recommended 0.44 layer coefficient in Table 4, the suggested layer coefficient for the current material would be 0.44 x 1.15 = 0.51.

$$a_{mterial,x} = \left(\frac{\frac{1}{Damage_{material,x}}}{\frac{1}{Damage_{reference}}} \right) \times a_{reference} \quad (10)$$

where $Damage_{material,x}$ is the fatigue or rutting damage for current materials and $Damage_{reference}$ is the fatigue or rutting damage for reference materials.

It should be noted that the ratio was calculated for rutting and fatigue separately and the minimum value was taken as the controlling factor. The inputs for these simulations were obtained from the NCSU materials database (both asphalt concrete and aggregate base courses), and the FHWA/NC 2015-02 pavement performance database. It should also be noted that the research team did investigate using 30-year performance window, owing the fact that NCDOT designs higher volume roads with a 30-year design life, but the final calibrated coefficients did not change in any systematic way and so for consistency elected to compute the final performance ratios using a 20-year basis.

Table 14 summarizes the parameters evaluated in these simulations and the levels of each factor. The simulation matrix is made-up of the permutation of these inputs. The specific input values for pavement structure and material properties are presented in Table 15 and Table 16, respectively. The inputs values were the same for both Pavement ME Design and FlexPAVE™ simulations, but the traffic inputs varied so that the simulations yielded (on average) rut depths of about 0.5 inch during the simulation period. The traffic inputs for Pavement ME and FlexPAVE™ simulations are summarized in Table 17 and Table 18, respectively.

Different combinations of inputs created 216 simulations for Pavement Design ME and 72 simulations for FlexPAVE™. The number of simulations for FlexPAVE™ is different than Pavement Design ME because a brief sensitivity analysis for FlexPAVE™ was conducted for the subgrade moduli values ranging from 8,000 to 14,000 psi (~55,000 to 96,500 kPa). The sensitivity analysis showed that the damage results and asphalt layer only rutting were not sensitive to this range of change, so it was decided that instead of three, only one soil types (silt) be used for FlexPAVE™ simulations.

Table 14. Matrix of Performance Simulation Inputs.

Material type	Pavement type[1]	Thickness type	Mix type	Soil type	Climate zone
Current	FDA	Thin	B-Mix	Sand	Piedmont (Raleigh)
Reference	ABC	Intermediate	C-Mix	Silt	Coastal (Wilmington)
	DS	Thick		Clay	Mountains (Asheville)

[1] FDA = full-depth asphalt pavement, ABC = pavement with aggregate base course, DS = pavement with asphalt base and aggregate base course

Table 15. Pavement Structures used in Performance Simulations.

Pavement Structure Type	Thickness Type	Thickness (in.)				
		Surface AC	Intermediate AC	Base AC	ABC	Total
FDA	Thin	3	0	4	0	7
	Intermediate	3	4	4	0	11
	Thick	3	4	10	0	17
ABC	Thin	3	0	0	8	11
	Intermediate	3	4	0	8	15
	Thick	3	4	0	10	17
DS	Thin	3	2.5	3	8	16.5
	Intermediate	3	4	3	8	18
	Thick	3	4	5.5	10	22.5

Table 16. Material Properties Used in Performance Simulations.

Poisson ratio		Moduli (psi)	
AC	0.30	ABC	29,008
ABC	0.35	Subgrade (Sand)	14,504
Subgrade	0.40	Subgrade (Silt)	10,878
		Subgrade (Clay)	7,252

Table 17. Traffic Inputs Used in Pavement Design ME Simulations.

Pavement Structure Type	Thickness Type	Trucks in Design Lane	Trucks in Design Direction	Two-Way AADTT	Speed (mph)	TTC	ALDF
FDA & ABC	Thin	100	50	1,000	60	12	1
	Intermediate	90	50	2,000	60	8	3
	Thick	60	50	6,000	60	1	4
DS	Thin	100	50	2,000	60	8	3
	Intermediate	90	50	2,000	60	8	3
	Thick	60	50	6,000	60	1	4

Table 18. Traffic Inputs Used in FlexPAVE™ Simulations.

Thickness Type	Daily ESALs	Growth Type	Growth Rate (%)	Speed (mph)
Thin	2,000	Linear	0.4	60
Intermediate	3,000			
Thick	6,000			

The results of the simulations are presented in detail in Appendix E. Table 19 summarizes the results of the simulations where the results are segregated by performance model and by surface layer type. This table shows the average performance ratio and the corresponding standard deviation based on analysis type and mix type. As shown in Table 19, the Pavment ME simulations

generally suggest that the current materials will underperform with respect to rutting and fatigue cracking in comparison to the reference materials. However, the standard deviation is large enough that a performance ratio of 1 is within the 95% confidence intervals. With respect to FlexPAVE, the simulations suggest on average increases in fatigue cracking performance, but a slight decrease with respect to rutting. However, it should be recalled that the same inherent damage properties were assumed for the reference and current mixtures. If anything, the research team believes that the inherent fatigue performance has improved and so the performance ratios from FlexPAVE for the current materials may likely represent an underestimation.

Table 19. Summary of Performance Ratios.

Simulation by	Mix Type	Analysis Type	Performance Ratio		Performance Ratio (Min.)
			Average	STDEV[1]	
Pavement ME	B-Mix	Fatigue Cracking (%)	0.94	0.36	0.86
		Total Pavement Rutting	0.86	0.09	
	C-Mix	Fatigue Cracking (%)	0.85	0.28	0.85
		Total Pavement Rutting	1.01	0.09	
FlexPAVE™	B-Mix	Fatigue Damage (%)	1.08	0.17	0.96
		Fatigue Cracking (%)	1.14	0.55	
		Total Pavement Rutting	0.96	0.01	
	C-Mix	Fatigue Damage (%)	1.04	0.16	1.00
		Fatigue Cracking (%)	1.20	0.63	
		Total Pavement Rutting	1.00	0.01	

[1] Standard deviation

3.5. Layer Coefficients for new mixtures

Calibrated layer coefficients for reference materials were discussed and presented in Table 4. Although there is considerable uncertainty in the performance predictions, the minimum performance value ratios can be used adjusted based on performance simulations. The layer coefficients for current materials are calculated based on the average performance ratios determined based on performance simulations as presented in Table 20. The simulations showed the performance of the current materials decreased or stayed the same (on average) comparing to reference materials. The largest change occurs in the C-mix and is based on Pavement ME rutting predictions.

While Table 20 shows calculated coefficients using the performance ratio, the research team's recommendation based on this analysis is to use the layer coefficients calibrated in Section 2 for current materials. This recommendation is based on the fact that the performance ratios suggest at most a 15% change in the coefficients and that in many cases (across simulation methods and distresses examined) performance ratios are above 1. Thus, there does not appear to be a universal bias (given the considerable variation) that provides sufficient evidence to reject the idea that the structural performance of asphalt mixtures has systematically changed in the 13 year period. FlexPAVE™ does suggest that the cracking performance may have improved while rutting was not affected. This finding suggests further study and investigation is warranted, but in the research team's opinion is not alone sufficient enough (given the other simulation results) to convince the team to recommend increases in the layer coefficients. Another factor contributing to this

recommendation is that the original layer coefficients calibrations also carry considerable uncertainty related to the conversion algorithms to relate *PCR* to *PSI*.

Table 20. Calculated Layer Coefficients for Current NCDOT Materials.

Simulation	Mix Type	Performance Ratio	Category	AC-surface/int.	AC-base
Pavement ME	B-Mix	0.86	Universal	0.35	0.17
			1	0.20	0.17
			2	0.37	0.17
	C-Mix	0.85	Universal	0.35	0.17
			1	0.20	0.17
			2	0.36	0.17
FlexPAVE™	B-Mix	0.96	Universal	0.40	0.19
			1	0.23	0.19
			2	0.41	0.19
	C-Mix	1.00	Universal	0.41	0.20
			1	0.24	0.20
			2	0.43	0.20

3.6. Discussion on Layer Coefficients

In this study, the calibration results suggests that the layer coefficients should be decreased from the default values. This conclusion in not in agreement with previous studies in other states, specifically two recent efforts (Timm et al. 2014; Dave et al. 2019) (see Appendix A for details). These studies concluded that layer coefficients should increase above what is currently in use in the locations of the respective studies. However, as the analysis shown in Figure 1 (where the AASHTO modulus to layer coefficient equation was used to show that the layer coefficient of NCDOT mixtures could potentially increase) demonstrates, the exact methodology must be carefully considered. One important distinction of the current study was the need to convert to *PSI* in two steps; *PCR* to *IRI* then *IRI* to *PSI*. However, in the previous studies *IRI* was converted to *PSI* directly thus their studies had one layer of conversion comparing to the current study, which had two. This difference could partly explain the discrepancy between studies. The following factors may contribute to the discrepancies between the Dave et al. (2019) study and the results obtained in this study:

1. The researchers considered *IRI* directly as the representative field performance index. However, in their study, *IRI* data was only available for a maximum of five years after construction. This should be compared against the current study which had, on average, 13 years of data at each site. Dave et al. (2019) observed a linear increase in *IRI* with time in the initial five year window and thus the researchers decided to extrapolate the data to 20-year *IRI* values using a linear function. Since *IRI* is known to exhibit exponential deterioration with time (Al-Suleiman and Shiyab 2003), this approach likely systematically underestimated the *IRI* values at the end of the 20-year period, which is an issue acknowledged by the authors. Since *IRI* is inversely related to *PSI*, an underestimation of the *IRI* translates to an overestimation of *PSI* and ultimately a condition that biases their results to yielding higher layer coefficients. If in the current study only the first few years of *PCR* data were considered and then this data was linearly extrapolated to 20 years, the calibration

results would also be higher than the current results. As shown and discussed in this report, North Carolina roadways, it seems, demonstrate a slower performance degradation early on, but then a much more rapid deterioration curve than the AASHTO equation suggests.

2. The Dave et al. (2019) study also evaluated new materials using laboratory tests and concluded again that the layer coefficient values for these materials should be higher than those for materials produced in the past. However, the new materials used in the laboratory investigation included asphalt rubber gap graded (ARGG) mixes and polymer-modified dense-graded mixes in addition to some conventional mixes. Most of these mixes indicated high performance in evaluation tests, for example, ARGG mixes had high stiffness values or polymer-modified mixtures showed a high resistance to fatigue cracking and transverse cracking. Presumably, these materials would perform very well over the years and would not deteriorate rapidly, which results in higher layer coefficients. In the current study, only conventional materials were used, which might have a lower performance compared to the mixtures used in Dave et al. (2019). It is further noted that the maximum binder replacement percentage for the dense graded mixtures in the Dave et al. study was 21.7 percent.
3. Dave et al. (2019) calculated the layer coefficients of non-surface course materials using the AASHTO equation that correlates the resilient modulus with the layer coefficient (the same used for the analysis in Figure 1). These coefficients were used only as the starting point to calibrate the coefficient of surface course. The structural number (SN) for non-surface course was calculated based on these coefficients and it was subtracted from the overall SN, calculated using field performance measurements and AASHTO equation, to determine the SN for surface course. Then, the SN of surface course was divided by the thickness of the layer to determine the layer coefficient. Unlike the data analyzed for North Carolina, Dave et al. (2019) believed that the resilient modulus to layer coefficient equation to underestimates the layer coefficients for some mixtures (the authors did not explain in detail the basis for this belief). It is possible that the underestimation of non-surface course layer coefficients resulted in higher values of layer coefficients for surface course.

The following factors may contribute to the discrepancies between the Davis and Timm (2009) study and the results obtained in this study.

1. Data from the NCAT test track sections were used for calibration in the Davis and Timm (2009) study where newer and more advanced HMA and base materials were placed in these sections. Also, construction of these sections took place under a relatively high level of control and supervision compared to typical practice. For calibration studies, the test sections were subjected to high volume traffic ranging from 1 to 14 million and in most sections the traffic volume was more than 3 million ESALs. On the basis of the higher level of variable certainty and attention to construction detail, the sections considered in the NCAT study are considered comparable with the Category 2 sections in the current study.
2. Since the data for the Davis and Timm (2009) study was collected at the NCAT test track, the loading was accelerated. Even though there were a large number of ESALs, these were applied over a period of two to three years. Thus, any environmental degradation and interaction between environmental and traffic effects was substantially lessened, which would systematically underestimate the performance degradation of the mixtures under real-world loading and environmental conditions and lead to overestimation of layer coefficients.

This page is intentionally blank

4. LONG-TERM PAVEMENT PERFORMANCE MODELING PLAN

The development of new pavement design and analysis methods that rely on large amounts of field performance data has increased the need for state highway agencies to monitor and record reliable information on the behaviors of their pavements. As part of the research effort described in this report, the research team has developed a guideline to aid the NCDOT in considering the development of its own performance monitoring program. As the previous sections have shown, accurate and detailed performance data is necessary, even when using mechanistic based design and analysis, to ensure that the resultant design equations accurately reflect real-world performance. Collecting this data by retrospective analysis, as was done in the previous sections, has several drawbacks with respect to data accuracy, certainty, and access to the necessary supplementary information to best use the data. Thus, a coordinated up front effort to collect and store performance data along with all necessary supplementary information (construction records, design contracts, material properties, etc.) is needed to ensure continual improvement and optimization of the roadway network performance.

The detailed plan developed for this purpose is provided in Appendix F of this report. This guideline covers, in the research team's view, the critical components that the NCDOT needs to consider before establishing a long-term monitoring program. The guideline first provides an overview of the need and status of the national long-term pavement performance program in North Carolina. It then describes the factors to consider for site selection and suggested categories for each (traffic, materials, structures, and climate). The guideline then discusses the potential for incorporating existing projects into the database as well as the benefits of focusing on including only new projects. While it is envisioned that the NCDOT would be primarily interested in cataloging existing designs, some examples of how a systematic performance database could be leveraged to catalog and analyze purpose-built sites to evaluate specific research questions are presented. Finally, the guideline also discusses data collection requirements, cataloging requirements, and data quality control issues to consider.

This page is intentionally blank

5. CONCLUSIONS AND RECOMMENDATIONS

This section presents the major conclusions derived from the review of pavement condition indices relationships and different agencies' truck factors, the results of layer coefficients calibration trials, experiments on materials, and performance simulations. It also presents key recommendations regarding the proposed calibrated layer coefficients for NCDOT.

5.1. Conclusions

- Based on the literature review and NCDOT database availability, it was concluded that *IRI* could be used as the intermediate parameter to correlate *PCR* and *PSI*.
- It was observed from the performance data that North Carolina roadways show a slower performance degradation early on, but then a much more rapid deterioration curve than the AASHTO equation suggests.
- The knowledge gained from the calibration trials show that layer coefficient calibration results are best achieved using the following guidelines:
    - adopt fixed, universal coefficients for asphalt base and aggregate base layers,
    - optimize the asphalt surface/intermediate layer coefficient on the basis of matching the measured and predicted *PSI* value that corresponds to an equivalent *PCR* equivalent of 60 instead of trying to match the entire performance degradation curve,
    - categorize sections based on the 20-year cumulative ESALs from the original contracts and whether the roadway was an interstate or not.
- The calibration results for reference materials suggests that the layer coefficients for asphalt concrete mixtures should decrease and for ABC should not change. This conclusion is not in agreement with other agencies' recent studies (Timm et al. 2014; Dave et al. 2019).
- The results of the laboratory testing found that practical and statistical differences exist in mixtures from the same classification. Some of these behaviors can be tracked back to compositional issues (binder content, RAP content, gradation, etc.), but there is no universal compositional factor that governs the observed behaviors. Some of the mixtures may be similar in respect to certain index performance parameters, such as S_{app} or RSI, but overall, the mixtures of the same classification exhibit differences. There is not a specific trend when it comes to these differences within each mixture classification.
- The performance simulations showed the performance of the current materials may be lower than the reference materials by up to 15 percent or that they may outperform the reference mixtures by as much 20 percent depending on the distress and simulation platform.

5.2. Recommendations

Based on these conclusions, the research team has made the following recommendations regarding layer coefficients.

- The calibrated layer coefficients for non-interstate pavements designed using a 20-year cumulative design ESAL less than 3 million, should be changed from 0.44 to 0.24 for asphalt concrete surface and intermediate mixtures and from 0.3 to 0.2 for asphalt concrete base mixtures. It is recommended to keep using the default value of 0.14 for ABC layer.
- The calibrated layer coefficients for interstate pavements at all traffic levels and all other roadways designed using a 20-year cumulative design ESAL equal to or greater than 3

million, should be kept at 0.44 for asphalt concrete surface and intermediate mixtures and changed from 0.3 to 0.2 for asphalt concrete base mixtures. It is recommended to keep using the default value of 0.14 for ABC layer.

The research team does not currently recommend adjusting the layer coefficients from the recommendations above for current mixtures because of the uncertainty and variation in the performance model predictions from AASHTO Pavement ME Design and FlexPAVE™. However, the team does recommend further study to identify ways to design and/or produce asphalt mixtures from the same traffic category that will exhibit more consistent performance.

Also, it is noted that this project investigated only new construction sites and it is unknown at this time whether the layer coefficients recommended above are applicable to overlay conditions. The research team found no evidence in the literature as to whether layer coefficients used for new design are equally applicable to overlays and the sites studied in this project did not permit the team to answer this question. Thus, the research team recommends that the NCDOT consider evaluating the efficacy of layer coefficients calibrated here for overlay pavements.

The project also identified some potential issues with respect to the NCDOT truck factors. The origin of the current truck factors used by the NCDOT could not be identified, but analysis in this project suggests that the DOTs current truck factors are different than adjacent states (systematically lower). Thus, it is recommended that the NCDOT conduct detailed analysis of their current WIM data to confirm that the truck factors it uses still represents the expected truck loading. The research team was unable to do such calibration given the information provided in the WIM data; however, such analysis is feasible. It may also be possible for the NCDOT to better leverage the traffic clustering analysis performed in FHWA/NC 2008-11 for the purpose of estimating truck loadings.

The above conclusions and recommendations rely on a two-step conversion process to relate measured *PCR* to *PSI*. This conversion carries an inherent uncertainty that limits the ability of this project and potentially other projects to reliably calibrate design equations for North Carolina. Thus, the research team recommends that the NCDOT allocate resources to either monitor a subset of pavements over several years in order to better facilitate calibration efforts or consider developing pavement design methods that are amenable to the current data collection efforts, i.e., compatible with *PCR*.

6. IMPLEMENTATION AND TECHNOLOGY TRANSFER PLAN

The Materials and Test Unit of the NCDOT are the primary users of this product. The layer coefficients provided in this report can be integrated into the pavement design guide to better reflect the long-term performance of NCDOT pavements. In addition, the long-term performance monitoring plan can be used to develop a formal program of detailed performance monitoring and continual design guide improvement. While the research team recommends reducing layer coefficients for lower volume roadways to better reflect the estimated performance, the data provided clearly shows that the layer coefficients should not be increased. Thus, the research findings can be used also as justification for not increasing the layer coefficients for pavement design.

For follow-up activities the research team believes that the NCDOT could consider the following activities:

- allocating resources to implement the long-term performance monitoring plan (or a variation thereof) in order to collect data for future calibration efforts (either of the AASHTO design equation or of AASHTO Pavement ME),
- allocating resources to investigate ways to create better consistency in the properties of asphalt mixtures designed for the same traffic levels,
- allocating resources to monitor roadway performance in ways that better align with *PSI* or develop design methodologies that are amenable to the currently collected *PCR* values.

This page is intentionally blank

7. REFERENCES

Al-Omari, B., and Darter, M. Relationships Between International Roughness Index and Present Serviceability Rating. *Transportation Research Record: Journal of the Transportation Research Board*, No. 1435, Washington, D.C., 1994, pp.130–136.

Al-Suleiman, T.I. and Shiyab, A.M. Prediction of pavement remaining service life using roughness data – case study in Dubai *International Journal of Pavement Engineering*, Vol. 4, No.2, 2003, pp. 121-129.

Arizona DOT (ADOT). *Pavement Design Manual*. Arizona DOT, Phoenix, AZ, 2017.

ASTM E1489-08 (Reapproved). *Standard Practice for Computing Ride Number of Roads from Longitudinal Profile Measurements Made by an Inertial Profile Measuring Device*, 2013.

Aultman-Hall, L., Jackson, E., Dougan, C. E., and Choi, S. Models Relating Pavement Quality Measures. *Transportation Research Record: Journal of Transportation Research Board*, No.1869, Washington, D.C., 2004, pp. 119–125.

Carey, W. N., and Irick, P. E. The pavement serviceability performance concept. *Highway Research Board Bulletin*, No.250, 1960, pp. 40–58.

Chandra, S., Sekhar, C. R., Bharti, A. K., and Kangadurai, B. Relationship Between Pavement Roughness and Distress Parameters for Indian Highways. *Journal of Transportation Engineering*, Vol. 139, No. 5, 2013, pp. 467–475.

Colorado DOT (CODOT). *Pavement Design Manual*. Colorado DOT, Denver, CO, 2008.

Connecticut DOT (CTDOT). Pavement Design Guidance. https://portal.ct.gov/DOT/Engineering/Pavement-Design/Design-Guidance. Accessed at Oct 11, 2021.

Dave, E., Sias, J. E., and Nemati, R. *Layer Coefficients for New Hampshire Department of Transportation Pavement Design*. FHWA Final Report No. FHWA-NH-RD-26962N, Federal Highway Administration, Washington, D.C., 2019.

Davis, K. and Timm, D.H. *Recalibration of the Asphalt Layer Coefficient*. National Center for Asphalt Technology (NCAT), Report No. 09-03, Auburn AL, 2009.

Dewan, S.A., and Smith, R.E. Estimating International Roughness Index from Pavement Distresses to Calculate Vehicle Operating Costs for the San Francisco Bay Area. *Transportation Research Record, Journal of Transportation Research Board*, No.1816, Washington, D.C., 2002, pp. 65–72.

Florida DOT (FDOT). *Flexible Pavement Design Manual*. Florida DOT, Tallahassee, FL, 2018.

Georgia DOT (GDOT). *Pavement Design Manual*. Georgia DOT, Atlanta, GA, 2005.

Ghanbari, A., Underwood, B.S., and Kim, Y.R.. Development of a Rutting Index Parameter Based on the Stress Sweep Rutting Test and Permanent Deformation Shift Model. *International Journal of Pavement Engineering*, 2020, pp. 1-13.

Gillespie, T.D., Sayers, M.W., and Segel, L. *Calibration of Response-Type Road Roughness Measuring Systems.* NCHRP Report No. 228, Washington, D.C., 1980.

Gulen, S., Woods, R., Weaver, J., and Anderson, V. L. Correlation of present serviceability ratings with international roughness index. *Transportation Research Record*, No. 1435, Washington, D.C., 1994, pp. 27-37.

Hall, K. T., and Muñoz, C.E.C. Estimation of Present Serviceability Index from International Roughness Index. *Transportation Research Record: Journal of the Transportation Research Board*, No. 1655, Washington, D.C., 1999, pp. 93–99.

Highway Research Board (HRB) *The AASHO Road Test*. Special Reports 61E. Highway

Research Board, Washington, D.C., 1962.
Illinois DOT (IDOT). *The Bureau of Design and Environmental Manual*. Chapter 42. Illinois DOT, Springfield, IL, 2013.
Kim, Y.R., Castorena, C., Wang, Y., Ghanbari, A., and Jeong, J. *Comparing Performance of Full-depth Asphalt Pavements and Aggregate Base Pavements in NC.* FHWA/NC Report No. HWY-2015-02, North Carolina DOT (NCDOT), 2018.
Lin, J., Yau, J., and Hsiao, L. Correlation Analysis Between International Roughness Index (*IRI*) and Pavement Distress by Neural Network. *82nd Annual Meeting (CD-ROM), Transportation Research Record,*Washington, D.C., 2003.
Loprencipe, G. and Zoccali, P. Ride Quality Due to Road Surface Irregularities: Comparison of Different Methods Applied on a Set of Real Road Profiles. *Coatings*, Vol. 7, No. 5, 2017.
Mactutis, J.A., Alavi, S.H., and Ott, W.C. Investigation of Relationship Between Roughness and Pavement Surface Distress Based on WesTrack Project. *Transportation Research Record: Journal of Transportation Research Board*, No. 1699, Washington, D.C., 2000, pp. 107–113.
Miller, J.S., and Bellinger, W.Y. *Distress Identification Manual for the Long-Term Pavement Performance Program*. Report No. FHWA-RD-03-031, Federal Highway Administration, McLean, VA, 2003.
Minnesota DOT (MNDOT). State Aid for Local Transportation. https://www.dot.state.mn.us/stateaid/esal.html. Accessed at Oct 11, 2021.
Janoff, M.S., Nick, J.B., Davit, P.S., and Hayhoe, G.F. *Pavement Roughness and Rideability*. NCHRP Report No. 275, Washington, D.C., 1985.
Janoff, M.S. *Pavement Roughness and Rideability Field Evaluation*. NCHRP Report No. 308, Washington, D.C., 1988.
New York DOT (NYDOT). *Comprehensive Pavement Design Manual*, Chapter 4 – New Construction/Reconstruction. New York DOT, Albany, NY, 2002.
Ohio DOT (ODOT). *Pavement Design Manual*. Ohio DOT, Columbus, OH, 2015.
Paterson, W.D.O. Road Deterioration and Maintenance Effects : Models for Planning and Management. The Highway Design and Maintenance Standards Model (HDM-III), Vol. III, World Bank, Washington, D.C., 1987.
Pennsylvania DOT (PennDOT). *Publication 242 Pavement Policy Manual*. Pennsylvania DOT, Harrisburg, PA, 2015.
Sayers, M.W., Gilespie, T.D., and Paterson, W.D.O. *Guidelines for Conducting and Calibrating Road Roughness Measurements.* World Bank Technical Paper 46, International Bank for Reconstruction, Washington, D.C., 1986.
Sayers, M.W. and Karamihas, S.M. *The Little Book of Profiling: Basic Information about Measuring and Interpreting Road Profiles*. University of Michigan, Ann Arbor MI, 1998.
Sayyady, F., Stone, J. R., List, G. F., Fadi, M. J., Kim, Y. R., and Sajjadi, S. Axle Load Distribution for Mechanistic–Empirical Pavement Design in North Carolina Multidimensional Clustering Approach and Decision Tree Development, *Transportation Research Record: Journal of the Transportation Research Board*, No. 2256, Washington, D.C., 2011, pp. 159–168.
South Carolina DOT (SCDOT). *Pavement Design Guidelines*. South Carolina DOT, Columbia, SC, 2008.
Stone, J.R., Kim, Y.R., List, G.F., Rasdorf, W., Sayyady, F., Jadoun, F.M., and Ramachandran, A.N. *Development of Traffic Data Input Resources for the Mechanistic Empirical-Pavement Design Process*. Final Report No. HWY-2008-11, North CarolinaDOT (NCDOT), 2010.

Timm, D.H., Robbins, M.M., Tran, N., and Rodezno, C. *Recalibration Procedures for the Structural Asphalt Layer Coefficient in the 1993 AASHTO Pavement Design Guide*. National Center for Asphalt Technology (NCAT), Report No. 14-08, Auburn, AL, 2014.

Underwood, B.S. and Kim, Y.R. Comprehensive Evaluation of Small Strain Viscoelastic Behavior of Asphalt Concrete. *ASTM Journal of Testing and Evaluation*, Vol. 40, No. 4, 2012, pp. 99-110.

U.S. Army Corps of Engineers (USACE). *Pavement Maintenance Manual*,Washington, D.C., 1982.

Van Til, C.J., McCullough, B.F., Vallerga, B.A., and Hicks R.G. *Evaluation of the AASHO Interim Guides for Design of Pavement Structures*. NCHRP No. 128, Washington, D.C., 1972.

Virgina DOT (VDOT). *Manual of Instructions*, Section 604 – Guidelines for Use of the 1993 AASHTO Pavement Design Procedure. Virgina DOT, Richmond, VA, 2018.

Wang, Y.D., Underwood, B.S., and Kim, Y.R.. Development of a Fatigue Index Parameter, S_{app}, for Asphalt Mixes Using Viscoelastic Continuum Damage Theory. *International Journal of Pavement Engineering*, 2020, pp. 1-15.

Wang, Y.D., Ghanbari, A., Underwood, B.S., and Kim, Y.R. Development of Preliminary Transfer Functions for Performance Predictions in the FlexPAVE^{TM} Program, *Construction and Building Materials*, Vol. 266 (Part B), 2021.

Zamora A.E.J. *A Discrete Roughness Index for Longitudinal Road Profiles*. Ph.D. Dissertation, Virginia Polytechnic Institute and State University, Blacksburg VA, 2016.

Zapata, C.E. *A National Catalog of Subgrade Soil Water Characteristic Curve (SWCC) Default Input and Selected Soil Properties for Use with the MEPDG*. NCHRP Report No. 9-23A, Washington, D.C., 2010.

This page is intentionally blank

APPENDIX A: DETAILED LITERATURE REVIEW

Introduction

The North Carolina Department of Transportation (NCDOT) uses the *AASHTO Guide for Design of Pavement Structures 1993* to determine the minimum pavement stiffness that ensures pavement longevity. During design, this stiffness is first determined using an iterative design process, charts, or software. Then, the engineer selects materials and layer thicknesses that provide the required stiffness by summing the contributions of individual layers. The contribution from any given layer is calculated by the product of that layer's thickness and a structural layer coefficient that captures the overall quality and structural benefit of the material. In the NCDOT procedure, the structural layer coefficient for asphalt concrete (AC) is 0.44 (surface and intermediate mixtures) or 0.30 (base mixtures), while other material types are lower, e.g., the structural layer coefficient for unbound aggregate base materials is 0.14.

The current study will undertake calibration of these layer coefficients to better reflect modern paving materials using three steps; a) a relationship between the AASHTO present serviceability index (*PSI*) and the NCDOT pavement condition rating will be established, b) the *PSI* will be calculated for each section in the pavement performance database, and c) the structural layer coefficients for different layers will be calibrated by adjusting the values until the measured and predicted performance curves match. The study will then evaluate the efficacy of adopting updated coefficients. In order to carry out this investigation, a review of some important topics is necessary. This review is divided into five sections; section 1 (this section) provides an overview of the research plan and description of the literature review organization, section 2 reviews the most recent and relevant studies regarding pavement indices to develop a framework for further analysis, section 3 describes the origin of the current layer coefficients and summarizes studies that have attempted to modify the layer coefficients, section 4 describes the calibration of truck factor and its relationship to layer coefficients since this factor has a direct effect on calibrating layer coefficients, and section 5 reviews the primary techniques and variables to conduct a life cycle cost analysis.

Pavement Condition Index

The introduction of the formal concept of pavement performance and pavement serviceability was presented by (Carey and Irick 1960), with the parameter denominated as Present Serviceability Rating – *PSR*. The *PSR* is the numerical average rating determined by a panel of individuals who traverse a pavement in question and independently rate it over a scale of 0 (the poor condition) and 5 (excellent condition). At the AASHO road test, the *PSR* was correlated to objective measurements made on the pavement surface, which included a measure of roughness, extent of cracking and patching, and for flexible pavement the average rut depth in the wheel track. The resultant correlated parameter was termed the Present Serviceability Index (*PSI*) and is shown in Equation (11).

$$PSI = 5.03 - 1.91 \times \log\left(1 + \overline{SV}\right) - 1.38 \times RD^2 - 0.01 \times \sqrt{C + P} \tag{11}$$

where;

SV = slope variance,
RD = rut depth in inches,
C = cracking area in $ft^2/1000\ ft^2$ and,
P = patching area in $ft^2/1000\ ft^2$.

Shortly, after the AASHO Road Test, two important events occurred in the United States in the area of pavement ride quality evaluation:

1. The introduction of the road meter, and
2. The introduction of the inertial profilometer.

In the early 1960s, two automotive vehicle-based road meters were introduced in the United States: 1) the Portland Cement Association (*PCA*) road meter (Brokaw 1967), and 2) the Mays road meter (*MRM*) (Walker and Hudson 1973). The operation of both road meters was based on the measurement and accumulation of the relative motion of the sprung and un-sprung masses of automotive vehicle suspension systems. The two road meters differed in how the measured displacement was weighted in the accumulation process. It was also during the 1960s that the inertial profilometer was developed by Spangler and Kelly (1966) at the General Motors research laboratory. These researchers, and others, also developed a series of indices that related the pavement profile with the pavement quality rating.

A recent example using profilometer measurements was research conducted to determine an objective means to correlate ride quality to the subjective opinions of highway users. It was found that some components of a road have a strong effect on user opinion, whereas others have a significantly lesser effect. Researchers studied these distresses and after a statistical analysis found that the pavement power spectral density (*PSD*) correlated at 90% with subjective opinions (Loprencipe and Zoccali 2017). On that basis, the profile was split into three wavelength bands: 0.6 to 1.5 m (2 to 5 ft), 1.5 to 7.6 m (5 to 25 ft), and 7.6 to 15.2 m (25 to 50 ft). Wavelengths shorter than 0.61 m (2 ft) mostly create tire noise and those longer than 15.2 m (50 ft) fail to disturb the vehicle suspension. They went on to propose a Ride Quality Index (*RQI*), which was calculated from these three *PSD* wavelength bands according to Equation (12):

$$RQI = 3.077 \ln\left(Var_1 \times 10^8\right) + 6.154 \ln\left(Var_2 \times 10^8\right) + 9.231 \ln\left(Var_3 \times 10^8\right) + 141.85 \quad (12)$$

where, Var_1, Var_2, and Var_3 are the variances for 7.6 to 15.2 m, 1.5 to 7.6 m, and 0.6 to 1.5 m wavelengths of the road profile, respectively. A *RQI* value from zero to 30 indicates excellent ride quality, *RQI* values from 31 to 54 indicate good ride quality, *RQI* values from 55 to 70 indicate fair ride quality, and *RQI* values of more than 70 indicate poor ride quality.

The National Cooperative Highway Research Program (NCHRP) sponsored two projects (NCHRP 1-23 and NCHRP 1-23(2)) that investigated the effect of surface roughness on ride comfort (Janoff et al. 1985, Janoff 1988). The objective of that research was to determine how features in road profiles were related with the subjective opinions of the public about the road, which were represented by the Mean Pavement Rating (*MPR*). NCHRP 1-23 developed the concept of Ride Number (*RN*), which is used to predict the *MPR* based on a *PSD* function of two longitudinal profiles (left and right). When derived, the *RN* seemed to have a great potential to grade pavement quality based on a set of pavement profiles; however, its mathematical procedure was never opened to the public and its use did spread as expected.

In 1995, the Federal Highway Administration (FHWA) developed a new portable profile analysis method that correlates *MPR* to the *RN*. The *RN* is an index that rates rideability of a road using a 0 to 5 scale, where a *RN* of 5.0 is a perfect ride quality road, and a *RN* of zero is an impassable road. The *RN* was chosen because it corresponds to users' perception of pavement roughness. The definition of this method is given in Section 4.3.2 of ASTM E1489-08 (ASTM, 2013). The Profile Index (*PI*) which is calculated using Equation (14), is derived from the longitudinal profile and

then processed through a non-linear mathematical transformation, Equation (13), to yield a *RN* value for each 0.1 mile or any other desired reporting interval.

$$RN = 5e^{-160PI} \tag{13}$$

$$PI = \sqrt{\frac{PI_L^2 + PI_R^2}{2}} \tag{14}$$

where, PI_L and PI_R are the profile index in the left and right wheel-path, respectively, in ft/ft. Due to its non-linear relationship, the *RN* for adjacent sections cannot be averaged in the same way as other ride profile indices (e.g., the International Roughness Index). For example, if one mile has a *RN* of 3 and the next has a *RN* of 4, the *RN* of the two-mile segment is not 3.5 (is about 3.37) (Sayers and Karamihas, 1998).

Another means of pavement condition rating is the U.S. Army Corps of Engineers' Pavement Condition Index (*PCI*) (USACE 1982). The *PCI* value is decreased by a cumulative deduct value score based upon the type, quantity, and severity level of distress and type of pavement. For calculating the *PCI,* the pavement condition is related to several factors, including structural integrity, structural capacity, roughness, skid resistance/hydroplaning potential, and rate of deterioration. These relationships are established based on USACE expert opinion. The PCI is a numerical indicator that varies from 0 (Failed) to 100 (Excellent).

IRI correlations

The study of the *RN* was followed by the development of the International Roughness Index (*IRI*), which is a computer-based virtual response system. The *IRI* was initially proposed by the World Bank in 1986 based on the results of a large research project conducted in Brazil from 1976 to 1981 to assess the perception of users on the condition of pavement surfaces, and right now constitute the roughness index most commonly used to characterize longitudinal road profiles. By definition, the *IRI* is a "scale for roughness based on the simulated response of a generic motor vehicle to the roughness in a single wheel path of the road surface" (MnDOT 2007). To calculate *IRI*, the road elevation profile is first filtered using the 250 mm (10 in.) moving average filter and then the Golden Quarter Car model is used to simulate the vehicle suspension response to the pavement surface at a reference vehicle speed of 80 km/h (50 mph). Figure A.1 shows the schematics of the quarter car model. By applying Newton's 2nd law of motion, the damped mass-spring model can be written as shown in Equation (15) and Equation (16).

$$m_s \ddot{z}_s + c_s\left(\dot{z}_s - \dot{z}_u\right) + k_s\left(z_s - z_u\right) = 0 \tag{15}$$

$$m_u \ddot{z}_u + c_s\left(\dot{z}_u - \dot{z}_s\right) + k_s\left(z_u - z_s\right) + k_t\left(z_u - Y\right) = 0 \tag{16}$$

where;

$m_s\ddot{z}_s$ = force acting on the sprung mass m_s,
$\ddot{z}_s$ = vertical acceleration of the sprung mass,
c_s = damping coefficient,
$\dot{z}_s$ = vertical motion of the sprung mass,
$\dot{z}_u$ = vertical motion of the un-sprung mass,
k_s = stiffness constant,
z_s = vertical displacement of the sprung mass,
z_u = vertical displacement of the un-sprung mass,

k_t = stiffness of the tire, and
Y = profile input.

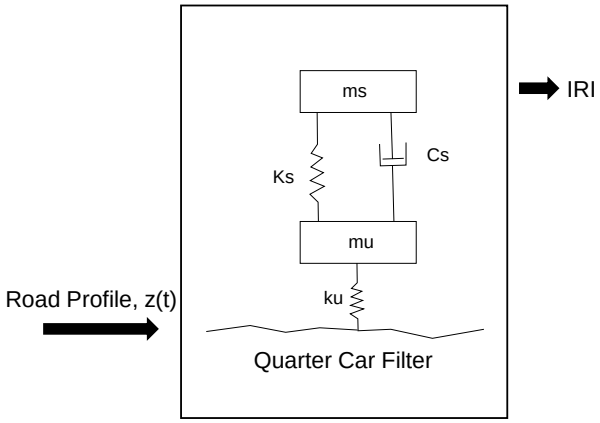

Figure A.1. *IRI* vehicle response model.

The parameters used to calculate *IRI* are known as the golden car parameters, which are summarized in Table A.1. These parameters are the suspension system constants that represents a typical passenger car from the 1980's when the *IRI* model was developed. Usually, the parameters are presented in *IRI* literature normalized to the sprung mass for applicability purposes to a wider range of vehicles (Zamora 2016). From the vehicle suspension response system and using the golden car parameters, *IRI* is calculated by taking the accumulated suspension travel over a distance traveled by a vehicle at a speed of 80 km/h (50 mph), Equation (17). Figure A.2 presents the typical values of this parameter according to the road type.

Table A.1. Golden Car Parameters for *IRI* Determination.

Parameter	Value
k_s/m_s (s^{-2})	63.3
k_u/m_s (s^{-2})	653
c_s/m_s (s^{-1})	6.0
m_u/m_s	0.15

$$IRI = \frac{1}{L}\int_{t_0}^{t_f} \left| \dot{z}_s(t) - \dot{z}_u(t) \right| dt \tag{17}$$

where;
L = longitudinal distance along the profile,
t_0 = the initial time traveled at a constant speed of 80 km/h (50 mph),
t_f = the final time traveled at a constant speed of 80 km/h (50 mph),
$\dot{z}_s$ = sprung vertical motion, and
$\dot{z}_u$ = unsprung vertical motion.

Most of the research underlaying the development of the *IRI* was articulated in NCHRP 1-18 (Gillespie et al. 1980). One of the advantages of the *IRI* is the fact that the values are directly proportional to the roughness, i.e., any percentual change in the profile elevation represent the same percentual change in the *IRI* value. Theoretically the *IRI* can take any value greater than or equal to zero (0 represents a perfectly flat profile); however, values above 8 m/km (approximately 507 in/mi) are associated with nearly impassable roads.

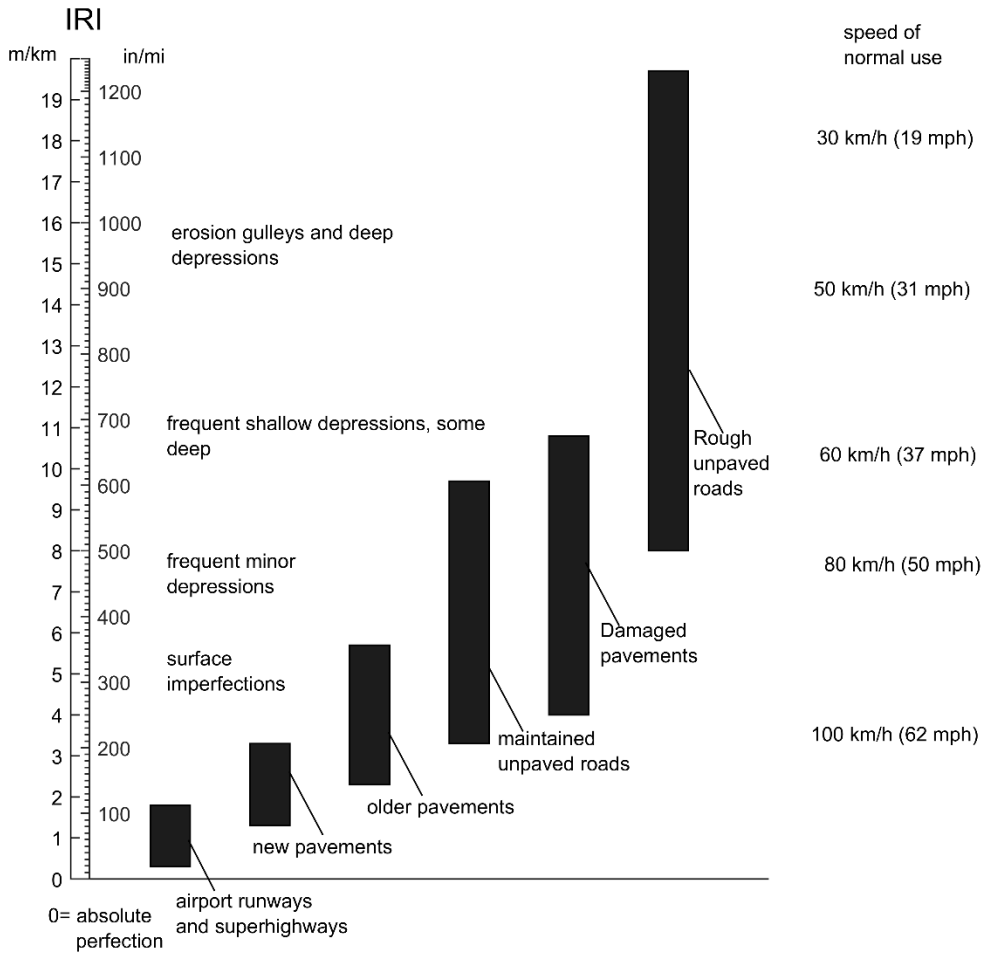

Figure A.2. *IRI* value ranges for each road type (After: Sayers et al. 1986).

The *IRI* is influenced by wavelengths (λ) ranging from 1.2 to 30 meters, the profile is filtered (with a moving average filter of 250 mm (9.85 mm) base length) and has maximum sensitivity to slope sinusoids with wave numbers of near 0.065 cycle/m (λ = 15 m) and 0.42 cycle/m (λ = 2.4 m). However, there is still some response for wavelengths outside this range (Sayers and Karamihas 1998).

Due to its widely use and practical methods for its measure, the *IRI* has been correlated with several indices. The first attempt was conducted by Paterson (1987) who proposed a non-linear relationship that generally fit data sets taken from Brazil, Texas, South Africa, and Pennsylvania. His functions are shown in Equation (18) (for *IRI* in m/km) and Equation (19) (for *IRI* in in./mi).

$$PSR = 5e^{-0.18IRI} \tag{18}$$

$$PSR = 5e^{-0.00286IRI} \tag{19}$$

Later, Al-Omari and Darter (1994) used data from Louisiana, Michigan, New Jersey, New Mexico, Indiana, and Ohio. The relationships between *IRI* and *PSI* ratings were analyzed. Their proposed functions are shown in Equation (20) (for *IRI* in m/km) and Equation (21) (for *IRI* in in./mi).

$$PSR = 5e^{-0.260RI} \tag{20}$$

$$PSR = 5e^{-0.0041IRI} \tag{21}$$

In the same year Gulen et al. (1994) proposed a correction to the Al-Omari and Darter functions, because they claimed that the predictions were not statistically correct due to the fact the relationship obtained were forced to pass through *PSI* = 5 when *IRI* is zero. The relation obtained by Gulen et al. (1994) is presented in Equation (22) (for *IRI* in m/km) and Equation (23) (for *IRI* in in./mi). Figure A.3 shows a plot of these three models and that visible differences in the relationship exist.

$$PSR = 9e^{-0.557\,IRI} \tag{22}$$

$$PSR = 9e^{-0.008784IRI} \tag{23}$$

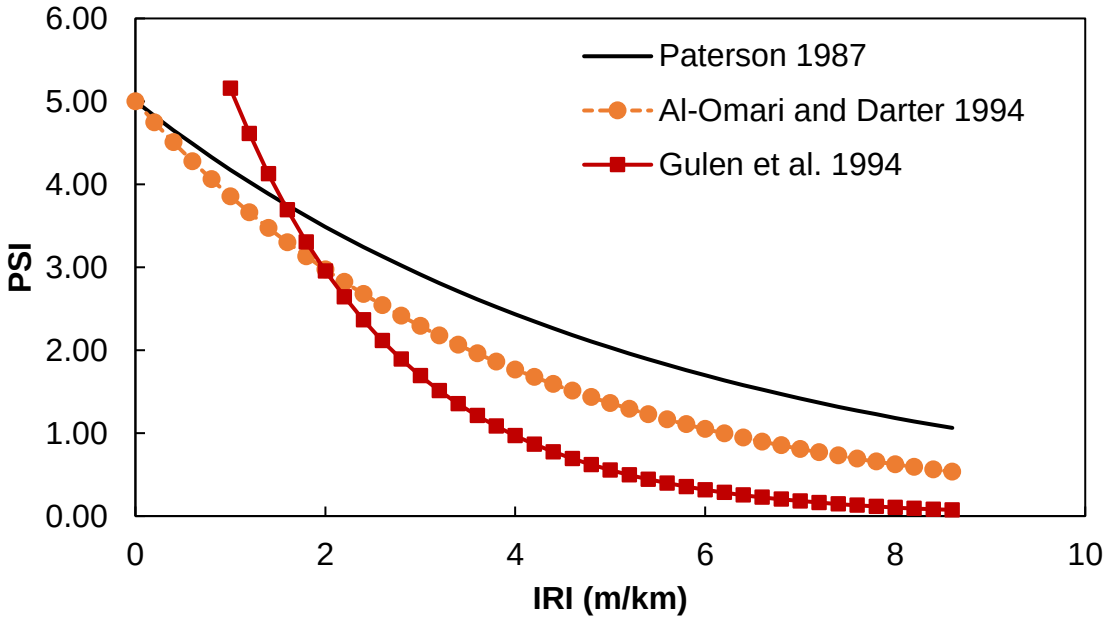

Figure A.3. Comparison of the *PSI* Models as Function of the *IRI*.

In the same line, Hall and Munoz (1999) proposed a relation between the Slope Variance (*SV*) and the *IRI*, mainly because the *SV* is an input for the calculation of the *PSI*, see Equation (11). The equation obtained is presented in Equation (24).

$$SV = 2.2704IRI^2 \tag{24}$$

The Minnesota Department of Transportation (*MnDOT*) also developed an index called the Minnesota Ride Quality Index (RQI_{Mn}) based on a correlation with the *IRI* values calculated for 120 test sections. Two different correlations were found, Equation (25) for asphalt pavement and Equation (26) for concrete pavements. In both Equations the *IRI* is in m/km. As for the *RN* the RQI_{Mn} varies from 0 (very poor) to 5 (very good). The *RQI* may be taken as a surrogate of the *PSI*, because both are calculated based on a rating panel with each rater assign a numerical value between zero and five based on their impression of the ride quality. The *RQI* categories used for these ratings are shown in Table A.2.

Table A.2. RQI Categories and Ranges.

Numerical Rating	Verbal Rating
4.1 – 5.0	Very Good
3.1 – 4.0	Good
2.1 – 3.0	Fair
1.1 – 2.0	Poor
0.0 – 1.0	Very Poor

$$RQI_{Mn,Flexible} = 5.697 - 2.104 \times \sqrt{IRI} \tag{25}$$

$$RQI_{Mn,Rigid} = 6.634 - 2.813 \times \sqrt{IRI} \tag{26}$$

Different attempts have been made in order to correlate the *IRI* with the different pavement distress that agencies collect for their Pavement Management System (*PMS*) database. For example, Al-Omari and Darter (1995) found no significant correlation between the *IRI* and either the average rut depth (*RD*) or the *RD* standard deviation when individual pavement sections were considered. However, when the data were grouped for ranges of *IRI* and the *RD* mean and standard deviation values were averaged over these ranges, it was found that the midpoint of *IRI* for these ranges correlates well with both mean *RD* and *RD* standard deviation (*SD*) as shown in Equation (27) and Equation (28).

$$IRI = 57.56RD - 334.28 \tag{27}$$

$$IRI = 136SD - 116.36 \tag{28}$$

where *IRI* is in cm/km, *RD* and *SD* are in mm.

A correlation between *IRI* and pavement distresses was also developed using the WestTrack data, which was a full-scale flexible pavement accelerated loading test where were measure pavement distresses under the repetition of nearly five million equivalent single axial loads. The model developed correlates *IRI* with initial *IRI* values, fatigue cracking, and rut depth according to Equation (29) (Mactutis et al. 2000):

$$IRI = 0.597(Initial\ IRI) + 0.0094(Fatigue\ \%) + 0.00847(Rut\ Depth) + 0.382 \tag{29}$$

Another important contribution was made by Dewan and Smith (2002) who developed a correlation between *IRI* and pavement distresses for the San Francisco Bay Area. They derived the following correlation between *IRI* (in m/km) and *PCI* (Dewan and Smith 2002):

$$IRI = 0.0171(153 - PCI),\ R^2 = 0.52 \tag{30}$$

Similarly, using neural network techniques, Lin et al. (2003) investigated the ability to predict accurately the *IRI* from the distress ratings obtained from an automatic road analyzer (*ARAN*) video-log vehicle. Data were collected from 125, 1-km long segments of provincial highways and country roads in Taiwan. Ten separate distress types (rutting, alligator cracking, cracking, digging and patching, potholes, corrugations, manholes, stripping, patching, and bleeding) were identified and studied for correlations. The authors results suggest that severe potholes, digging and patching, and rutting have the largest impact on *IRI*.

Chandra et al. (2013) also developed a correlation between pavement roughness and distress parameters like potholes, raveling, rut depth, cracked areas, and patch work. The pavement distress

data collected on four national highways in India using a network survey vehicle (*NSV*) were used to develop linear, see Equation (31), and nonlinear regression models, see Equation (32), between roughness and distress parameters. Analysis of variance of these models indicated that nonlinear relation is better than a linear model (Chandra et al. 2013).

$$IRI = 2.198 + 0.418(RD) + 0.122(C) + 0.518(PH) + 0.002(P) + 0.002(R),\ R^2 = 0.77 \quad (31)$$

$$IRI = 2.01 + 0.442(RD)^{0.92} + 0.092(C)^{1.032} + 0.575(PH)^{0.168} + 0.046(P)^{0.539} + 0.174(R)^{0.13},\ R^2 = 0.80 \quad (32)$$

where;

IRI = *IRI* in m/km,
RD = Rut Depth in mm,
C = the area of total cracks in m^2 per 3750 m^2,
PH = the area of potholes in m^2 per 3750 m^2,
P = the area of path work in m^2 per 3750 m^2, and
R = the area of raveling in m^2 per 3750 m^2.

Current State of Practice

The current state of practice with respect to pavement condition indices is based on two needs; 1) the need to determine the pavement structural and functional conditions for rehabilitation/reconstruction planning of an individual roadway segment (i.e., project level) and 2) support pavement management decisions (i.e., network level). Data collection for network-level decision making is generally different from data collection for project-level decision making in purpose, methods, and the actual data collected. This means the quality, periodicity and quantity of the data collected will be different.

Network level

Owing to the large quantity of required data, collection methods at the network level typically involve windshield surveys or automated methods since these techniques can generally be performed at or near highway speeds without affecting traffic or posing a hazard to data collection teams. This information is normally used to obtain an overall index of the pavement condition that allows taking decisions and budget distribution. Flintsch and McGhee (2009) conducted an electronic survey of most states in US as well as different provincial agencies in Canada to gain insight into the practices and data collection from contractors and agency members. Figure A.4 presents the types of data that agencies collect to define the pavement condition at both the project and network levels. At the network level, it can be observed that the most common types of information include surface distresses and smoothness. To define pavement distresses and severities, most of the agencies use approaches like the one used in the Long-Term Pavement Performance (*LTPP*) Distress Identification Manual for the Long-Term Pavement Performance Program (Miller and Bellinger 2003). Smoothness data are typically reported using the International Roughness Index (*IRI*), expressed in in./mile or m/km.

Project level

At the project level, more specific data are typically collected in terms of individual distress identification and severity. Friction and structural capacity measurements are more prevalent at this level of data collection as more specific information is needed to determine specific preservation methods and budgeting requirements for individual pavement projects. At this level of analysis, data collection methods often include a higher prevalence of walking surveys, in

addition to the other methods used for collecting network-level data. Structural capacity evaluation is performed mostly at the project level to support the "design" of the maintenance or rehabilitation projects that have been recommended through network-level analysis.

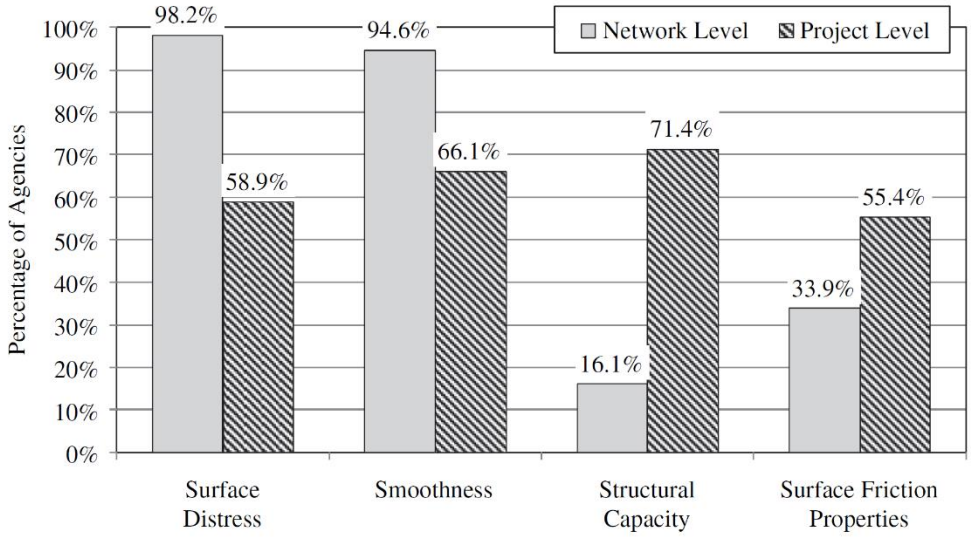

Figure A.4. Types of pavement condition data collected by agencies (Source: Flintsch and McGhee 2009).

As seen in Figure A.4 there are four types of pavement condition indicators normally used in the practice, these may be grouped as follows:

- Surface distress: Commonly represented by the measures of different distresses types or by the calculation of a single index as a function of the different pavement damages.
- Smoothness: Typically represented by the International Roughness Index (*IRI*).
- Structural capacity: Normally this is measured by a following weight deflectometer test and may be represented by an index that is a function of the different deflections. Also, it is possible to use the Structural Number (*SN*) as an indicator of the structural capacity.
- Surface friction properties: Transportation agencies monitor pavement friction because it affects wet-pavement friction and wet-pavement crashes; inadequate friction often leads to higher rates of crashes. Normally the pavement friction is expressed by the International Friction Index (*IFI*).

The above information may be complemented with the work of Robbins and Tran (2018), who performed a survey of different DOTs to determine the actual timing of a major rehabilitation of their interstates. From the responses, it can be inferred that each DOT utilizes a process that is unique to their state and dependent on several factors. Generally, DOTs indicated that their decision-making process consisted of reviewing pavement condition data from annual surveys. In many cases, the process also incorporated other factors such as funding and/or functional classification of the roadways. The following table summarizes the findings of Robbins and Tran in terms of the different performance measures considered for each DOT for actual service life or rehabilitation triggers.

As can be seen from Table A.3, most agencies measure the *IRI* for roughness and ride quality, rutting and cracking as the main type of distresses, and sometimes complement these values with measurements of surface defects like raveling and bleeding. Figure A.5 compliments this analysis and summarizes the different distresses typically measured by the agencies to describe pavement condition.

Table A.3. Indices Used by the Different Agencies to Trigger a Rehabilitation Action.

State	Survey/Score	Function of
AK	PSR	Rut depth and *IRI*
AL	*PCR*	Composite index based on semi-automated distress survey
AR	PCI	*IRI*, rutting and cracking
CT	ECI	Transverse and non-wheelpath cracking
	RI	*IRI* transformed to 0-10 scale
	SCI	Wheelpath and some non-wheelpath longitudinal cracking
FL	Distresses	Rutting and Cracking
	IRI	*IRI*
IA	PCI	Pavement type, individual distress type
KS	PL	Multiple factors including *IRI*, transverse cracking, and rutting.
MI	DI	Surface distress (current and projected) and project history
	RSL	Estimated number of years until DI = 50
MT	Ride	*IRI*
	Rut	Rutting
	ACI & MCI	Alligator cracking & Transverse/longitudinal cracking
NC	*PCR*	Function of cracking, rutting, ride, raveling and bleeding
NJ	SDI	Severity of extent of distress
NV	PRI	*IRI*, friction, rutting, cracking, patching, flushing, raveling
OR	PCI	Includes cracking, rutting, roughness, and friction
UT	Ride & RUT	*IRI* & Rutting
	Joint	Joint index from spalling and asphalt patching
	ECI	Environmental cracking (transverse, longitudinal, block cracking)
	WPCK	Wheel-path cracking (cracking due to fatigue)
WA	PSC	Cracking
	PRC	Rutting
	PPC	*IRI*
WV	CCI	Minimum of *PSI*, *SCI*, *ECI* and *RDI*
	PSI	*IRI*
	RDI	Rutting
	SCI	Fatigue cracking and longitudinal cracking
	ECI	Transverse cracking and block cracking
	NCI	Index is a function of a combined *ECI* and *SCI*

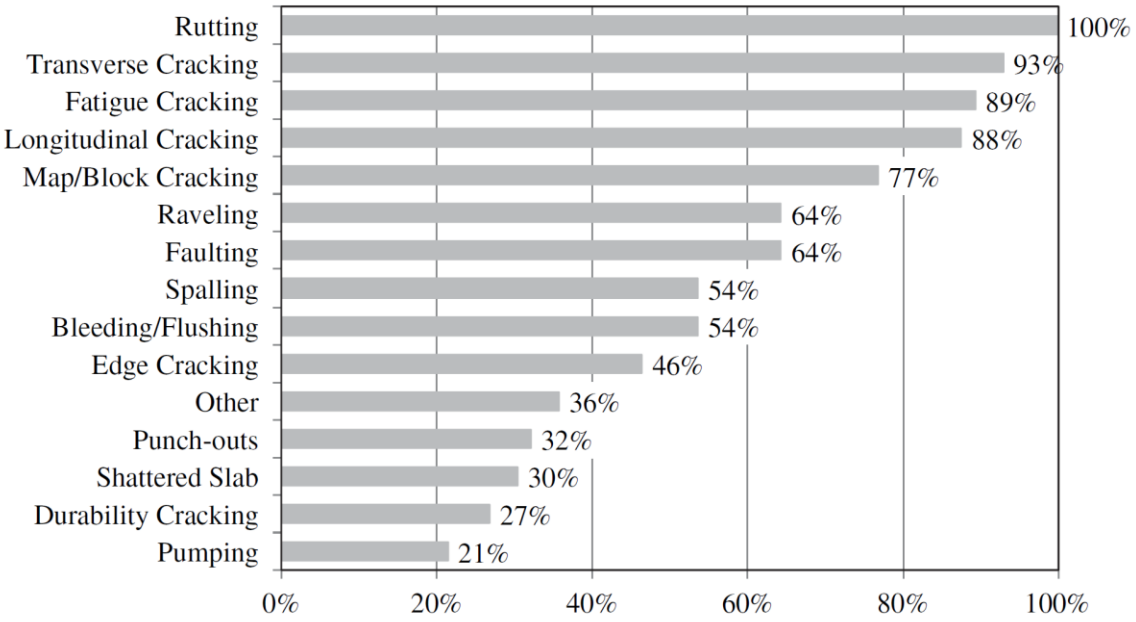

Figure A.5. Type of distresses normally collected by agencies (Source: Flintsch and McGhee 2009).

Dual Pavement Condition Rating

Most of the current systems for rating pavement condition are primarily based on the pavement ride quality, distresses, or both. The problem with this approach is that the system does not account for the pavement deterioration rates into the derivation. Musunuru et al. (2015) proposed a dual system for rating pavement condition based on functional and structural characteristics and rates of deterioration. The new rate system contemplates two different criteria: Functional and Structural.

- Functional: Depends on the ride quality, expressed in terms of the *IRI*, and safety which is expressed in terms of the skid resistance and rutting.
- Structural: Is based on cracking (transversal, longitudinal, alligator cracks, cracks on the edge and block cracking), faulting, and rutting.

Correspondingly, for a given pavement section, two quantities are defined; the Remaining Functional Period (*RFP*) and the Remaining Structural Period (*RSP*). The *RFP* and the *RSP* are defined as the period when a pavement reaches the minimum performance index threshold. This means that, for a given pavement section or network, one will have an *RFP* for the *IRI* (and possibly the Skid Number) and another for the rutting or cracking. The representative functional period is the minimum of these individual remaining periods. The above definition indicates that the *RFP* and the *RSP* are not combined indices. Each condition and distress type are analyzed separately, and the results are retained for further analyses. Additionally, neither the *RFP* nor *RSP* indicates the treatment type to be applied to a pavement section. Rather, they are flagging mechanism for identifying pavement sections that are in need for further attention. In summary, the dual-condition rating systems are designed to be adaptable to the needs and constrain of users. This rating system is based on the following information:

- Time-dependent pavement condition and distress data, and

- Threshold values

In their study, (Musunuru et al. 2015) consider that the mathematical relationships for modeling pavement distress and condition data as function of time are the following: exponential function for the *IRI*, Equation (33); power functions for rut depth, Equation (34); and logistic (S-shaped) function for cracking, not shown in the literature.

$$IRI = \alpha e^{\beta t} \tag{33}$$

$$RD = \alpha \times t^{\beta} \tag{34}$$

Where α and β are parameters to be determined, and t represents the time.

Summary and Conclusions

One of the objectives of the present research is create a relationship between the *PSI* and the *NCDOT* pavement condition rating (*PCR*). In order to do this task, it is necessary to structure a database at a network level with the information of the pavement distresses, the ride quality (*IRI*), and the *PCR* value. It is important to note that the database must include the historical information of all these parameters, in order to capture the deterioration pattern of the different distresses and pavement indices.

First, in those sections where is available both the *PSI* and the *PCR* the correlation of these indices can be established directly, however, in those sections where the *PSI* is not available the research team will proceed using one of these procedures:

i. Using Equation (11) in conjunction with the Equation (24) one can obtain the *PSI*, or,
ii. Based on Equation (11) and Equation (24) is possible to generate an expression similar to Equation (18) through Equation (22), which relates the *IRI* with the *PSI*, and,
iii. In the case that the *IRI* is not available, is necessary to develop a relationship between the *IRI* and the different distresses. This relationship will have a structure like the ones presented in Equation (27) through Equation (32).

The procedure presented above is important because is the foundation for the calibration of the layer coefficients.

Calibration of layer coefficient

Origin of Layer Coefficients

The primary objective of American Association of State Highway Officials (*AASHO*) Road Test was to determine the effect of different axle loading on the performance of the pavement during the pavement service life (HRB 1962). During the analysis of the test data, an empirical model was developed based on serviceability trends for various axle loads (Figure A.6) was develop and fit to the data. In this model, experimental and analytical procedures were used to estimate constants and variables in the model. Also, the precision associated with the estimations were investigated. If the pavement design and axle load are specified, this model can be used to predict the number of applications that a pavement section will experience before reaching a certain serviceability level, but fundamentally the relationship developed from the test road was that between serviceability, axle loads, and pavement structure.

The model was first developed based on the assumption that serviceability loss behaves as a power function with respect to axle load applications,

$$c_0 - p = KW^{\beta}, \tag{35}$$

where β is a positive power and K and/or β may depend on load and design variables. If ρ is the value of W in Equation (35) when $p = c_1$, Equation (35) may be written as:

$$c_0 - p \;=\; (c_0 - c_1)\left(\frac{W}{\rho}\right)^{\beta}. \tag{36}$$

Then, if logarithmic transformation is applied to both sides,

$$\log\left(\frac{c_0 - p}{c_0 - c_1}\right) = \beta\left(\log W - \log \rho\right), \tag{37}$$

and the left side is defined as the variable G it can be computed using,

$$G = \beta\left(\log W - \log \rho\right). \tag{38}$$

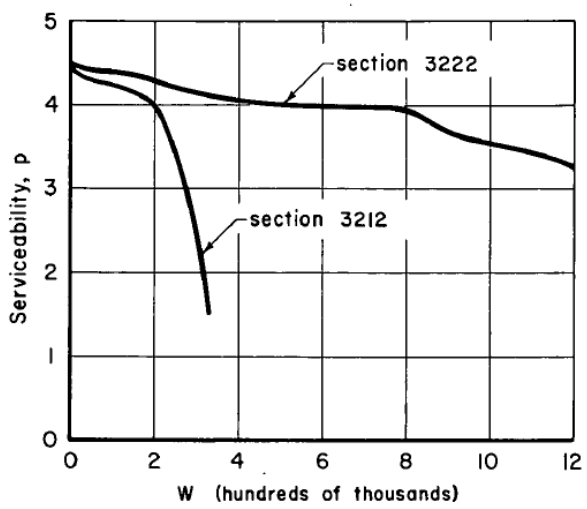

Figure A.6. Performance curves for two illustrative sections (Source: HRB 1962).

The significance of Equation (38) is that it produces a linear relationship between axle loads and a serviceability function. When these are plotted in logarithmic domain Equation (38) suggests that the function has a slope of β and an intercept of log ρ. During the test road experiment researchers tracked axle load applications and serviceability and then during analysis extracted the values for G and log W and fitted lines between them. Figure A.7 shows a conceptual mapping of these variables and Figure A.8 shows transformed data and fitted lines for four actual test road sections. In this figure, the lines were fitted by minimizing the sum of squared vertical deviations from the data for each section, and the slope of line was considered $\hat{\beta}$ (estimation for β). The $\hat{\beta}$-values were determined for each section, and they were graphed against pavement design and load variables. An analysis of variance was used to find that the $\hat{\beta}$-value was statistically dependent on design and load variable. Based on the analysis, β is related to design and load variables.

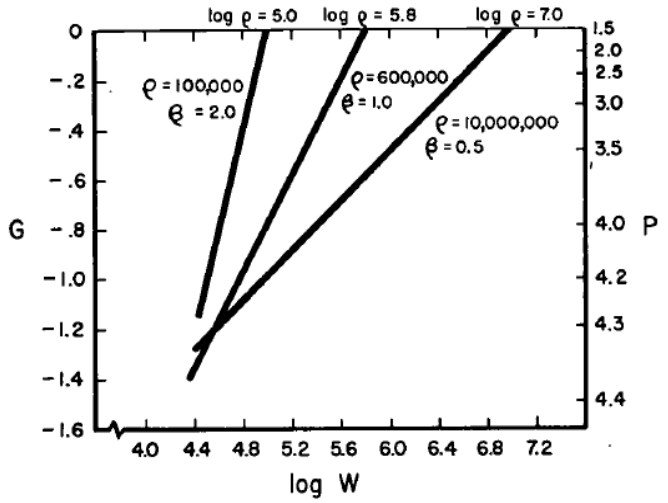

Figure A.7. Conceptual graphs of *G* (Source: HRB 1962).

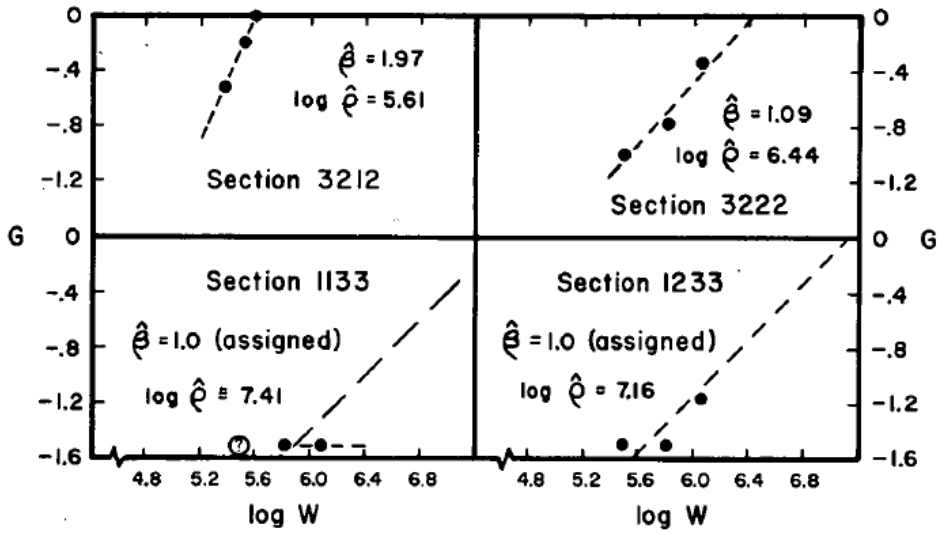

Figure A.8. Illustrative estimates for β and log ρ from section data (Source: HRB 1962).

Furthermore, since β was related to design and load variables, a model was developed based on these parameters, Equation (39).

$$\beta = \beta_0 + \frac{B_0 (L_1 + L_2)^{B_2}}{(a_1 D_1 + a_2 D_2 + a_3)^{B_1} \; L_2^{B_3}} \tag{39}$$

where

β_0 = minimum value for β,
L_1 = nominal load axle weight, in kips,
L_2 = 1 for single axle vehicles, 2 for tandem axle vehicles,
D_1 = the first pavement design factor, slab thickness, in inch, and
D_2 = the second pavement design factor, subbase thickness, in inch.

During calibration, β_0 was assumed equal to 1, and a_2 was assumed equal to zero while $a_{1,3}$ were assumed equal to one. With these assumptions, Equation (39) could be rewritten as;

$$\log(\beta - 1.0) = \log B_0 + B_2 \log(L_1 + L_2) - B_3 \log\ L_2 - B_1 \log(D_1 + 1). \quad (40)$$

Subsequently, log (β - 1.0) was plotted against log (D_1+1) in order to determine B_1 which is the slope of fitted line regression. The regression analysis was done for each lane, and the average of slopes gave $\hat{B}_1$ which is the final estimate for B_1. Moreover, the same regression analysis (Figure A.9) was done to determine other constants, B_0, B_2, and B_3. The final equation for $\tilde{\beta}$ (final estimate for β) is shown in Equation (41).

$$\tilde{\beta} \ = \ 1.0 \ + \ \frac{0.22\ (L_1 + L_2)^{4.54}}{(D_1 + 1)^{5.90}\ L_2^{3.12}} \quad (41)$$

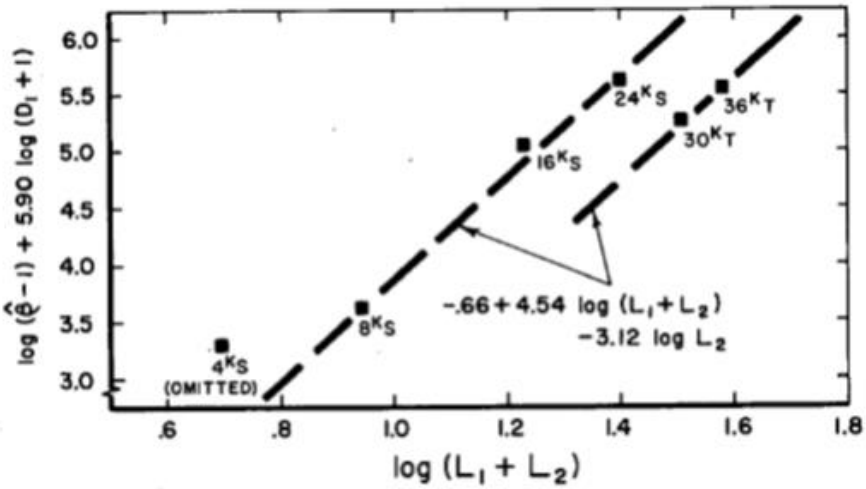

Figure A.9. Adjusted mean log ($\widehat{\beta}$– 1) vs (L_1+L_2) (Source: HRB 1962).

The same analyses were conducted for ρ which resulted in Equation (42) for $\tilde{\rho}$ (final estimate for ρ).

$$\tilde{\rho} \ = \ \frac{10^{5.98}(D_1 + 1)^{6.79}\ L_2^{\ 3.18}}{(L_1 + L_2)^{4.40}} \quad (42)$$

Until this stage of analysis, only the thickness of the top layer, D_1 was considered, and the official report states that to determine layer coefficients further regression analyses should be done.

In summary, in order to determine the thickness index and layer coefficients, analysis of variance for log ρ for 6 variations in terms of considering thickness index in the equation log ρ. Since the linear effects of the variables were highly significant in almost every case, the linear expression of (a_1D_1+a_2D_2+a_3D_3) was considered for thickness index (the term given during the test road analysis to what is now called the structural number) and further analysis. Estimates for a_1, a_2, and a_3 were obtained from the variance analyses, and weighted average of these estimates are presented in Equation (43) and (44). The first equation is for weighted applications (considering environmental effects) and the second one is for unweighted applications (not considering environmental effects).

$$D = 0.44D_1 + 0.14D_2 + 0.11D_3 \quad (43)$$

$$D = 0.37D_1 + 0.14D_2 + 0.10D_3 \quad (44)$$

Updates to Layer Coefficient Values

It was recognized early that direct adoption of the AASHO test road regression values might not be acceptable to all states. The first effort to correct this shortcoming was 1972 when Van Til et al. conducted a layered elastic analysis using a range of material moduli and examined the resulting vertical deflections, tensile strains in the asphalt concrete layer, and compressive strains on the subgrade to propose functional relationships between individual layer coefficients and the moduli of the materials in the layer. The resulting relationships appeared first in the 1972 American Association of State Highway and Transportation Officials (*AASHTO*) design guide and still appear in the 1993 guidelines. The Van Til approach to layer coefficient characterization was largely analytical, although the final recommendations involved some experimental observations. Others have also examined this issue and developed different conclusions based on their own local conditions.

Test Road Reanalysis

Shook and Finn (1962) statistically reanalyzed the test road data and suggested that 1 in. of asphalt concrete equated to 2 inches of crushed stone and 2.67 inches of granular subbase (i.e., coefficients of 0.44, 0.22, and 0.16 for asphalt concrete, aggregate base, and aggregate subbase respectively). These equivalency factors were determined based on a survey on the results from AASHO road test and previous studies. For example, Skok and Finn (1962) showed that the effectiveness of asphaltic concrete can be two to six times relative to good crushed stone. Based on these results, Shook and Finn carried out regression analyses with Equations (45)-(47) and the AASHO road test data to determine the relation of Structural Number (*SN*) that gave the lowest error. This analysis showed that the approximate errors were identical. Thus, 1 in. of a high-quality asphaltic concrete surfacing should be equivalent to 2 to 3 in. of good dense-graded crushed stone base, while the equivalency for asphaltic concrete base would be approximately 2 in. Also, in order to interpret AASHO road test data, layered elastic theory was used to compare vertical pressures on the subgrade. Skok and Finn's analysis with this theory found an equivalency factor of at least 2 to 1 was acceptable.

$$SN = 2.0D_1 + 1.0D_2 + 0.75D_3 \tag{45}$$

$$SN = 2.5D_1 + 1.0D_2 + 0.75D_3 \tag{46}$$

$$SN = 3.0D_1 + 1.0D_2 + 0.75D_3 \tag{47}$$

Two later studies also used the test road data to develop layer coefficient estimates. Kamel et al. (1973) utilized experimental results at the Brampton Road Test along with layered elastic analysis and found similar relative weights as the Shook and Finn study. Elliott (1981) analyzed the AASHO test road rehabilitations and found that for thick asphalt concrete surface courses the structural layer coefficient could be 0.57.

Penn State-Test Track

The Penn State-Test track experiment was also used to evaluate layer coefficients. This track was built using different materials and thicknesses as shown in Figure A.10. The data from this track was analyzed by Dunn in 1974 and Wang and Larson in 1977 and it was suggested that structural coefficients have a nonlinear relationship with thickness. The suggested values ranged between 0.67 to 0.48 for asphalt concrete, 0.55 to 0.28 for aggregate base, and 0.01 to 0.12 for aggregate subbase. In this study, surface roughness was measured using the *MacBeth* profilograph on both wheel paths, and the roughness factors were converted to *PSI* using the equation developed by

Bureau of Materials Testing and Research of the *PennDOT*. For the analysis of pavement responses the *BISAR* program was used, and the layer thicknesses were determined by limiting the maximum vertical strain, maximum tensile strain, and maximum surface deflection. To arrive at their conclusions, the researchers found, the relationship between Equivalent Axle Loads (*EAL*s) and maximum strains and surface deflection for different thicknesses. The maximum surface deflection for instance was limited to 0.51 mm for flexible pavements with a life of 1 million *EAL*s.

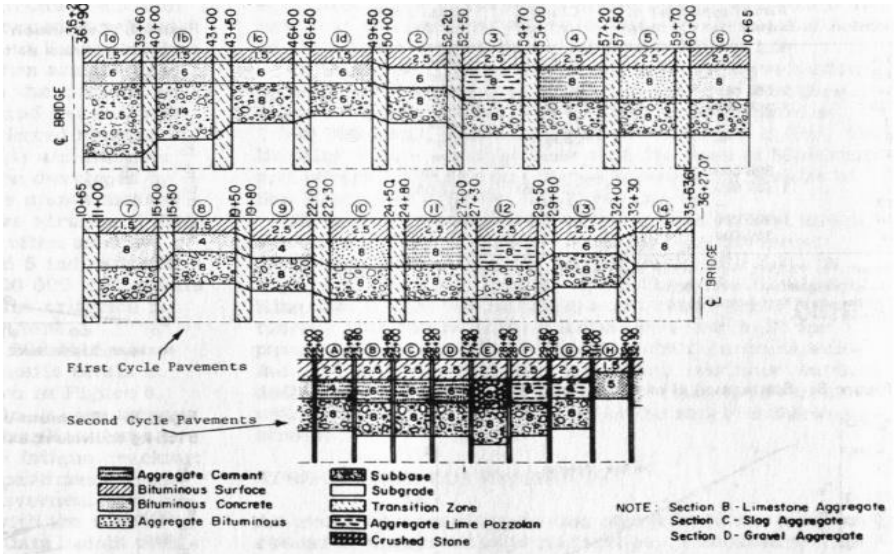

Figure A.10. Penn-test track (Source: Wang and Larson 1977).

Van Wijk Study

Van Wijk et al. (1983) used Falling Weight Deflectometer (*FWD*) testing, performance correlations, and layered elastic analysis to develop a structural coefficient for a recycled layer based on field data. Measurements were taken from the Dynaflect *FWD* and Dynamic Cone Penetrometer (*DCP*) tests at three different times. The process for determining the layer coefficient is shown in Figure A.11. Using test results and the *BISTRO* program, a range of coefficients between 0.11 and 0.39 was found for foamed-asphalt recycled layer. This study only considered changes to the asphalt concrete layer and did not consider how other layers may also be different.

Gomez and Thompson Study

Gomez and Thompson (1983) reviewed the methods for calibration of layer coefficients and based on their investigation concluded that the layer coefficient cannot be considered constant since it varies with different parameters including layer thickness, material type, material quality, layer location, traffic level, and limiting stress, strain, and deflection. They further conclude that in order to calibrate the layer coefficient, extensive field test or mechanistic pavement modeling should be conducted. They considered the former approach to be too difficult and time consuming and instead used *ILLI-PAVE*. However, in such an approach, many factors need to be determined which makes it difficult to use and not easily adaptable to new materials or design concepts. Thus, further efforts to calibrate layer coefficients for *IDOT* was discontinued.

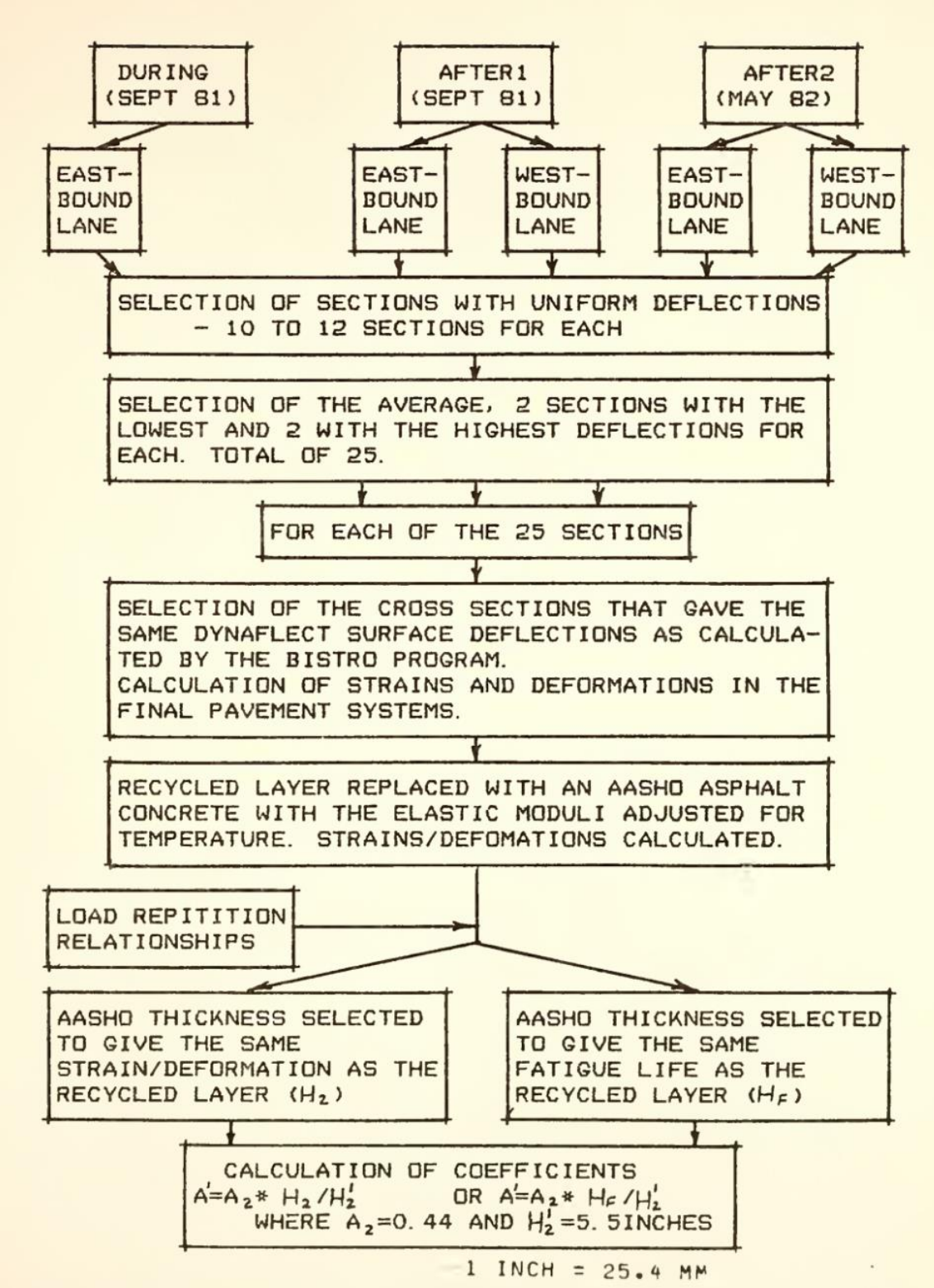

Figure A.11. Procedure for determination of structural coefficient (Source: Van Wijk 1983).

Van Til Study

Van Til et al. (1972) summarized the procedures for determining the structural layer coefficient for different states at the time. In Arizona the layer coefficients were revised, and in most cases the results were lower than the layer coefficients established by the AASHO road test. The method they used for determining the layer coefficient for aggregate base, bituminous-treated base, and asphaltic concrete is summarized in Table A.4 through Table A.7. For all layers, the basic method involved establishing a base or average representative value for all materials, for example with Select Material the base value was 0.05 for sand and gravel (S&G) and 0.04 when the material was made of cinders. Then, adjustments to this base value are made depending on certain compositional characteristics like gradation, plasticity, thickness, etc.

Van Til also presented modifications to the Illinois method. There, the state modified the structural layer coefficient because of the variability of layer coefficient with the strength of the material. The Marshall stability values were used as a basis for adjusting the layer coefficient for surface course, which were found to vary from 0.2 for a material with the lowest stability to 0.44 for bituminous concrete (Figure A.12). Furthermore, various tests were performed to obtain the layer coefficients for base layer materials in four categories: granular material, bituminous-stabilized granular material, portland cement-stabilized granular material, and lime-stabilized granular material. The layer coefficients for granular materials were determined based on the California Bearing Ratio (*CBR*) values, specifically varying between 0.07 and 0.14. The coefficients for bituminous-stabilized granular material correlated with Marshall stability values, and the range of coefficient values was from 0.15 to 0.34.

For cement and lime-fly-ash stabilized granular materials the 7-day compressive strength and 21-day compressive strength were used respectively to determine the variation of structural layer coefficient. Based on their study, the coefficient values for portland cement-stabilized materials varied from 0.14 to 0.23, and this range for lime-fly-ash-stabilized material was 0.15 to 0.23. Furthermore, the layer coefficient for subbase material was determined based on *CBR*, and same as surface layer, graphs for variation of layer coefficient for different layers were developed.

For Louisiana, the structural coefficients for surface course and asphalt-stabilized base materials were based on Marshall stability. Texas triaxial values were used to determine the coefficients of the untreated and lime-treated base and subbase courses. The coefficients for cement stabilized base correlated with compressive strength. The coefficients for surface course varied in a narrow range between 0.43 and 0.44, whereas a range from 0.06 to 0.34 was observed for the base course. Layer coefficients for subbase materials were found to change from 0.04 to 0.15. The coefficients for both bituminous concrete and portland cement concrete pavements were also determined and varied between 0.1 to 0.5.

New Mexico calibrated the layer coefficients based on strength of material. The layer coefficient of the surface layer was calibrated based on Marshall stability, and the coefficients for the untreated granular bases and subbases were calibrated with *R*-values.

Table A.4. Methods Used to Calibrate Coefficient for Select Material (After: Van Til et al. 1972).

Select Material - Use base coefficient of 0.05 for S&G and 0.04 for cinders.						
Add Value	**P.I.**	**Pass #200**	**Pass #8**	**Pass ¼-in.**	**Pass 3-in.**	**Pass 3-in.**
0.01	N.P.					
0.01		0-15				
0.02		0-10*				
0.01			30-75			
0.02				30-75		
0.01					100	
0.02						100

Table A.5. Methods Used to Calibrate Coefficient for Aggregate Base (After: Van Til et al. 1972).

Aggregate Base - Use base coefficient of 0.08 for S&G and 0.06 for cinders.					
Add Value	**P.I.**	**Pass #200**	**Pass ¼-in.**	**Abrasion**	**Crushing**
0.01	N.P.				
0.01		0-12			
0.02		0-10			
0.01		0-8			
0.02			45-75		
0.01				<40	35% Ret. ¼-in. sieve
0.02					

Table A.6. Methods Used to Calibrate Coefficient for Asphaltic Matls. (After: Van Til et al. 1972).

Asphaltic Pavement and Bases – For asphalt pavement use base 0.25 for S&G and 0.2 for cinders, For BTB use 0.2 for S&G and 0.15 for cinders.					
Add Value	**Grading**	**Stab.**	**AC Thickness**	**Abrasion**	**Asphalt**
	¾-in. coarse (Class A)				
0.02	¾-in. medium, or ½-in. coarse				
0.01	¾-in. fine (Class B)				
0.00	½-in. fine, open graded				
0.02		>35			
0.01		28-35			
0.00		<28			
0.02				<25	
0.01				25-40	
0.00				>40	
0.01 to 0.6			0.01 per inch		
0.05					Pen 60-70 or 85-100
0.00					Liq. 250-800

Table A.7. Methods used to Calibrate Coefficient for Cement Treated Base (After: Van Til et al. 1972).

Cement treated Base – Use base of 0.12						
Add Value	**Mixing**	**Pass #8**	**Pass #4**	**Strength, psi**	**P.I.**	**AC Thickness**
0.05	Central plant					
0.00	Road Mix					
0.01		30-65				
0.02			45-75			
0.07				>500		
0.05				300-500		
0.00				<300		
0.01					N.P.	
0.01						4 in.
0.02						in.

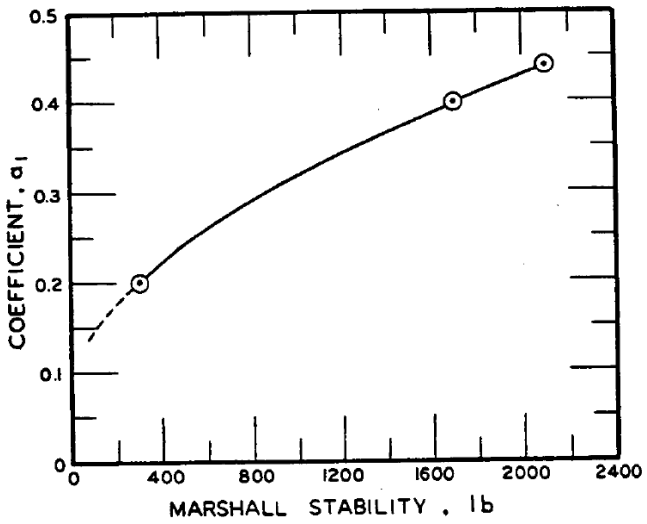

Figure A.12. Surface layer coefficient with Marshall stability values (Source: Van Til et al. 1972).

Texas provided layer coefficients as a supplement to the coefficients developed by the AASHO road test rather than as a replacement. Their development of layer coefficients were based on tests and the local engineering experience. For granular bases and subbases, untreated and lime-treated, the results of Texas triaxial test were used. The resulting range of layer coefficients was 0.045 to 0.35. For asphalt-treated bases the same test was conducted at 140°F, and the coefficients varied between 0.1 and 0.5. The layer coefficient for cement-treated bases was determined based on the 7-day unconfined compressive strength test, and the range of the coefficient values was 0.10 to 0.32. Furthermore, coefficients for asphaltic concrete were correlated with cohesiometer values in a range from 0.25 to 0.51.

Wyoming modified layer coefficients based on results of strength tests. Marshall stability and stabilometer *R*-values were used to calibrate layer coefficients for surfadfce course and granular subbase and base material, respectively.

Coree and White Study

Coree and White (1989) applied Odemark's method of equivalent stiffness to propose a third order relationship between modulus and layer coefficient and applied this function to Indiana mixtures. While they found a large range, they finally concluded that the representative layer coefficient was 0.44. In this study, two methods were considered for determining the layer coefficient, direct and relative method. The direct method was based on a regression between layer coefficient and resilient modulus. The relative method was similar to Odemark's equation. That being said, the two methods were assumed to be identical, and Odemark's concept was used to ultimately calibrate the layer coefficient. In order to calculate modulus or stiffness of the mixtures, three methods were used; Van der Poel nomograph (Van der Poel 1954), the Ullidtz approach (Ullidtz 1979), and the Bonnaure method (Bonnaure 1976). Laboratory tests were conducted to verify the application of these methods.

Richardson Study

Richardson et al. (1994) also used Odemark's method of equivalent stiffness and compared the results with layer coefficients obtained from AASHTO nomographs for the Missouri Highway and Transportation Department (MHTD). Based on this comparison, it was concluded that the layer coefficients determined using the AASHTO nomographs were more realistic. Odemark's equation, Equation (48), was used to relate the MHTD resilient modulus (M_r) to the AASHO Road Test M_r. The resilient modulus used in both methods were determined by test or estimated by general regression equation. In the second method, a correction for temperature was applied. The first option resulted in a fixed layer coefficient per material; asphaltic cement concrete had a layer coefficient of 0.42 and bituminous base had a layer coefficient of 0.34.

The second option developed was a method for pavement designers to calculate layer coefficients for a specific mix and location in the state. Also, in this study, the effects of changes in asphalt cement grade, aggregate gradation, testing temperature, aggregate source, and asphalt content on layer coefficient in 48 mix designs were investigated. The same analysis was carried out for unbound materials.

$$a_{n,MHTD} = a_{n,AASHO}\left[\frac{Modulus_{MHTD}}{Modulus_{AASHO}}\right]^{1/3} \tag{48}$$

where a_n is layer coefficient for layer *n* and Modulus is one the several types such as resilient modulus (M_r), dynamic modulus ($|E^*|$), or mixture stiffness (S_m).

Janoo Study

Janoo (1994) conducted a research study to calibrate layer coefficients mainly for subgrade soils, aggregate courses and recycled stabilized base course (*RSB*). The method adopted used a combination of values proposed by AASHTO in the 1960s and by Janoo (Table A.8). In this study, Heavy Weight Deflectometer (*HWD*) testing with the Strategic Highway Research Program (*SHRP*) protocol for pavement evaluation was conducted on ten test sections with different materials. In addition, dynamic cone penetrometer (*DCP*), in-situ California Bearing Ratio (*CBR*), level survey, and Clegg hammer were performed. The *WESDEF* software was used to determine layer moduli. Furthermore, layer thicknesses were determined from level survey, and *SN* was

calculated using Rohde's method (Rohde 1994). Layer coefficients were calculated using AASHTO relationships and back calculated moduli. Janoo used multiple methods to estimate the layer coefficients. Based on the work of Rohde (1994) *SN* and *CBR* which were first used to estimate layer coefficients. Then the World Bank HDM-111 method, (Watanatada et al. 1987) which utilizes in-situ CBR was used to determine layer coefficients. In addition, two sets of layer coefficients were calculated based on data obtained from Clegg hammer and *DCP* test. Comparison between layer coefficients based on different method showed that coefficients determined from in-situ *CBR* are very low, but that a good correlation between coefficients calculated based on backcalculated data from *FWD*, Rohde's method, Clegg hammer, and *DCP* test. The collective findings from these evaluations were coupled with the experience and expectations of the researcher and agency respectively to recommend the final layer coefficients.

Table A.8. Layer Coefficients Used by NHDOT.

Material	Layer Coefficient (a_i)
Hot bituminous base course	0.34
Hot bituminous binder and surface course	0.38
Crushed gravel base	0.10
Gravel base	0.07
Crushed stone	0.14
Sand	0.05
Reclaimed stabilized base	0.17

Hossain Study

Hossain et al. (1997) used *FWD* testing and the effective *SN* equation from AASHTO to estimate layer coefficients for crumb rubber modified mixtures. They found a large range, but an average of 0.35. They also applied layered elastic analysis to find a median layer coefficient of 0.30. In this study, three methods were used to backcalculate layer moduli; forward calculation using *ELSYM5* and two backcalculation programs *MODULUS* 4.0 and *BKCHEVM*.

Pologruto Study

FWD testing in Vermont was used by Pologruto in 2001 to estimate an asphalt concrete layer coefficient as high as 0.639. The effective structural number (SN_{eff}) was determined in each interface, and the layer coefficient was calculated by taking the difference between SN_{eff} on top and below each layer and dividing it by the layer thickness (Figure A.13), and this analysis was done for all the layers. The determined layer coefficient values were verified by statistical analysis. It was concluded that the high values for calibrated layer coefficient were reasonable considering the fact that the *FWD* tests were done on new pavement. The authors go on to mention that determining the layer coefficient by direct assessment of the pavement is difficult, which makes the designing of pavement using AASHTO design equation more challenging, but possible through the usage of *FWD* testing.

Von Quintus Study

Von Quintus (2007) evaluated layer coefficients for the Kansas DOT. The report justified the need for calibration of layer coefficients based on changes in materials and specifications for designing and constructing flexible pavements. One change included the increased use of polymer modified asphalts (*PMA*). In this study, it was recommended that the structural layer coefficient of the HMA surface course and base mixtures be increased; however, the authors did not make any specific

recommendation on what those increased values should be. Also, important points regarding the calibration of structural layer coefficient are noted.

Huang Study

Huang and Drumm (2007) used laboratory testing of asphalt concrete and aggregate base materials from across Tennessee along with the published relationships between modulus and layer coefficients. They estimated a wide range in resulting layer coefficients, but ultimately suggested retaining the current values.

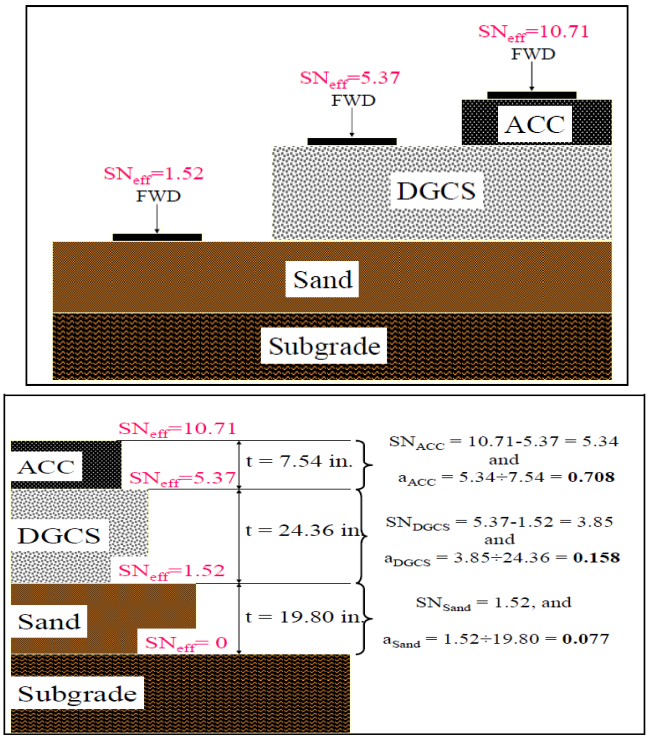

Figure A.13. Determination of layer coefficient from FWD testing (Source: Pologruto, 2004).

Timm Studies

Jess and Timm (2005) applied the AASHTO procedure using backcalculated moduli to estimate the layer coefficient for asphalt concrete layers at the National Center for Asphalt Technology (*NCAT*) and found an average coefficient of 0.59. This study calculated the surface layer coefficients by keeping the base layer coefficients as default values.

Recently, Davis and Timm (2009) also used the *NCAT* test track, but used *IRI* instead of FWD to estimate an average layer coefficient for the asphalt concrete of 0.54. Again, differences in performance were attributed solely to errors in the surface layer coefficient. It was pointed out that this layer coefficient should be used for pavements with HMA layer thickness greater than 5 in. since the thinnest HMA layer was used in test was 5 in. For designs that result in HMA layer thinner than 5 in., the coefficient of 0.44 was recommended.

Davis and Timm also demonstrated why choosing the layer coefficient as the main parameter to recalibrate. This was done by performing a sensitivity analysis on different design parameters in the 1993 AASHTO design equation, Equation (49). Based on the results of this analysis, HMA layer coefficient is the most influential parameter on *HMA* layer thickness.

$$\log W_{18} = Z_R S_0 + 9.36\ \log(SN+1) - 0.20 + \frac{\log\left[\frac{\Delta PSI}{4.2-1.5}\right]}{0.4 + \frac{1094}{(SN+1)^{5.19}}} + 2.32 \log M_R - 8.07 \quad (49)$$

Based on another analysis on Equivalent Single Axle Loads (ESALs) values, the recalibration of the layer coefficient was justified. Predicted and calculated *ESAL*s using a_1=0.44 were plotted, and as shown in Figure A.14 using a_1= 0.44 causes underestimation of the observed performance.

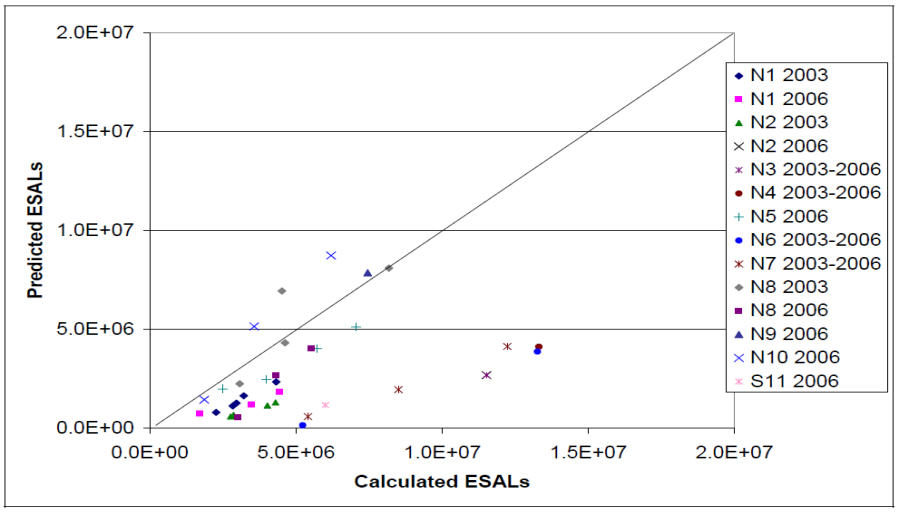

Figure A.14. Calculated vs. predicted ESALs using a_1=0.44 (Source: Davis and Timm 2009).

The process followed by Davis and Timm is shown in Figure A.15. After the recalibration of the layer coefficient, a forensic investigation was done. It was found that those sections that had signs of debonding between HMA lifts had recalibrated layer coefficients lower than 0.44.

Prowell Study

Prowell et al. (2017) evaluated the layer coefficient for South Carolina's asphalt base materials using dynamic modulus testing and the AASHTO modulus to layer coefficient relationship. The researchers concluded that the layer coefficients for the asphalt base could be greater than 0.44. The calibration of the layer coefficient was necessary because of the several changes to South Carolina DOT's mix designs and materials such as using Reclaimed Asphalt Pavement (RAP) in asphalt mixtures. Four mixtures were used for dynamic modulus testing that contained 23 to 35 percent *RAP*. The resilient modulus values at 1.59 Hz and 68°F were predicted from the dynamic modulus master curves for each mixture. Based on this analysis, the estimated structural layer coefficients were greater than 0.44, but the ultimate recommendation was that South Carolina DOT uses a_1= 0.44 for asphalt base materials.

Dave Study

Dave et al. (2019) updated the layer coefficients for the New Hampshire DOT by conducting a laboratory study of asphalt concrete properties. These properties were linked to performance models to suggest changes in the current layer coefficients, which was verified by examining in-service pavement performance.

A set of 18 asphalt mixtures were selected to represent all the conventional traffic levels, climatic conditions, cross sectional designs, production methods, aggregate size and binder types, recycled asphalt pavement (RAP) amount and recycled binder ratio (RBR) as well as gyration levels in use in New Hampshire. The mixtures include two asphalt rubber gap graded (ARGG), four cold central plant recycled (CCPR) mixtures as well as other different types of conventional and polymer modified hot mixed asphalt (HMA) mixtures used in surface, binder, and base course layers. In the process of calibration, the layer coefficients were backcalculated from field *IRI* data. The initial and terminal *IRI* (20^{th} year *IRI*) were converted to *PSI* values using Al-Omari equation (Al-Omari et al. 1994). The initial serviceability was deducted from the terminal serviceability to obtain the Δ*PSI* value as the allowable serviceability loss at the end of design life. Δ*PSI* is a key input in the AASHTO 1993 design equation which can significantly affect the layer coefficient back calculation using the field data. The AASHTO design equation was used to first identify the overall structural number (SN) was determined for a given cross section. Then, the SN of the granular material as well as other base and binder course asphalt mixtures could be determined using their thickness and layer coefficients. The SN of all the non-surface course material was identified and differentiated from the SN of the surface course materials.

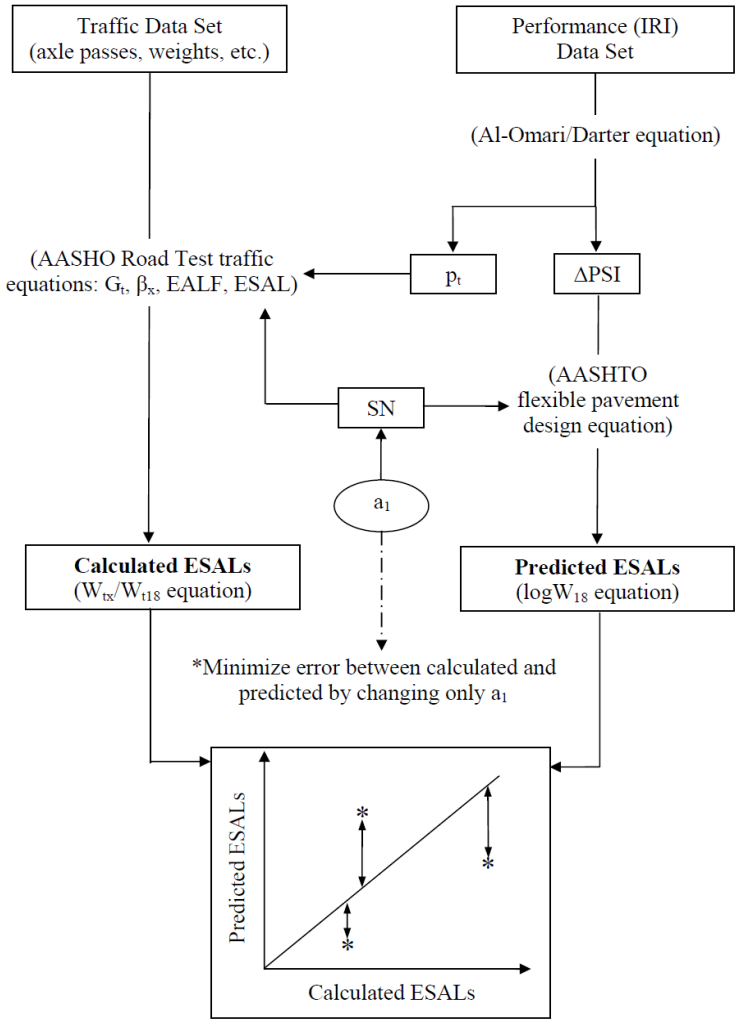

Figure A.15. Recalibration process illustration (Source: Davis and Timm 2009).

Based on the analysis, a set of average and minimum a-values at different levels of reliability have been proposed for future New Hampshire pavement designs. Using a normal distribution function, the average layer coefficient for surface course of non-AARG mix was determined to be 0.58. ARGG mixes had a very high layer coefficient compared to the rest of the mixtures. Also, there were some cases where a similar mixture from different project sites had significantly different layer coefficient values. It was concluded that this occurrence could have happened because of over designed non-surface course material or difference between the assumed subgrade soil resilient modulus and actual modulus value.

Summary

The methodologies used in previous studies can be summarized into five categories, shown in Table A.9. In addition, a summary of calibration of the layer coefficients for different states is presented in Table A.10 while a summary of the layer coefficients currently being used by other states or agencies are shown in Table A.11.

Table A.9. Calibration Methodologies Summarized from Dave et al. (2017) and Davis and Timm (2014).

Method	Param.	Procedure/Basic concept	Advantage	Disadvantage	Used by
Pavement perf.	*IRI*, *PSI*, SN	Regression analysis on SN	Based on the performance of materials	Need detailed records of traffic and pavement performance.	ALDOT
Pavement struc. Res.	D, ε_t, ε_z, N_f	Equivalent deflection	-	-	IDOH
Material properties char.	M_r	Determining M_r and using AASHTO equation.	-	-	WisDOT
Using FWD	Deflections and Back. moduli	1. Assuming properties for sub-AC layers and using Ullitdz equations. 2. Using ΔSN approach.	Requires relatively little data	Relies on empirical equations	NHDOT
ME approach	Pavement ME inputs	Analyzing with Pavement ME and calculate equivalent layer coefficients.	Relatively more sophisticated way	Requires a detailed database	WSDOT

Table A.10. Summary of Layer Coefficient Calibrations.

State/ Agency	New Layer Coefficient			Method	Reference
	AC	Base	Subbase		
-	0.44	0.22	0.16	Reanalyzed the AASHO test road data	Shook and Finn (1962)
-	0.57	-	-	Reanalyzed the AASHO test road data	Elliott (1981)
PA	0.48 - 0.67	0.28 - 0.55	0.01 - 0.12	Test track	Wang and Larson (1977)
-	0.11 – 0.39	-	-	Using FWD and DCP data in layered elastic analysis	Van Wijk et al. (1983)
IL	-Study discontinued-				Gomez and Thompson (1983)
AZ	Varies depending on the material				Van Til et al. (1972)
IL	0.2 – 0.44	0.07 – 0.34	-	Material test	
LA	0.43 – 0.44	0.06 - 0.34	0.1 - 0.5	Material test	
TX	0.25 – 0.51	0.045 – 0.5			
IN	0.44	-	-	Odemark's method	Coree and White (1989)
MO	0.42	0.34	-	Odemark's method	Richardson et al. (1994)
NH	0.38	0.05 – 0.17	-	FWD	Janoo (1994)
-	0.35	-	-	FWD	Hossain et al. (1997)
VT	0.639	-	-	FWD	Pologruto (2001)
KS	-Coefficient should be increased (specific values are not defined)-			-	Von Quintus (2007)
TN	-Suggested retaining the current values-			Material test	Huang and Drumm (2007)
AL	0.59	-	-	Pavement performance	Jess and Timm (2005)
	0.54	-	-		Davis and Timm (2011)
	0.55				Timm et al. (2014)
NC	≥0.44	-	-	Material Properties Characterization (M_r)	Prowell et al. (2017)
NH	0.58	-	-	Pavement performance	Dave et al. (2019)

Table A.11. Layer Coefficients Used by other Agencies (Source: Dave et al. 2017).

Layer Type	Layer coefficients (a_i)	DOTs
Surface Course	0.54	ALDOT
	0.50	WSDOT
	0.44	FDOT, SCDOT, CTDOT, MaineDOT, MassDOT, IADOT, PADOT, WisDOT, NJDOT, MDOT, GDOT, ConnDOT
	0.43	ODOT
	0.42	NYCDOT
	0.40	DelDOT, IDOT
	0.35	NDOT, VTDOT
Non-Surface Course	0.44	FDOT, PADOT, SCDOT
	0.42	NYCDOT
	0.40	DelDOT, ConnDOT
	0.36	ODOT
	0.35	NDOT
	0.34	MassDOT, MaineDOT, MDOT
	0.33	VTDOT
	0.31	WisDOT
	0.30	GDOT, IDOT

Calibration of Truck Factors

Truck factors and the method for calculation of Equivalent Single Axle Loads (ESALs) were determined from the design guidelines of multiple DOTs across the US. Truck factors for single unit (SU) and multi-unit (MU) trucks, which were identified from this study are presented in Table A.12. Note that in this table the values for some agencies are presented with lower and upper range limits. While many agencies compile truck factors in the same way as NCDOT (by SU or MU), many disaggregate the truck factors into more finely divided groupings. For these agencies, the truck factors were grouped into SU and MU classes and the upper range and lower range values represent the extreme values within that agency's own classification system.

To more clearly identify agency differences, truck volumes from NCDOT traffic data were used to compute the cumulative ESALs for a hypothetical roadway using the agency specific truck factors. The results are plotted in Figure A.16 as the ratio of cumulative ESALs from the individual agency to that of the NCDOT. Where lower and higher range estimates exist, the data is shown using error bars. As can be seen in this figure, the estimated ESALs based on NCDOT truck factors are lower than all other DOT's using their average factors and approximately the same or slightly higher for agencies with a low range.

Table A.12. Truck factors for different DOTs.

State	Average Truck Factor		Lower Range Truck Factor		Higher Range Truck Factor	
	SU	MU	SU	MU	SU	MU
NC	0.30	0.85	-	-	-	-
AZ	0.96	1.96	0.39	0.91	0.61	3.50
PA	0.82	2.33	0.24	0.44	4.50	2.33
OH	0.47	0.90	-	-	-	-
IL	0.36	1.32	-	-	-	-
GA	0.40	1.50	-	-	-	-
MN	0.58	1.13	0.25	0.39	0.58	2.40
SC	0.63	1.09	0.18	0.77	0.63	1.09
VA	0.46	1.05	-	-	-	-
NY	1.35	1.35	-	-	-	-
CT	1.14	3.07	0.20	0.80	3.48	3.07
FL	0.90	0.90	-	-	-	-
CO	0.25	1.09	-	-	-	-

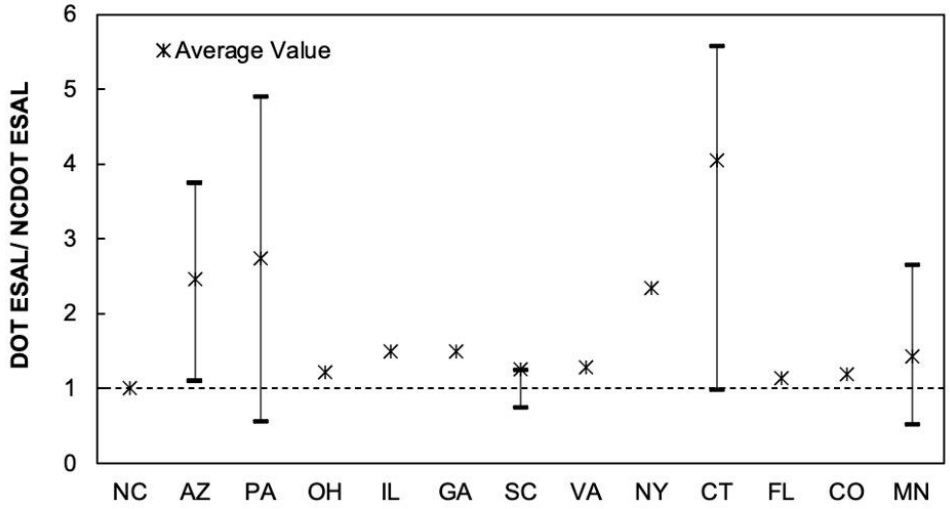

Figure A.16. Calculated ESALs for different DOTs.

Smith and Diefenderfer (2009) calibrated truck factors for Virginia DOT using WIM data from 15 locations around Virginia. The procedure to calibrate truck factors began with converting WIM data to LEFs and ESALs per vehicle based on the AASHTO functions, Equations (50)-(52) using a custom MATLAB script. The MATLAB program used various inputs other than WIM data including a site identification number, date range, *SN*, and p_t as specified by the user. The script also required the vehicle count and average number of axles for each vehicle class with respect to lane for each month in a Microsoft Excel worksheet.

$$\log\left(\frac{W_{tx}}{W_{t18}}\right) = 4.79\log(18+1) - 4.79\log(L_x + L_2) + 4.33\log(L_2) + \frac{G_t}{\beta_x} - \frac{G_t}{\beta_{18}} \quad (50)$$

$$G_t = \log\left(\frac{4.2 - p_t}{4.2 - 1.5}\right) \quad (51)$$

$$\beta_x = 0.40 + \frac{0.081\,(L_x + L_2)^{3.23}}{(SN + 1)^{5.19}\,L_2^{3.23}} \quad (52)$$

where;

W_{tx} = number of applications of given axle,
W_{t18} = number of standard axle passes (single 18-kip axle),
L_x = load in kips of axle group,
L_2 = axle code (1 for single axle, 2 for tandem axles, 3 for tridem axles, and 4 for quad axles),
β_{18} = value of β_x when $L_x = 18$ and $L_2 = 1$,
p_t = terminal serviceability, and
SN = structural number.

The MATLAB results provide the site-specific truck factors for each WIM location and for each vehicle classification. A sensitivity analysis of the truck ESAL factors was conducted using DARWin 2.01 and comparing the required *SN*. In order to obtain maximum variations of *SNs*, sections with high truck traffic were used. Ultimately, two test sections were used to represent interstate and primary routes. The authors compared VDOT's single-unit/combination truck classifications and 13 classes of FHWA classification with the site-specific truck ESAL factors (Table A.13).

Table A.13. Average Truck Factors for Flexible Pavement by Vehicle Classification and Administrative Roadway Classification (Source: Smith and Diefenderfer, 2009).

Vehicle Classification	Interstate		Primary	
	No. of Vehicles	Average Truck Factor	No. of Vehicles	Average Truck Factor
4	83,584	0.44	42,445	0.35
5	91,173	0.28	87,006	0.36
6	69,069	0.42	102,112	0.60
7	5,043	1.00	27,921	1.09
8	71,606	0.47	36,751	0.50
9	2,307,904	1.06	467,982	1.01
10	20,160	1.07	16,307	1.06
11	114,922	1.52	13,574	1.19
12	44,496	0.83	2,933	0.70
13	227	1.59	39	2.23
VDOT Representative Classification				
Single-unit trucks	248,869	0.39	259,484	0.53
Combination trucks	2,559,315	1.06	537,587	0.98

Based on the results of these comparisons, changes to the required SN for single unit/combination of trucks and FHWA classifications were minimal; therefore, grouping truck vehicles into single unit/combination of trucks was deemed sufficient for traffic characterization. Also, separate truck ESAL factors for interstate and primary routes were found to be unnecessary, and instead, statewide average truck ESAL factor values were recommended. The final results for updated truck factors and old truck factors before modifying for flexible and rigid pavements are presented in Table A.14, which shows that for single unit trucks, factors increase and for combination trucks these values decrease.

Table A.14. Comparison Between Old and Updated Truck Factors for Flexible and Rigid Pavements (Source: Smith and Diefenderfer, 2009).

Pavement Type		Single-unit trucks	Combination trucks
Flexible pavement	Old truck factors	0.37	1.28
	Updated truck factors	0.46	1.05
Rigid pavement	Old truck factors	0.56	1.92
	Updated truck factors	0.59	1.59

Knowledge Gaps and Applications

The literature review prepared for this research confirmed that the current layer coefficients are the result of statistical analysis of the sections in the 1956-1962 AASHO test road. Despite looking through numerous studies pertaining to pavement evaluation and design at NCDOT, no mention of the origin of the current NCDOT layer coefficients were found. Multiple studies from different agencies have been conducted to evaluate whether these original coefficients are universally applicable and to identify possible modifications to the values. Methodologies have ranged from purely empirical and involve in-situ evaluation of pavement stiffness to purely theoretical using layered elastic analysis. The most successful and long-lasting approaches have relied on combined experimental and analytical study. However, the general applicability of these approaches across agencies has not been demonstrated likely due to differences in performance measurement, construction, mixture design, and management practices (i.e., maintenance, rehabilitation, reconstruction timings and their relationship to design practices). Current asphalts used by the NCDOT are stiffer than the binder used in the AASHO road test and mixtures are designed using the Superpave system. Thus, it is important in the calibration efforts to recognize this condition and not only develop calibrated structural layer coefficients, but also develop relationships or a methodology to determine layer coefficients for future materials.

Literature Review References

American Association of State Highway and Transportation Officials (AASHTO). AASHTO Guide for Design of Pavement Structures. *American Association of State Highway and Transportation Officials*, Washington, D.C., 1993.

Al-Omari, B., and Darter, M. Relationships Between International Roughness Index and Present Serviceability Rating. *Transportation Research Record: Journal of the Transportation Research Board*, No. 1435, Washington, D.C., 1994, pp.130–136.

Al-Omari, B. and Darter, M. Effect of Pavement Deterioration Types on *IRI* and Rehabilitation. *Transportation Research Record: Journal of the Transportation Research Board*, No. 1505, Washington, D.C.,, 1994, pp. 57–65.

American Society for Testing and Materials (ASTM). ASTM E1489-08 (Reapproved) *Standard Practice for Computing Ride Number of Roads from Longitudinal Profile Measurements*

Made by an Inertial Profile Measuring Device. West Conshohocken, PA, 2013.
Bahia, H.U., Bosscher, P.J., Christensen, J., and Hu, Y. *Layer Coefficients for New and Reprocessed Asphaltic Mixes*. Wisconsin DOT (WisDOT), Final Report No. WI/SPR-04-00, Madison, WI, 2000.
Bonnaure, F. Gest, G., Gravais, A., and Uge, P. A New Method of Predicting the Stiffness of Asphalt Paving Mixtures. *Journal of the Association of Asphalt Paving Technologists*, Vol. 46, 1977, pp. 64-104.
Brokaw, M.P. Development of the PCA Road Meter: A Rapid Method for Measuring Slope Variance. *Highway Research Record*, Vol. 189, 1967, pp. 137-149.
Carey, W.N. and Irick, P.E. The Pavement Serviceability Performance Concept. *Highway Research Board Bulletin*, No. 250, 1960, pp. 40–58.
Chandra, S., Sekhar, C.R., Bharti, A.K., and Kangadurai, B. Relationship Between Pavement Roughness and Distress Parameters for Indian Highways. *Journal of Transportation Engineering*, Vol. 139, No. 5, 2013, pp. 467–475.
Coree, B.J. and White, T.D. The Synthesis of Mixture Strength Parameters Applied to the Determination of AASHTO Layer Coefficient Distributions. *Journal of the Asphalt Paving Technologists*, No. 58, 1989, pp. 109-141.
Dave, E. *Layer Coefficients for NHDOT Pavement Design*. New Hampshire DOT (NHDOT), Project Number 26962N, Concord NH, 2017.
Dave, E., Sias, J. E., and Nemati, R. *Layer Coefficients for New Hampshire Department of Transportation Pavement Design*. FHWA Final Report No. FHWA-NH-RD-26962N, Federal Highway Administration, Washington, D.C., 2019.
Davis, K. and Timm, D.H. *Recalibration of the Asphalt Layer Coefficient*. National Center for Asphalt Technology Report No. 09-03, Auburn AL, 2009.
Davis, K. and Timm, D.H. Structural Coefficients and Life Cycle Cost. *Proceedings of the First T&DI Congress 2011, American Society of Civil Engineers*, Chicago, IL., 2011, pp. 646-655.
Dewan, S.A. and Smith, R.E. Estimating International Roughness Index from Pavement Distresses to Calculate Vehicle Operating Costs for the San Francisco Bay Area. *Transportation Research Record, Journal of Transportation Research Board*, No. 1816, Washington, D.C., 2002, pp. 65–72.
Dunn, H.D. Jr. *A study of Four Stabilized Base Courses*. Ph.D. Dissertation, The Pennsylvania State University, Department of Civil Engineering, State College, PA, 1974.
Elliot, R.P. *Rehabilitated AASH(T)O Road Test-Analysis of Performance Data Reported in Illinois*. National Asphalt Pavement Association, Physical Research Report 76, 1981.
Flintsch, G.W. and McGhee, K.K. *Quality Management of Pavement Condition Data Collection*. NCHRP Synthesis 401, Washington, D.C., 2009.
Gillespie, T.D., Sayers, M.W., and Segel, L. *Calibration of Response-Type Road Roughness Measuring Systems.* NCHRP Report No. 228, Washington, D.C., 1980.
Gomez, R. and Thompson, M.R. *Structural Coefficients and Thickness Equivalency Ratios*. Illinois Cooperative Highway and Transportation Research Program Final Report UILU-Eng-83-2009, Urbana IL, 1983.
Gulen, S., Woods, R., Weaver, J., and Anderson, V.L. Correlation of Present Serviceability Ratings with International Roughness Index. *Transportation Research Record: Journal of the Transportation Research Board*, No. 1435, Washington, D.C., 1994, pp. 27-37.
Hall, K.T. and Munoz, C.E.C. Estimation of Present Serviceability Index from International

Roughness Index. *Transportation Research Record: Journal of the Transportation Research Board*, No. 1655, Washington, D.C., 1999, pp. 93–99.
Highway Research Board (HRB) *The AASHO Road Test*. Special Reports 61E. Highway Research Board, Washington, D.C., 1962.
Hossain, M., Habib A., and LaTorella, T.M. Structural Layer Coefficients of Crumb Rubber-Modified Asphalt Concrete Mixtures. *Transportation Research Record: Journal of the Transportation Research Board*, No. 1583,Washington, D.C., 1997, pp. 62-70.
Huang, B. and Drumm, E. *Laboratory Evaluation of Layer Structural Coefficients for HMA Pavements*. Tennessee DOT (TDOT), Final Report No. RES1271 116-2004, Knoxville, TN., 2007.
Janoff, M.S., Nick, J.B., Davit, P.S., Hayhoe, G.F. *Pavement Roughness and Rideability*. NCHRP Report No. 275, Washington, D.C., 1985.
Janoff, M.S. *Pavement Roughness and Rideability Field Evaluation.* NCHRP Report No. 308, Washington, D.C., 1988.
Janoo, V.C. *Layer Coefficients for NHDOT Pavement Materials*. US. Army Corp of Engineers Cold Regions Research & Engineering Laboratory, Special Report No. 94-30, 1994.
Jess, J.C., and Timm, D.H. *Structural coefficients for new asphalt mixtures*. Alabama DOT (ALDOT), Final Report Project No. 930-559, Montgomery, AL, 2005.
Kamel, N.I., Phang, W., Morris, J., and Haas, R.C.G. Layer Analysis of the Brampton Test Road and Application to Pavement Design. *Highway Research Record*, No. 466, 1973, pp. 113 – 126.
Lin, J., Yau, J., and Hsiao, L. Correlation Analysis Between International Roughness Index (*IRI*) and Pavement Distress by Neural Network. *82nd Annual Meeting (CD-ROM), Transportation Research Record*,Washington, D.C., 2003.
Loprencipe, G. and Zoccali, P. Ride Quality Due to Road Surface Irregularities: Comparison of Different Methods Applied on a Set of Real Road Profiles. *Coatings*, Vol. 7, No. 5, 2017.
Mactutis, J.A., Alavi, S.H., and Ott, W.C. Investigation of Relationship Between Roughness and Pavement Surface Distress Based on WesTrack Project. *Transportation Research Record: Journal of Transportation Research Board*, No. 1699, Washington, D.C., 2000, pp. 107–113.
Miller, J.S., and Bellinger, W. Y. *Distress Identification Manual for the Long-Term Pavement Performance Program*. Report No. FHWA-RD-03-031, Federal Highway Administration, McLean, VA, 2003.
Minnesota Department of Transportation (MnDOT). *Introduction to the International Roughness Index*. Bituminous Smoothness Training Workshop. 2007.
Musunuru, G., Baladi, G., Dawson, T., Jiang, J., and Prohaska, M. Effective Systems for Rating Pavement Condition. *Transportation Research Record: Journal of the Transportation Research Board*, No. 2523, Washington, D.C., 2015, pp. 32–39.
North Carolina Department of Transportation (NCDOT). *Pavement Design Procedure AASHTO 1993 Method*. North Carolina Department of Transportation: Materials and Tests Unit – Pavement Section, Raleigh, NC, 2017.
Pologruto, M. Procedure for Use of Falling Weight Deflectometer to Determine AASHTO Layer Coefficients. *Transportation Research Record: Journal of the Transportation Research Board*, No. 1764, Washington, D.C., 2001, pp. 11-19.
Pologruto, M. *A Study of In Situ Pavement Material Properties Determined from FWD Testing. Vermont Agency of Transportation Pavement Design Committee*, Report No. RSCH008-

936, Montpelier, VT, 2004.
Prowell, B.D., James T., Bennert, T., and Jordan, J. Evaluation of Moduli and Structural Coefficients of South Carolina's Asphalt Base Mixtures. *Transportation Research Record: Journal of the Transportation Research Board*, No. 2641, Washington, D.C., 2017, pp. 21–28.
Richardson, D.N., Lambert, J.K., and Kremer, P.A. *Determination of AASHTO Layer Coefficients*. Missouri DOT (MODOT), Final Report 90-5: Volume I - Bituminous Materials, Jefferson City, MO, 1994.
Robbins, M. and Tran, N. *Review of Initial Service Life Determination in Life-Cycle Costs Analysis (LCCA) Procedures and in Practice*. National Center for Asphalt Technology Report No. 18-02, Auburn AL, 2018.
Robbins, M., Tran, N., & Copeland, A. Determining the Age and Smoothness of Asphalt and Concrete Pavements at the Time of First Rehabilitation using Long-Term Pavement Performance Program Data. *Transportation Research Record: Journal of the Transportation Research Board*, No. 2672, Washington, D.C., 2018, pp. 1-10.
Rohde, G. Determining Pavement Structural Number from FWD Testing. *Transportation Research Record: Journal of the Transportation Research Board*, No. 1448, Washington, D.C., 1994, pp. 61–68.
Sayers, M.W., Gilespie, T.D., and Paterson, W.D.O. *Guidelines for Conducting and Calibrating Road Roughness Measurements.* World Bank Technical Paper 46, International Bank for Reconstruction, Washington, D.C., 1986.
Sayers, M.W. and Karamihas, S.M. *The Little Book of Profiling: Basic Information about Measuring and Interpreting Road Profiles*. University of Michigan, Ann Arbor MI, 1998.
Shook, J.F. and Finn, F.N. Thickness Design Relationships for Asphalt Pavements. Proceedings, *1st International Conference on Structural Design of Asphalt Pavements*, Ann Arbor, MI, 1962, pp. 640-687.
Skok, E.L., JR., and Finn, F.N. Theoretical Concepts Applied to Asphalt Concrete Pavement Design, Proceedings, *1st International Conference on Structural Design of Asphalt Pavements*, Ann Arbor, MI, 1962, pp. 412-440.
Smith B.C. and Diefenderfer B.K. *Development of Truck Equivalent Single-Axle Load (ESAL) Factors Based on Weigh-in-Motion Data for Pavement Design in Virginia*. Virginia Transportation Research Council, Report No. VTRC 09-R18, Charlottesville, VA, 2009.
Spangler, E. B. and Kelly, W. J. GMR Road Profilometer - A Method for Measuring Road Profile. *Highway Research Record*, No. 121, 1966, pp. 27-54.
Timm, D.H., Robbins, M.M., Tran, N., and Rodezno, C. *Recalibration Procedures for the Structural Asphalt Layer Coefficient in the 1993 AASHTO Pavement Design Guide*. National Center for Asphalt Technology (NCAT), Report No. 14-08, Auburn, AL, 2014.
Ullidtz, P. A Fundamental Method for Prediction of Roughness, Rutting and Cracking of Pavements. *Journal of the Association of Asphalt Paving Technologists*, No. 48, 1979, pp. 557-586.
United States Army Corps of Civil Engineers (USACE). *Pavement Maintenance Manual*. Washington, D.C., 1982.
Van der Poel, C. *A General System Describing the Visco-Elastic Properties of Bitumens and its Relation to Routine Test Data*. Shell Bitumen, Reprint No. 9, Shell Laboratorium-Koninklijke, Amsterdam, 1954.
Van Til, C.J., McCullough, B.F., Vallerga, B.A., and Hicks R.G. *Evaluation of the AASHO*

Interim Guides for Design of Pavement Structures. NCHRP No. 128, Washington, D.C., 1972.

Van Wijk, A.J. *Determination of the Structural Coefficients of a Foamed Asphalt Recycled Layer*. Joint Highway Research Program (JHRP) Report No. 84-1, Purdue University, West Lafayette, IN, 1984.

Von Quintus, H.L. *Evaluation of Procedure to Assign Structural Layer Coefficients for Use in Flexible Pavement Design*. Kansas DOT (KDOT), Final Report No. KS-07-9, Topeka, KS, 2007.

Walker, R.S. and Hudson, W.R. *A Correlation Study of the Mays Road Meter with the Surface Dynamics Profilometer*. Research Report No. 156-1, Center for Highway Research, The University of Texas at Austin, Austin, TX, 1973.

Wang, M.C. and Larson T.D. Performance Evaluation for Bituminous Concrete Pavements at the Pennsylvania State Test Track. *Transportation Research Record: Journal of the Transportation Research Board*, No. 632, Washington, D.C., 1977, pp. 21–27.

Watanatada, T., Harral, C.G., Paterson, W.D.O., Dhareshwar, A.M., Bhandari, A., and Tsunokawa, K. *The Highway Design and Maintenance Standard Model: Volume 1*. World Bank, International Bank for Reconstruction, Washington, D.C., 1987.

Zamora A.E.J. *A Discrete Roughness Index for Longitudinal Road Profiles*. Ph.D. Dissertation, Virginia Polytechnic Institute and State University, Blacksburg VA, 2016.

APPENDIX B: SUPPLEMENTARY INFORMATION ON PAVEMENT PERFORMANCE MODELS

This appendix provides an overview of the models and supplementary information supporting the pavement performance model development. These models are used to convert between *PCR* and *PSI*.

Data

The NCDOT has collected pavement condition data since 1982. Every two years, 100% of its flexible pavements and 0.2 mile of every mile of rigid pavement are surveyed. Historically this data was collected via windshield survey carried out by trained teams of raters that drove the roads and inspected them for different distresses. A description of the procedure followed by NCDOT personnel to rate the severity of each distress type can be found in the pavement condition survey manual (NCDOT 2012).

The windshield survey database was downloaded from the NCDOT PMS, as shown in Figure B.1. The database contains the *PCR* (a composite index calculated by applying a series of discount factors based on the distress type and severity), referred in the database as NCDOT Rating Number), and the different distresses categorized in four severity levels N: None, L: Low, M: Moderate, and S: Severe. The only numeric value is reported for the alligator cracking.

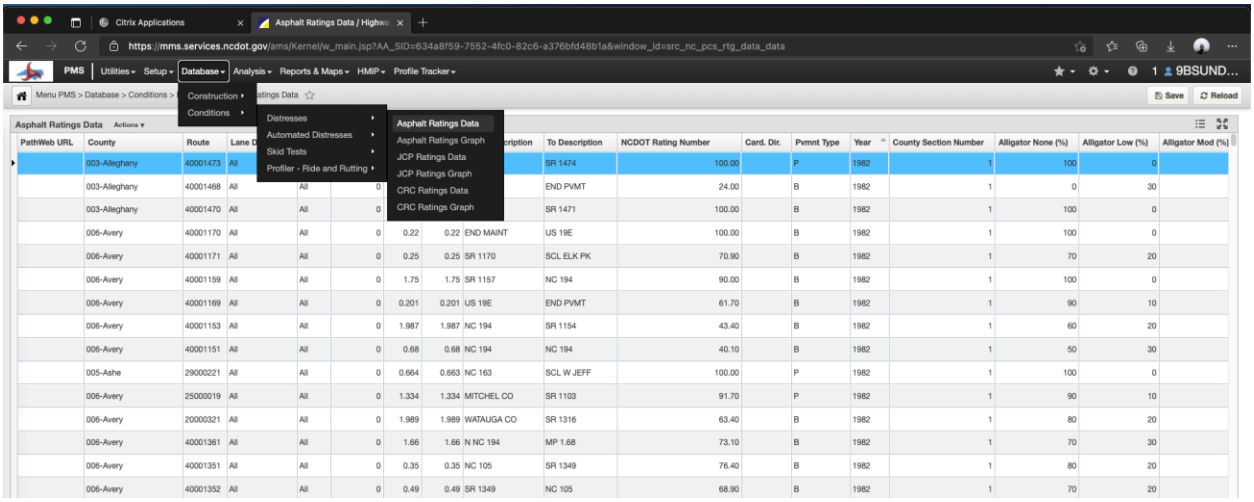

Figure B.1. Windshield survey database in the PMS.

Starting with the 2013 cycle (started in November of 2012), the NCDOT began performing automated surveys on their primary network. These condition data contain various distress ratings collected from asphalt, composite, jointed concrete (JCP), and continuously reinforced concrete (CRC) pavements as well as shoulders. The NCDOT has only collected automated data from Interstate, US, and NC routes. The condition data for SR routes continues to be collected by windshield surveys. The automated survey was downloaded from the PMS as indicated in Figure B.2, and the list of distresses with their respective unit measured in the automated survey is summarized in Table B.1. Note that after the implementation of the automated survey, the NCDOT started to compute the *PCR* using the distresses collected with the automated survey. For this project, these *PCR* values were also downloaded and used to develop the performance models.

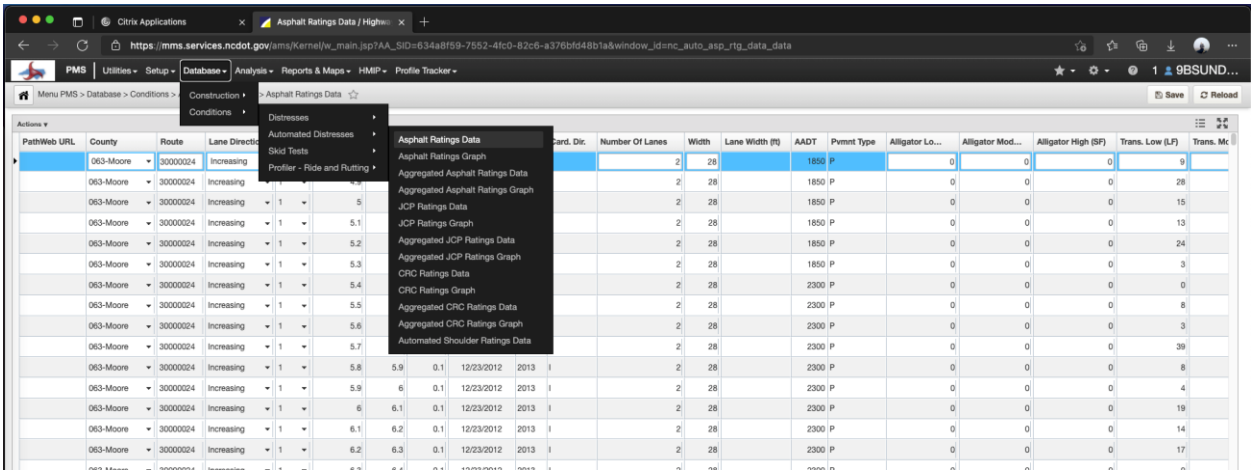

Figure B.2. Automated survey database in the PMS.

Table B.1. List of Asphalt Pavement Distresses.

Distress	Unit	Low Severity	Moderate Severity	High Severity
Alligator Cracking	Square feet	x	x	x
Bleeding	Square feet	x		x
Delamination	Square feet		Single Rating	
Longitudinal Cracking	Linear feet	x	x	x
Longitudinal Lane Joint	Linear feet	x	x	x
Patching Area – Non Wheel Path	Square feet			
Patching Area – Wheel Path	Square feet		Single Rating	
Ravelling	Square feet	x	x	x
Reflective Longitudinal Cracking	Linear feet	x	x	x
Reflective Transverse Cracking	Linear feet	x	x	x
Rutting – Maximum Average Depth	Inch.		Single Rating	
Transverse Cracking	Linear feet	x	x	x

After downloading and organizing the data, the procedure of analysis depicted in Figure B.3 was used. First individual performance models were obtained for the *PCR* and *IRI*. For the former index, a sigmoidal model was selected and for the latter one an exponential model was chosen. Afterwards, the two models were combined to derive an expression that relates *PCR* and *IRI*.

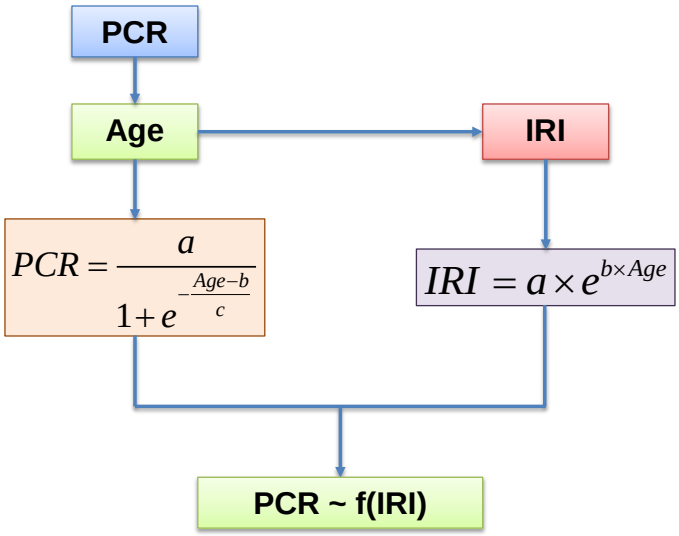

Figure B.3. Procedure of analysis used to calibrate a relationship between *PCR* and *IRI*.

***PCR* Deterioration Model**

To develop *PCR* deterioration models, the roads were first grouped by functional class, i.e., interstates, US Routes and NC Routes. For each of the road classes, a box plot like the one shown in Figure B.4 was created, so that the research team could appreciate the distribution of values by each year and to identify the respective outliers. In in the case of Figure B.4, the outliers are identified by a red cross and are based on the interquartile range (IQR), (P_{25} - 1.5(IQR) < x < P_{75} + 1.5(IQR)). Table B.2 summarizes the initial number of records used for each road class and the final number that were used for calibration after following the filtering process above and removing the outliers.

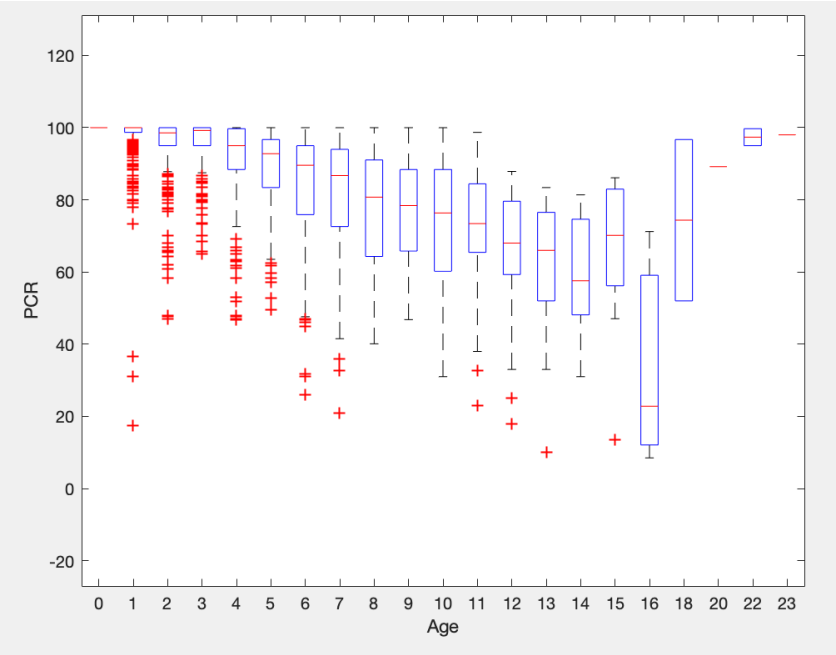

Figure B.4. *PCR* Box Plot for Interstates.

Table B.2. Number of *PCR* Records Used in the Analysis.

Road Class	Original Number of Records*	Remaining Number of Records after the filtering process
Interstates	39,960	3,782
US Routes	245,828	12,145
NC Routes	237,133	16,843

*A record is a *PCR* value taken at a year *t* in each pavement section.

The sigmoidal model shown in Figure B.3 has three coefficients. These coefficients were calibrated by minimizing the sum of squared errors. The resulting coefficients for each deterioration model of each road category are summarized in Table B.3. In addition, the fitted models as well as the dataset used for their calibration are presented in Figure B.5. The two data sources used in the calibration process are indicated in the figure, the 'Before 2013' purple crosses represent the windshield survey measurements, and the black filled dots represent the automated survey measurements. As indicated overall the two datasets are consistent and follow the same trend.

Table B.3. Coefficients of the *PCR* Deterioration Models.

Parameters	Interstates	US Routes	NC Routes
a	102.77	111.00	116.00
b	12.97	12.98	12.68
c	-3.61	-5.88	-6.92

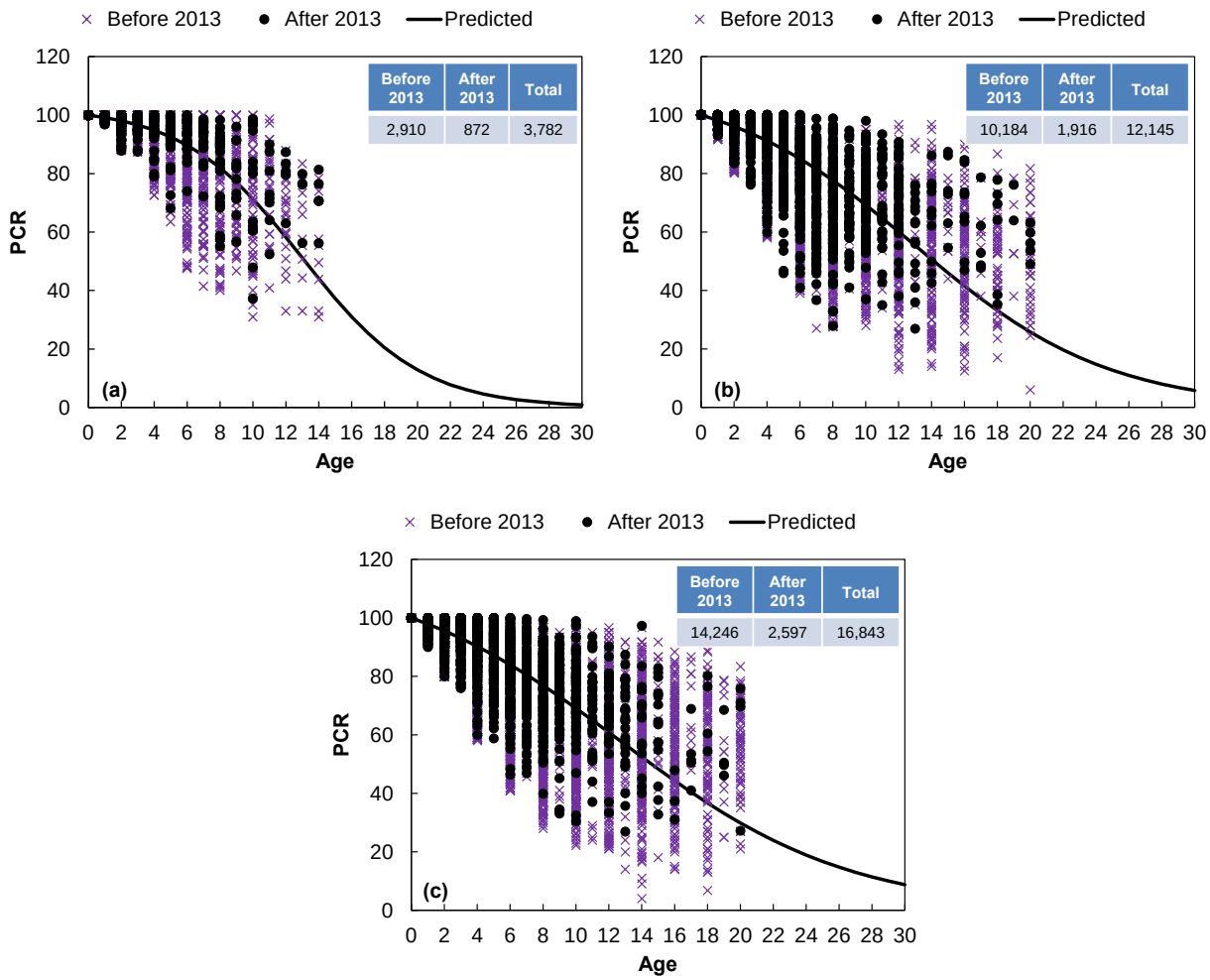

Figure B.5. *PCR* deterioration models, (a) Interstates, (b) US Routes, and (c) NC Routes.

IRI Deterioration Model

Similarly, the *IRI* deterioration models were established based on the road class. Attempts to segregate the models more finely (for example based on traffic level) did not improve the overall model fit. The same outlier identification process was applied, and the resulting sample size is indicated in Table B.4. The functional form used to fit the model is exponential and the coefficients of the model for each road category are presented in Table B.5. Likewise, the fitted deterioration models are plotted over the *IRI* records used in the calibration process (Figure B.6).

Table B.4. Number of *IRI* Records Used in the Analysis.

Road Class	Original Number of Records*	Remaining Number of Records after the filtering process
Interstates	39,960	2,249
US Routes	245,828	4,816
NC Routes	237,133	5,729

*A record is a *IRI* value taken at a year *t* in each pavement section

Table B.5. *IRI* Deterioration Model Coefficients.

Parameters	Interstates	US Routes	NC Routes
a	61.8196	76.5420	90.9158
b	0.0242	0.0239	0.0227

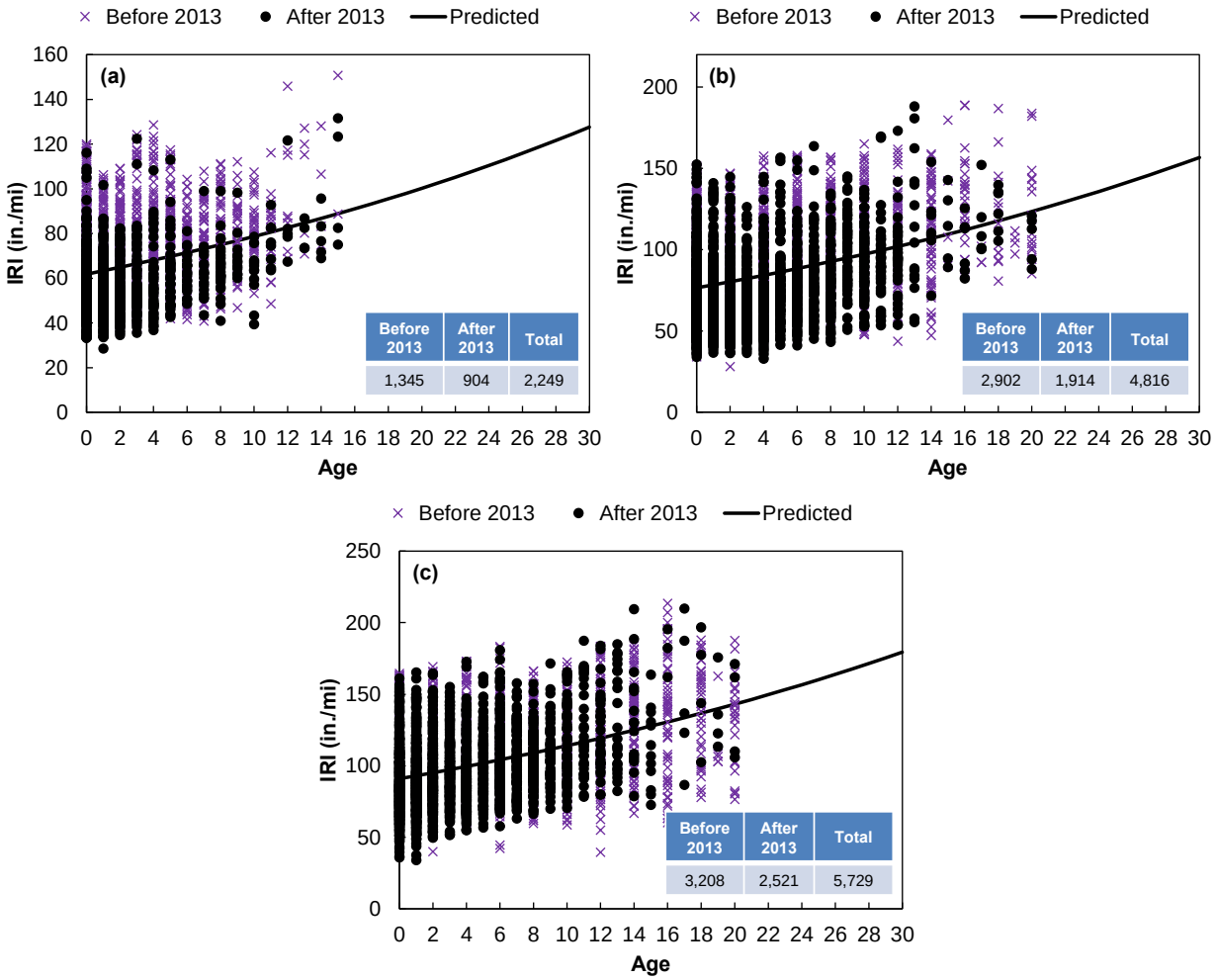

Figure B.6. *IRI* deterioration models, (a) Interstates, (b) US Routes, and (c) NC Routes.

Appendix B References

North Carolina DOT (NCDOT). *Pavement Condition Survey Manual*. North Carolina DOT, Raleigh, NC, 2012.

APPENDIX C: SUPPLEMENTARY INFORMATION ON LAYER COEFFICIENT CALIBRATION

Calibration Trials

Two separate performance databases were used in this research. The first database (referred to as the Support Model Database) consisted of *PCR* and *IRI* data from more than 76 pavement sites and was used to develop the support models to predict *PSI* from *PCR*. The second database (referred to as the Calibration Database) consisted of 33 separate pavement sites and was used to calibrate the layer coefficients. The properties of pavement sites is summarized in Table C.1.

To calibrate the layer coefficients that best represent the structures in this study and categorize them in a practical way, many different calibration methods have been explored. Table C.2 and Table C.3 summarize the different trials, the associated parameters/values used in those trials, and the resulting layer coefficients. As can be seen from Table C.2, the trials varied by whether analysis was done on a section-by-section basis (i.e., determining the optimal layer coefficients independently for each section) or Universal basis; by the number of points on the performance curve that were used for optimization; how the roads were categorized (or not categorized); and whether the base and ABC layer structural number values were set to constant values or included in the optimization process. A total of 45 trials have been performed using different combinations of these factors, and the knowledge gained from these has provided the team with a number of principle guidelines for the final coefficient determinations.

The first finding from the trials was that calibration could not be completed on a section-by-section basis, as done in Trials 1-6 because there was a uniqueness issue. The team found that while the total optimized structural number would be consistent, that the values of the individual layer coefficients could vary substantially depending on the initial values selected for the coefficients. The team also learned from the early simulations that using all of the measured *PCR* values for optimization was problematic because the AASHTO performance equation did not do a good job of capturing the total pavement deterioration function. North Carolina roadways, it seems, demonstrate a slower performance degradation early on, but then a much more rapid deterioration curve than the AASHTO equation suggests should occur. As result, the research team found that it was necessary to use only those points with *PCR* values less than 100. In Trials 4 through 16 (except for Trial 7) the team investigated the ideal points to use for the optimization by performing two different analyses; (a) using only the last data point and (b) using all points with *PSI* less than certain threshold (0.1 less than maximum *PSI* value). Through these trials, it was found that using the last data point resulted in better identification of the design life and so this approach was the only one followed for subsequent analysis.

Trials 4-16 also showed some limitations with using universal coefficients because the resulting average errors were higher than desirable. Thus, in subsequent trials, pavement sections were categorized according to factors such as road type, overall fitting error, traffic levels, surface type, and pavement type (ABC or FDA). In Trials 17, 18, 30, and 31, sections were categorized based on the squared error (SE) associated with their previous calibration trials. In Trials 19, 20, 34, and 35, sections were grouped based on the ESALs at the construction year as calculated from de-aging traffic volumes from the NCDOT interactive GIS map. For de-aging the traffic volumes, the growth rate was first calculated based on the multiple years of survey traffic volumes that were available. Then, this growth rate was used, along with the year of construction, year of the first available survey traffic data, and the traffic data at the first available survey traffic data year, to

calculate the traffic volume at the year of construction. The standard NCDOT traffic equation, Equation (53), was used for this calculation.

$$ADT_a = ADT_c \times \left(1 + \frac{\%Growth}{100 \times 365.25}\right)^{((Year_a - Year_c) \times 365.25)} \quad (53)$$

where ADT_a is Average Annual Daily Traffic in year of the first available survey traffic data, ADT_c is Average Annual Daily Traffic in year of construction, $Year_a$ is year of the first available survey traffic data, $Year_c$ is the year of construction, and $\%Growth$ is the percent growth rate.

In Trials 21, 22, 32, and 33, sections were categorized based on the 20-year cumulative ESALs from the project design contracts. The 20-year ESALs based on the NCDOT interactive GIS map traffic volumes were used to categorize sections in Trials 23, 24, 25, 26, 36, 37, 38, and 39. In Trials 27, 28, 40, and 41, the pavement sections were categorized based on their surface mix type. The structural number (SN) for each pavement section depends on the mathematical combination of layer thicknesses and coefficients, and Trials 10 through 16 (except for 14) indicated that, mathematically, the calibration results are sensitive to the combination of layers, i.e., considering the AC-surface and AC-intermediate layers as one layer or two separate layers or considering the AC-intermediate and AC-base layers as one layer or two separate layers. Most of the pavement sections in this analysis are ABC pavements and it was presumed that the overall calibration results might be driven by these sections which might not be representable for FDA pavements. So, in Trials 42 through 45, sections were grouped based on the pavement types.

It was also observed that fixing the coefficient of AC-Base and/or ABC layers to constant (universal) values could be practical. Therefore, in Trials 9, 11, 13, 31, 33, 35, 37, 39, 41, and 45, the coefficient of ABC layer was fixed to the current value of 0.14 and the coefficient of other layers were calibrated. Also, in Trials 14, 15, 16, 18, 20, 22, 24, 26, 28, and 43, the coefficient of AC-base and ABC layer was fixed to the current values of 0.3 and 0.14, respectively. It was also observed that when the AC-base layer was not fixed that most of the results suggested decreasing the coefficient of this layer to a value between 0.1 and 0.3. However, these values are substantially lower than any reported in the literature for AC-base layers. These results might be due to numerous unknown elements inherent in the performance prediction and calibration process. Thus, the research team chose to fix the AC-base coefficient to a slightly lower value of 0.25 in Trials 29, 30, 32, 34, 36, 38, 40, and 44 to examine how the errors were affected. In addition, minor modifications such as using two conversion models that relate *IRI* to *PSI* (Gulen and Al-Omari), eliminating sections with unusually long or short life, changing the initial *PSI* values in analysis, and using SN equations as the basis for calibrations were tried in Trials 4 through 7.

In summary, the calibration process was evaluated and modified by changing the influential elements in the calibration analysis through a total of 45 trials. The knowledge gained from these trials established that the calibration results are better fitted and more practical if the following guidelines are followed: universal coefficients for categorized sections calibrated based on fitting the last data point. To be more specific, categorization should be practical from the design standpoint. This requirement means that factors that would be known at design, such as ESALs, surface mix type or other elements should be chosen. It was decided that the 20-year ESAL value from the design contract yielded a practical and effective categorization.

In the initial set of trials discussed above, a set of guidelines were established on how to approach the calibration process. In a supplementary set of trials, the categorization of the sections and the

best fitting predefined values to fix the coefficients in calibration were explored as presented in Table C.4.

- In Trial 1, NCDOT categorization of ESALs was followed (less than 3 million, between 3 and 30 million, and more than 30 million) and sensitivity analysis was conducted to determine a set of predefined values for AC-base and ABC layers that yield to lowest SSE. The results were not practical specifically for the category with high volume of traffic (more than 30 million) because the coefficients for AC-base and ABC were unreasonably high and low, respectively.
- Trials 2 – 5 were created in order to explore other approaches to categorization of ESALs. Among these trials, Trial 5 showed better fitting results because in other trials the results were equal to calibration constraints, i.e., the coefficients for AC-base and ABC were unreasonably high or low.
- Trials 6 – 8, evaluated different predefined fixed values of 0.25 and 0.3 for AC-base and 0.14 for ABC. In Trial 9 a comprehensive sensitivity analysis was conducted by calibrating a universal values for AC-surface/int. and fixing both AC-base and ABC. The AC-base values were changed in a range between 0.15 and 0.3. The ABC values varied from 0.1 to 0.23. These values were dictated by the observations from the sensitivity analysis. The sensitivity analysis is summarized in Figure C.1. In this figure, the SSE vs. AC-surface/int. coefficients is plotted and each symbol represents a certain AC-b value and each color represents a certain ABC value. The label for certain data points is shown in this figure to determine the range on changes in values. The result of the sensitivity analysis indicated that AC-b value of 0.18 and ABC value of 0.19 results in the lowest SSE. At this point of the analysis, the research team made two adjustments which resulted in exploring additional set of calibration trials. The first adjustment was modifying the mixed truck factor (*MTF*) due to an error in the ESALs calculations. The research team revisited the truck factor calibration and found an error regarding the consideration of lane distribution factor (LD) and directional distribution factor (DD). This error was fixed and mixed truck factors (*MTF*) and ESALs were modified. The second adjustment was the elimination of one section that seemed to be driving the calibration results to a certain direction. In order to show how the elimination of that one section improve the calibration results is presented in Figure C.2 as one example. In this figure, after elimination of that one section the data points are better distributed and the SSE is lower.
- Trials 10 – 15 tried to find universal coefficients for all sections. The results from calibrating the coefficients for all layers in Trial 10 showed that the ABC coefficient was higher than the AC-base coefficient, which in terms of structural performance was not intuitive or expected. In fact, this analysis showed that all layer coefficients except the ABC coefficients were lower than those currently used by the DOT. Because of this observation, it was decided to fix ABC and AC-base to predefined values, and freely optimize the other two. In order to define fixed values, the sensitivity analysis conducted in Trial 9 was considered as the initial estimation. Based on that analysis it was decided to fix the AC-base value to 0.2 and since it is more intuitive to have a lower coefficient for ABC than the AC-base, the ABC coefficient was fixed to 0.14. Since a lower ABC coefficient than the sensitivity analysis was considered, higher values (0.25 and 0.3) were also evaluated in trials to determine a combination with best fit and the lowest SSE values. In Trial 13, the coefficient of AC-base was fixed to 0.2 and in Trial 14, the coefficient of ABC was fixed to 0.14. The calibration results of optimizations conducted fixing ABC or

AC-base indicate that the coefficients of AC-base and ABC are close to each other, which means these two layers have the same structural effect in pavements (which is unexpected). Based on these observations, it was decided perform calibration by fixing both AC-base and ABC coefficients. Trials 11, 12, and 15 were created. In the first, both ABC and AC-base coefficients were chosen as the current DOT values. In the second and third trials, the ABC coefficient was kept at the current default value (0.14), but AC-base was set to 0.25 and 0.20, respectively. The results of these calibrations show that the calibrated coefficient of AC-surface/int. are very close to each other in all three cases (0.419, 0.416, and 0.412), but that the last values (Trial 15) yielded the lowest error.

- Trials 16 – 30 evaluated different approaches for categorization. In Trial 16, the coefficient for ABC layer was higher than that for AC-base layer for all traffic levels. In Trial 17, the coefficients for AC-base and ABC were unreasonably low for moderate and low levels of traffic (in the respective traffic categorization). In Trial 18, for high level of traffic (in the respective traffic categorization) the coefficients for AC-base and ABC were unpractically high and low, respectively. The calibrated coefficients for Trials 19 and 25 were better fitted than other trials. For these two categorization approaches in Trials 19 and 25, predefined fixed values (based on Trial 9 as discussed before in Trials 11 – 15) were tried in Trials 20 – 24 and Trials 26 – 30. In Trials 19 – 25, it was evident that the trend of the coefficients with traffic levels is unexpected, i.e., it is expected that the coefficient increases from low traffic level to moderate traffic level and again it decreases as the traffic level increases from moderate to high traffic level (in the respective traffic categorization), and this issue is not resolved with using different predefined values for different combination of layers. Therefore, the categorization approach in Trials 25 – 30 was chosen as the final categorization approach (less than 2.5 million and more than 2.5 million ESALs) in the calibration process. The results of the calibration in Trial 25 when all layers were optimized showed that the coefficients of ABC for low traffic level (less than 2.5 mil.) and AC-base for high traffic level (more than 2.5 mil.) were much lower than default values. In Trial 28 where the ABC coefficient was fixed to 0.14, a very small value of AC-base coefficient for high traffic level was found and in Trial 29 where the AC-base coefficient was fixed to 0.2, a very high value of ABC coefficient for high traffic level was found. Based on these observations, it was decided to fix both AC-base and ABC to default values or certain values (AC-base to 0.25 or 0.2 and ABC to 0.14) in Trials 26, 27, and 30. The results of the calibration showed that fixing the AC-base and ABC values to 0.2 and 0.14 (Trial 30) yields the lowest SSE error compared to the alternative calibrations.

In summary, the calibration process was further evaluated and finalized through a total of 30 trials. The knowledge gained from these trials established that the calibration results would be fitted better and more practically if the calibration was conducted either universally or categorically. The categorization was established to be two categories: less than 2.5 million and more than 2.5 million 20-year ESALs. It was also determined that the AC-base and ABC coefficients need to be fixed to a predefined value. Through different trials it was determined that these predefined values should be 0.2 and 0.14 for AC-base and ABC, respectively.

Table C.1. Summary of Properties of Pavement Sites.

Route ID	County	Road Name	Structure	Cum. ESAL	Const. Year	Cont. Avail.
40001324067 (1)	Onslow	Ramsey	1.5 in., S9.5C, 3 in., I19.0C	--	2011	×
40001324067 (2)	Onslow	Ramsey	1.5 in., S9.5C, 3 in., I19.0C	--	2011	×
40002323097	Wilkes	Berrys	2 in., S9.5B, 2.5 in., I19.0B, 6 in., ABC	--	2002	×
40001134099	Yadkin	Billy Reynolds	2 in., S9.5B, 1.5 in., I19.0B, 6 in., ABC	--	2002	×
40001199099	Yadkin	Short	2 in., S9.5B, 1.5 in., I19.0B, 6 in., ABC	--	2004	×
40001209099	Yadkin	Jim West	2.75 in., S12.5B, 6 in., ABC	--	2004	×
40001210099	Yadkin	Trails End	2.75 in., S9.5B, 6 in., ABC	--	2004	×
40001444099	Yadkin	Vanhoy	2.75 in., S9.5B, 6 in., ABC	--	2004	×
40001141099	Yadkin	Reavis	1.25 in., S9.5B, 3 in., I19.0B, 10 in., ABC	--	2002	×
40001141099	Yadkin	Reavis	1.25 in., S9.5B, 3 in., I19.0B, 10 in., ABC	--	2002	×
40001150099	Yadkin	Hoots	2 in., S9.5B, 3 in., I19.0B, 10 in., ABC	--	2002	×
40001166099	Yadkin	Bethel Church	1.25 in., S9.5B, 3 in., I19.0B, 10 in., ABC	--	2002	×
40001415099	Yadkin	Beamer	2 in., S9.5B, 3 in., I19.0B, 10 in., ABC	--	2004	×
40002325097	Wilkes	Antioch Church	2 in., S9.5B, 3 in., I19.0B, 10 in., ABC	--	2002	×
40002325097	Wilkes	Antioch Church	2 in., S9.5B, 3 in., I19.0B, 10 in., ABC	--	2002	×
40001150099	Yadkin	Hoots	2 in., S9.5B, 3 in., I19.0B, 10 in., ABC	--	2002	×
30000012028	Dare	NC 12	2.5 in., S9.5B, 3 in., I19.0B, 8 in., ABC	--	2002	×
40001002096	Wayne	East Main	2 in., S9.5B, 2.5 in., I19.0B, 8 in., ABC	--	2002	×
40001002096	Wayne	East Main	2 in., S9.5B, 2.5 in., I19.0B, 8 in., ABC	--	2002	×
40002309097 (1)	Wilkes	Cedar Forest	2 in., S9.5B, 2.5 in., I19.0B, 10 in., ABC	--	2002	×
40002309097 (2)	Wilkes	Cedar Forest	2 in., S9.5B, 2.5 in., I19.0B, 10 in., ABC	--	2002	×
40002345097	Wilkes	Mcgamp	2 in., S9.5B, 2.5 in., I19.0B, 3 in., B25.0B, 8 in., ABC	--	2002	×
40003632060 (1)	Mecklenburg	Ardrey Kell	3 in., S12.5B, 3 in., I19.0B, 6 in., ABC	--	2000	×
40003632060 (2)	Mecklenburg	Ardrey Kell	3 in., S12.5B, 3 in., I19.0B, 6 in., ABC	--	2000	×
40003632060 (3)	Mecklenburg	Ardrey Kell	3 in., S12.5B, 3 in., I19.0B, 6 in., ABC	--	2000	×
40001430013 (2)	Cabarrus	Kannapolis	2.5 in., S9.5B, 3 in., I19.0B, 8 in., ABC	--	2007	×
20000070049 (1)	Iredell	US 70	2.75 in., S12.5C, 4.25 in., I19.0C, 9 in., B25.0B	--	2002	×
20000064019	Chatham	US 64	2.75 in., S12.5B, 3 in., I19.0B, 10 in., ABC	--	2002	×
20000421099 (1)	Yadkin	US 421	2.75 in., S12.5C, 3.5 in., I19.0C, 10 in., ABC	--	2002	×
20000421099 (2)	Yadkin	US 421	2.75 in., S12.5C, 3.5 in., I19.0C, 10 in., ABC	--	2002	×
20000421099 (3)	Yadkin	US 421	2.75 in., S12.5C, 3.5 in., I19.0C, 10 in., ABC	--	2002	×
20000421099 (4)	Yadkin	US 421	2.75 in., S12.5C, 3.5 in., I19.0C, 10 in., ABC	--	2002	×
20000421099 (5)	Yadkin	US 421	2.75 in., S12.5C, 2.75 in., I19.0C, 4 in., B25.0B, 10 in., ABC	--	2003	×
20000421099 (6)	Yadkin	US 421	2.75 in., S12.5C, 2.75 in., I19.0C, 4 in., B25.0B, 10 in., ABC	--	2003	×
20400421099 (1)	Yadkin	US 421	2.75 in., S12.5C, 2.75 in., I19.0C, 4 in., B25.0B, 10 in., ABC	--	2003	×
20400421099 (2)	Yadkin	US 421	2.75 in., S12.5C, 2.75 in., I19.0C, 4 in., B25.0B, 10 in., ABC	--	2003	×
20400421099 (3)	Yadkin	US 421	2.75 in., S12.5C, 2.75 in., I19.0C, 4 in., B25.0B, 10 in., ABC	--	2003	×

Route ID	County	Road Name	Structure	Cum. ESAL	Const. Year	Cont. Avail.
20400421099 (4)	Yadkin	US 421	2.75 in., S12.5C, 3.5 in., I19.0C, 8 in., ABC	--	2002	×
20400421099 (5)	Yadkin	US 421	2.75 in., S12.5C, 3.5 in., I19.0C, 8 in., ABC	--	2002	×
20400421099 (6)	Yadkin	US 421	2.75 in., S12.5C, 3.5 in., I19.0C, 8 in., ABC	--	2002	×
20400421099 (7)	Yadkin	US 421	2.75 in., S12.5C, 3.5 in., I19.0C, 8 in., ABC	--	2002	×
20400421099 (8)	Yadkin	US 421	1.25 in., S12.5C, 3.5 in., I19.0C, 10 in., ABC	--	2001	×
20400421099 (9)	Yadkin	US 421	1.25 in., S12.5C, 3.5 in., I19.0C, 10 in., ABC	--	2001	×
40001125099	Yadkin	Asbury Ch.	2.75 in., S9.5B, 2 in., I19.0B, 4 in., B25.0B	187,033	1999	✓
40001211051	Johnston	Morgan	2.5 in., S9.5B, 5 in., B25.0B	230,263	2000	✓
40001412033	Edgecombe	Morn.Star Ch.	2.5 in., S9.5B, 2.5 in., I19.0B, 6 in., ABC	315,607	2002	✓
40001933026	Cumberland	Pembroke	2 in., S9.5B, 6 in., B25.0B	366,385	1999	✓
40001452077	Richmond	Millstone	3 in., S9.5B, 3 in., B25.0B	437,827	2004	✓
40002705023 (1)	Cleveland	Kings Mnt.	2.5 in., S9.5B, 2 in., I19.0B, 3 in., B25.0B	925,811	2006	✓
40002705023 (2)	Cleveland	Kings Mnt.	2.5 in., S9.5B, 2 in., I19.0B, 3 in., B25.0B	925,811	2006	✓
40001546041	Guilford	Guilford College	2.5 in., S12.5B, 4.5 in., I19.0B, 6 in., ABC	1,577,518	1999	✓
40003632060 (4)	Mecklenburg	Ardrey Kell	3 in., S12.5B, 3 in., I19.0B, 6 in., ABC	1,765,043	2000	✓
40002200036	Gaston	Cox	2.5 in., S12.5B, 2.5 in., I19.0B, 8 in., ABC	1,810,820	1999	✓
40002433001	Alamance	Moore	2.5 in., S9.5B, 3.5 in., I19.0B, 6 in., ABC	1,843,185	2000	✓
30000054001 (1)	Alamance	NC 54	2.5 in., S9.5B, 4.5 in., I19.0B, 3 in., B25.0B, 6 in., ABC	2,126,676	1999	✓
30000054001 (2)	Alamance	NC 54	2.5 in., S9.5B, 4.5 in., I19.0B, 3 in., B25.0B, 6 in., ABC	2,126,676	1999	✓
30000054001 (3)	Alamance	NC 54	2.5 in., S9.5B, 4.5 in., I19.0B, 3 in., B25.0B, 6 in., ABC	2,126,676	1999	✓
40001765099	Yadkin	Unifi Industrial	2.5 in., S12.5B, 3 in., I19.0B, 8 in., ABC	2,496,268	1999	✓
10000140065	N. Hanover	I-140	2.5 in., S9.5B, 3.5 in., I19.0B, 8 in., ABC	2,804,319	2000	✓
10600140065 (1)	N. Hanover	I-140	2.5 in., S9.5B, 3.5 in., I19.0B, 8 in., ABC	2,804,319	2000	✓
10600140065 (2)	N. Hanover	I-140	2.5 in., S9.5B, 3.5 in., I19.0B, 8 in., ABC	2,804,319	2000	✓
40001954032	Durham	NE Creek Pkwy	2.5 in., S9.5B, 4.5 in., I19.0B, 6 in., ABC	2,888,616	1997	✓
30000024013	Cabarrus	NC 24	2.5 in., S12.5C, 3.5 in., I19.0C, 8 in., ABC	2,896,821	1998	✓
20000001077	Richmond	US 1	3 in., S9.5C, 2.5 in., I19.0C, 8 in., ABC	3,310,087	2006	✓
30000087043 (1)	Harnett	NC 87	2.5 in., S12.5C, 3 in., I19.0C, 8 in., ABC	3,499,288	1998	✓
30000087043 (2)	Harnett	NC 87	2.5 in., S12.5C, 3 in., I19.0C, 8 in., ABC	3,499,288	1998	✓
30000157032 (1)	Durham	NC 157	3 in., S12.5C, 4 in., I19.0C, 7 in., B25.0C	4,670,465	2000	✓
30000157032 (2)	Durham	NC 157	3 in., S12.5C, 4 in., I19.0C, 7 in., B25.0C	4,670,465	2000	✓
30000109029	Davidson	NC 109	2.5 in., S9.5B, 4.5 in., I19.0B, 8 in., ABC	4,773,060	2000	✓
20000070041 (3)	Guilford	US 70	2.5 in., S12.5B, 4.5 in., I19.0B, 4.5 in., B25.0B	6,500,644	2002	✓
20000070049 (2)	Iredell	US 70	2.75 in., S12.5B, 4.25 in., I19.0B, 9 in., B25.0B	6,719,539	1999	✓
30000055092 (1)	Wake	NC 55	2.5 in., S12.5C, 4 in., I19.0C, 8 in., B25.0C	8,321,784	2002	✓
30000055092 (2)	Wake	NC 55	2.5 in., S12.5C, 4 in., I19.0C, 8 in., B25.0C	8,321,784	2002	✓
10800485060	Mecklenburg	I-485	2.75 in., S12.5D, 2.75 in., I19.0D, 4 in., B25.0C, 8 in., ABC	11,172,986	2000	✓
10000074078	Robeson	I-74	4 in., S12.5C, 2.5 in., I19.0C, 3 in., B25.0C, 10 in., ABC	19,133,718	2004	✓
10600074078	Robeson	I-74	4 in., S12.5C, 2.5 in., I19.0C, 3 in., B25.0C, 10 in., ABC	19,133,718	2004	✓

Table C.2. Calibration Trials and Corresponding Calibration Elements.

Trial	Coefficient basis		Data points used for fitting				Categorized by:					Fix to current values:		Fix coefficient of AC-Base and ABC to 0.25 and 0.14
	Section-by-section	Univ.	All Points	Only *PCR* < 100	Only last point	Only points below threshold	Road type	Sq. error (SE)	ESALs	Surface mix type	Pave. type	ABC layer	AC-Base and ABC layers	
Trial 1	✓		✓				✓							
Trial 2	✓			✓			✓							
Trial 3	✓			✓										
Trial 4	✓			✓	✓	✓								
Trial 5	✓			✓	✓	✓								
Trial 6	✓			✓	✓	✓								
Trial 7		✓		✓										
Trial 8		✓		✓	✓	✓								
Trial 9		✓		✓	✓	✓						✓		
Trial 10		✓		✓	✓	✓								
Trial 11		✓		✓	✓	✓						✓		
Trial 12		✓		✓	✓	✓								
Trial 13		✓		✓	✓	✓						✓		
Trial 14		✓		✓	✓	✓							✓	
Trial 15		✓		✓	✓	✓							✓	
Trial 16		✓		✓	✓	✓							✓	
Trial 17		✓		✓	✓			✓						
Trial 18		✓		✓	✓			✓					✓	
Trial 19		✓		✓	✓				✓					
Trial 20		✓		✓	✓				✓				✓	
Trial 21		✓		✓	✓				✓					
Trial 22		✓		✓	✓				✓				✓	
Trial 23		✓		✓	✓				✓					
Trial 24		✓		✓	✓				✓				✓	
Trial 25		✓		✓	✓				✓					
Trial 26		✓		✓	✓				✓				✓	
Trial 27		✓		✓	✓					✓				
Trial 28		✓		✓	✓					✓			✓	
Trial 29		✓		✓	✓									✓
Trial 30		✓		✓	✓			✓						✓

Trial	Coefficient basis		Data points used for fitting				Categorized by:					Fix to current values:		Fix coefficient of AC-Base and ABC to 0.25 and 0.14
	Section-by-section	Univ.	All Points	Only *PCR* < 100	Only last point	Only points below threshold	Road type	Sq. error (SE)	ESALs	Surface mix type	Pave. type	ABC layer	AC-Base and ABC layers	
Trial 31		✓		✓	✓			✓				✓		
Trial 32		✓		✓	✓				✓					✓
Trial 33		✓		✓	✓				✓			✓		
Trial 34		✓		✓	✓				✓					✓
Trial 35		✓		✓	✓				✓			✓		
Trial 36		✓		✓	✓				✓					✓
Trial 37		✓		✓	✓				✓			✓		
Trial 38		✓		✓	✓				✓					✓
Trial 39		✓		✓	✓				✓			✓		
Trial 40		✓		✓	✓					✓				✓
Trial 41		✓		✓	✓					✓		✓		
Trial 42		✓		✓	✓						✓			
Trial 43		✓		✓	✓						✓		✓	
Trial 44		✓		✓	✓						✓			✓
Trial 45		✓		✓	✓						✓	✓		

Table C.3. Summary of Calibration Trials.

Calibration Trial	Description	Category	Results				SSE (Avg)
			AC-surface	AC-int.	AC-base	ABC	
Trial 1	-	NC Routes		0.490*	0.387*	0.155*	0.776
		US & Int. Routes		0.522*	0.379*	0.168*	1.867
Trial 2	-	NC Routes		0.359*	0.244*	0.102*	0.683
		US & Int. Routes		0.422*	0.278*	0.131*	0.62
Trial 3	• To determine the appropriate number of points, four last points, and last point, and points with *PSI* less than certain threshold (0.1 less than maximum *PSI* value) were considered.	Last point		0.318*	0.272*	0.147*	0.054
		Four last points		0.385*	0.288*	0.160*	0.430
		Points below threshold		0.375*	0.296*	0.166*	0.525
Trial 4	• Two conversion models, Gulen and Al-Omari models were used. In other trials, Gulen conversion model was used.	Last point (Gulen)		0.324*	0.270*	0.146*	0.03
		Last point (Al-Omari)		0.429*	0.320*	0.187*	0.00
		Pts below thr (Gulen)		0.357*	0.283*	0.158*	0.26
		Pts below thr (Al-Omari)		0.483*	0.375*	0.232*	0.04
Trial 5	• Sections with projection years to *PCR* of 60 more than 18 years were eliminated.	Last point		0.322*	0.270*	0.146*	0.03
		Points below threshold		0.355*	0.284*	0.159*	0.25
Trial 6	• Initial *PSI* based on NCDOT design guide was used and observed *PSI* values were shifted according to the difference between previous initial *PSI* values and NCDOT initial *PSI* values.	Last point		0.314*	0.248*	0.155*	0.03
		Points below threshold		0.347*	0.308*	0.162*	0.25
Trial 7	• Layer coefficients were optimized by solving an overdetermined system of SN equations, and • Sections with short life (less than 5 years) were eliminated.	-		0.542*	0.193*	0.036*	-
Trial 8	-	Last point		0.472	0.176	0.141	0.379
		Points below threshold		0.550	0.151	0.132	0.894
Trial 9	-	Last point		0.473	0.175	0.140	0.379
		Points below threshold		0.540	0.154	0.140	0.895
Trial 10	• AC-surface and AC-int layers were considered separately.	Last point	0.468	0.482	0.177	0.138	0.379
		Points below threshold	0.428	0.593	0.193	0.150	0.883
Trial 11	• AC-surface and AC-int layers were considered separately.	Last point	0.465	0.479	0.178	0.140	0.379
		Points below threshold	0.428	0.613	0.193	0.140	0.883
Trial 12	• AC-surface was considered separately. AC-int. and AC-base were considered as one layer.	Last point	0.900	0.189		0.127	0.409
		Points below threshold	0.900	0.237		0.155	0.955

Calibration Trial	Description	Category	Results				SSE (Avg)
			AC-surface	AC-int.	AC-base	ABC	
Trial 13	• AC-surface was considered separately. AC-int. and AC-base were considered as one layer.	Last point	0.859	0.197		0.140	0.410
		Points below threshold	0.900	0.247		0.140	0.958
Trial 14	-	Last point	0.464		0.300	0.140	0.421
		Points below threshold	0.522		0.300	0.140	0.965
Trial 15	• AC-surface and AC-int layers were considered separately.	Last point	0.213	0.671	0.300	0.140	0.406
		Points below threshold	0.204	0.758	0.300	0.140	0.920
Trial 16	• AC-surface was considered separately. AC-int and AC-base were considered as one layer.	Last point	0.499	0.440		0.140	0.449
		Points below threshold	0.625	0.440		0.140	1.017
Trial 17	-	SE less than 0.6	0.461		0.180	0.135	0.231
		SE more than 0.6	0.430		0.010	0.284	0.620
Trial 18	-	SE less than 0.6	0.444		0.300	0.140	0.285
		SE more than 0.6	0.674		0.300	0.140	0.673
Trial 19	• Categorized based on survey ESALs at construction year.	ESALs ≤ 100,000	0.454		0.183	0.114	0.601
		100,000 < ESALs ≤ 1 mil.	0.100		0.511	0.464	0.172
		1 mil. < ESALs ≤ 2 mil.	0.495		0.130	0.010	0.094
		ESALs > 2 mil.	0.443		0.219	0.072	0.06
Trial 20	• Categorized based on survey ESALs at construction year.	ESALs ≤ 100,000	0.409		0.300	0.140	0.659
		100,000 < ESALs ≤ 1 mil.	0.545		0.300	0.140	0.234
		1 mil. < ESALs ≤ 2 mil.	0.313		0.300	0.140	0.184
		ESALs > 2 mil.	0.360		0.300	0.140	0.089
Trial 21	• Categorized based on contract design 20 years ESALs.	ESALs ≤ 3 mil.	0.303		0.254	0.040	0.132
		3 mil. < ESALs ≤ 30 mil.	0.542		0.091	0.125	0.204
		ESALs > 30 mil.	0.400		0.900	0.010	0.001
Trial 22	• Categorized based on contract design 20 years ESALs.	ESALs ≤ 3 mil.	0.301		0.300	0.140	0.360
		3 mil. < ESALs ≤ 30 mil.	0.483		0.300	0.140	0.273
		ESALs > 30 mil.	0.588		0.300	0.140	0.008
Trial 23	• Categorized based on survey 20 years ESALs.	ESALs ≤ 3 mil.	0.487		0.164	0.119	0.569
		3 mil. < ESALs ≤ 30 mil.	0.636		0.010	0.036	0.228
Trial 24	• Categorized based on survey 20 years ESALs.	ESALs ≤ 3 mil.	0.405		0.300	0.140	0.578
		3 mil. < ESALs ≤ 30 mil.	0.471		0.300	0.140	0.287
Trial 25	• Categorized based on survey 20 years ESALs.	ESALs ≤ 1 mil.	0.303		0.254	0.202	0.574
		1 mil. < ESALs ≤ 10 mil.	0.368		0.311	0.214	0.190
		10 mil. < ESALs ≤ 20 mil.	0.670		0.010	0.010	0.278
		ESALs > 20 mil.	0.485		0.156	0.371	0.000

Calibration Trial	Description	Category	Results				SSE (Avg)
			AC-surface	AC-int.	AC-base	ABC	
Trial 26	• Categorized based on survey 20 years ESALs.	ESALs ≤ 1 mil.	0.409		0.300	0.140	0.654
		1 mil. < ESALs ≤ 10 mil.	0.459		0.300	0.140	0.215
		10 mil. < ESALs ≤ 20 mil.	0.477		0.300	0.140	0.382
		ESAL > 20 mil.	0.355		0.300	0.140	0.093
Trial 27	-	S9.5B	0.303		0.254	0.330	0.442
		S9.5C	0.360		-	0.136	0.000
		S12.5B	0.134		0.764	0.347	0.197
		S12.5C	0.386		0.206	0.083	0.095
		S12.5D	0.420		0.281	0.353	0.000
Trial 28	-	S9.5B	0.544		0.300	0.140	0.524
		S9.5C	0.354		-	0.140	0.000
		S12.5B	0.450		0.300	0.140	0.269
		S12.5C	0.287		0.300	0.140	0.102
		S12.5D	0.716		0.300	0.140	0.000
Trial 29	-	Last point	0.462		0.250	0.140	0.403
Trial 30	-	SE less than 0.6	0.444		0.250	0.140	0.269
		SE more than 0.6	0.677		0.250	0.140	0.673
Trial 31	-	SE less than 0.6	0.455		0.180	0.140	0.231
		SE more than 0.6	0.677		0.240	0.140	0.673
Trial 32	• Categorized based on contract design 20 years ESALs.	ESALs ≤ 3 mil.	0.304		0.250	0.140	0.250
		3 mil. < ESALs ≤ 30 mil.	0.484		0.250	0.140	0.249
		ESALs > 30 mil.	0.622		0.250	0.140	0.008
Trial 33	• Categorized based on contract design 20 years ESALs.	ESALs ≤ 3 mil.	0.303		0.250	0.140	0.242
		3 mil. < ESALs ≤ 30 mil.	0.524		0.110	0.140	0.204
		ESALs > 30 mil.	0.206		0.900	0.140	0.002
Trial 34	• Categorized based on survey ESALs at construction year.	ESALs ≤ 100,000	0.406		0.250	0.140	0.650
		100,000 < ESALs ≤ 1 mil.	0.545		0.250	0.140	0.233
		1 mil. < ESALs ≤ 2 mil.	0.338		0.250	0.140	0.185
		ESALs > 2 mil.	0.388		0.250	0.140	0.117
Trial 35	• Categorized based on survey ESALs at construction year.	ESALs ≤ 100,000	0.412		0.200	0.140	0.603
		100,000 < ESALs ≤ 1 mil.	0.546		0.010	0.140	0.225
		1 mil. < ESALs ≤ 2 mil.	0.321		0.300	0.140	0.183
		ESALs > 2 mil.	0.340		0.400	0.140	0.073
Trial 36	• Categorized based on survey 20 years ESALs.	ESALs ≤ 3 mil.	0.402		0.250	0.140	0.567
		3 mil. < ESALs ≤ 30 mil.	0.472		0.250	0.140	0.27

Calibration Trial	Description	Category	Results				SSE (Avg)
			AC-surface	AC-int.	AC-base	ABC	
Trial 37	• Categorized based on survey 20 years ESALs.	ESALs ≤ 3 mil.		0.407	0.200	0.140	0.528
		3 mil. < ESALs ≤ 30 mil.		0.491	0.130	0.140	0.244
Trial 38	• Categorized based on survey 20 years ESALs.	ESALs ≤ 1 mil.		0.406	0.250	0.140	0.645
		1 mil. < ESALs ≤ 10 mil.		0.461	0.250	0.140	0.204
		10 mil. < ESALs ≤ 20 mil.		0.477	0.250	0.140	0.364
		ESALs > 20 mil.		0.406	0.250	0.140	0.076
Trial 39	• Categorized based on survey 20 years ESALs.	ESALs ≤ 1 mil.		0.411	0.200	0.140	0.598
		1 mil. < ESALs ≤ 10 mil.		0.476	0.100	0.140	0.191
		10 mil. < ESALs ≤ 20 mil.		0.492	0.100	0.140	0.327
		ESALs > 20 mil.		0.677	0.010	0.140	0.025
Trial 40	-	S9.5B		0.549	0.250	0.140	0.520
		S9.5C		0.354	-	0.140	0.000
		S12.5B		0.456	0.250	0.140	0.269
		S12.5C		0.310	0.250	0.140	0.111
		S12.5D		0.753	0.250	0.140	0.000
Trial 41	-	S9.5B		0.539	0.150	0.140	0.479
		S9.5C		0.354	-	0.140	0.000
		S12.5B		0.454	0.270	0.140	0.269
		S12.5C		0.291	0.290	0.140	0.101
		S12.5D		0.637	0.410	0.140	0.000
Trial 42	-	FDA		0.459	0.181	-	0.179
		ABC		0.668	-	0.010	0.44
		AC-Base & ABC		0.598	0.010	0.010	0.203
Trial 43	-	FDA		0.366	0.300	-	0.315
		ABC		0.482	-	0.140	0.442
		AC-Base & ABC		0.339	0.300	0.140	0.273
Trial 44	-	FDA		0.395	0.250	-	0.284
		ABC		0.482	-	0.140	0.442
		AC-Base & ABC		0.361	0.250	0.140	0.267
Trial 45	-	FDA		0.459	0.181	-	0.179
		ABC		0.482	-	0.140	0.442
		AC-Base & ABC		0.468	0.010	0.140	0.244

*averaged through all sections

Table C.4. Summary of Supplementary Calibration Trials.

Calibration Trials	Description	Category (Design 20 years Contract ESALs)	Results			SSE (Avg)
			AC-surface/int.	AC-base	ABC	
Trial 1	• Categorized • Sensitivity analysis	ESALs ≤ 3 mil.	0.304	0.250	0.100	0.239
		3 mil. < ESALs ≤ 30 mil.	0.534	0.100	0.130	0.204
		ESALs > 30 mil.	0.400	0.900	0.010	0.001
Trial 2	• Categorized • Calibrate all layers	ESALs ≤ 3 mil.	0.303	0.254	0.040	0.132
		3 mil. < ESALs ≤ 10 mil.	0.100	0.254	0.471	0.226
		ESALs > 10 mil.	0.534	0.105	0.173	0.079
Trial 3	• Categorized • Calibrate all layers	ESALs ≤ 5 mil.	0.303	0.254	0.121	0.185
		5 mil. < ESALs ≤ 20 mil.	0.530	0.106	0.152	0.193
		ESALs > 20 mil.	0.100	0.422	0.413	0.005
Trial 4	• Categorized • Calibrate all layers	ESALs ≤ 1 mil.	0.303	0.254	0.040	0.165
		1 mil. < ESALs ≤ 5 mil.	0.100	0.512	0.264	0.035
		5 mil. < ESALs ≤ 10 mil.	0.100	0.190	0.502	0.188
		10 mil. < ESALs ≤ 20 mil.	0.501	0.142	0.010	0.088
		ESALs > 20 mil.	0.100	0.422	0.413	0.005
Trial 5	• Categorized • Calibrate all layers	ESALs ≤ 1 mil.	0.303	0.254	0.040	0.165
		1 mil. < ESALs ≤ 10 mil.	0.414	0.036	0.230	0.209
		ESALs > 10 mil.	0.534	0.105	0.173	0.079
Trial 6	• Categorized • ABC Coefficient fixed	ESALs ≤ 1 mil.	0.303	0.250	0.140	0.311
		1 mil. < ESALs ≤ 10 mil.	0.509	0.010	0.140	0.229
		ESALs > 10 mil.	0.538	0.100	0.140	0.079
Trial 7	• Categorized • AC-base and ABC Coefficients fixed	ESALs ≤ 1 mil.	0.303	0.300	0.140	0.447
		1 mil. < ESALs ≤ 10 mil.	0.508	0.300	0.140	0.275
		ESALs > 10 mil.	0.380	0.300	0.140	0.117
Trial 8	• Categorized • AC-base and ABC Coefficients fixed	ESALs ≤ 1 mil.	0.304	0.250	0.140	0.322
		1 mil. < ESALs ≤ 10 mil.	0.508	0.250	0.140	0.268
		ESALs > 10 mil.	0.415	0.250	0.140	0.102
Trial 9	• Universal calibration • Sensitivity analysis	-	0.460	0.180	0.190	0.230
Trial 10	• Calibrate all layers • Universal calibration	-	0.349	0.138	0.224	0.350
Trial 11	• AC-base and ABC Coefficients fixed • Universal calibration	-	0.419	0.300	0.140	0.473

Calibration Trials	Description	Category (Design 20 years Contract ESALs)	Results			SSE (Avg)
			AC-surface/int.	AC-base	ABC	
Trial 12	• AC-base and ABC Coefficients fixed • Universal calibration	-	0.416	0.250	0.140	0.461
Trial 13	• ABC Coefficients fixed • Universal calibration	-	0.397	0.121	0.140	0.380
Trial 14	• AC-base Coefficients fixed • Universal calibration	-	0.309	0.200	0.254	0.408
Trial 15	• AC-base and ABC Coefficients fixed • Universal calibration	-	0.412	0.200	0.140	0.447
Trial 16	• Categorized • Calibrate all layers	ESALs ≤ 1 mil.	0.238	0.193	0.624	0.469
		1 mil. < ESALs ≤ 5 mil.	0.336	0.073	0.226	0.374
		ESALs > 5 mil.	0.412	0.073	0.243	0.020
Trial 17	• Categorized • Calibrate all layers	ESALs ≤ 2 mil.	0.266	0.178	0.010	0.406
		2 mil. < ESALs ≤ 4 mil.	0.100	0.010	0.405	0.316
		ESALs > 4 mil.	0.403	0.078	0.182	0.127
Trial 18	• Categorized • Calibrate all layers	ESALs ≤ 2.5 mil.	0.238	0.197	0.169	0.410
		2.5 mil. < ESALs ≤ 10 mil.	0.408	0.072	0.216	0.267
		ESALs > 10 mil.	0.221	0.900	0.010	0.011
Trial 19	• Categorized • Calibrate all layers	ESALs ≤ 2.5 mil.	0.238	0.404	0.034	0.384
		2.5 mil. < ESALs ≤ 5 mil.	0.402	0.010	0.221	0.326
		ESALs > 5 mil.	0.412	0.073	0.243	0.020
Trial 20	• Categorized • AC-base and ABC Coefficients fixed	ESALs ≤ 2.5 mil.	0.238	0.300	0.140	0.481
		2.5 mil. < ESALs ≤ 5 mil.	0.483	0.300	0.140	0.406
		ESALs > 5 mil.	0.254	0.300	0.140	0.132
Trial 21	• Categorized • AC-base and ABC Coefficients fixed	ESALs ≤ 2.5 mil.	0.238	0.250	0.140	0.468
		2.5 mil. < ESALs ≤ 5 mil.	0.482	0.250	0.140	0.400
		ESALs > 5 mil.	0.285	0.250	0.140	0.108
Trial 22	• Categorized • ABC Coefficient fixed	ESALs ≤ 2.5 mil.	0.238	0.193	0.140	0.392
		2.5 mil. < ESALs ≤ 5 mil.	0.444	0.010	0.140	0.356
		ESALs > 5 mil.	0.417	0.069	0.140	0.025
Trial 23	• Categorized • AC-base Coefficient fixed	ESALs ≤ 2.5 mil.	0.237	0.200	0.130	0.417
		2.5 mil. < ESALs ≤ 5 mil.	0.212	0.200	0.367	0.328
		ESALs > 5 mil.	0.315	0.200	0.250	0.075

Calibration Trials	Description	Category (Design 20 years Contract ESALs)	Results			SSE (Avg)
			AC-surface/int.	AC-base	ABC	
Trial 24	• Categorized • AC-base and ABC Coefficient fixed	ESALs ≤ 2.5 mil.	0.237	0.200	0.140	0.419
		2.5 mil. < ESALs ≤ 5 mil.	0.481	0.200	0.140	0.393
		ESALs > 5 mil.	0.316	0.200	0.140	0.080
Trial 25	• Categorized • Calibrate all layers	ESALs ≤ 2.5 mil.	0.238	0.404	0.034	0.384
		ESALs > 2.5 mil.	0.407	0.074	0.219	0.226
Trial 26	• Categorized • AC-base and ABC Coefficients fixed	ESALs ≤ 2.5 mil.	0.238	0.300	0.140	0.481
		ESALs > 2.5 mil.	0.437	0.300	0.140	0.366
Trial 27	• Categorized • AC-base and ABC Coefficients fixed	ESALs ≤ 2.5 mil.	0.238	0.250	0.140	0.468
		ESALs > 2.5 mil.	0.433	0.250	0.140	0.346
Trial 28	• Categorized • ABC Coefficient fixed	ESALs ≤ 2.5 mil.	0.238	0.193	0.140	0.392
		ESALs > 2.5 mil.	0.477	0.015	0.140	0.233
Trial 29	• Categorized • AC-base Coefficient fixed	ESALs ≤ 2.5 mil.	0.237	0.200	0.130	0.417
		ESALs > 2.5 mil.	0.312	0.200	0.288	0.253
Trial 30	• Categorized • AC-base and ABC Coefficient fixed	ESALs ≤ 2.5 mil.	0.237	0.200	0.140	0.419
		ESALs > 2.5 mil.	0.428	0.200	0.140	0.324

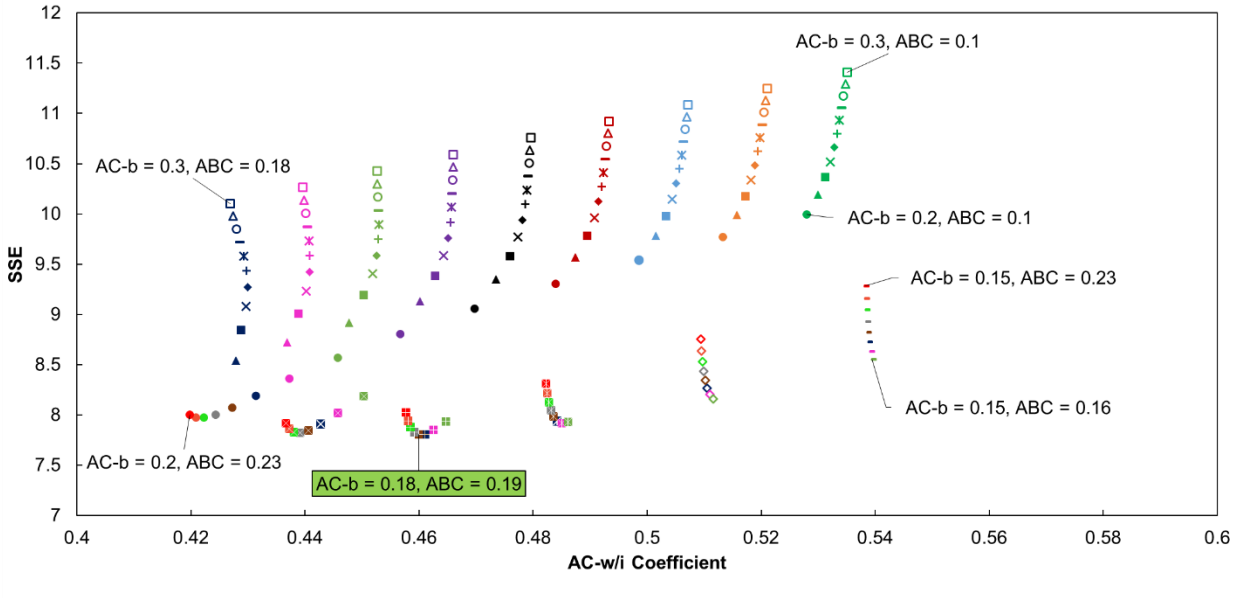

Figure C.1. Sensitivity analysis on SSE values (calibration Trial 9).

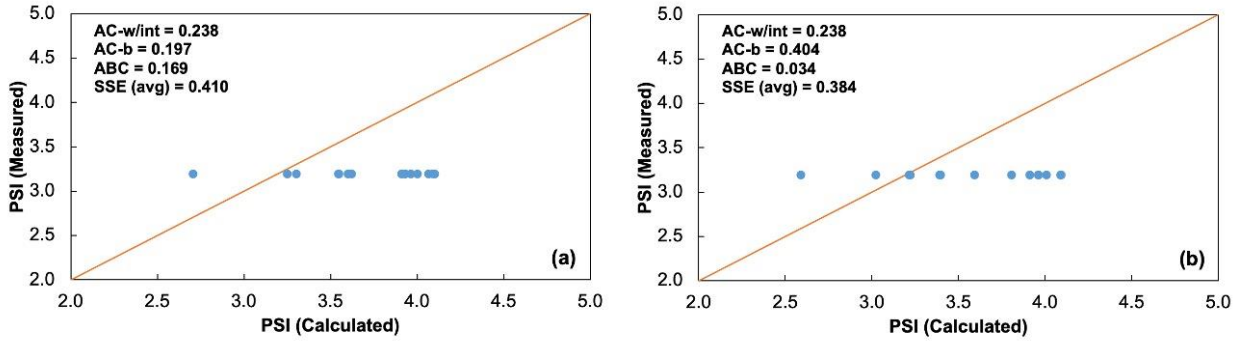

Figure C.2. Correlation of measured *PSI* and calculated *PSI* by calibrated coefficients (a) before elimination of one section and (b) after elimination of one section.

The calibration results are further evaluated by comparing the deterioration of *PSI* using calibrated and default coefficients. The comparisons are shown for each pavement section in Figure C.3 and Figure C.4. Figure C.3 represents the comparison graphs for sections with 20-year cumulative ESALs less than 3 million and Figure C.4 shows the comparison graphs for sections with 20-year cumulative ESALs more than 3 million or interstates. As shown in this figures, the calibration was successful in matching the last data point in some cases and it was not in others.

40001211051

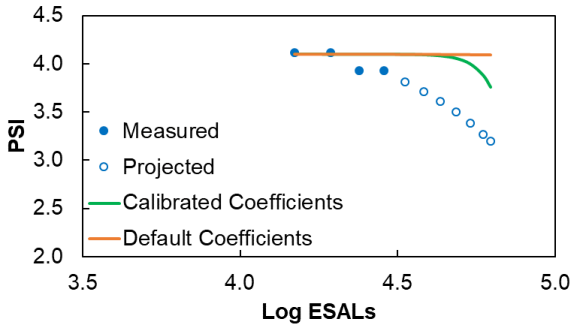

40001933026

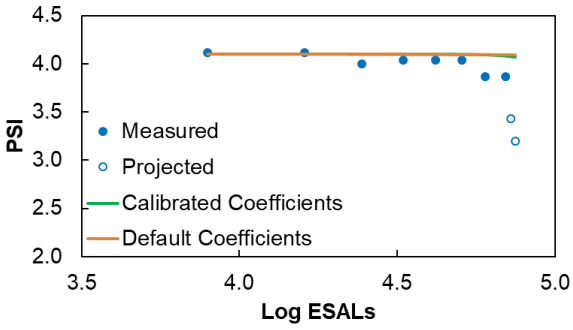

40001452077

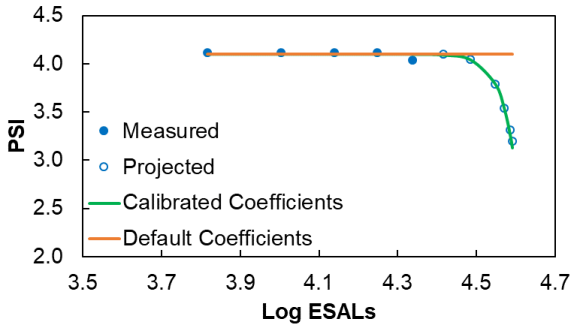

40001125099

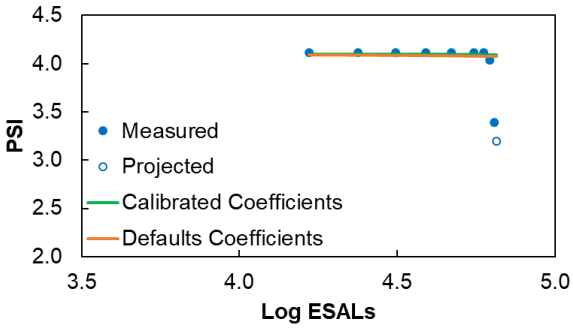

40002705023 (1)

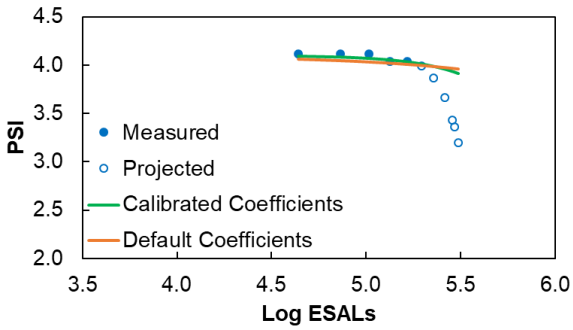

40002705023 (2)

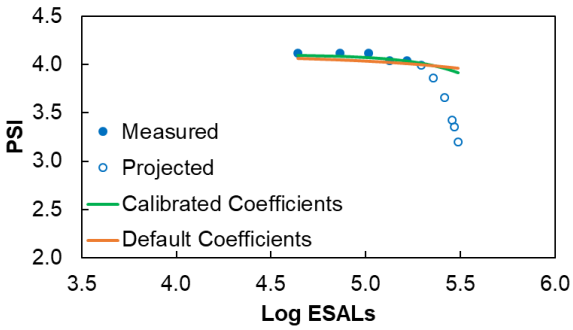

30000054001 (1)

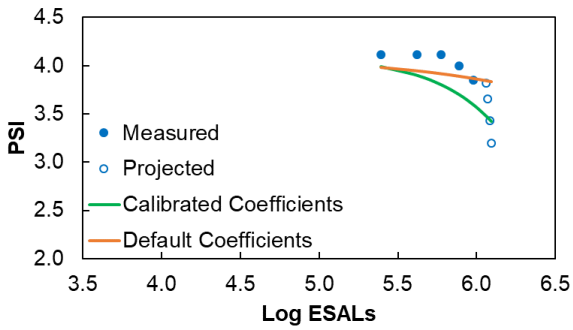

30000054001 (2)

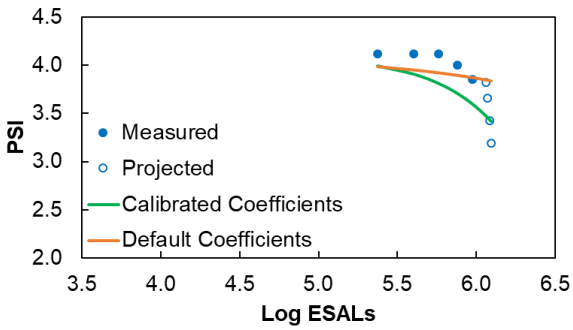

30000054001 (3)

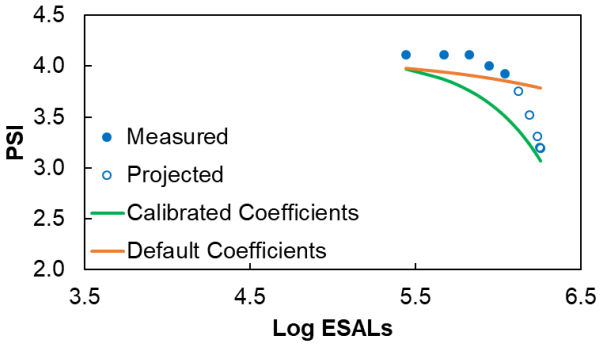

40001412033

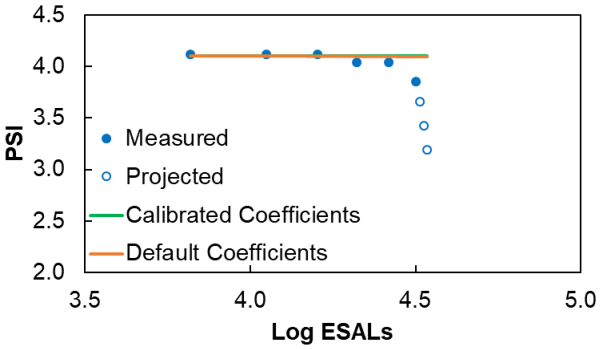

40001765099

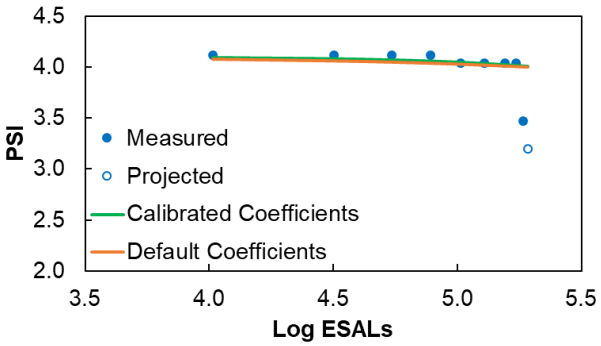

40002200036

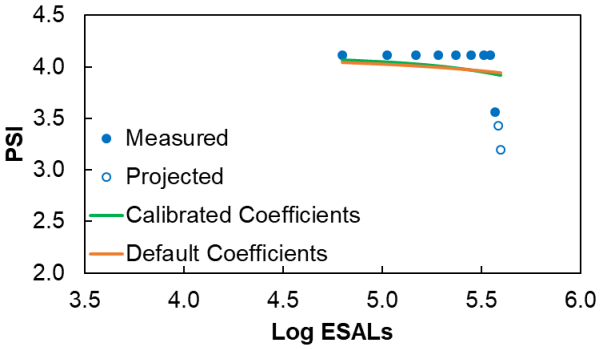

40003632060 (4)

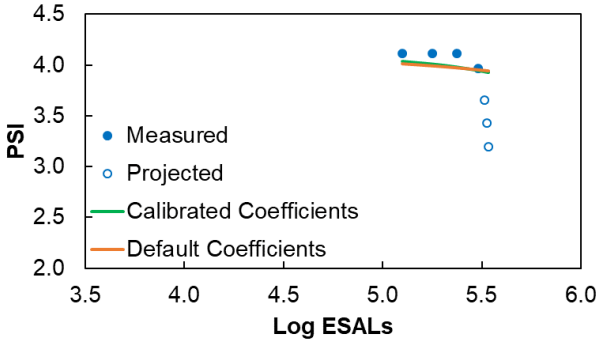

40002433001

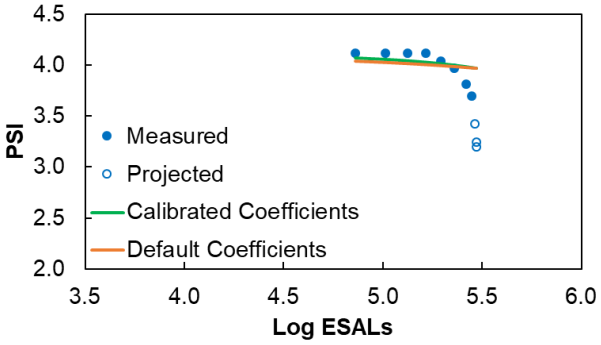

40001546041

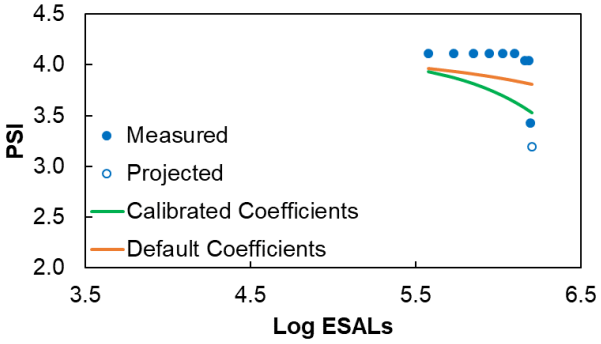

30000024013

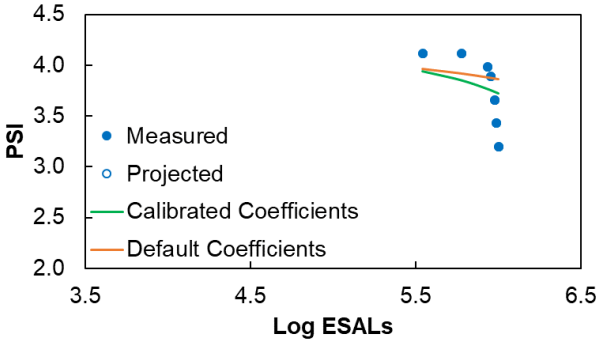

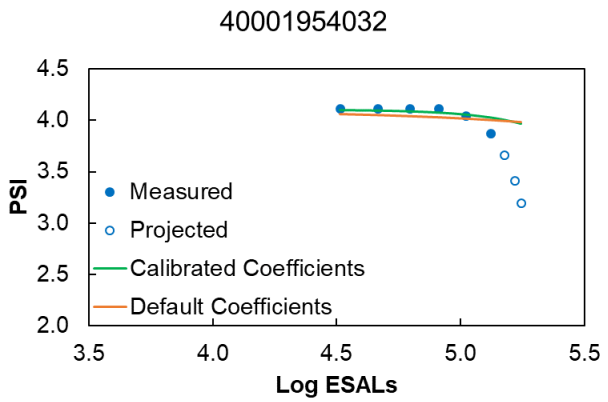

Figure C.3. Comparing the deterioration of *PSI* calculated based on calibrated and default coefficients for sections with less than 3 million ESALs.

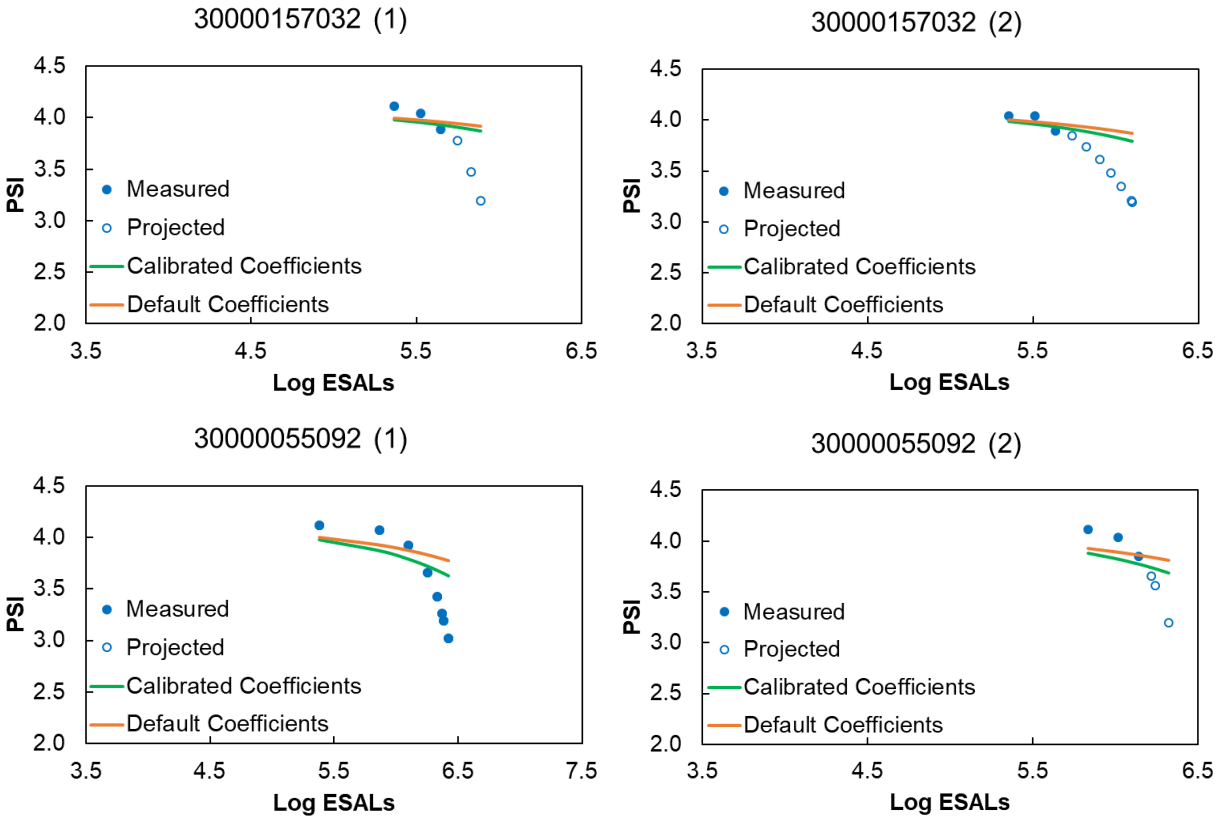

30000087043 (1)

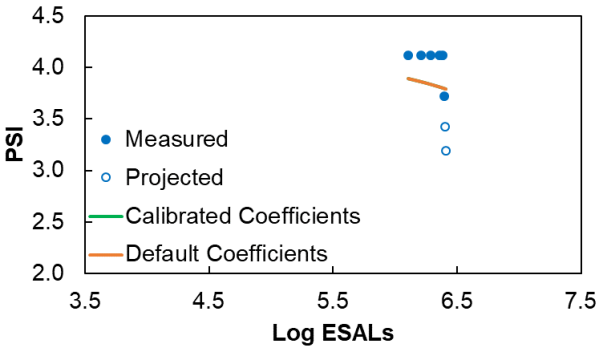

30000087043 (2)

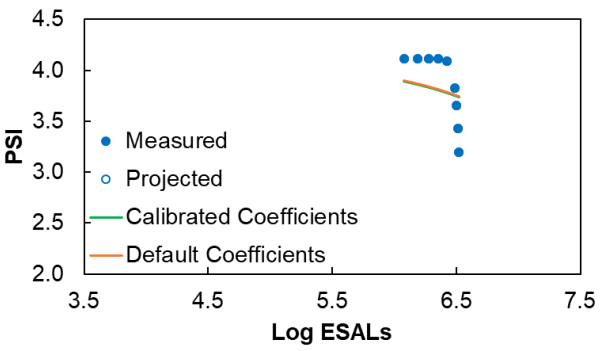

30000109029

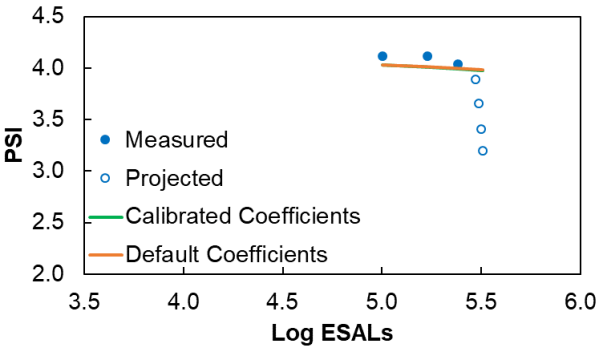

20000070041 (3)

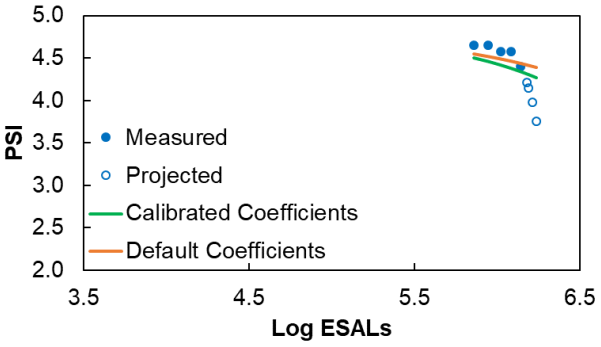

20000070049 (2)

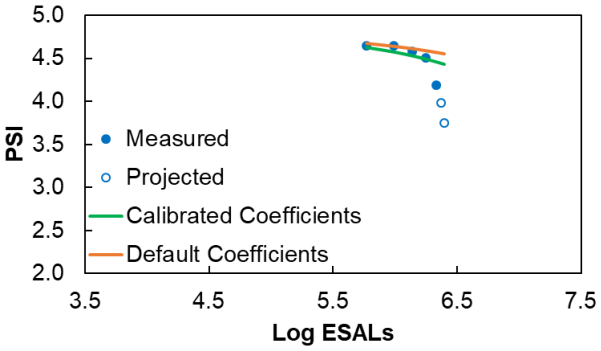

10800485060

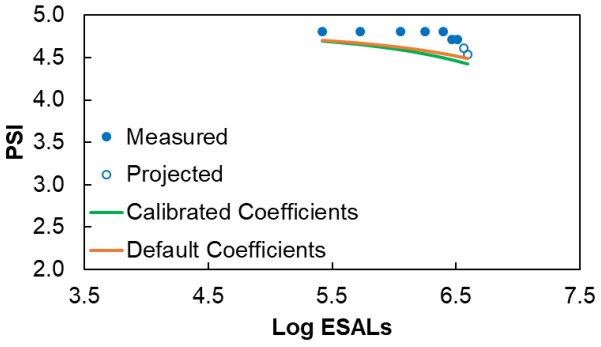

10000074078

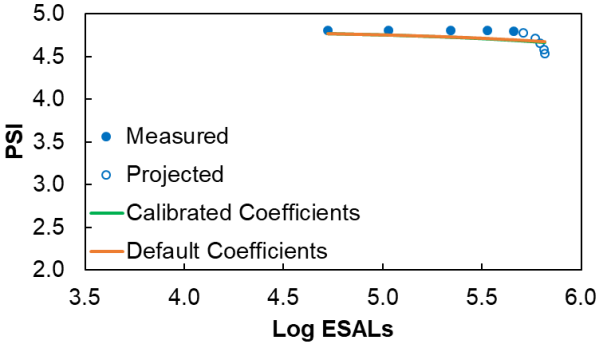

10600074078

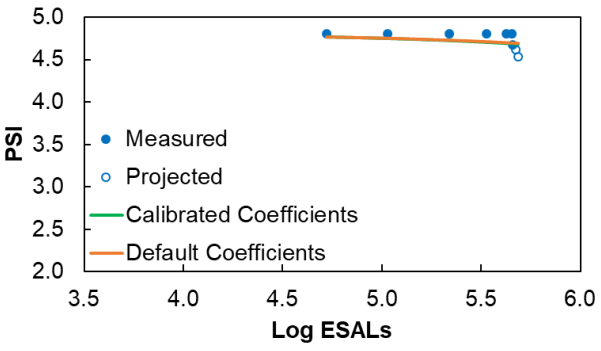

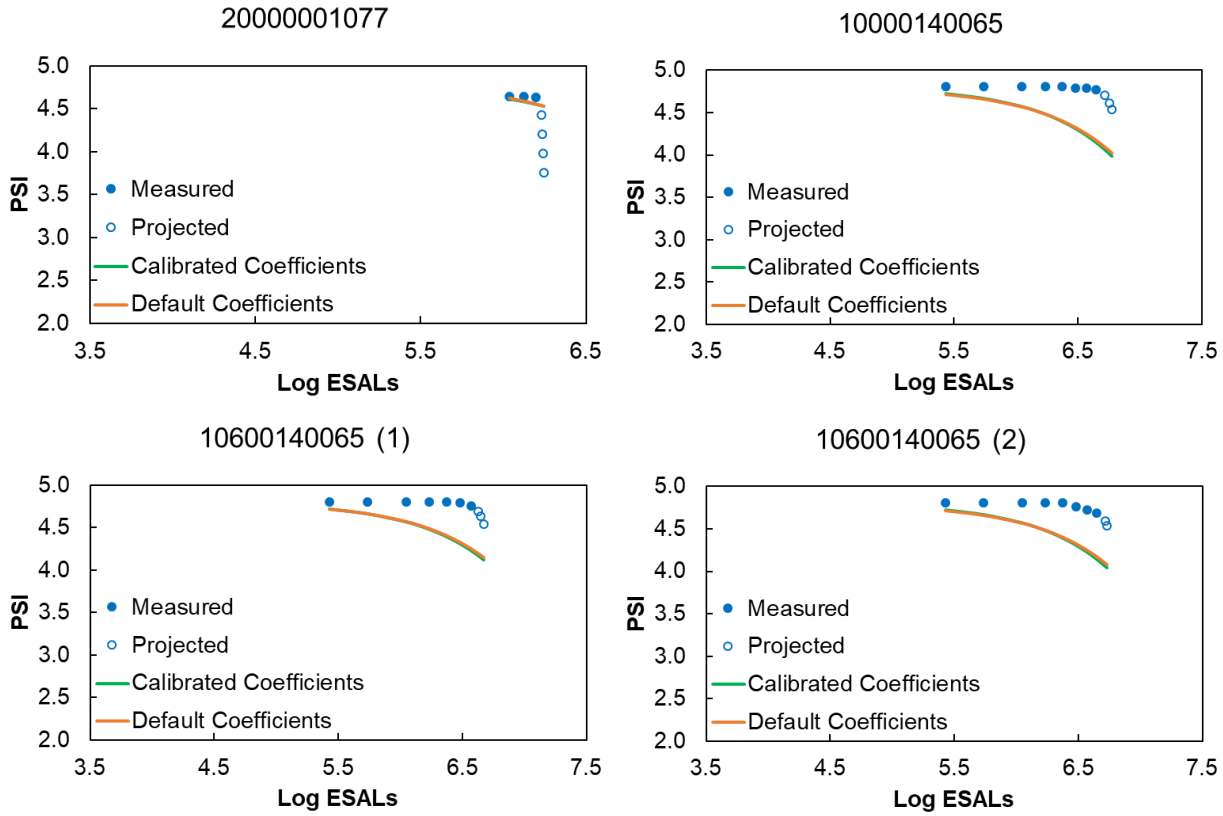

Figure C.4. Comparing the deterioration of *PSI* calculated based on calibrated and default coefficients for sections with more than 3 million ESALs or interstate routes.

The PCR raw data along with fitting coefficients used to model and project PCR values to PCR of 60 for all 76 sections is presented in Table C.5. In addition the raw traffic data for all sections is summarized in Table C.6.

Table C.5. Summary of PCR raw data and fitting coefficients.

Category	Route ID	Year															Fitting Coefficients		
		2002	2003	2004	2005	2006	2007	2008	2009	2010	2011	2012	2013	2014	2015	2016	2017	a	b	n
ESALs < 3 mil.	40001125099			100		100		100		100		96.7		68.6				100	-1E-12	12.4
	40001211051	100		100		91.7		91.7										100	-1E+00	1.3
	40001412033							100		100		96.7		96.7	88.4			100	-1E-12	13.0
	40001933026			100		95		96.7		96.7		96.7		89.2	89.2			100	-1E-10	9.8
	40001452077									100		100		100	96.7			100	-5E-11	10.0
	40002705023 (1)											100		96.7	96.7			100	-9E-04	3.8
	40002705023 (2)											100		96.7	96.7			100	-9E-04	3.8
	40001546041	100		100		100		100		96.7		96.7		70.1				100	-7E-13	12.2
	40003632060 (4)					100		93.4										100	-2E-08	11.0
	40002200036					100		100		100		100		100	75.9			100	-1E-10	9.8
	40002433001					100		100		96.7		93.4		86.8	81.8			100	-1E-10	10.1
	30000054001 (1)	100		100		100		95		88.4								100	-1E-12	13.0
	30000054001 (2)	100		100		100		95		88.4								100	-1E-12	13.0
	30000054001 (3)	100		100		100		95		91.7								100	-3E-02	2.7
	40001765099			100		96.7		96.7		96.7		96.7		71.9				100	-1E-10	10.0
	40001954032					100		100		100		96.7		89.2				100	-2E-05	5.7
	30000024013	100		100		57.5												100	-2E-05	9.0
3 mil. ≤ ESALs or Interstate	10000140065						100	100	100	100	100	97.7	96.7	94.4				100	-2E-09	8.2
	10600140065 (1)						100	100	100	100	98.4	91.3						100	-7E-09	8.4
	10600140065 (2)						100	100	100	100	100		92.7	85.5	80.8			100	-6E-08	7.3
	20000001077												100	100	99.3			100	-1E-08	12.9
	30000087043 (1)			100		100		100		82.6								100	-7E-09	11.1
	30000087043 (2)			100		100		100		93.4		80.1	63.5					100	-1E-10	11.1
	30000157032 (1)					100		96.7		90.1								100	-3E-01	2.2
	30000157032 (2)				100	96.7		96.7		90.1								100	-1E+00	1.2
	30000109029			100		100		96.7										100	-8E-09	12.3
	20000070041 (3)	100		100		96.7		96.7		88.4								100	-2E-02	3.1
	20000070049 (2)	100		100		96.7		93.4		79.3								100	-1E-02	3.5

Category	Route ID	Year																Fitting Coefficients		
		2002	2003	2004	2005	2006	2007	2008	2009	2010	2011	2012	2013	2014	2015	2016	2017	a	b	n
	30000055092 (1)					100		83.4				52.9						100	-5E-01	2.1
	30000055092 (2)					100		96.7		88.4								100	-9E-01	1.8
	10800485060			100	100	100	100	100	84.2	85.1								100	-2E-05	5.9
	10000074078							100		100		98						100	-1E-08	9.2
	10600074078							100		100		77.7						100	-2E-09	11.1
	40001324067 (1)											100		100	90.1			100	-3E-11	19.1
	40001324067 (2)											100		88.4				100	-3E-03	7.4
	40002323097	100		96.7		96.7		91.7		91.7		84.2		84.2				100	-9E-01	1.2
	40001134099	100		100		100		96.7		91.7								100	-4E-03	3.7
	40001199099			100		100		100		100		100		95	95	95	95	100	-1E-02	2.5
	40001209099			100		100		100		100		100		86.7				100	-6E-12	12.4
	40001210099			100		100		100		100		100		80.1				100	-4E-10	10.6
	40001444099			100		100		100		100		95		83.4	83.4	83.4	83.4	100	-9E-02	2.1
	40001141099 (1)	100		100		100		100		100		93.4		67.6	67.6	67.6	57.6	100	-8E-03	3.2
	40001141099 (2)	100		100		100		100		100		93.4		67.6	67.6	67.6	57.6	100	-8E-03	3.2
	40001150099 (1)	100		100		100		100		100		96.7		86.4	86.4	86.4	66.4	100	-6E-06	5.7
Non-Contract Route	40001166099	100		100		100		100		100		91.7		80.1	68.4	68.4	68.4	100	-1E-02	3.0
	40001415099			100		100		100		100		93.4		88.4	88.4	88.4	78.4	100	-1E-02	2.9
	40002325097 (1)					100		87.5		88.4		66.7		60.1				100	-2E-01	2.2
	40002325097 (2)	100		91.7		88.4		83.4		71.7		45.1						100	-7E-02	2.6
	40001150099 (2)			100		100		100		100		96.7		86.4	86.4			100	-9E-05	4.7
	30000012028	100		100		100		95.0										100	-7E-09	11.4
	40001002096 (1)			100		95.0		95.0										100	-6E-01	1.3
	40001002096 (2)									100		100		100	91.7			100	-5E-11	10.0
	40002309097 (1)	100		100		100				96.7		89.2		80.1	75.1			100	-1E-02	2.9
	40002309097 (2)	100		100		100				96.7		89.2		80.1	75.1			100	-1E-02	2.9
	40002345097					100		96.7		93.4		85.9		75.9				100	-6E-01	1.8
	40003632060 (1)					100		96.7		96.7		93.4		79.3				100	-2E-02	3.4
	40003632060 (2)					100		90.1		86.8		76.0		76.0	71.0	71.0		100	-6E+00	0.7
	40003632060 (3)					100		93.4		75.2		68.6		57.5				100	-5E+00	1.0

Category	Route ID	Year															Fitting Coefficients		
		2002	2003	2004	2005	2006	2007	2008	2009	2010	2011	2012	2013	2014	2015	2016	2017	a	b	n
	40001430013 (2)							100		100		91.7		91.7	88.4			100	-2E-01	1.9
	20000070049 (1)	100		100		100		96.7		96.7								100	-6E-02	2.0
	20000064019	100		100		100		100		100				91.4	83.7			100	-1E-08	8.1
	20000421099 (1)			100		100		100		91.7			78.1					100	-4E-02	2.9
	20000421099 (2)			100		100		100		91.7			80.7	47.8				100	-7E-08	8.9
	20000421099 (3)			100		100		100		91.7								100	-2E-08	11.0
	20000421099 (4)			100		100		100		91.7								100	-2E-08	11.0
	20000421099 (5)			100		100		100		91.7								100	-2E-08	11.0
	20000421099 (6)			100		100		100		96.7								100	-1E-08	11.0
	20400421099 (1)			100		100		100		91.7								100	-2E-08	11.0
	20400421099 (2)			100		100		96.7		80.9								100	-8E-03	4.3
	20400421099 (3)			100		100		96.7		88.4								100	-4E-02	3.2
	20400421099 (4)			100		100		100		84.2								100	-2E-09	12.8
	20400421099 (5)			100		100		100		91.7								100	-2E-09	12.8
	20400421099 (6)			100		100		100		91.7			73.9	72.8	61.4			100	-8E-02	2.6
	20400421099 (7)			100		100		100		88.4			68.8					100	-5E-02	2.9
	20400421099 (8)			100		100		100		88.4			68.8					100	-5E-02	2.9
	20400421099 (9)			100		100		100		88.4								100	-6E-09	11.9

Table C.6. Summary of 1000 AADT raw data and growth rate.

Category	Route ID	Year																Growth Rate (%)
		2002	2003	2004	2005	2006	2007	2008	2009	2010	2011	2012	2013	2014	2015	2016	2017	2018	
ESALs < 3 mil.	40001125099		1.1		1.0		1.1		1.1		1.0		1.1		1.1			1.1	2.0
	40001211051	0.7		0.8		0.7		0.6		0.8		0.7		0.7		0.8		0.9	1.2
	40001412033		0.5		0.5		0.8		0.7		0.8		0.6		0.6		0.7	0.5	2.1
	40001933026					1.3		1.7		1.8		1.2		1.6		1.4		1.4	1.3
	40001452077		0.4		0.6		0.39		0.5		0.5		0.6		0.55			0.5	2.4
	40002705023 (1)								4.7				4.8		5.1		5	4.9	0.7
	40002705023 (2)								4.7				4.8		5.1		5	4.9	0.7
	40001546041		29		33		33		32		31		22		24		23	23.5	2.0
	40003632060 (4)			8.8		12		12		11		15		16		19		19	5.9
	40002200036	9.5		7.9		8.6		9.3		9.4		9.5		11.2		10.6		10.9	0.6
	40002433001								5				4.7		5.4		5.4	5.5	0.9
	30000054001 (1)		13		13		14		14		14		13.5		15		16	16.5	1.3
	30000054001 (2)		12.5		12.5		13		13		14		14		15		18.5	19.3	2.2
	30000054001 (3)		14.5		15		13.5		14.5		15		14.5		16		21	22	1.8
	40001765099								4.1					4.3		4.6		5.4	2.4
	40001954032		1.8		2.9		3.5		3.1		4.2		4.4		4.6				8.8
	30000024013	14.5		17.5		20		19		17.5		18		19.5		22.5		24.8	3.1
3 mil. ≤ ESALs or Interstate	10000140065					15.5	17	18	16.5	16	16.5	14.5	15.5	17	19	17	21	26.8	2.4
	10600140065 (1)					15.5	17	18	16.5	16	16.5	14.5	15.5	17	19	17	21	26.8	2.0
	10600140065 (2)					15.5	17	18	16.5	16	16.5	14.5	15.5	17	19	17	21	26.8	2.0
	20000001077	8	7.7	7.4	7.7	7.6	8.1	7.6	8.1	8.4	7.8	7.6	8.3	8.1	8.1	9.5	8.7	9.1	0.4
	30000087043 (1)		13	14		14	15	15	13	15	14	14			19	12	13	14.5	0.9
	30000087043 (2)		13	16	16.5	15.5	17	18	15.7	17	16.5	16		18	21.7	12.5	16.3	18.7	2.5
	30000157032 (1)		16.5		17.3		19.7		21.3		21		23.3		24		24.3	24.8	3.0
	30000157032 (2)		16		17		20		21		20		22		23		25	25.5	3.2
	30000109029				9.3		10		9.5		9.8		11		11		11	11.5	1.6
	20000070041 (3)		19		16.5		18.5		17.5		19		18		18		22	22.3	0.4
	20000070049 (2)	20.5	22	22.5	23	23.5	23.5	22.5	20	18.5	20.5	22	23	16	20.5	20	21	22.8	0.2

	30000055092 (1)			37		43		44		44		43		43		44	43.8	2.0
	30000055092 (2)		25		22.5		27		29.5		32		27		28.5		24.5	24.8	0.6
	10800485060			38	45	53	51	47	47	47	47	45	48	51	64	73	75	78.5	4.7
	10000074078		10	11	12					8.7	9.5	9.6	10	11	11.5	12	17	19	2.2
	10600074078		10	11	12					8.7	9.5	9.6	10	11	11.5	12	17	19	0.7
	40001324067 (1)	3				3.1		3.2		3.1		4.3				4.9		5.6	3.4
	40001324067 (2)	1.3		1.4		1.6		1.7		1.7		2.3		2.2		2.4		2.8	4.6
	40002323097		0.31		0.3		0.27		0.26		0.19		0.21		0.2			0.2	2.0
	40001134099								1.3					1.4		1.6			2.5
	40001199099			0.9		0.9		0.9		0.9		0.9		0.9	0.9	0.9	0.9		2.0
	40001209099			0.2		0.2		0.2		0.2		0.2		0.2	0.2	0.2	0.2		2.0
	40001210099			0.1		0.1		0.1		0.1		0.1		0.1	0.1	0.1	0.1		2.0
	40001444099			0.04		0.04		0.04		0.04		0.04		0.04	0.04	0.04	0.04		2.0
	40001141099 (1)								2.5					2.3		2.6		2.7	0.4
	40001141099 (2)								2.6					2.8		2.8		2.9	1.2
	40001150099 (1)		0.6		0.7		0.8		0.7		1.1		1.1		1		0.84	0.9	3.6
	40001166099		0.7		0.6		0.6		0.6		0.5		0.6		0.5			0.6	2.0
	40001415099		0.2		0.3		0.3		0.4		0.4		0.5		0.5		0.4	0.5	8.6
Non-Contract Route	40002325097 (1)	2.1		2.4		3.1		2.8		3.3		3.3		2.5		3.1		3.7	3.4
	40002325097 (2)	2.1		2.4		3.1		2.8		3.3		3.3		2.5		3.1		3.7	3.4
	40001150099 (2)		1.1		1.0		1.1		1.1		1.0		1.1		1.1			1.1	2.0
	30000012028	6.2		6.9		8		8		6.4									4.9
	40001002096 (1)	N/A	N/A																
	40001002096 (2)	N/A	N/A																
	40002309097 (1)								1.4				1.2	1.6		1.2		1.3	2.0
	40002309097 (2)								3				2.7	3		2.6		3.3	2.0
	40002345097					0.1		0.1		0.1		0.1		0.1	0.1	0.1	0.1		2.0
	40003632060 (1)			8.8		12		12		11		15		16		19		19	5.9
	40003632060 (2)					13		19		18		19		22		21		21	5.0
	40003632060 (3)					10		14		14		18		17		19		18	6.1
	40001430013 (2)							10		12		14						22	7.9
	20000070049 (1)	20.5	22	22.5	23	23.5	23.5	22.5	20	18.5	20.5	22	23	16	20.5	20	21	22.8	0.2

20000064019	6.6	7.5	7.7	7.8	8	8.6	6.9	7.6	8	12	9		9.8	11	11	12	14	4.0
20000421099 (1)		16	16	16	17	17	19	16	17	18	16	18		18	18	20	20	1.2
20000421099 (2)		16	16	16	17	17	19	16	17	18	16	18		18	18	20	20	1.2
20000421099 (3)			16	16	17	18	18	15	17	18	15	17		18	18	19	19	1.0
20000421099 (4)	16	15	16	16	18	17	18	15	17	17	16	17		17	17	20	21.5	1.0
20000421099 (5)	13	13	15	14	15	15	17	14	15	16	13		15	15	15	17	16	1.4
20000421099 (6)			13	13	15	15	16	12	13	15		14	14	14	14	16	16.5	1.2
20400421099 (1)			13	13	15	15	16	12	13	15		14	14	14	14	16	16.5	1.2
20400421099 (2)			13	13	15	15	16	12	13	15		14	14	14	14	16	16.5	1.2
20400421099 (3)	13	13	15	14	15	15	17	14	15	16	13		15	15	15	17	16	1.4
20400421099 (4)	16	15	16	16	18	17	18	15	17	17	16	17		17	17	20	21.5	1.0
20400421099 (5)			16	16	17	18	18	15	17	18	15	17		18	18	19	19	1.0
20400421099 (6)		16	16	16	17	17	19	16	17	18	16	18		18	18	20	20	1.2
20400421099 (7)		16	16	16	17	17	19	16	17	18	16	18		18	18	20	20	1.2
20400421099 (8)		16	16	16	17	17	19	16	17	18	16	18		18	18	20	20	1.2
20400421099 (9)	18	16	17	16	18	18	19	17	18	18	16			19	19	20	22	0.4

Estimating Cumulative Traffic for Calibration Sites

To calculate the cumulative ESAL values for the calibration, the research team leveraged the data and method developed in FHWA/NC 2008-11 to create mix-traffic inputs for AASHTO Pavement ME Design. The data included traffic and load counts from 12 WIM stations across North Carolina. Each pavement in the calibrate dataset was first grouped according to the FHWA/NC 2008-11 traffic cluster by calculating the percentage of single unit (SU%) and multi-unit (MU%) trucks at each site according to Equations (54) and (55).

$$SU\%_{\text{Section}} = \left(\frac{SU_{fraction}}{SU_{fraction} + MU_{fraction}} \right) \times 100 \tag{54}$$

$$MU\%_{\text{Section}} = \left(\frac{MU_{fraction}}{SU_{fraction} + MU_{fraction}} \right) \times 100 \tag{55}$$

Then, to determine the cluster that the WIM data is associated with based the flowchart presented in Figure C.5 was used.

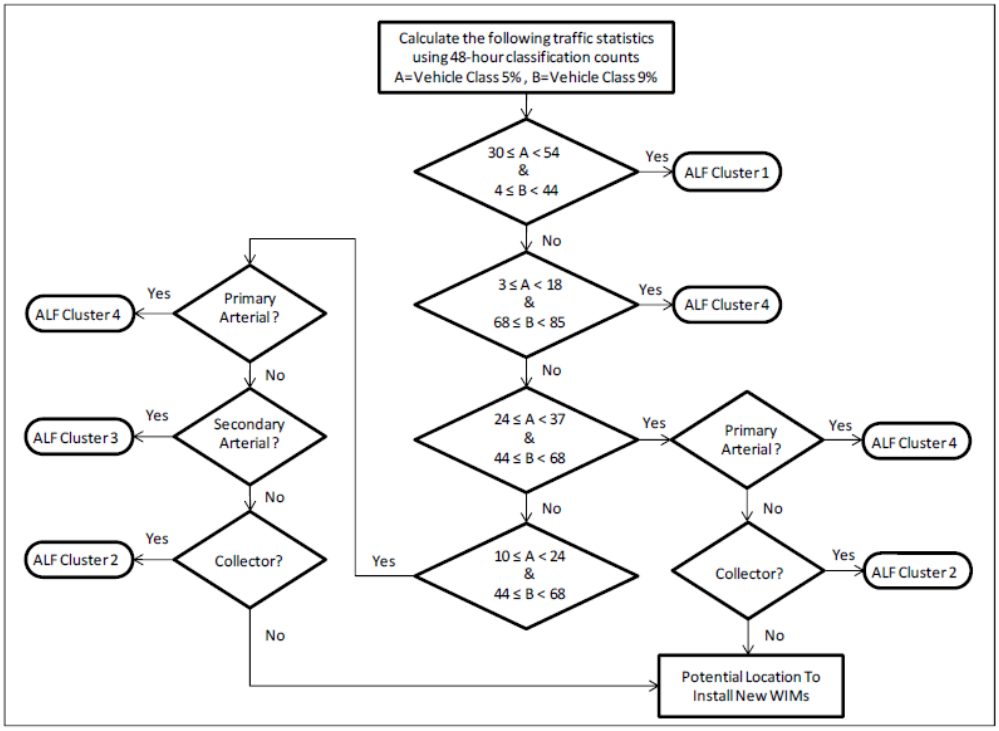

Figure C.5. Decision tree to identify WIM site (Sayyady et al. 2011).

For this calculation, the Class 5% and Class 9% were determined for each section using Equation (56) – (59).

$$Class\ 5\%_{\text{Section}} = \frac{SU\%_{\text{Section}} \times Class\ 5\%_{WIM}}{SU\%_{WIM}} \tag{56}$$

$$SU\%_{WIM} = \left(Class\ 4\% + Class\ 5\% + Class\ 6\% + Class\ 7\% \right)_{WIM} \tag{57}$$

$$Class\ 9\%_{Section} = \frac{MU\%_{Section} \times Class\ 9\%_{WIM}}{MU\%_{WIM}} \tag{58}$$

$$MU\%_{WIM} = \left(Class\ 8\% + Class\ 9\% + ... + Class\ 13\%\right)_{WIM} \tag{59}$$

Then, the following steps were carried out to calculate the mixed truck factor (*MTF*):

a. Calculate LEF for each axle type and weight for each WIM station within the cluster that was identified for the site in question from the aforementioned flowchart using Equations (50) – (52),
b. Multiply LEF by axle weight frequency distribution for each axle type in each WIM station,
c. Sum the results for axle types in each WIM station to determine ESALs in each WIM station,
d. Calculate *MTF* from each WIM station using the calibration site specific traffic volumes using Equation (8), and
e. Calculate the representative *MTF* by averaging the *MTF* from each of the applicable WIM station data.

The AADTTs, truck percentages, and number of lanes for multiple years were acquired for each station from the NCDOT interactive map. Based on the AADTTs data, the growth rate was calculated using Equation (60) and the AADTT was cumulated over the years in which the *PCR* data was collected using Equation (61). Finally, Equation (62) was used to compute the cumulative ESALs for each *PCR* location.

$$\%Growth = (10^{\frac{\log_{10}(\frac{ADT_{Future}}{ADT_{Initial}})}{(Year_{Future} - Year_{Initial}) \times 365.25}} \times 365.25 - 365.25) \times 100 \tag{60}$$

$$Cumulative\ AADTs_{PCR} = \frac{((1 + \frac{\%Growth}{100 \times 365.25})^{(365.25 \times N_D)} - 1) \times AADTT_{PCR}}{\ln(1 + \frac{\%Growth}{100 \times 365.25})} \tag{61}$$

$$ESAL_{PCR} = Cumulative\ AADTT_{PCR} \times DD \times LD \times MTF \tag{62}$$

where;

$ESAL_{PCR}$	=	the ESAL for *PCR* location i,
$Cumulative\ AADTT_{PCR}$	=	the sum of AADTTs for multiple years in which *PCR* data was collected,
LD	=	the lane distribution factor,
DD	=	the direction distribution factor, and
N_D	=	the number of years.

A summary of calibrated *MTF*s for 33 analysis sections are presented in Table C.7. The *MTF* is calculated for each WIM station (MTF_{WIM}) and the average of MTF_{WIM} for the WIM station in each cluster is the *MTF* for each section. As shown in the table, the average *MTF* values for sections that belong to Cluster 1 and 4 are about 0.6 and 1.1, respectively. The ESALs for each pavement section was calculated at the *PCR* of 60 (the combination used for calibration). In one set of

calculations, the NCDOT truck factors were used and in another set the *MTF*s were used. The log ESALs calculated based on these two sets were plotted in Figure C.6. As shown in this figure, the log ESALs based on *MTF*s are fairly similar to the ones based on NCDOT truck factors. The ESALs based on *MTF*s varies within a range of -1.5 to 5.1% with respect to the corresponding ESALs based on TF.

Table C.7. Summary of *MTF*s.

Section ID	Cluster	*MTF* (STDEV. of MTF_{WIM})	*MTF* (Avg. of MTF_{WIM})
40003632060 (4)	Cluster 1	0.138	0.578
40001211051		0.144	0.602
40001125099		0.141	0.593
40001412033		0.142	0.597
40001452077		0.141	0.594
40001933026		0.144	0.601
40002705023 (1)		0.139	0.584
40002705023 (2)		0.139	0.584
40002433001		0.138	0.578
40002200036		0.138	0.579
30000054001 (1)		0.139	0.577
30000054001 (2)		0.139	0.577
30000054001 (3)		0.139	0.577
40001765099		0.140	0.578
40001954032		0.138	0.580
30000024013		0.139	0.585
40001546041		0.139	0.577
30000157032 (1)		0.140	0.578
30000157032 (2)		0.140	0.578
30000109029		0.140	0.578
20000070041 (3)		0.138	0.579
30000055092 (1)		0.140	0.578
30000055092 (2)		0.140	0.578
20000070049 (2)		0.141	0.580
10000074078		0.142	0.581
10600074078		0.141	0.579
30000087043 (1)	Cluster 4	0.345	1.107
30000087043 (2)		0.345	1.107
10000140065		0.342	1.119
10600140065 (1)		0.342	1.119
10600140065 (2)		0.342	1.119
20000001077		0.343	1.124

10800485060	0.364	1.108

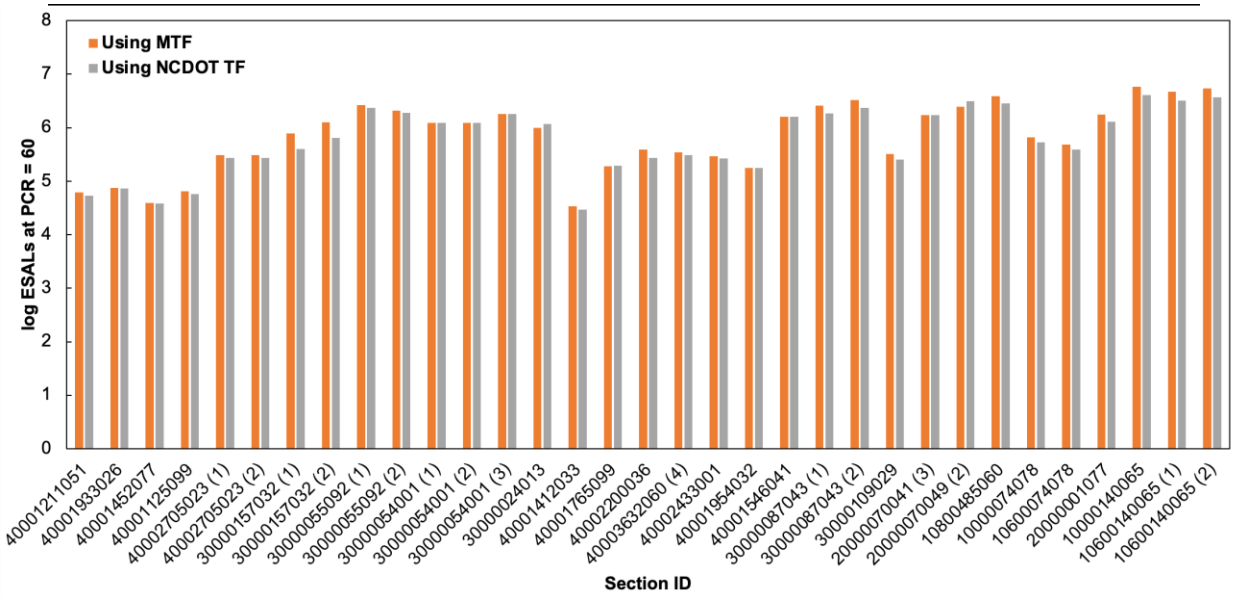

Figure C.6. Comparing ESALs calculated based on NCDOT truck factors and *MTF*s.

Additional analysis was carried out to determine the sensitivity of the *MTF* values to layer coefficients. The reason for this analysis was to determine whether, during the calibration process, it would be critical to update the truck factors with the new layer coefficients at the same time as the calibration or if this process could be reasonably accomplished in a sequential manner. The former is more complicated, and the research team believes it would be easier to do the latter. However, if the *MTF* values are very sensitive then the latter will likely not be successful.

In this analysis the layer coefficient for the asphalt layer in a pavement structure consisting of 5.5 inches of asphalt, 8 inches of aggregate base, and 10 inches of subbase was considered. Then the *MTF* was calculated for Cluster 1 and 4 by varying the asphalt layer coefficients from 0.12 to 0.92. The analysis was performed for terminal serviceability values of 2. The layer coefficients for base and subbase layers were fixed to 0.14 and 0.1, respectively. The results are summarized in Figure C.7 where *MTF* values based on Cluster 1 and 4 are plotted for each of the layer coefficients used. Based on these results there is only a slight change in *MTF* by varying the layer coefficient. It should be noted that this does not mean that the performance properties are not sensitive to layer coefficient, only the step of calculating ESALs.

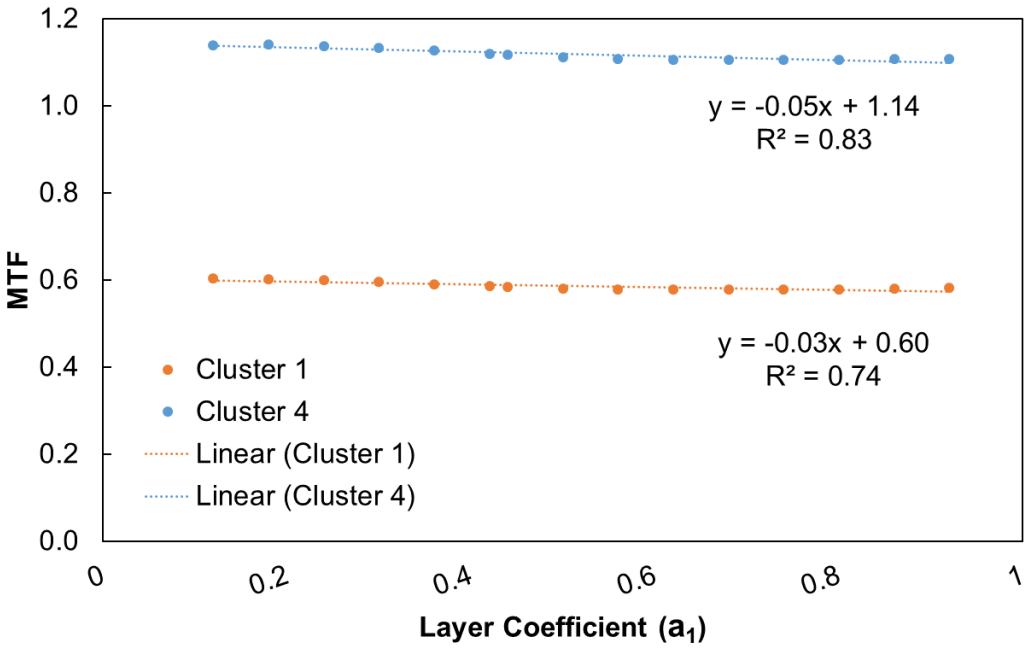

Figure C.7. Variation of *MTF* by changes of asphalt layer coefficient.

APPENDIX D: SUPPLEMENTARY INFORMATION ON ASPHALT CONCRETE EXPERIMENTS

Testing Methods

Sample Preparation and Mixture Volumetric Testing

For each of the mixtures used in this research, specimens were prepared in accordance with AASHTO R 83 for large cylinder test specimens and AASHTO PP 99 for small cylindrical test specimens. Specimens were cored from samples compacted to a 150 mm diameter and 180 mm using a Pine G2 Superpave gyratory compactor.

Mixture volumetric testing falls under sample preparation as these standards are listed in AASHTO R 83 and AASHTO PP 99. First, the theoretical maximum specific gravity was measured for each mixture in accordance with AASHTO T 209. The measured results were compared with the values given by the JMF. For each measurement, two samples were used, and the average was taken to compare to the JMF value. The average Gmm value was used for each mixture to get a more accurate representation of the mixture that was being tested.

Using the measured Gmm values, an air void study for each mixture was conducted by targeting three different air void percentages: usually 6%, 8%, and 10%. With these specimens prepared in accordance with AASHTO R 83 and PP 99, the next task was to measure the bulk specific gravity (AASHTO T 166) and air void percentage (AASHTO T 269). A target air void content for each mixture was then chosen after this process and was 5% +/- 0.5% for all test specimens.

Dynamic Modulus Test

For dynamic modulus testing, AASHTO TP 132 and T378 were followed to ensure the correct mechanical characterization of the mixtures. The temperatures used were determined as in the standard based on the stiffness of the binder. Data quality indicators were followed to an extent. The limits exhibited in the standard were met in most cases but for some mixtures, it was difficult to meet all the requirements due to the properties of the mixtures. For all tested mixtures the average deformation standard error limit was difficult to meet for the 40°C – 10Hz tests as well as a couple of the 40°C – 1Hz and 40°C – 0.1Hz tests. For the RS9.5B mm mixtures, deformation uniformity was an issue for 4°C tests but was resolved for the higher temperature tests. For RS9.5C mm mixtures, there was only one test that went slightly above the limit for phase uniformity. For RI19.0C mm mixtures, only one test was over the limit for load standard error, and for RB25C mixtures, only one test went slightly above the limit for phase uniformity.

Cyclic Fatigue Test

For cyclic fatigue testing, AASHTO TP 133 and TP 107 were followed to ensure correct mechanical characterization of the mixtures. The temperatures for each test were chosen from the table in the standard based on the binder grade of the mixture. For all mixtures, the target test temperature was 18°C. This temperature was chosen based off the binder grade for each mix. Each specimen was conditioned in the AMPT chamber for 1 hour and 30 minutes total. The strain level for each test was determined in accordance with the table in the standard. All the temperatures and input values used for testing are shown in Table D.1. All DQI were met in accordance with the limits set in the standard. If a test resulted in an end failure, as described in the standard, the data was not used for this research and another test was conducted.

Table D.1. Cyclic Fatigue Test Temperatures and Input Strain for Tested Mixtures.

Mixture	Region	Specimen	Test Temperature (°C)	Input Strain Level
RS9.5B	CO	1-2	18	475
		2-2	18	475
		3-2	18	475
	PI	1-4	18	600
		2-2	18	600
		3-4	18	600
		1-3	18	600
	MO	1-2	18	530
		1-3	18	420
		2-1	18	420
RS9.5C	CO	2-4	18	440
		3-4	18	440
		4-4	18	440
	PI	1-2	18	530
		2-4	18	530
		2-1	18	530
		1-1	18	530
	MO	1-3	18	390
		2-1	18	320
		2-2	18	320
RI19.0C	CO	1-3	18	350
		2-3	18	350
		3-3	18	350
	PI	9-2	18	400
		10-1	18	290
		11-3	18	290
	MO	1-1	18	380
		2-1	18	300
		3-1	18	300
		4-1	18	300
RB25C	CO	3	18	160
		8	18	160
		14	18	150
	PI	6	18	160
		9	18	160
		11	18	160
	MO	1	18	240
		3	18	160
		5	18	160

Stress Sweep Rutting Test

For the stress sweep rutting testing, AASHTO TP 134 was followed. Table D.2 below summarizes the test temperatures followed for each mixture. The high temperature was determined by the calculation using the number of degree days and the design depth to the top of the layer. The low temperature was determined from a table in the standard, which was based on the climatic performance grade for the location of interest. The number of degree days and climatic binder grade were found using the asphalt mixture location and LTPPBind v. 3.1.

If the difference between the final permanent strain values of two specimens was above 25%, a third specimen was tested. This third specimen would ideally result in a permanent strain that falls between the other two specimens' permanent strains within the 25% difference.

Table D.2. SSR Test Temperatures.

Mixture	Region	Low Temperature (°C)	High Temperature (°C)
RS9.5B	CO	29	52
	PI	29	51
	MO	18	49
RS9.5C	CO	29	52
	PI	29	51
	MO	18	49
RI19.0C	CO	29	46
	PI	29	45
	MO	18	43
RB25C	CO	29	43
	PI	29	42
	MO	18	40

Experimental Results and Discussion

Introduction

This section presents the experimental results collected during this study, results from the analysis of this data using FlexMAT™, and the statistical analysis of those results. The discussion covers the differences shown between mixes of the same variation and is supported by the statistical analysis. There are two methodologies for this statistical analysis. The methodology of the statistical analysis for dynamic modulus test parameters follows the flowchart in Figure D.1. The methodology of the statistical analysis for cyclic fatigue and stress sweep rutting test parameters follows the flowchart in Figure D.2.

From dynamic modulus testing, the dynamic modulus and phase angle were identified and examined on a temperature and frequency basis. From cyclic fatigue testing, the properties included pseudo stiffness (C), D^R, number of cycles to failure (Nf), representative damage (S_{app}), and fingerprint modulus (FP). From the stress sweep rutting testing, the properties included delta viscoplastic permanent-strain (grouped from cycles 0 – 200, 201 – 400, and 401 – 600) and rutting strain index (RSI).

For the dynamic modulus test parameters, the first step of the statistical analysis process was to develop a Q-Q plot and perform the Shapiro-Wilk Test to potentially flag problematic data when drawing conclusions. For this statistical analysis, there was a limit to what could be done because

of the extremely small sample sizes. Although the Shapiro-Wilk test has limited statistical power to reject if the data is normally distributed, it was used as guidance to flag potentially problematic data. A decision was made whether to transform the entirety of the data to better suit normality based on the totality of results across all temperatures and frequencies. Some methods of transformation included exponential, inverse, Boxcox, and flipping data. The assumption of normally distributed data was a given, even if the data needed to be transformed or not. With less-than-ideal sample sizes, this led to low statistical power for identifying significant differences within the data. Therefore, the data was analyzed parametrically, as the low statistical power of small sample sizes would be compounded by nonparametric tests. The next step of this analysis was to run the Levene and Bartlett tests for unequal variances. Both tests were performed because the Levene test is less sensitive to data that defers from the normal distribution, but for normally distributed data, Barlett's test has a more robust performance. If the variances of the data, as an entirety, exhibit equality then an ANOVA test was to be performed to determine if there was a significant difference in means. If there was a significant difference, then Tukey-Kramer HSD was used to determine which means are statistically different. If the variances of the data, as an entirety, exhibited inequality, then a Welch's ANOVA test was to be performed to determine if there was a significant difference in means. If there was a significant difference, then the Games-Howell test was used to identify the means that were statistically different. The Welch's ANOVA and Games-Howell tests are the unequal variances equivalent to ANOVA and Tukey-Kramer HSD.

Just as with the dynamic modulus parameters, the cyclic fatigue and SSR parameters have extremely small sample sizes. In fact, the sample sizes for these parameters are smaller than the dynamic modulus parameter sample sizes. For this data, there is no need to try and transform the data to better meet the normality assumption, thus the normality of data is assumed from the beginning of the analysis. For cyclic fatigue and SSR test parameters, the first step of the statistical analysis process was to develop a Q-Q plot and perform the Shapiro-Wilk Test to potentially flag problematic data when drawing conclusions. The rest of the analysis was the same as the dynamic modulus analysis.

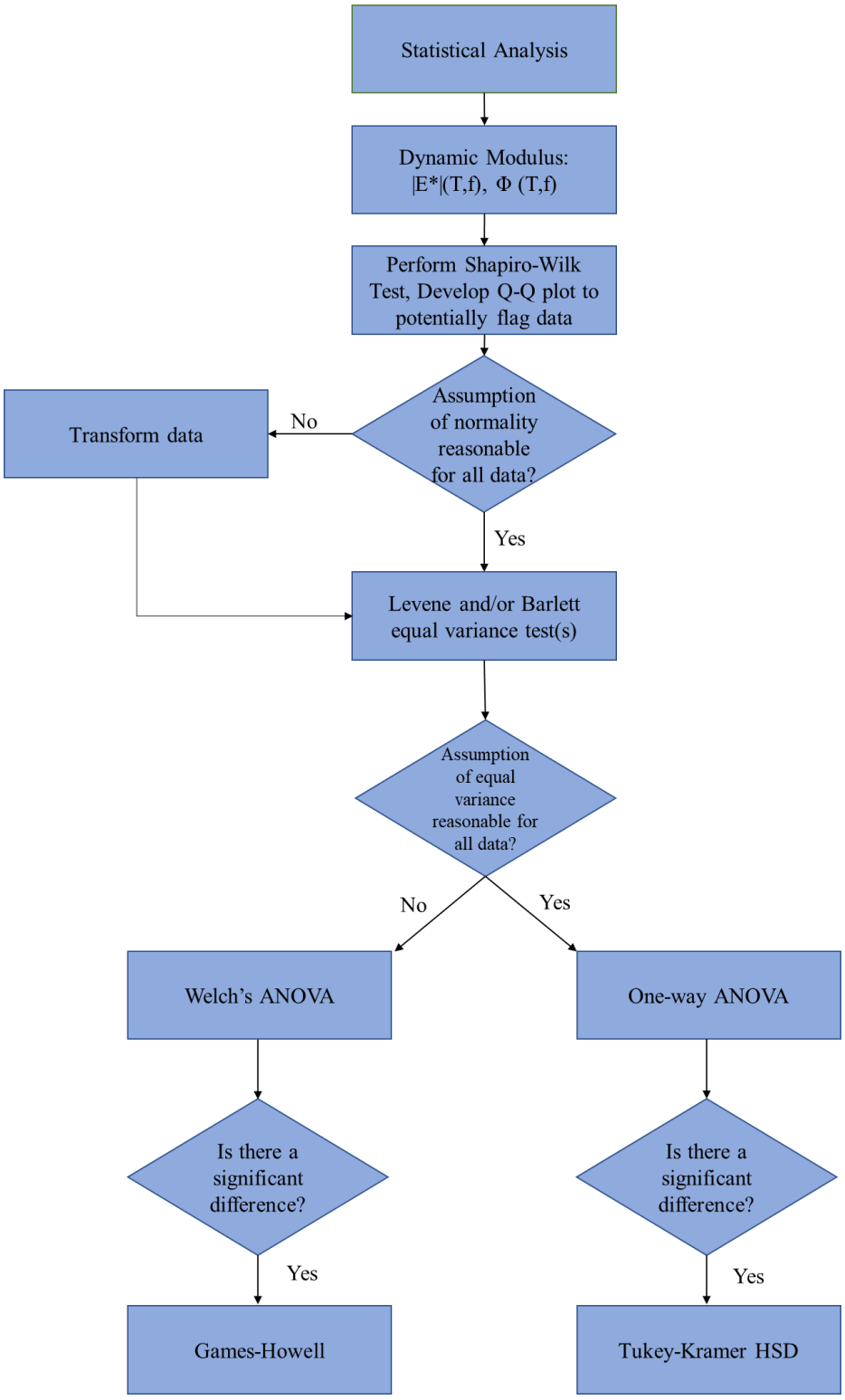

Figure D.1. Statistical analysis procedure for dynamic modulus test parameters.

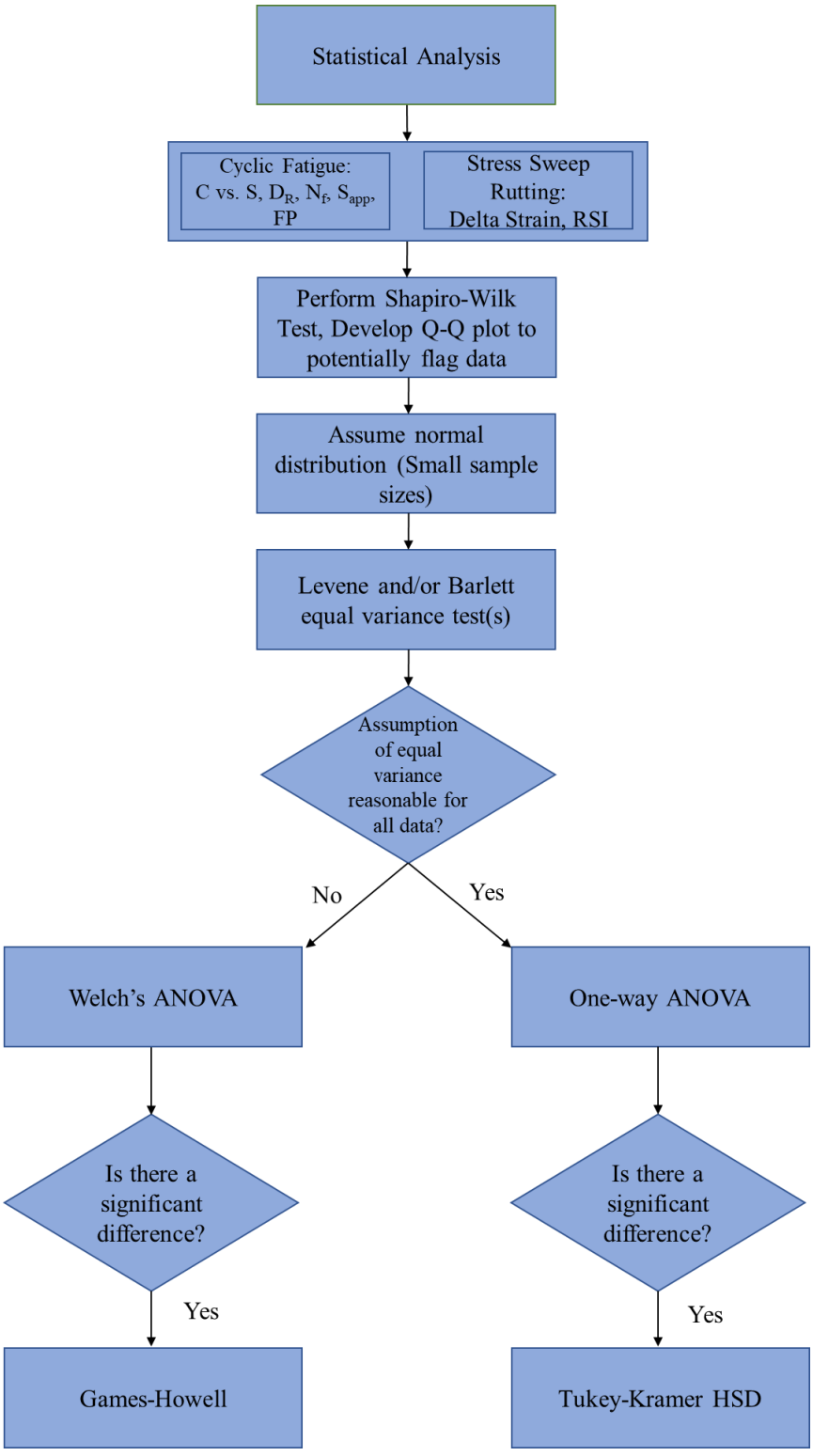

Figure D.2. Statistical analysis procedure for cyclic fatigue and stress sweep rutting parameters.

North Carolina RS9.5B Experimental Results

Dynamic Modulus Tests

The dynamic modulus results for each of the three surface mixtures are shown in Figure D.3 and Figure D.4. The phase angle results from the dynamic modulus testing are shown in Figure D.5. Overall, the modulus of CO_RS9.5B looks to be higher than PI_RS9.5B and MO_RS9.5B. In addition, MO_RS9.5B looks to have the higher phase angle values than the other two mixtures. CO_RS9.5B has a courser gradation in respect to the largest aggregates and has the lowest binder content and effective binder content. This explains as to why this mixture has the higher modulus values. The phase angle values follow that MO_RS9.5B has a higher binder content and higher effective binder content.

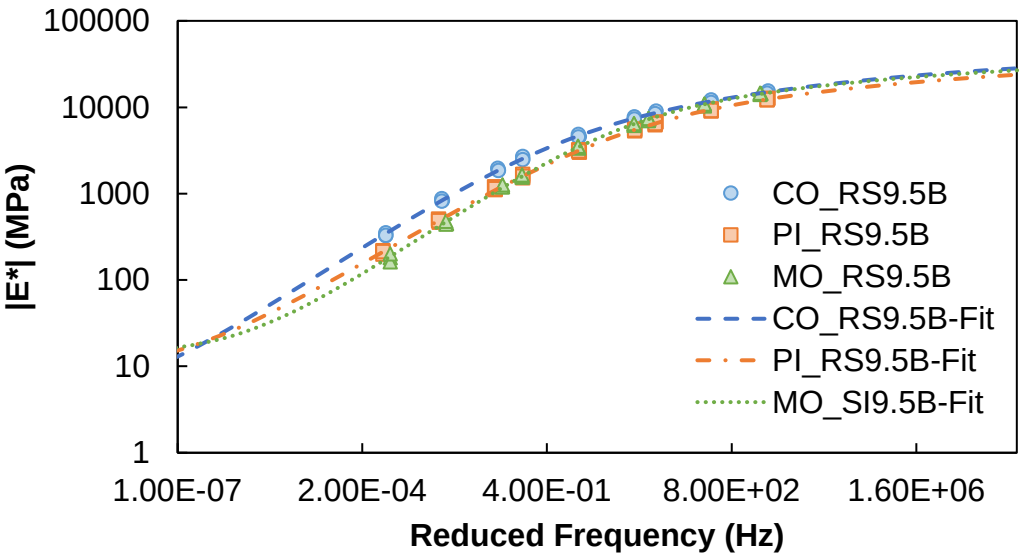

Figure D.3. Dynamic modulus results (log-log plot).

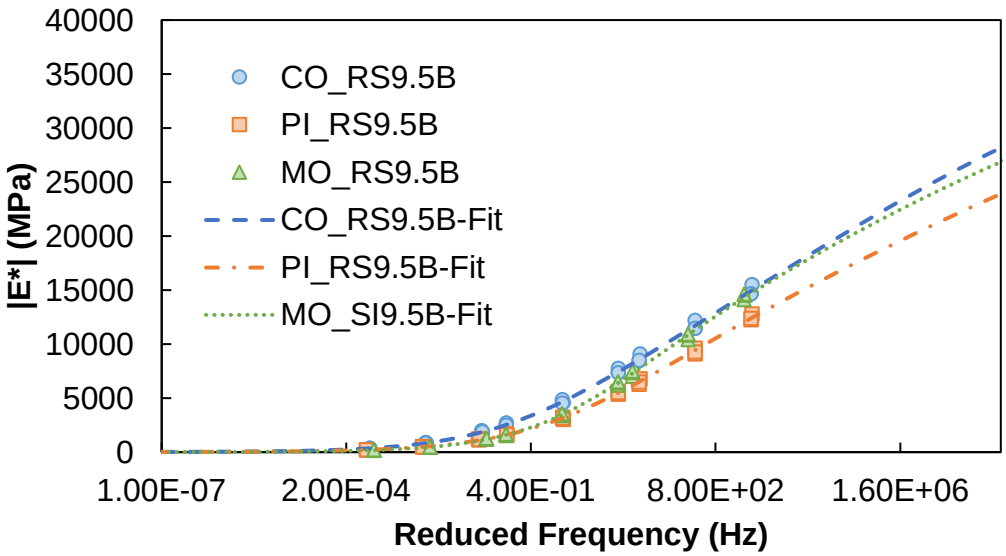

Figure D.4. Dynamic modulus results (semi-log plot).

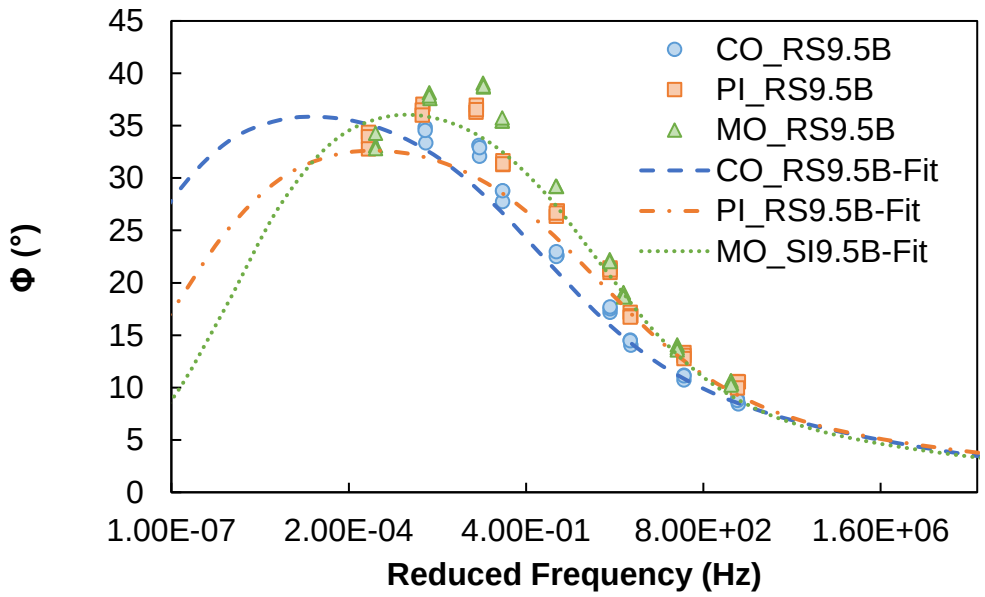

Figure D.5. Phase angle results.

For the statistical analysis of the dynamic modulus results, the modulus values from each temperature and frequency combination were compared. For example, for 4°C-10 Hz, three specimens were tested for each of the mixes. Therefore, there are three dynamic modulus values for each mix for this temperature and frequency combination. The three values for each mix were grouped together and compared against each other to see if there is a significant difference. The dynamic modulus values used in the statistical analysis are shown in Table D.3. For the statistical analysis, the test results for normality and equal variances are shown in Table D.4. Table D.5 provides a summary of the results and the resultant statistical analysis method chosen for each of the relevant parameters.

In summary, for the dynamic modulus data, four of the combinations above were flagged for non-normality. After examining the results for transformed data and non-transformed data it was determined to not perform an overall transformation on the data because applying a transformation to all data caused some data to have a relatively high variation that affected the overall significant differences. All the data passed the equal variances check; thus, it was concluded to run an ANOVA test to find significant differences. The results of the statistical analysis are shown in Table D.6 in terms of the p-values from the hypothesis test. In this table, cases where the p-value is less than a significance level of 95% are highlighted in red. By examining the p-values shown, CO_RS9.5B is statistically different from PI_RS9.5B and MO_RS9.5B. PI_RS9.5B is also different from MO_RS9.5B, except for 40°C.

Table D.3. Dynamic Modulus Results for Statistical Analysis.

Mixture	4°C-10Hz	4°C-1Hz	4°C-0.1Hz	20°C -10Hz	20°C-1Hz	20°C-0.1Hz	40°C-10Hz	40°C -1Hz	40°C -0.1Hz
CO_RS9.5B	14668	11448	8459	7398	4582	2506	1878	836.4	328.5
	15519	12209	9076	7770	4858	2706	1982	879.9	353.8
	14666	11452	8484	7355	4540	2491	1862	822.6	329.9
PI_RS9.5B	12247	9087	6288	5357	3028	1533	1117	466.5	199.1
	12791	9633	6769	5632	3243	1684	1202	511.6	219.6
	12369	9253	6486	5502	3127	1601	1147	489.4	213
MO_RS9.5B	14114	10406	7029	6200	3373	1550	1201	450.7	181.6
	14537	10832	7359	6407	3489	1612	1203	443.7	162.6
	14637	10926	7480	6506	3561	1652	1268	481.1	201.3

Table D.4. Statistical Values for Dynamic Modulus Data.

Comparison	Normality (Shapiro-Wilk Test) Prob<W	Equal Variance (Levene and Bartlett tests) Prob>F	ANOVA or Welch's ANOVA (significant difference in means) α = 0.05
4°C-10Hz	0.1051	0.2672, 0.6928	0.0004**
4°C-1Hz	0.6399	0.3986, 0.7864	0.0004**
4°C-0.1Hz	0.4847	0.5162, 0.8409	0.0002**
20°C-10Hz	0.3945	0.4365, 0.7882	0.0001**
20°C-1Hz	0.0592	0.3584, 0.7073	0.0001**
20°C-0.1Hz	0.0040*	0.2321, 0.5652	0.0001**
40°C-10Hz	0.0044*	0.4059, 0.7619	0.0001**
40°C-1Hz	0.0035*	0.6619, 0.8627	0.0001**
40°C-0.1Hz	0.0472*	0.6923, 0.7407	0.0001**

*Significant values based on significance level
**Significantly different means

Table D.5. Summary of Statistical Analysis Method for Dynamic Modulus.

Data	Comparison	Normality Check (Passed)	Trans. Method	Equal Variance Check (Passed)	Trans. Method	Statistical Analysis Method
Dynamic Modulus	4°C-10Hz	Yes	None	Yes	None	ANOVA, Tukey-Kramer HSD
	4°C-1Hz	Yes		Yes		
	4°C-0.1Hz	Yes		Yes		
	20°C-10Hz	Yes		Yes		
	20°C-1Hz	Yes		Yes		
	20°C-0.1Hz	No		Yes		
	40°C-10Hz	No		Yes		
	40°C-1Hz	No		Yes		
	40°C-0.1Hz	No		Yes		

Table D.6. Significant Differences for Dynamic Modulus Data.

Comparison	p-values (α = 0.05)								
	4°C-10Hz	4°C-1Hz	4°C-0.1Hz	20°C-10Hz	20°C-1Hz	20°C-0.1Hz	40°C-10Hz	40°C-1Hz	40°C-0.1Hz
CO9.5B vs. PI9.5B	0.0004	0.0003	0.0002	0.0001	0.0001	0.0001	0.0001	0.0001	0.0001
CO9.5B vs. MO9.5B	0.2640	0.0285	0.0022	0.0006	0.0001	0.0001	0.0001	0.0001	0.0001
PI9.5B vs. MO9.5B	0.0014	0.0057	0.0338	0.0023	0.0411	0.9998	0.2885	0.3416	0.1273

The phase angle results were statistically compared just as the dynamic modulus results. The phase angle results used in the statistical analysis are found in Table D.7. For the statistical analysis, the test results for normality and equal variances are shown in Table D.8. Table D.9 above provides a summary of the results and the resultant statistical analysis method chosen for each of the relevant parameters.

In summary, all phase angle data passed the normality check except the data for 4°C-10Hz and 20°C-10Hz tests. Based on the entirety of the data, it was concluded to not transform the data to better fit the assumption of normality. All the data passed the equal variance check except 20°C-0.1Hz; thus, an ANOVA test was used to detect significant differences. The results of the statistical analysis are shown in Table D.10 in terms of the p-values from the hypothesis test. In this table, cases where the p-value is less than a significance level of 95% are highlighted in red. For the phase angle data, CO_RS9.5B, PI_RS9.5B, and MO_RS9.5B are significantly different except for a couple of combinations.

Table D.7. Phase Angle Results for Statistical Analysis.

Mixture	4°C-10Hz	4°C-1Hz	4°C-0.1Hz	20°C-10Hz	20°C-1Hz	20°C-0.1Hz	40°C-10Hz	40°C-1Hz	40°C-0.1Hz
CO_RS9.5B	8.89	11.19	14.54	17.19	22.61	28.76	32.1	33.38	33.19
	8.44	10.72	14.05	17.52	22.52	27.75	33.12	34.85	34.19
	8.76	11.11	14.46	17.69	22.97	28.79	32.91	34.56	33.81
PI_RS9.5B	10.58	13.35	17.18	21.41	26.86	31.67	36.95	37.05	34.36
	10.53	13.06	16.85	21	26.37	31.28	36.29	36.49	33.93
	9.96	12.75	16.72	21.23	26.67	31.35	36.54	36.03	32.78
MO_RS9.5B	10.65	14.07	19.08	22.21	29.18	35.43	38.69	37.59	33.08
	10.39	13.81	18.78	22.06	29.23	35.47	39.08	38.14	34.29
	10.24	13.59	18.64	22.03	29.23	35.74	38.78	37.85	32.83

Table D.8. Statistical Values for Phase Angle Data.

Comparison	Normality (Shapiro-Wilk Test) Prob<W	Equal Variance (Levene and Bartlett tests) Prob>F	ANOVA or Welch's ANOVA (significant difference in means) α = 0.05
4°C-10Hz	0.0380*	0.4162, 0.7823	0.0003**
4°C-1Hz	0.1222	0.94, 0.9545	0.0001**
4°C-0.1Hz	0.1837	0.9042, 0.9792	0.0001**
20°C-10Hz	0.0111*	0.4037, 0.5082	0.0001**
20°C-1Hz	0.0567	0.1156, 0.0815	0.0001**
20°C-0.1Hz	0.1424	0.0363, 0.2171*	0.0001**
40°C-10Hz	0.1464	0.2154, 0.4895	0.0001**
40°C-1Hz	0.5424	0.2181, 0.4587	0.0007**
40°C-0.1Hz	0.1594	0.5448, 0.8150	0.8313

*Significant values based on significance level
**Significantly different means

Table D.9. Significant Differences for Phase Angle Data.

Comparison	p-values (α = 0.05)								
	4°C-10Hz	4°C-1Hz	4°C-0.1Hz	20°C-10Hz	20°C-1Hz	20°C-0.1Hz	40°C-10Hz	40°C-1Hz	40°C-0.1Hz
CO9.5B vs. PI9.5B	0.0007	0.0002	0.0001	0.0001	0.0001	0.0001	0.0001	0.0063	0.8754
CO9.5B vs. MO9.5B	0.0005	0.0001	0.0001	0.0001	0.0001	0.0001	0.0001	0.0006	0.8426
PI9.5B vs. MO9.5B	0.9456	0.0278	0.0002	0.0036	0.0001	0.0002	0.0009	0.0601	0.9974

Table D.10. Summary of Statistical Analysis Method for Phase Angle Data.

Data	Comparison	Normality Check (Passed)	Trans. Method	Equal Variance Check (Passed)	Trans. Method	Statistical Analysis Method
Phase Angle	4°C-10Hz	No	None	Yes	None	ANOVA, Tukey-Kramer HSD
	4°C-1Hz	Yes		Yes		
	4°C-0.1Hz	Yes		Yes		
	20°C-10Hz	No		Yes		
	20°C-1Hz	Yes		Yes		
	20°C-0.1Hz	Yes		No		
	40°C-10Hz	Yes		Yes		
	40°C-1Hz	Yes		Yes		
	40°C-0.1Hz	Yes		Yes		

Cyclic Fatigue Tests

The cyclic fatigue test data resulting in *C* vs. *S* damage curves are shown in Figure D.6 and Figure D.7. The representative S_{app} values, DR values, and Nf vs. Cum. (1-C) data are shown in Figure D.8, Figure D.9, and Figure D.10 respectively. The linear viscoelastic and S-VECD fatigue properties are shown in Table D.11. For the damage curves, CO_RS9.5B has the highest *C* values through the whole damage curve. PI_RS9.5B has the highest S_{app} values followed by CO_RS9.5B and then MO_RS9.5B. PI_RS9.5B has the lowest dynamic modulus values as well as the softest binder which seems to govern the S_{app} value. PI_RS9.5B has the highest D^R values followed by CO_RS9.5B and then MO_RS9.5B. The Cum. (1-*C*) vs. N_f graph shows different results for all three of the mixes. CO_RS9.5B and PI_RS9.5B have similar slopes in this graph.

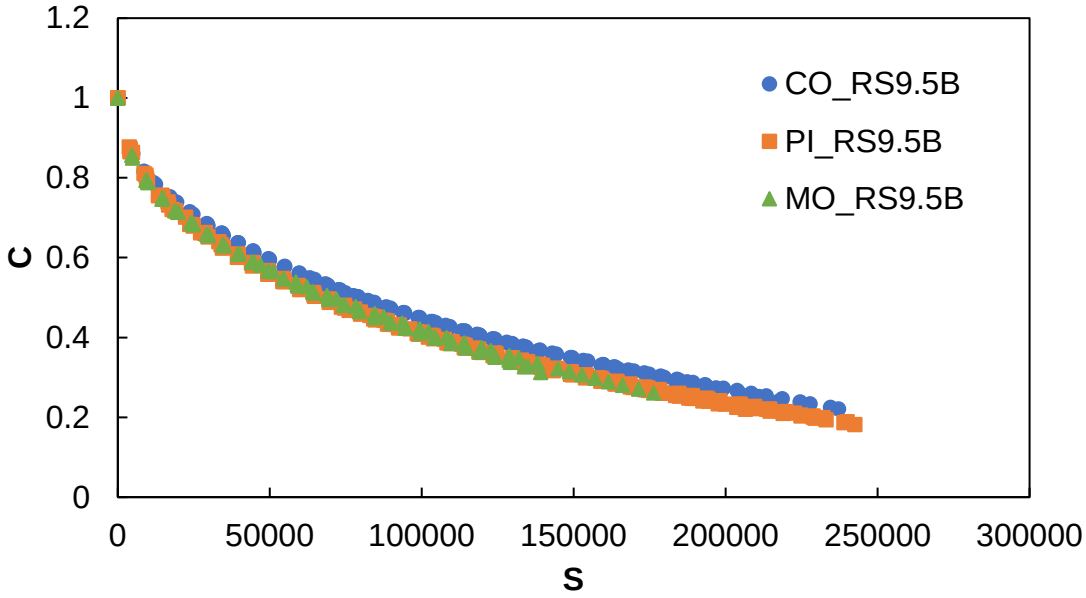

Figure D.6. *C* vs. *S* damage curves (individual specimen values).

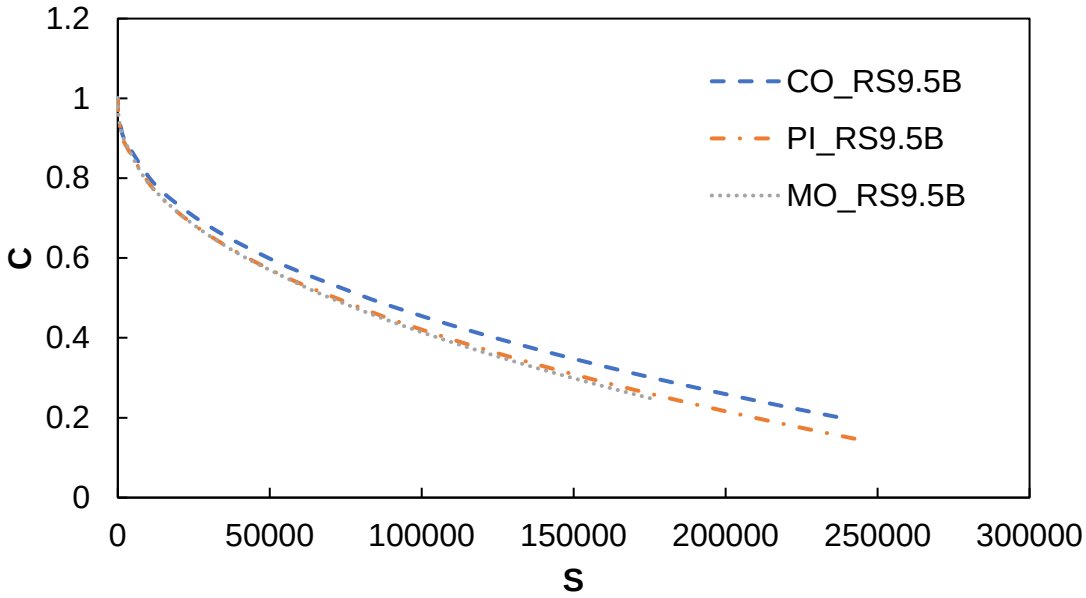

Figure D.7. *C* vs. *S* damage curves (fitted values).

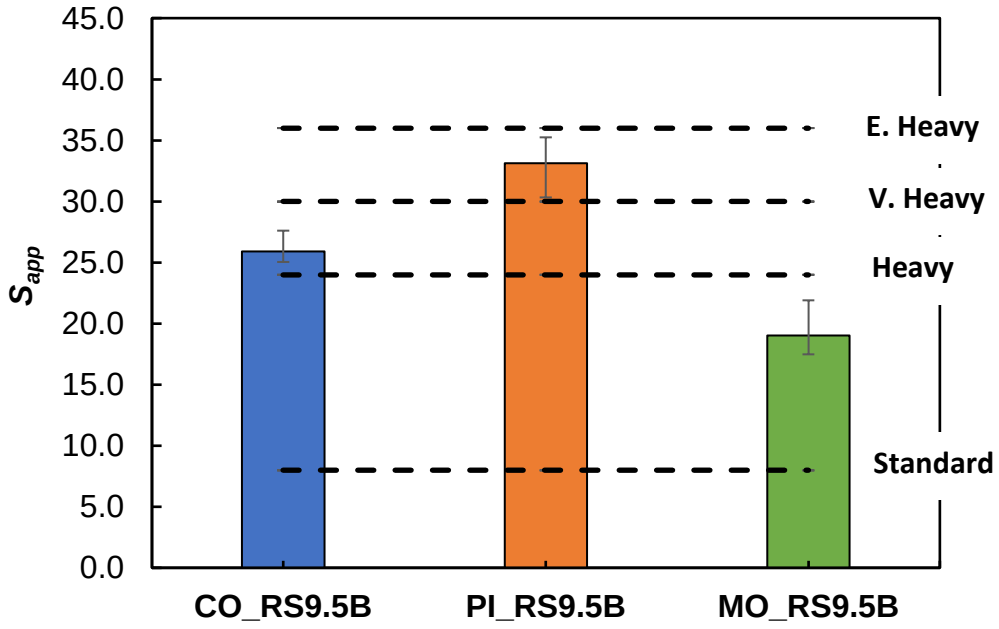

Figure D.8. Representative S_{app} values.

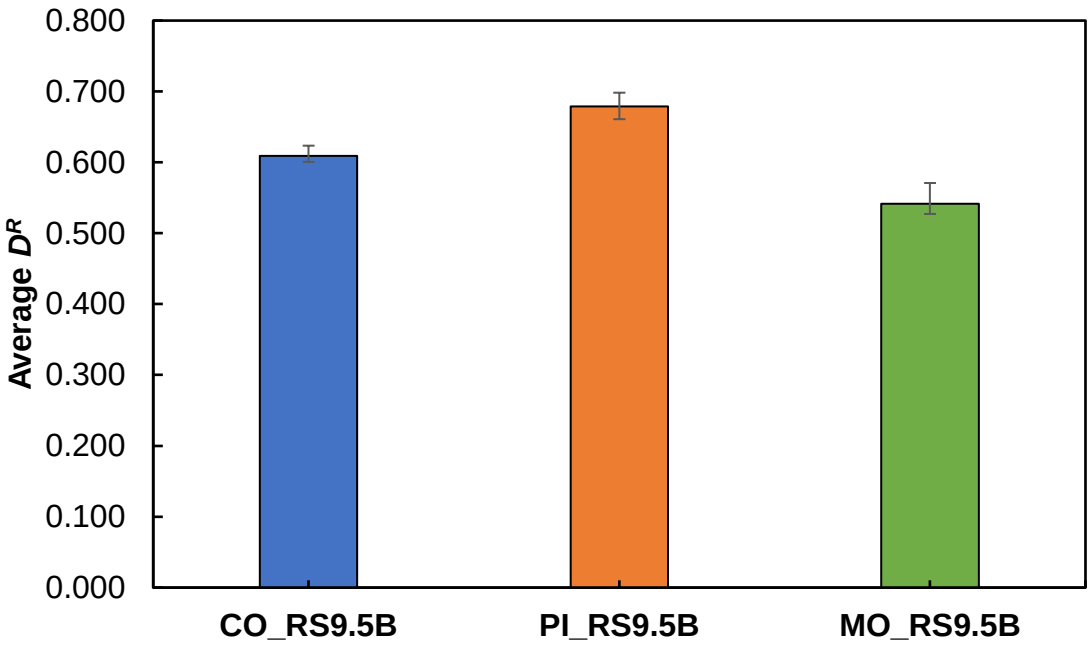

Figure D.9. Average D^R values.

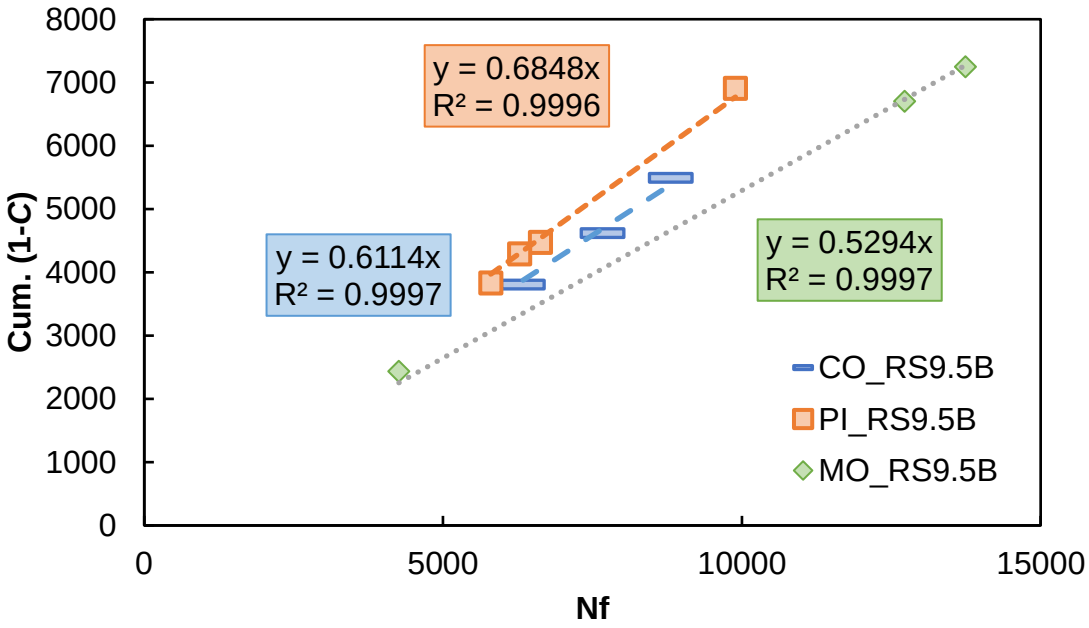

Figure D.10. Cum. (1-*C*) vs. N_f.

Table D.11. Linear Viscoelastic and FlexPAVE™ S-VECD Fatigue Properties.

Properties	CO_RS9.5B	PI_RS9.5B	MO_RS9.5B
α	3.48	3.73	3.46
C_{11}	0.0034	0.0038	0.0036
C_{12}	0.44	0.44	0.44
a_1	0.0008	0.0007	0.0007
a_2	-0.17	-0.17	-0.16
a_3	3.19	3.19	3.03

For the cyclic fatigue data results, the following parameters were statistically compared; fingerprint modulus, number of cycles to failure (N_f), D^R, S_{app}, and pseudo stiffness values (C) associated with two fixed damage parameter values (S). The temperatures for calculating S_{app} are the same for the statistical analysis. For the cyclic fatigue tests, three or four specimens were used to conduct the tests for each mix, therefore the specimens for each mix were grouped together and compared against each other. The two S values chosen for the statistical analysis were 20,000 and 120,000. These values were chosen based on the length of the damage curves. The average C values targeted for these S values were 0.72 and 0.38. The C values that correspond to these two values were interpolated from the C vs. S curves characterized for each specimen from FlexMAT™. The values used in the statistical analysis for fingerprint modulus, N_f, D^R, and S_{app} are shown in Table D.12. The C values used in the statistical analysis are shown in Table D.13.

For the statistical analysis, the tests of normality and variance are shown in Table D.14. Table D.15 provides a summary of the results and the resultant statistical analysis method chosen for each of the relevant parameters. Even though the data for C at S = 20,000 and C at S = 120,000 did not appear to pass the normality check, the data was assumed normal as described by the description of the statistical analysis. All the data passed the equal variance checks, except for N_f, thus equal variances were assumed, and an ANOVA test was used for all data.

The p-values that show the significant differences for the cyclic fatigue data are shown in Table D.16. This table shows the same trend as shown in the dynamic modulus data, that all mixtures are different in terms of modulus. This also shows that the mixtures are also different in terms of D^R and S_{app}. For the *C* vs. *S* data, this table shows that CO_RS9.5B is different from the other two mixtures.

Table D.12. Cyclic Fatigue Results for Statistical Analysis.

Mixture	Fingerprint |E*| (MPa)	N_f	D^R	S_{app}
CO_RS9.5B	8215	7670	0.60	25.06
CO_RS9.5B	8318	8810	0.62	27.61
CO_RS9.5B	8440	6340	0.60	25.07
PI_RS9.5B	6099	9890	0.70	35.25
PI_RS9.5B	6501	5800	0.66	30.32
PI_RS9.5B	6372	6630	0.67	32.92
PI_RS9.5B	6426	6280	0.68	34.07
MO_RS9.5B	7278	4260	0.57	21.91
MO_RS9.5B	7115	12720	0.53	17.49
MO_RS9.5B	7574	13740	0.53	17.70

Table D.13. *C* Values used for Statistical Analysis.

Mixture	*C* at *S* = 20,000	*C* at *S* = 120,000
CO_RS9.5B	0.73	0.40
CO_ RS9.5B	0.74	0.40
CO_ RS9.5B	0.74	0.40
CO_ RS9.5B	0.74	0.41
PI_ RS9.5B	0.71	0.36
PI_ RS9.5B	0.71	0.36
PI_ RS9.5B	0.72	0.37
PI_ RS9.5B	0.71	0.37
PI_ RS9.5B	0.72	0.37
MO_ RS9.5B	0.71	0.37
MO_ RS9.5B	0.71	0.36
MO_ RS9.5B	0.71	0.36
MO_ RS9.5B	0.71	0.36

Table D.14. Statistical Values for Cyclic Fatigue Data.

Attribute	Normality (Shapiro-Wilk Test) Prob<W	Equal Variance (Levene and Bartlett tests) Prob>F	ANOVA or Welch's ANOVA (significant difference in means) α = 0.05
Fingerprint |E*|	0.2395	0.5229, 0.6650	<0.0001**
N_f	0.2987	0.0309*, 0.1403	0.4385
D^R	0.4109	0.3017, 0.6477	<0.0001**
S_{app}	0.4763	0.6025, 0.7987	0.0001**
C at S = 20,000	0.0067*	0.0733, 0.2072	<0.0001**
C at S = 120,000	0.0035*	0.4036, 0.5156	<0.0001**

*Significant value based on significance level
**Significantly different means

Table D.15. Summary of Statistical Analysis Method for Cyclic Fatigue Data.

Attribute	Normality Check (Passed)	Trans. Method	Equal Variance Check (Passed)	Trans. Method	Statistical Analysis Method
Fingerprint |E*|	Yes	None	Yes	None	ANOVA, Tukey-Kramer HSD
N_f	Yes		No		
D^R	Yes		Yes		
S_{app}	Yes		Yes		
C at S = 20,000	No		Yes		
C at S = 120,000	No		Yes		

Table D.16. Significant Differences for Cyclic Fatigue Data.

Comparison	p-values (α = 0.05)					
	Fingerprint |E*| (MPa)	N_f	D_R	S_{app}	C at S = 20,000	C at S = 120,000
CO_RS9.5B vs. PI_RS9.5B	0.0001	0.9798	0.0038	0.0063	0.0001	0.0001
CO_RS9.5B vs. MO_RS9.5B	0.0006	0.5784	0.0069	0.0115	0.0001	0.0001
PI_RS9.5B vs. MO_RS9.5B	0.0005	0.4378	0.0001	0.0001	0.9996	0.9565

Stress Sweep rutting Tests

The permanent micro-strain curves for each mixture are shown in Figure D.11 and Figure D.12. The rutting strain index (RSI) values are shown in Figure D.13, Figure D.14, and Figure D.15. For the North Carolina mixtures, each mixture is from a specific region, therefore the RSI values in three different locations are shown. Table D.17 shows the percent difference between each test.

CO_RS9.5B exhibits the highest micro-strain in the high temperature tests, followed by PI_RS9.5B and MO_RS9.5B. As shown in Table D.2, the temperatures for these SSR tests were different. CO_RS9.5B had the highest temperature, then PI_RS9.5B, and MO_RS9.5B. The difference was only two degrees Celsius and three degrees Celsius, respectively, but this could influence the results of these strain curves. For low temperature, PI_RS9.5B has the highest permanent strain, followed by CO_RS9.5B and MO_RS9.5B. In these tests, CO_RS9.5B and PI_RS9.5B have the same test temperature, while MO_RS9.5B has a test temperature nine degrees Celsius lower. Even though CO_RS9.5B and PI_RS9.5B have the same temperature, PI_RS9.5B has a higher permanent strain accumulation. This could be due to that PI_RS9.5B, has a higher RAP and binder content than CO_RS9.5B.

The RSI values represent the values from three different locations. MO_RS9.5B has the best rutting performance in all locations, followed by PI_RS9.5B and CO_RS9.5B. MO_RS9.5B has a lower RAP content, %RBR and higher modulus values resulting in better rutting performance than PI_RS9.5B. PI_RS9.5B also has a softer binder which could be affecting the performance. CO_RS9.5B shows a greater variation in RSI when changing locations, 8.39%, compared to MO_RS9.5B, which shows a variation of 1.47%. This variation arises with this mixture because the β value, a coefficient of the incremental model within FlexMAT™, is lower than normal. For most mixtures, this value is between 0.65 and 0.70, but for this mixture, it is 0.56. The curve fitting for the model calibration regarding this mixture is causing this value to be lower than normal. If this β value was within the average range, the RSI value for CO_RS9.5B would be lower than shown here.

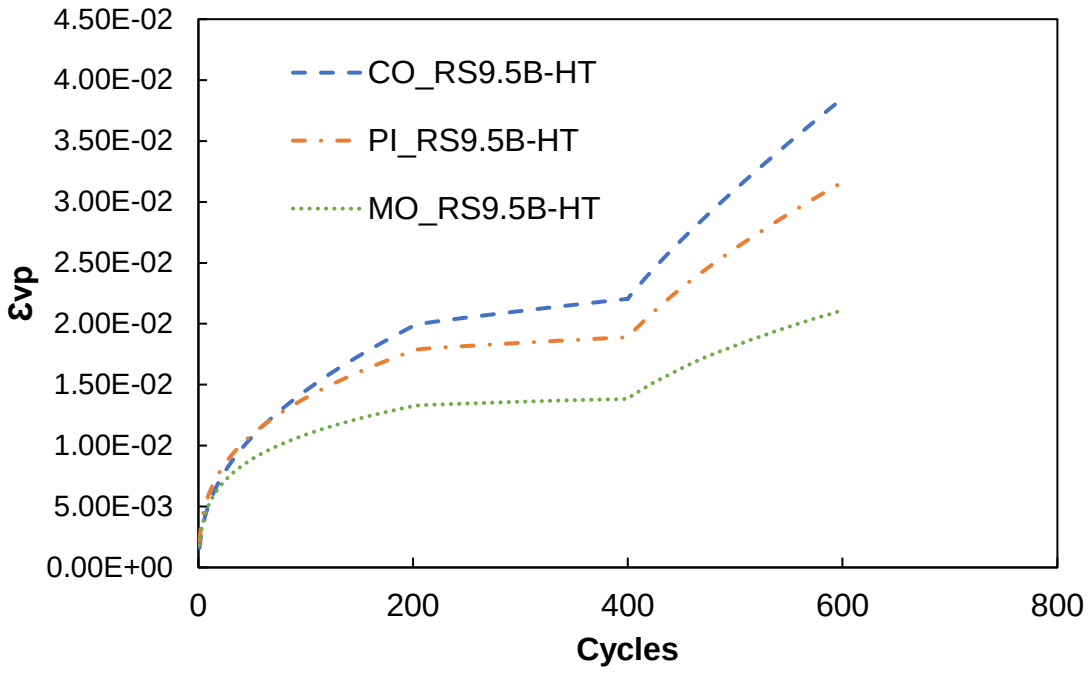

Figure D.11. Permanent micro-strain curves for high temperature tests.

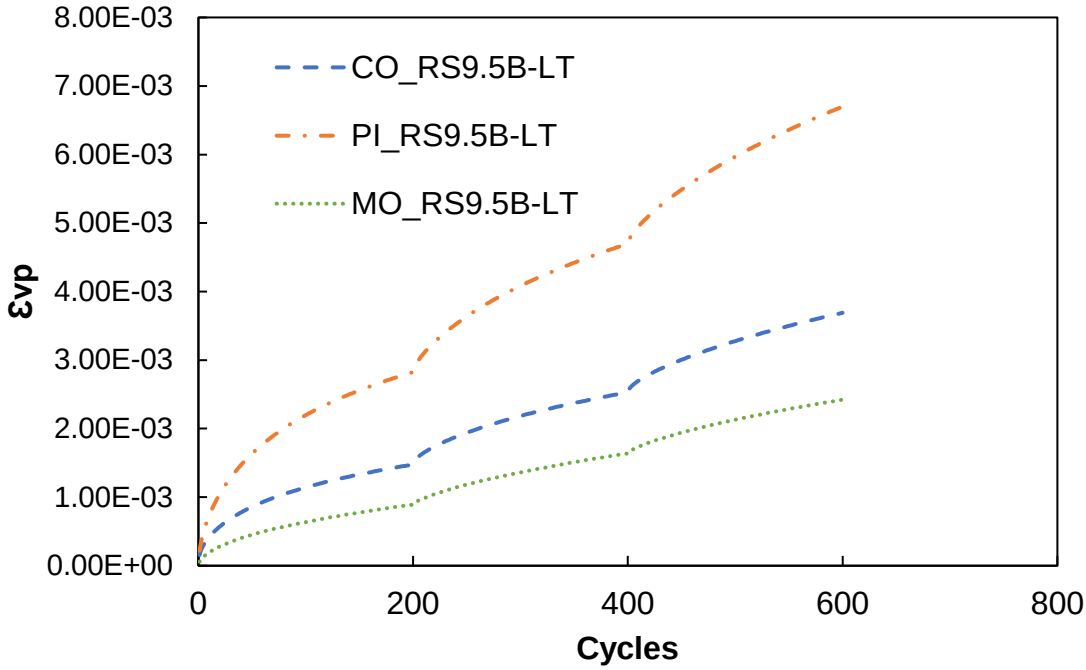

Figure D.12. Permanent micro-strain curves for low temperature tests.

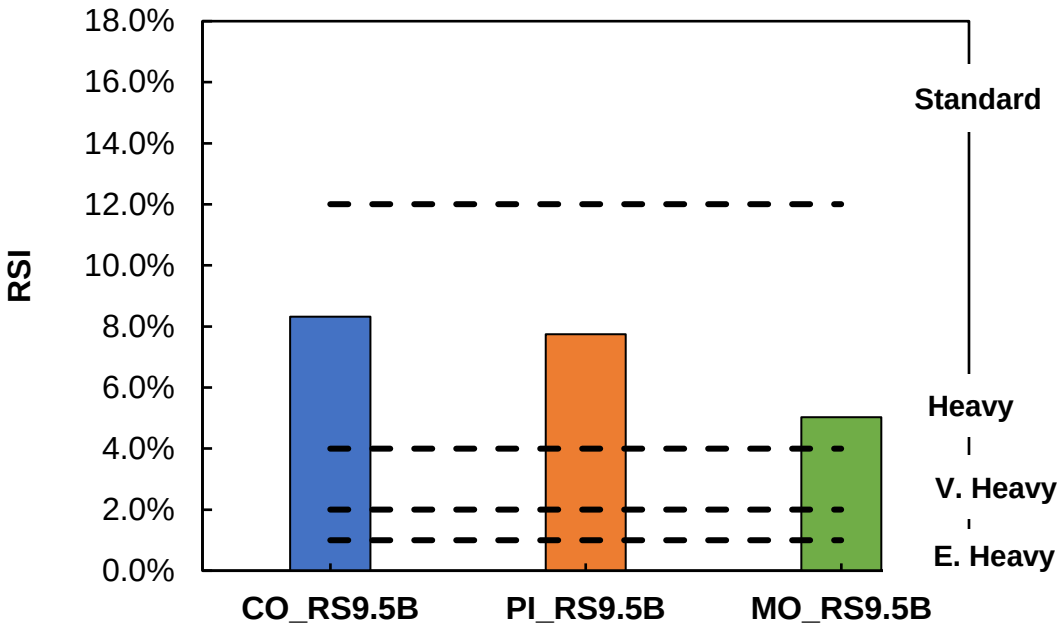

Figure D.13. Rutting strain index values (Wilmington, NC).

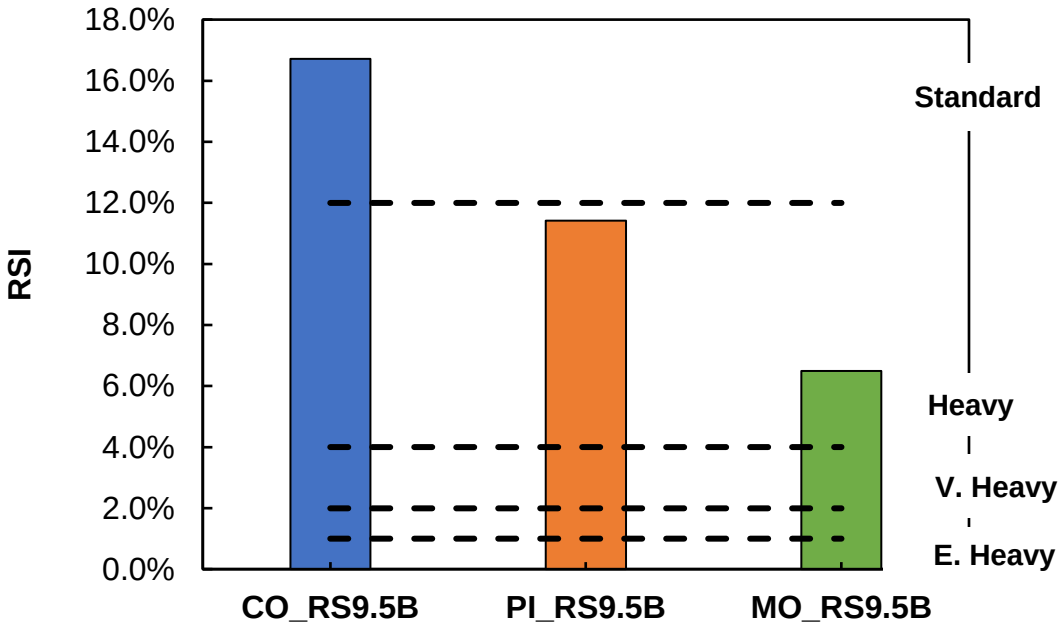

Figure D.14. Rutting strain index values (Wake Forest, NC).

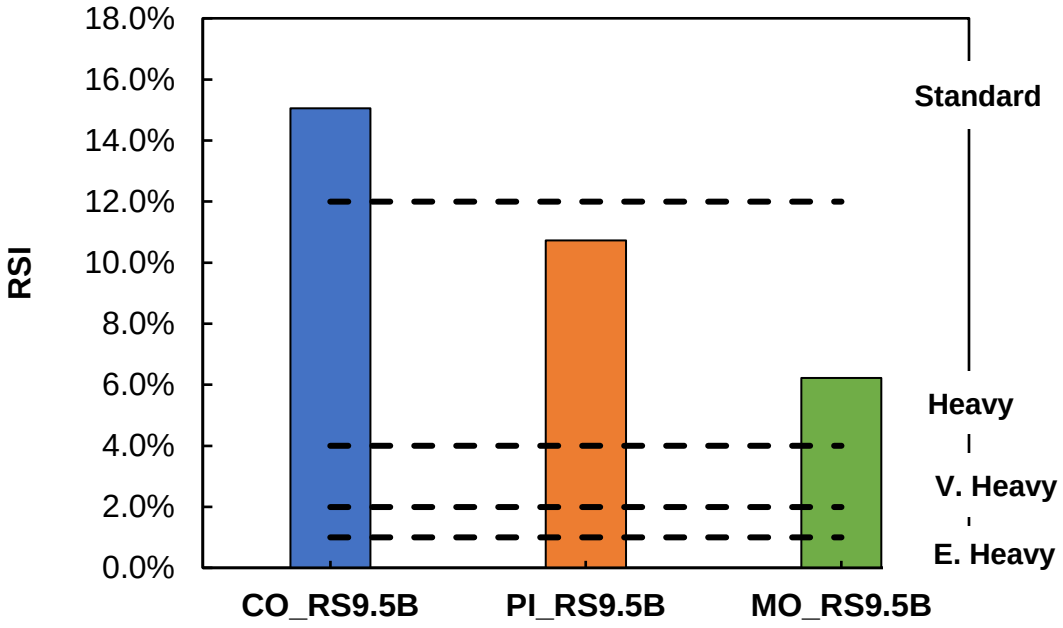

Figure D.15. Rutting strain index values (Asheville, NC).

Table D.17. Percent Difference in Permanent Micro-Strain for SSR Testing.

Mixture	Temperature	Percent Difference
CO_RS9.5B	HT	13.70
	LT	4.39
PI_RS9.5B	HT	15.83
	LT	2.09
MO_RS9.5B	HT	1.00
	LT	14.93

For the North Carolina mixtures, as mentioned before, the test temperatures for the SSR tests were different. Because of this, a statistical analysis of the permanent strain curves was not done. The RSI values for the statistical analysis are shown in Table D.18, Table D.19, and Table D.20. With so much variation in the CO_RS9.5B mixture, it was decided to run a statistical analysis on the RSI values from all three locations mentioned. The temperatures for calculating RSI were the same for all mixtures.

Table D.18. RSI Values for SSR Tests (Wilmington, NC).

Mixture	HT-H: LT-H	HT-H: LT-L	HT-L: LT-L	HT-L: LT-H	All temp.
CO_RS9.5B	10.26	9.94	7.33	7.57	8.32
PI_RS9.5B	8.08	7.95	7.38	7.50	7.75
MO_RS9.5B	4.99	4.78	5.09	5.31	5.03

Table D.19. RSI Values for SSR Tests (Wake Forest, NC).

Mixture	HT-H: LT-H	HT-H: LT-L	HT-L: LT-L	HT-L: LT-H	All temp.
CO_RS9.5B	19.89	14.35	14.01	19.42	16.71
PI_RS9.5B	12.17	10.74	10.63	12.05	11.42
MO_RS9.5B	6.41	6.79	6.22	6.58	6.50

Table D.20. RSI Values for SSR Tests (Asheville, NC).

Mixture	HT-H: LT-H	HT-H: LT-L	HT-L: LT-L	HT-L: LT-H	All temp.
CO_RS9.5B	17.96	17.52	12.70	13.03	15.05
PI_RS9.5B	11.40	11.28	10.02	10.13	10.72
MO_RS9.5B	6.14	5.95	6.30	6.51	6.22

For the statistical analysis, the normal distribution checks, equal variance checks, statistical results are all shown in Table D.21. Table D.22 below provides a summary of the results and the resultant statistical analysis method chosen for each of the relevant parameters.

In summary, the data for the RSI values passed the normality check, but each one was flagged for unequal variances. Even though other cyclic fatigue and SSR data have assumed equal variances, here an ANOVA test and Welch's ANOVA were used to identify significant differences.

The p-values for the SSR data that have significantly different means are shown in Table D.23. For RSI from Wilmington, NC, CO_RS9.5B is similar to PI_RS9.5B, while MO_RS9.5B is different from these two mixtures. For Wake Forest and Asheville, all mixtures show significant differences in RSI. The p-values in Table D.24 from the Games-Howell test show the exact same

results as the Tukey-Kramer HSD test, but by accounting for unequal variances, the Games-Howell test shows that CO_RS9.5B and PI_RS9.5B are closer to the significance threshold.

Table D.21. Statistical Values for SSR Data.

Attribute	Normality (Shapiro-Wilk Test) Prob<W	Equal Variance (Levene and Bartlett tests) Prob>F	ANOVA, (significant difference in means) α = 0.05	Welch's ANOVA, (significant difference in means) α = 0.05
RSI (Wilmington, NC)	0.0846	0.0002*, 0.0010*	<0.0001**	<0.0001**
RSI (Wake Forest, NC)	0.1094	0.0013*, 0.0002*	<0.0001**	<0.0001**
RSI (Asheville, NC)	0.1195	0.0011*, 0.0003*	<0.0001**	<0.0001**

*Significant values based on significance level

**Significantly different means

Table D.22. Summary of Statistical Analysis Method for SSR Data.

Attribute	Normality Check (Passed)	Trans. Method	Equal Variance Check (Passed)	Trans. Method	Statistical Analysis Method
RSI (Wilmington, NC)	Yes	None	No	None	ANOVA, Welch's ANOVA
RSI (Wake Forest, NC)	Yes		No		
RSI (Asheville, NC)	Yes		No		

Table D.23. Significant Differences for SSR Data (ANOVA, Tukey-Kramer HSD).

Comparison	p-values (α = 0.05)		
	RSI (Wilmington, NC)	RSI (Wake Forest, NC)	RSI (Asheville, NC)
CO_9.5B vs. PI_9.5B	0.1891	0.0005	0.001
CO_9.5B vs. MO_9.5B	0.0001	0.0001	0.0001
PI_9.5B vs. MO_9.5B	0.0005	0.0013	0.0011

Table D.24. Significant Differences for SSR Data (Welch's ANOVA, Games-Howell).

Comparison	p-values (α = 0.05)		
	RSI (Wilmington, NC)	RSI (Wake Forest, NC)	RSI (Asheville, NC)
CO_9.5B vs. PI_9.5B	0.3589	0.0211	0.0274
CO_9.5B vs. MO_9.5B	0.0077	0.0023	0.0025
PI_9.5B vs. MO_9.5B	0.0001	0.0001	0.0001

RS9.5B Analysis Summary

Table D.25 and Table D.26 show the overall significant differences for the tests' parameters. The tables use the letters to signify if the mixtures are the same or different. The letters also signify the

numerical value of that particular parameter. The lower the letter in the alphabet, the greater the value. Therefore, if a parameter is given "A", it has the higher values for that parameter. For the dynamic modulus and phase angle summary table, if two of the three temperature–frequency combinations were different with respect to two mixtures, then there were assumed different. Also, if a mixture is given two letters, such as "AB", then this mixture is similar to both of the other mixtures.

For dynamic modulus, CO_RS9.5B is different than the other two mixtures. PI_RS9.5B is different than MO_RS9.5B until the temperature is increased to 40°C. The same trend is shown for the phase angle data. For *C* vs. *S* data, CO_RS9.5B is different than the other two mixtures but all mixtures are different in terms of S_{app}. For RSI, CO_RS9.5B is similar to PI_RS9.5B, but for the other two locations, all mixtures are different.

For S_{app}, PI_RS9.5B is classified as "Very Heavy", CO_RS9.5B is classified as "Heavy", and MO_RS9.5B is classified as "Standard". For RSI, CO_RS9.5B is classified outside of "Standard" in two of the locations, but for Wilmington, NC, it has a designation of "Standard". The other two mixtures are classified as "Standard" in all three locations. The traffic designation for all three mixtures, therefore, falls under "Standard" as it is controlled by the rutting performance. CO_RS9.5B would not even be a "Standard" classification in the other two locations. According to the North Carolina DOT QMS manual, these mixtures are classified to handle 0 to 3 million ESALs. According to the S_{app} thresholds defined by Wang et al. (2020), CO_RS9.5B and PI_RS9.5B overperform, while MO_RS9.5B meets its design requirement. For RSI as defined by Ghanbari et al. (2020), all three mixtures meet the category in which they were designed.

Table D.25. Summary of Dynamic Modulus Test Parameters.

Mixtures	DM parameters			PA parameters		
	4°C	20°C	40°C	4°C	20°C	40°C
CO_RS9.5B	A	A	A	C	C	B
PI_RS9.5B	C	C	B	B	B	A
MO_RS9.5B	B	B	B	A	A	A

Table D.26. Summary of Cyclic Fatigue and Stress Sweep Rutting Test Parameters.

Mixtures	CF and SSR parameters					
	S_{app}	*C* at *S* = 20,000	*C* at *S* = 120,000	RSI Wilmington)	RSI (Wake Forest)	RSI (Asheville)
CO_RS9.5B	B	A	A	A	A	A
PI_RS9.5B	A	B	B	A	B	B
MO_RS9.5B	C	B	B	B	C	C

North Carolina RS9.5C Experimental Results

Dynamic Modulus Tests

The dynamic modulus results for each of the three surface RS9.5C mixtures are shown in Figure D.16 and Figure D.17. The phase angle results from the dynamic modulus testing are shown in Figure D.18. Overall, the modulus of MO_RS9.5C looks to be higher than PI_RS9.5C and CO_RS9.5C. PI_RS9.5C looks to have the higher phase angle values than the other two mixtures. MO_RS9.5C has a courser gradation than the other mixtures and has the lowest effective binder

content. This explains as to why this mixture has the higher modulus values. The phase angle values follow that PI_RS9.5C has a higher binder content and higher effective binder content. Even though CO_RS9.5C has the highest effective binder content, PI_RS9.5C has the higher RAP percentage eight percent.

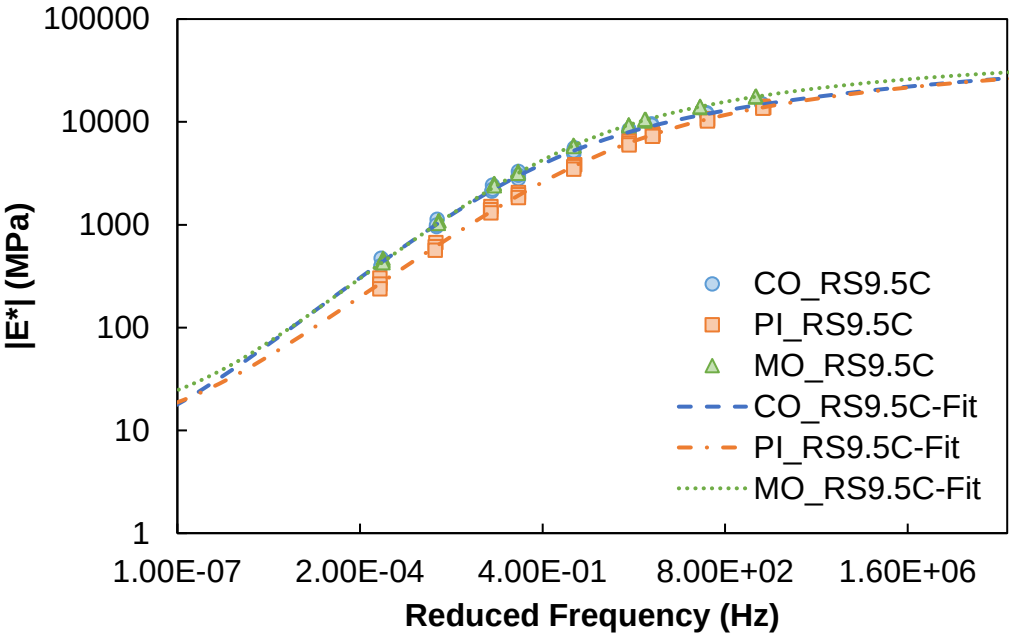

Figure D.16. Dynamic modulus results (log-log plot).

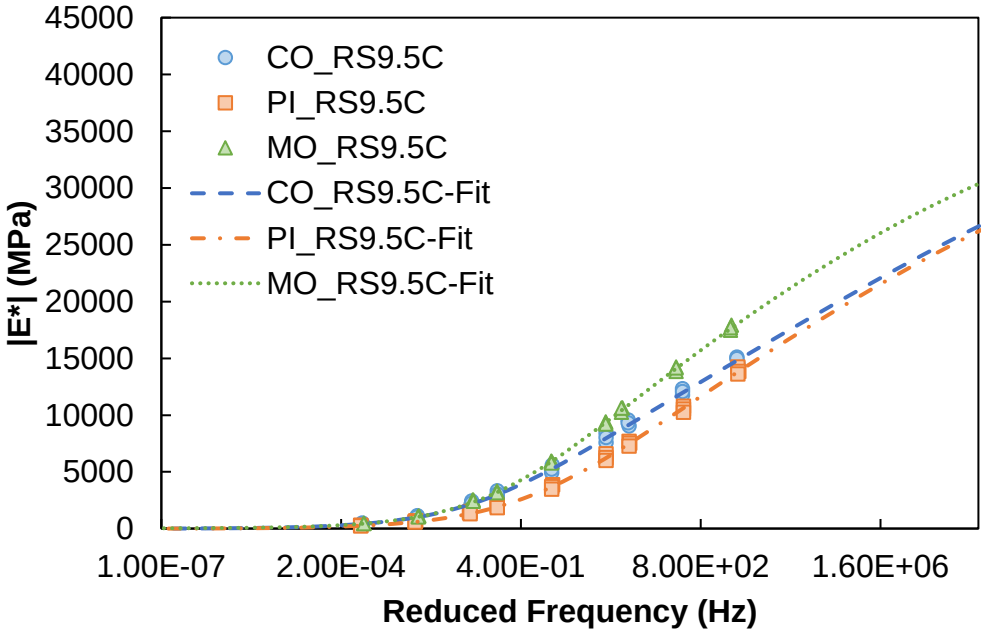

Figure D.17. Dynamic modulus results (semi-log plots).

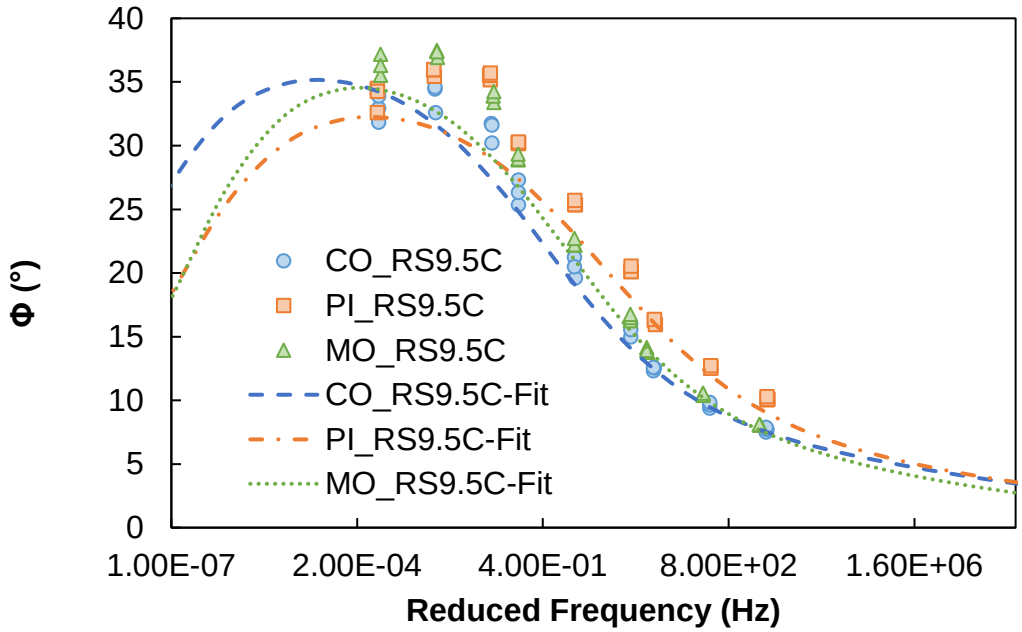

Figure D.18. Phase angle results.

The statistical analysis for the dynamic modulus results was done the exact same as in the other surface "B" mixtures. The dynamic modulus values used in the statistical analysis are shown in Table D.27. For the statistical analysis, the test results for normality and equal variances are shown in Table D.28. Table D.29 provides a summary of the results and the resultant statistical analysis method chosen for each of the relevant parameters.

In summary for the dynamic modulus data, three of the combinations above were flagged for non-normality. After examining the results for transformed data and non-transformed data it was determined to not perform an overall transformation on the data because applying a transformation to all data caused some data to have a relatively high variation that affected the overall significant differences. All the data passed the equal variances check; thus, it was concluded to run an ANOVA test to find significant differences. The results of the statistical analysis are shown in Table D.30 in terms of the p-values from the hypothesis test. In this table, cases where the p-value is less than a significance level of 95% are highlighted in red.

By examining the p-values shown, CO_RS9.5C is statistically different than PI_RS9.5C. CO_RS9.5C different from MO_RS9.5C until the temperature is increased. PI_RS9.5C is statistically different from MO_RS9.5C.

Table D.27. Dynamic Modulus Results for Statistical Analysis.

Mixture	4°C-10Hz	4°C-1Hz	4°C-0.1Hz	20°C-10Hz	20°C-1Hz	20°C-0.1Hz	40°C-10Hz	40°C-1Hz	40°C-0.1Hz
CO_RS9.5C	15110	12315	9577	8423	5612	3317	2429	1132	474.2
	14528	11749	9037	7583	4917	2810	2129	958.9	398.7
	14959	12068	9313	8011	5236	3035	2218	993.9	400.9
PI_RS9.5C	14231	10777	7678	6585	3860	2061	1507	672.8	304.9
	13839	10518	7517	6262	3679	1958	1402	614.2	266.3
	13627	10245	7256	5986	3475	1836	1307	566.1	238.6
MO_RS9.5C	17472	13830	10251	9303	5855	3222	2515	1096	473.4
	17905	14240	10639	9393	5949	3312	2507	1091	450.7
	17698	14135	10600	9208	5766	3171	2400	1032	427.4

Table D.28. Statistical Values for Dynamic Modulus Data.

Temperature - Frequency	Normality (Shapiro-Wilk Test) Prob<W	Equal Variance (Levene and Bartlett tests) Prob>F	ANOVA or Welch's ANOVA (significant difference in means) α = 0.05
4°C-10Hz	0.0572	0.7170, 0.8910	<0.0001**
4°C-1Hz	0.245	0.9415, 0.9321	<0.0001**
4°C-0.1Hz	0.209	0.9517, 0.9386	<0.0001**
20°C-10Hz	0.2428	0.3434, 0.2419	<0.0001**
20°C-1Hz	0.0765	0.3131, 0.2897	<0.0001**
20°C-0.1Hz	0.0273*	0.2683, 0.2702	0.0002**
40°C-10Hz	0.0342*	0.3562, 0.5550	<0.0001**
40°C-1Hz	0.0479*	0.2177, 0.4908	0.0002**
40°C-0.1Hz	0.1527	0.4074, 0.7394	0.0013**

*Significant values based on significance level
**Significantly different means

Table D.29. Summary of Statistical Analysis Method for Dynamic Modulus Data.

Data	Comparison	Normality Check (Passed)	Trans. Method	Equal Variance Check (Passed)	Trans. Method	Statistical Analysis Method
Dynamic Modulus	4°C-10Hz	Yes	None	Yes	None	ANOVA, Tukey-Kramer HSD
	4°C-1Hz	Yes		Yes		
	4°C-0.1Hz	Yes		Yes		
	20°C-10Hz	Yes		Yes		
	20°C-1Hz	Yes		Yes		
	20°C-0.1Hz	No		Yes		
	40°C-10Hz	No		Yes		
	40°C-1Hz	No		Yes		
	40°C-0.1Hz	Yes		Yes		

Table D.30. Significant Differences for Dynamic Modulus Data.

Comparison	p-values (α = 0.05)								
	4°C-10Hz	4°C-1Hz	4°C-0.1Hz	20°C-10Hz	20°C-1Hz	20°C-0.1Hz	40°C-10Hz	40°C-1Hz	40°C-0.1Hz
CO_RS9.5C vs. PI_RS9.5C	0.0126	0.0008	0.0002	0.001	0.0004	0.0004	0.0002	0.0006	0.0035
CO_RS9.5C vs. MO_RS9.5C	0.0001	0.0002	0.0019	0.0046	0.0465	0.4271	0.124	0.6891	0.6425
PI_RS9.5C vs. MO_RS9.5C	0.0001	0.0001	0.0001	0.0001	0.0001	0.0002	0.0001	0.0003	0.0015

The phase angle results were statistically compared just as the dynamic modulus results. The phase angle results used in the statistical analysis are found in Table D.31.

For the statistical analysis, the test results for normality and equal variances are shown in Table D.32. Table D.33 provides a summary of the results and the resultant statistical analysis method chosen for each of the relevant parameters. In summary, all phase angle data passed the normality check except the data for 4°C-10Hz and 20°C-10Hz tests. Based on the entirety of the data, it was concluded to not transform the data to better fit the assumption of normality. All the data passed the equal variance check except 20°C-0.1Hz and 40°C-1Hz; thus, an ANOVA test was used to detect significant differences. The results of the statistical analysis are shown in Table D.34 in terms of the p-values from the hypothesis test. In this table, cases where the p-value is less than a significance level of 95% are highlighted in red. For the phase angle data, CO_RS9.5C, PI_RS9.5C, and MO_RS9.5C are significantly different except for a couple of combinations.

Table D.31. Phase Angle Results for Statistical Analysis.

Mixture	4°C-10Hz	4°C-1Hz	4°C-0.1Hz	20°C-10Hz	20°C-1Hz	20°C-0.1Hz	40°C-10Hz	40°C-1Hz	40°C-0.1Hz
CO_RS9.5C	7.50	9.38	12.31	14.97	19.61	25.34	30.2	32.58	31.82
	7.69	9.63	12.54	15.99	21.24	27.29	31.74	34.44	32.92
	7.87	9.83	12.58	15.53	20.47	26.31	31.61	34.59	33.88
PI_RS9.5C	10.04	12.6	16.27	20.11	25.34	30.18	35.16	35.43	32.59
	10.09	12.5	15.95	20.09	25.36	30.16	35.52	35.94	34.49
	10.28	12.7	16.34	20.54	25.7	30.27	35.68	35.96	34.27
MO_RS9.5C	8.04	10.52	14.15	16.24	22.18	28.86	33.37	36.91	35.52
	8.04	10.37	13.77	16.5	22.21	28.95	33.89	37.47	37.17
	8.10	10.56	13.92	16.74	22.70	29.32	34.24	37.37	36.29

Table D.32. Statistical Values for Phase Angle Data.

Temperature - Frequency	Normality (Shapiro-Wilk Test) Prob<W	Equal Variance (Levene and Bartlett tests) Prob>F	ANOVA or Welch's ANOVA (significant difference in means) α = 0.05
4°C-10Hz	0.0091*	0.2625, 0.1889	<0.0001**
4°C-1Hz	0.057	0.3874, 0.4598	<0.0001**
4°C-0.1Hz	0.119	0.7670, 0.8996	<0.0001**
20°C-10Hz	0.0375*	0.4746, 0.5552	<0.0001**
20°C-1Hz	0.2873	0.2368, 0.1843	<0.0001**
20°C-0.1Hz	0.1438	0.1379, 0.0132*	0.0005**
40°C-10Hz	0.4303	0.0974, 0.3470	0.0003**
40°C-1Hz	0.5482	0.0256, 0.1427*	0.0029**
40°C-0.1Hz	0.9285	0.8335, 0.9486	0.0117*

*Significant values based on significance level
**Significantly different means

Table D.33. Summary of Statistical Analysis Method for Phase Angle Data.

Data	Comparison	Normality Check (Passed)	Trans. Method	Equal Variance Check (Passed)	Trans. Method	Statistical Analysis Method
Phase Angle	4°C-10Hz	No	None	Yes	None	ANOVA, Tukey-Kramer HSD
	4°C-1Hz	Yes		Yes		
	4°C-0.1Hz	Yes		Yes		
	20°C-10Hz	No		Yes		
	20°C-1Hz	Yes		Yes		
	20°C-0.1Hz	Yes		No		
	40°C-10Hz	Yes		Yes		
	40°C-1Hz	Yes		No		
	40°C-0.1Hz	Yes		Yes		

Table D.34. Significant Differences for Phase Angle Data.

Comparison	p-values (α = 0.05)								
	4°C-10Hz	4°C-1Hz	4°C-0.1Hz	20°C-10Hz	20°C-1Hz	20°C-0.1Hz	40°C-10Hz	40°C-1Hz	40°C-0.1Hz
CO_RS9.5C vs. PI_RS9.5C	0.0001	0.0001	0.0001	0.0001	0.0001	0.0004	0.0002	0.0343	0.5222
CO_RS9.5C vs. MO_RS9.5C	0.03	0.0011	0.0002	0.0337	0.0089	0.0029	0.0032	0.0024	0.0113
PI_RS9.5C vs. MO_RS9.5C	0.0001	0.0001	0.0001	0.0001	0.0008	0.1096	0.0315	0.0887	0.042

Cyclic Fatigue Tests

The cyclic fatigue test data resulting in *C* vs. *S* damage curves are shown in Figure D.19 and Figure D.20. The representative S_{app} values, D^R values, and N_f vs. Cum. (1-*C*) data are shown in Figure

D.21, Figure D.22, and Figure D.23 respectively. The linear viscoelastic and S-VECD fatigue properties are shown in Table D.35. For the damage curves, MO_RS9.5C has the higher *C* values throughout the plot. PI_RS9.5C has the highest S_{app} values followed by CO_RS9.5C and then MO_RS9.5C. PI_RS9.5C has the highest D^R values followed by CO_RS9.5C and then MO_RS9.5C. The Cum. (1-*C*) vs. N_f graph shows different results for all three of the mixes. The S_{app} values shown below make sense because of MO_RS9.5C having the lowest effective binder content and coarsest gradation. The stiffer mixture translates to lower S_{app} values. As discussed before, PI_RS9.5C has lower dynamic modulus values with a softer binder than the other two mixtures, therefore resulting in better fatigue performance.

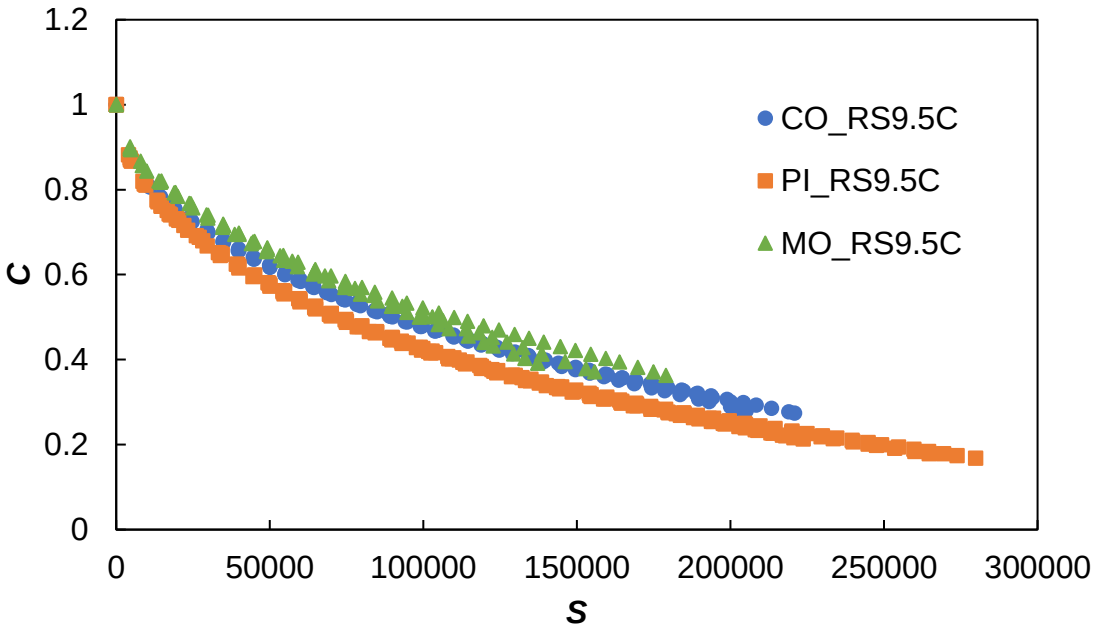

Figure D.19. *C* vs. *S* damage curves (individual specimen values).

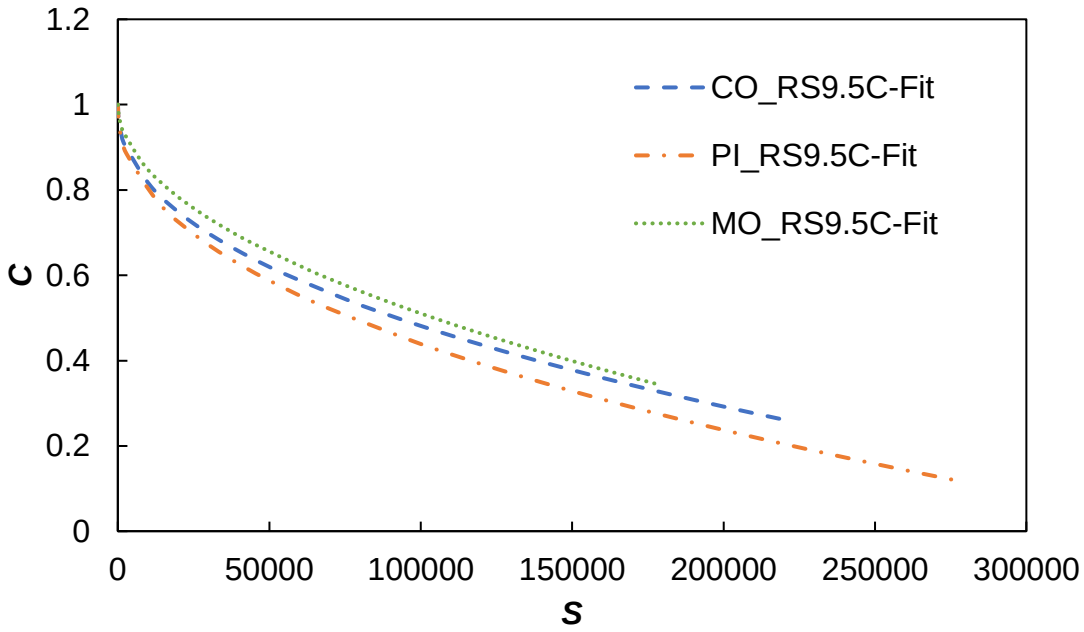

Figure D.20. *C* vs. *S* damage curves (fitted values).

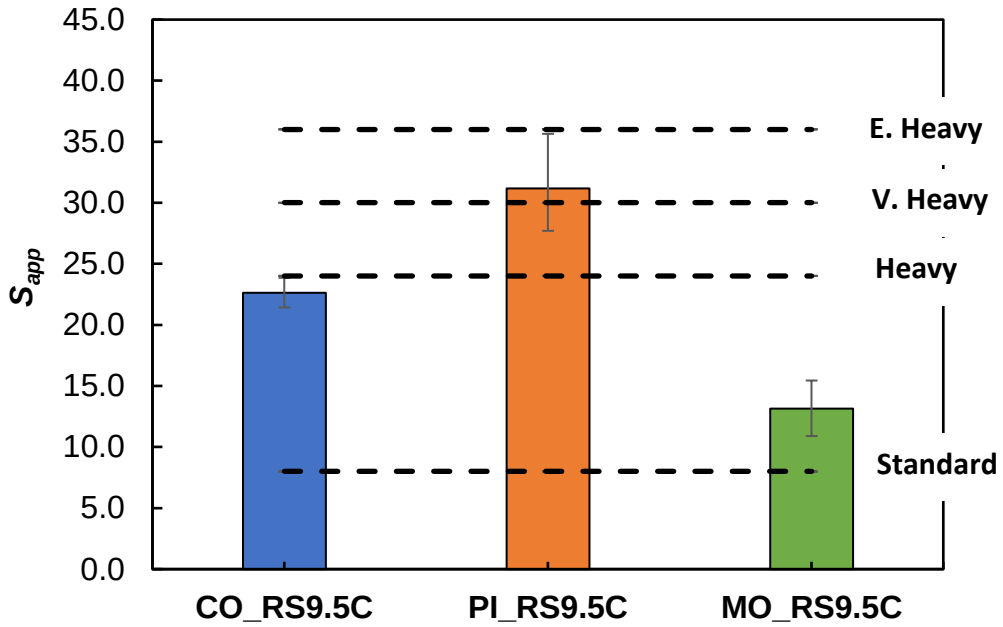

Figure D.21. Representative S_{app} values.

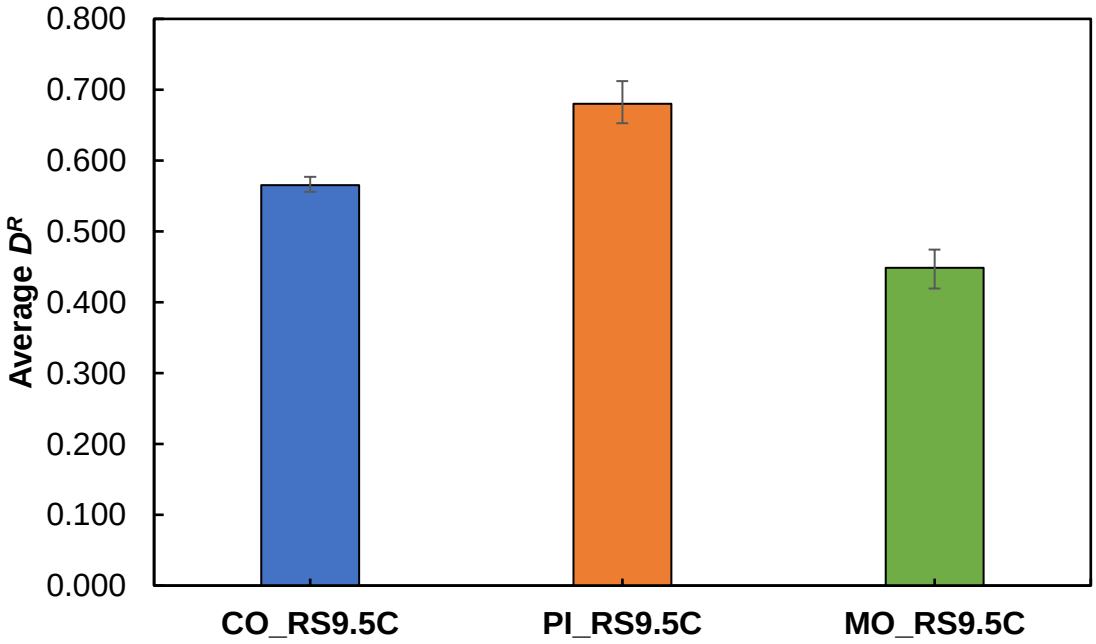

Figure D.22. Average D^R values.

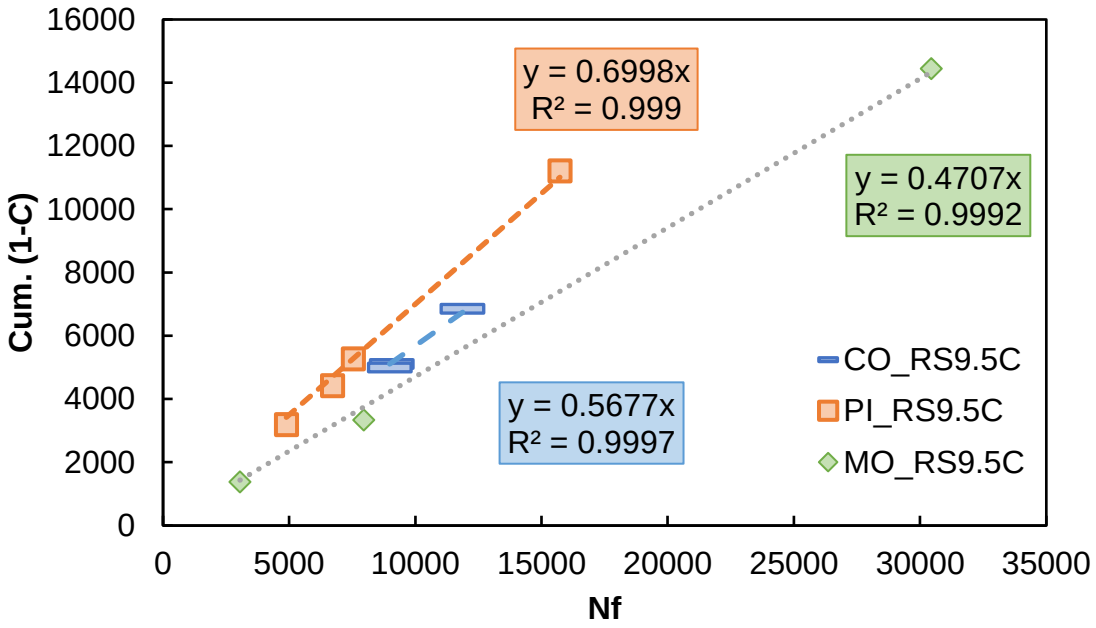

Figure D.23. Cum. (1-*C*) vs. N_f.

Table D.35. Linear Viscoelastic and FlexPAVE™ S-VECD Fatigue Properties.

Properties	CO_RS9.5C	PI_RS9.5C	MO_RS9.5C
α	3.53	3.76	3.57
C_{11}	0.0030	0.0034	0.0015
C_{12}	0.45	0.44	0.51
a_1	0.0008	0.0008	0.0006
a_2	-0.17	-0.17	-0.16
a_3	3.23	3.25	3.08

The statistical analysis for the North Carolina RS9.5C surface mixtures includes the same parameters that were used for the statistical analysis from the RS9.5B mixtures. Just as with the other mixtures set, the temperature when calculating S_{app} is the same for all mixtures. The *C* values correspond to *S* = 20,000 and *S* = 120,000 were used in the analysis. The average *C* values targeted for these *S* values were 0.72 and 0.38. The *C* values that correspond to these two values were interpolated from the *C* vs. *S* curves characterized for each specimen from FlexMAT™. The values used in the statistical analysis for fingerprint modulus, N_f, D^R, and S_{app} are shown in Table D.36. The *C* values used in the statistical analysis are shown in Table D.37.

For the statistical analysis, the tests of normality and variance are shown in Table D.38. Table D.39 provides a summary of the results and the resultant statistical analysis method chosen for each of the relevant parameters. As mentioned in the methodology for the statistical analysis, the data was assumed normal even though N_f and *C* at *S* = 20,000 data is flagged as non-normal. Even though other mixtures have assumed equal variances, for these mixtures, an analysis using ANOVA and Welch's ANOVA was used.

The p-values that show the significant differences for the cyclic fatigue data is shown in Table D.40. This table shows the same trend as shown in the dynamic modulus data, that all mixtures are different in terms of modulus. This also shows that the mixtures are also different in terms of D^R and S_{app}. For the *C* vs. *S* data, this table shows that all three mixtures are different but CO_RS9.5C and MO_RS9.5C are close to the significance threshold. The p-values shown in Table D.41 are from using Games-Howell's test, which accounts for unequal variances. With this the same trends are shown for the data, but instead of CO_RS9.5C and MO_RS9.5C having a slight significant difference, they are similar.

Table D.36. Cyclic Fatigue Results for Statistical Analysis.

Mixture	Fingerprint |E*| (MPa)	N_f	D^R	S_{app}
CO_9.5C	8637	11870	0.58	23.86
CO_9.5C	8701	9070	0.56	22.62
CO_9.5C	8677	8990	0.56	21.44
PI_9.5C	6983	6720	0.66	27.93
PI_9.5C	7419	7540	0.70	33.55
PI_9.5C	7065	4890	0.65	27.71
PI_9.5C	6770	15730	0.71	35.64
MO_9.5C	10230	3050	0.45	13.19
MO_9.5C	10002	7950	0.42	10.89
MO_9.5C	10181	30440	0.47	15.44

Table D.37. *C* Values for Statistical Analysis.

Mixture	*C* at *S* = 20,000	*C* at *S* = 120,000
CO_9.5C	0.75	0.43
CO_9.5C	0.75	0.44
CO_9.5C	0.75	0.43
CO_9.5C	0.75	0.44
PI_9.5C	0.72	0.38
PI_9.5C	0.73	0.38
PI_9.5C	0.73	0.38
PI_9.5C	0.73	0.38
PI_9.5C	0.73	0.39
MO_9.5C	0.79	0.46
MO_9.5C	0.78	0.44
MO_9.5C	0.79	0.48
MO_9.5C	0.78	0.46

Table D.38. Statistical Values for Cyclic Fatigue Data.

Attribute	Normality (Shapiro-Wilk Test) Prob<W	Equal Variance (Levene and Bartlett tests) Prob>F	ANOVA (significant difference in means) $\alpha = 0.05$	Welch's ANOVA (significant difference in means) $\alpha = 0.05$
Fingerprint |E*|	0.1226	0.2429, 0.0603	<0.0001**	0.0002**
N_f	0.0074*	0.0201*, 0.0390*	0.7341	0.8320
D^R	0.4888	0.0905, 0.4411	<0.0001**	0.0016**
S_{app}	0.7759	0.0236*, 0.3086	0.0003**	0.0036**
C at S = 20,000	0.0201*	0.5778, 0.8339	<0.0001**	<0.0001**
C at S = 120,000	0.0846	0.1231, 0.0203*	<0.0001**	<0.0001**

*Significant value based on significance level

**Significantly different means

Table D.39. Statistical Analysis Method for Cyclic Fatigue Data.

Attribute	Normality Check (Passed)	Trans. Method	Equal Variance Check (Passed)	Trans. Method	Statistical Analysis Method
Fingerprint |E*|	Yes	None	Yes	None	ANOVA, Welch's ANOVA
N_f	No		No		
D^R	Yes		Yes		
S_{app}	Yes		No		
C at S = 20,000	No		Yes		
C at S = 120,000	Yes		No		

Table D.40. Significant Differences for Cyclic Fatigue Data (ANOVA, Tukey-Kramer HSD).

Comparison	p-values ($\alpha = 0.05$)					
	Fingerprint |E*| (MPa)	N_f	D^R	S_{app}	C at S = 20,000	C at S = 120,000
CO_RS9.5C vs. PI_RS9.5C	0.0001	0.9794	0.0014	0.0164	0.0001	0.0001
CO_RS9.5C vs. MO_RS9.5C	0.0001	0.8472	0.0019	0.0139	0.0001	0.0117
PI_RS9.5C vs. MO_RS9.5C	0.0001	0.7212	0.0001	0.0002	0.0001	0.0001

Table D.41. Significant Differences for Cyclic Fatigue Data.

Comparison	p-values (α = 0.05)					
	Fingerprint |E*| (MPa)	N_f	D^R	S_{app}	*C* at *S* = 20,000	*C* at *S* = 120,000
CO_RS9.5C vs. PI_RS9.5C	0.0023	0.8813	0.0047	0.0385	0.0001	0.0001
CO_RS9.5C vs. MO_RS9.5C	0.0023	0.8987	0.0197	0.0153	0.0001	0.1025
PI_RS9.5C vs. MO_RS9.5C	0.0001	0.8416	0.0005	0.0018	0.0001	0.0025

Stress Sweep Rutting Tests

The permanent micro-strain curves for each mixture are shown in Figure D.24 and Figure D.25. The rutting strain index (RSI) values are shown in Figure D.26, Figure D.27, and Figure D.28. For the North Carolina mixtures, each mixture is from a specific region, therefore the RSI values in three different locations are shown. Table D.42 shows the percent difference between each test.

PI_RS9.5C exhibits the highest permanent strain in both the high and low temperature tests. As shown in Table D.2, the temperatures for these SSR tests were different. CO_RS9.5C had the highest temperature, then PI_RS9.5C, and MO_RS9.5C. The difference was only two degrees Celsius and three degrees Celsius, respectively, but this could influence the results of these strain curves. PI_RS9.5C has the softest binder, second-highest binder content, and the highest RAP percentage, thus showing that this mixture is softer overall, resulting in higher permanent strain.

The RSI values represent the values from three different locations. MO_RS9.5C has the best rutting performance in all locations, followed by CO_RS9.5C and PI_RS9.5C. MO_RS9.5C has the lowest effective binder content and the coarsest gradation resulting in this performance. These mixtures do not show a large range in RSI based on the location as with the North Carolina 9.5B mixtures. With these mixtures, the highest range is only 2.11%.

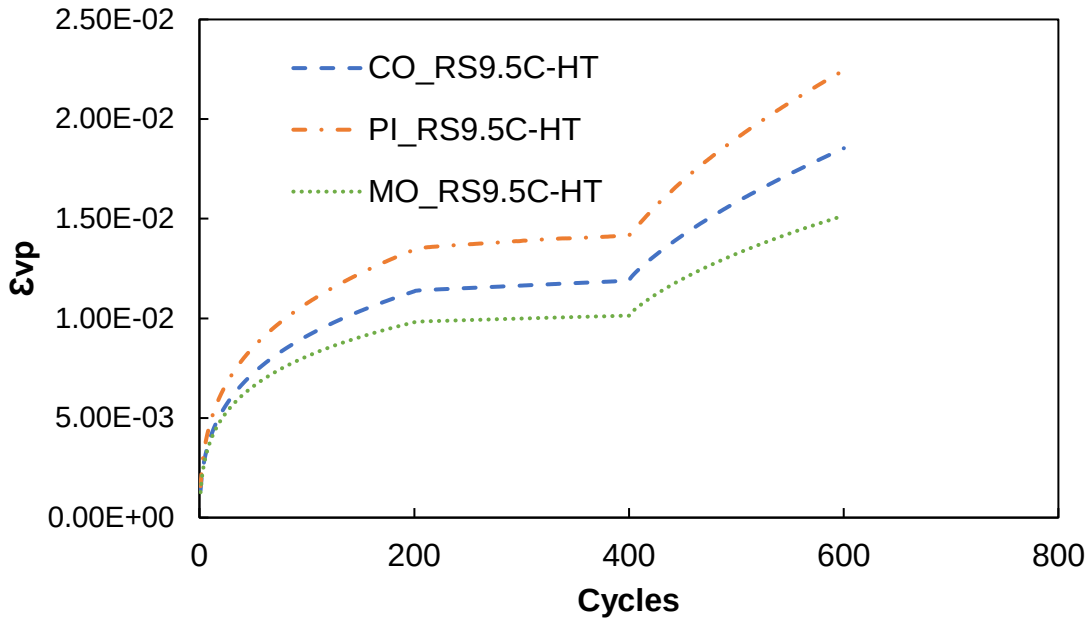

Figure D.24. Permanent micro-strain curves for high temperature tests.

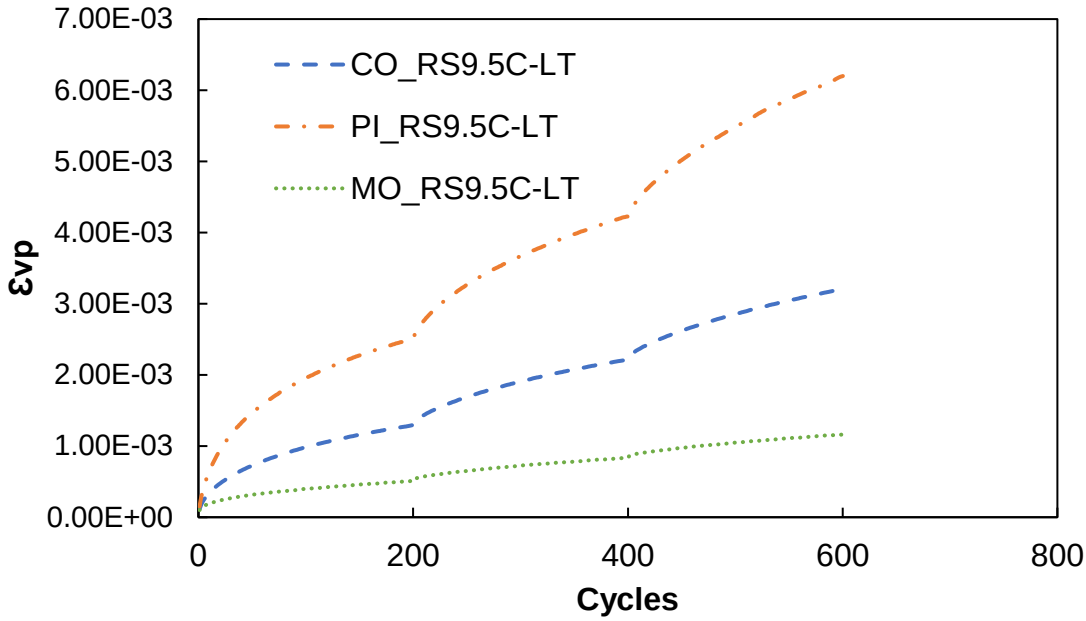

Figure D.25. Permanent micro-strain curves for low temperature tests.

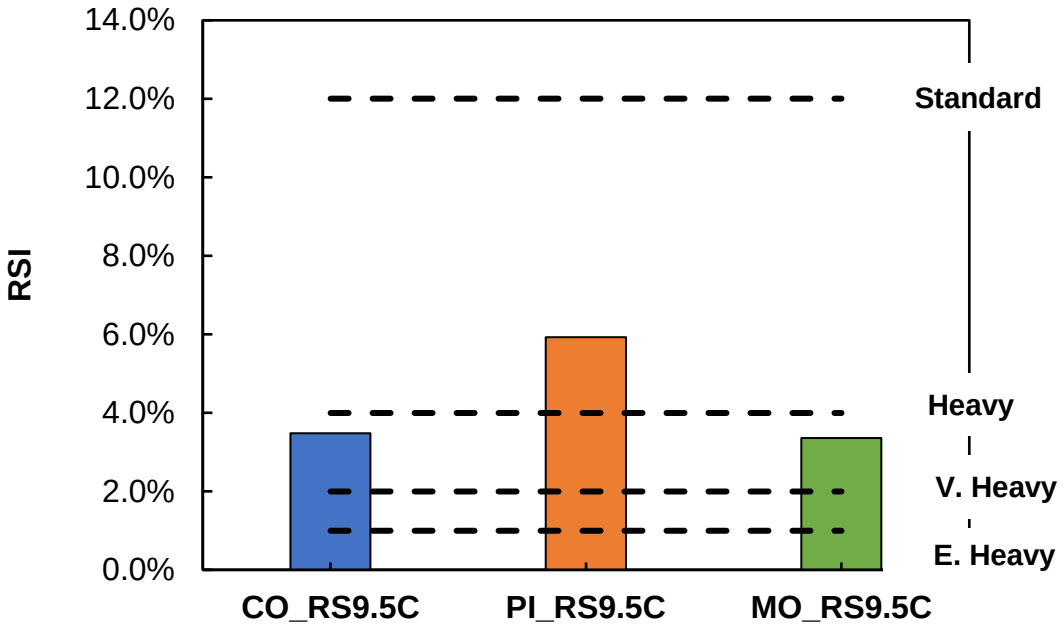

Figure D.26. Rutting strain index values (Wilmington, NC).

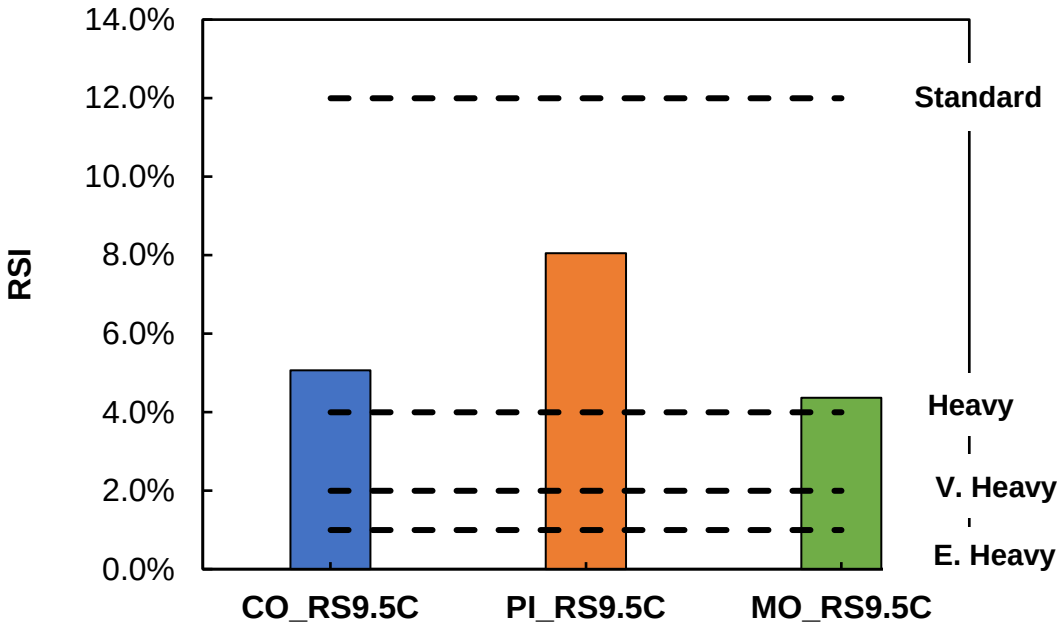

Figure D.27. Rutting strain index values (Wake Forest, NC).

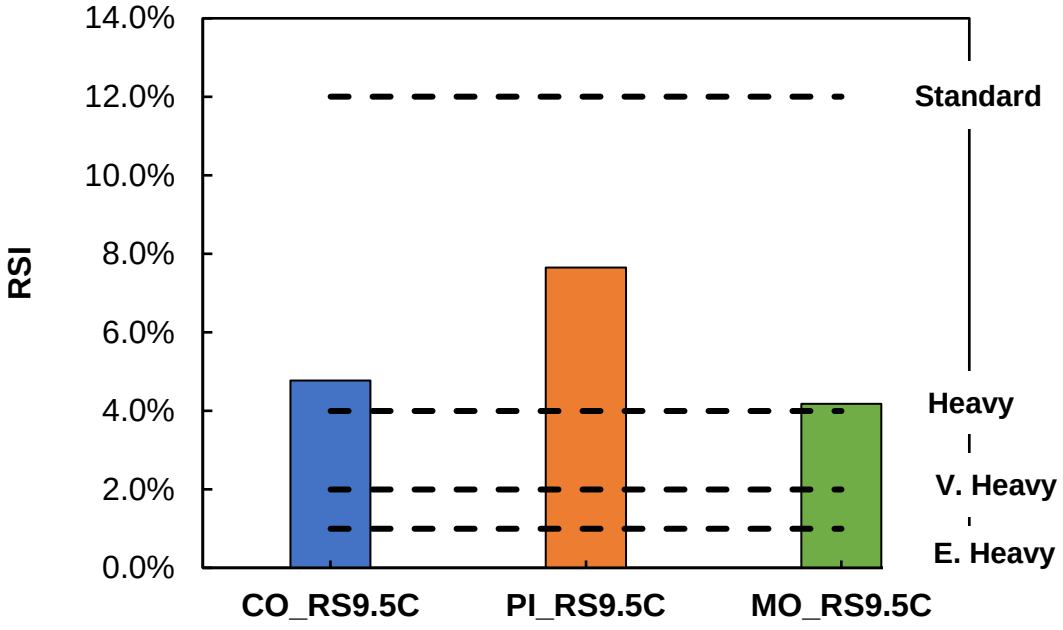

Figure D.28. Rutting strain index values (Asheville, NC).

Table D.42. Percent Difference in Permanent Micro-Strain for SSR Testing.

Mixture	Temperature	Percent Difference
CO_RS9.5C	HT	24.82
	LT	2.49
PI_RS9.5C	HT	9.50
	LT	11.42
MO_RS9.5C	HT	0.31
	LT	16.70

For the North Carolina mixtures, as mentioned before, the test temperatures for the SSR tests were different. Because of this, a statistical analysis of the permanent strain curves was not done. Table D.43 shows the RSI values used for the statistical analysis. There was hardly any variation from location to location for the RSI values, therefore the location with the middle RSI values was chosen for the analysis. The temperatures for calculating RSI were the same for all mixtures.

For the statistical analysis, the normal distribution checks and equal variance checks results are all shown in Table D.44. Table D.45 provides a summary of the results and the resultant statistical analysis method chosen for each of the relevant parameters.

In summary, the data for the RSI values did not pass the normality check and was flagged for unequal variances. As with the previous North Carolina mixtures, it was concluded to run an ANOVA test and Welch's ANOVA test to identify significant differences and compare.

The p-values for the SSR data that have significantly different means are shown in Table D.46. For RSI, PI_RS9.5C is significantly different than the other two mixtures. For Table D.47, the same trends are shown.

Table D.43. RSI Values for SSR Tests (Asheville, NC).

Mixture	HT-H: LT-H	HT-H: LT-L	HT-L: LT-L	HT-L: LT-H	All temp.
CO_RS9.5C	5.57	5.50	3.98	4.03	4.77
PI_RS9.5C	8.67	8.47	6.73	6.87	7.65
MO_RS9.5C	4.26	4.13	4.10	4.23	4.18

Table D.44. Statistical Values for SSR Data.

Attribute	Normality (Shapiro-Wilk Test) Prob<W	Equal Variance (Levene and Bartlett tests) Prob>F	ANOVA (significant difference in means) α = 0.05	Welch's ANOVA (significant difference in means) α = 0.05
RSI (Asheville, NC)	0.0088*	0.0098*, 0.0010*	<0.0001**	0.0008**

*Significant values based on significance level

**Significantly different means

Table D.45. Summary of Statistical Analysis Method for SSR Data.

Attribute	Normality Check (Passed)	Trans. Method	Equal Variance Check (Passed)	Trans. Method	Statistical Analysis Method
RSI (Asheville, NC)	No	None	No	None	ANOVA, Welch's ANOVA

Table D.46. Significant Differences for SSR Data (ANOVA, Tukey-Kramer HSD).

Comparison	p-values (α = 0.05) RSI (Asheville, NC)
CO_RS9.5C vs. PI_RS9.5C	0.0001
CO_RS9.5C vs. MO_RS9.5C	0.3839
PI_RS9.5C vs. MO_RS9.5C	0.0001

Table D.47. Significant Differences for SSR Data (Welch's ANOVA, Games-Howell).

Comparison	p-values (α = 0.05) RSI (Asheville, NC)
CO_RS9.5C vs. PI_RS9.5C	0.0015
CO_RS9.5C vs. MO_RS9.5C	0.3045
PI_RS9.5C vs. MO_RS9.5C	0.002

RS9.5C Analysis Summary

Table D.48 and Table D.49 show the overall significant differences for the tests' parameters. The convention for the tables is the same as it was described for the RS9.5B mixtures. For dynamic modulus, PI_RS9.5C is different than the other two mixtures. CO_RS9.5C is different than MO_RS9.5C until the temperature is increased to 40°C. For phase angle data, the mixtures are different for all temperatures. For cyclic fatigue data, all three mixtures are different. For RSI, CO_RS9.5C is similar to MO_RS9.5C.

For S_{app}, PI_RS9.5C is classified as "Very Heavy", CO_RS9.5C is classified as "Standard", and MO_RS9.5C is classified as "Standard". For RSI, each mixture is classified as "Standard" based on the location chosen for statistical analysis but are classified as "Heavy" for the other two locations. The traffic designation for all three mixtures therefore falls under "Standard". For CO_RS9.5C, depending on location, the designation could be controlled by fatigue performance and the same goes for MO_RS9.5C. According to the North Carolina DOT QMS manual, these mixtures are classified to handle 3 to 30 million ESALs. This shows according to the S_{app} thresholds defined by Wang et al. (2020), these mixtures could be classified as "Standard" or "Heavy". For S_{app}, PI_RS9.5C overperforms with a classification of "Very Heavy". For RSI as defined by Ghanbari et al. (2020), all three mixtures meet the category in which they were designed.

Table D.48. Summary of Dynamic Modulus Test Parameters.

Mixtures	DM parameters			PA parameters		
	4°C	20°C	40°C	4°C	20°C	40°C
CO_RS9.5C	B	B	A	C	C	C
PI_RS9.5C	C	C	B	A	A	B
MO_RS9.5C	A	A	A	B	B	A

Table D.49. Summary of Cyclic Fatigue and Stress Sweep Rutting Test Parameters.

Mixtures	CF and SSR parameters			
	S_{app}	C at S = 20,000	C at S = 120,000	RSI (Asheville, NC)
CO_RS9.5C	B	B	B	B
PI_RS9.5C	A	C	C	A
MO_RS9.5C	C	A	A	B

North Carolina RI19.0C Experimental Results

Dynamic Modulus Tests

The dynamic modulus results for each of the three intermediate mixtures are shown in Figure D.29 and Figure D.30. The phase angle results from the dynamic modulus testing are shown in Figure D.31. Overall, the modulus of CO_RI19.0C looks to be higher than PI_RI19.0C and MO_RI19.0C. Overall, PI_RI19.0C looks to have the higher phase angle values than the other two mixtures. By examining the information in the materials section (section 3.2.2), CO_RI19.0C has a lower binder content but also exhibits the highest %RBR accounting for a softer binder grade. This %RBR increases the stiffness of the mixture, thus increasing the dynamic modulus. The phase angle values follow that PI_RI19.0C has a higher binder content overall and has the lower dynamic modulus values.

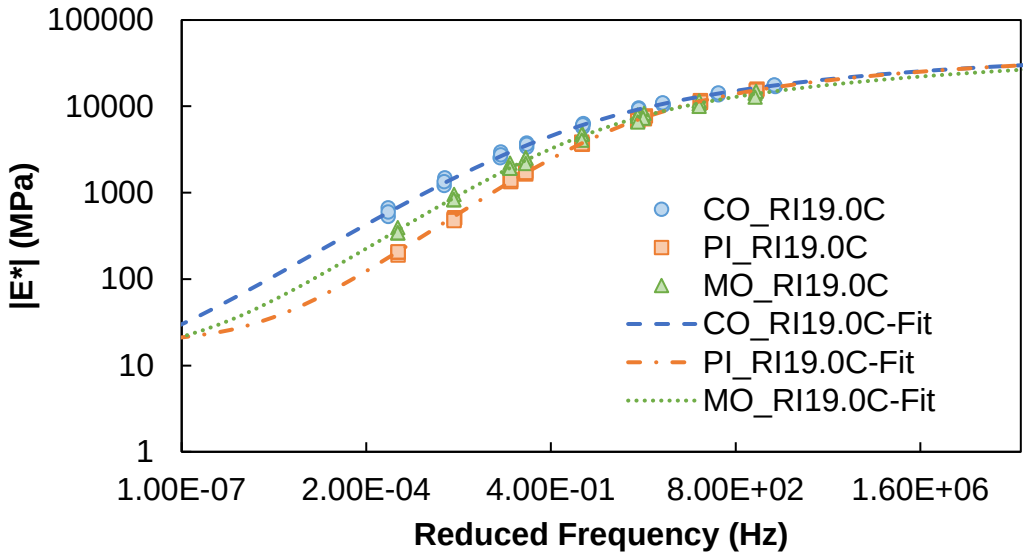

Figure D.29. Dynamic modulus results (log-log plot).

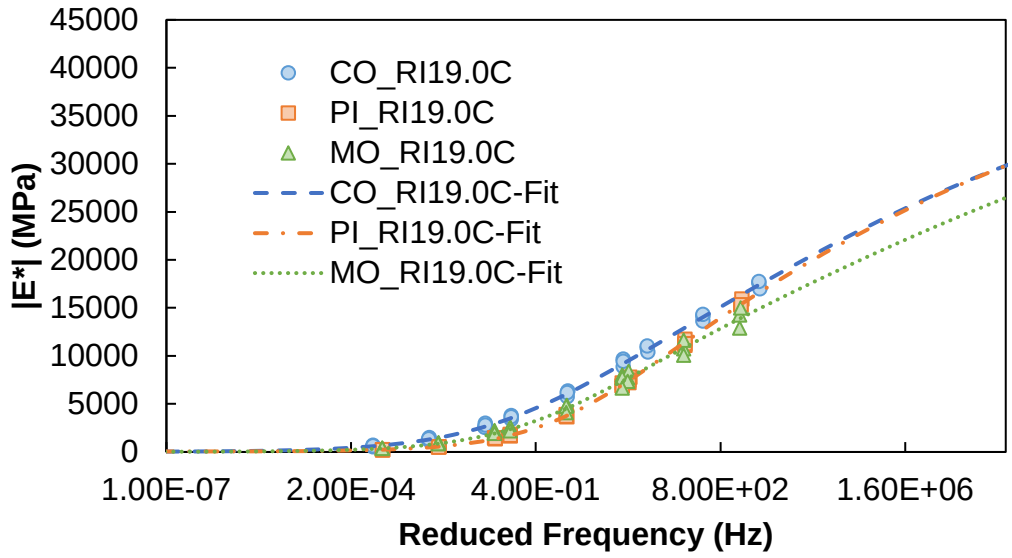

Figure D.30. Dynamic modulus results (semi-log plots).

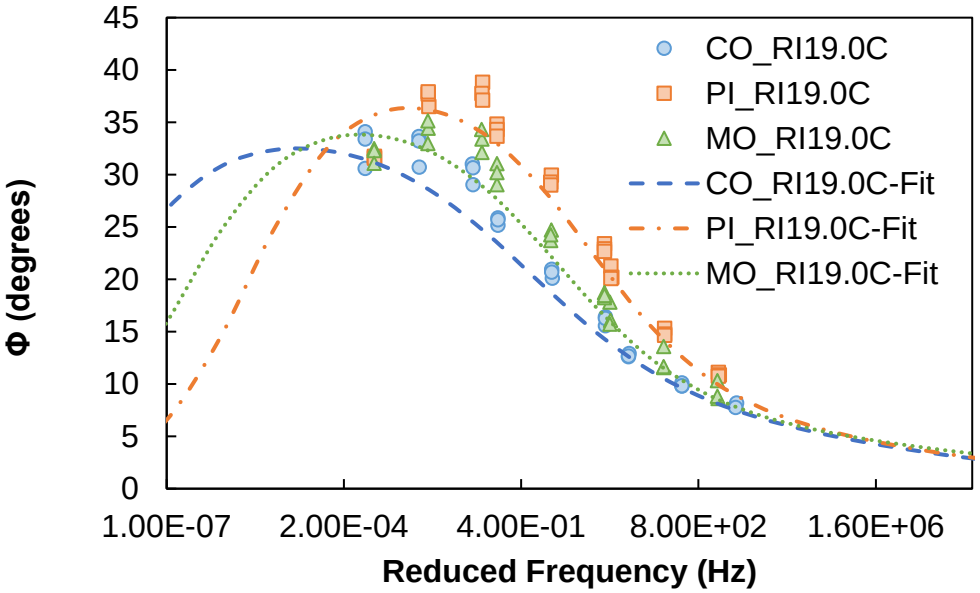

Figure D.31. Phase angle results.

The statistical analysis for the dynamic modulus results was done the exact same as in the other mixtures. The dynamic modulus values used in the statistical analysis are shown in Table D.50. For the statistical analysis, the test results for normality and equal variances are shown in Table D.51. Table D.52 provides a summary of the results and the resultant statistical analysis method chosen for each of the relevant parameters.

In summary for the dynamic modulus data, only one combination was flagged for non-normal data. All the data passed the equal variances check; thus, it was concluded to run an ANOVA test to find significant differences. The results of the statistical analysis are shown in Table D.53 in terms of the p-values from the hypothesis test. In this table, cases where the p-value is less than a

significance level of 95% are highlighted in red. By examining the p-values shown, CO_RI19.0C is statistically different than PI_RI19.0C and MO_RI19.0C. PI_RI19.0C is similar to MO_RI19.0C until 20°C and 40°C. By examining the p-values comparing PI_RI19.0C and MO_RI19.0C, there is an abrupt change in the p-values from 20°C-10Hz and 20°C-1Hz. One data point from MO_RI19.0C at 20°C-10Hz varies more from the other two data points exaggerating the similarity between the two mixtures. This data point from MO_RI19.0C has less variation from the other two values at 20°C-1Hz, therefore decreasing the exaggeration shown before, resulting in a slightly significant difference.

Table D.50. Dynamic Modulus Results for Statistical Analysis.

Mixture	4°C-10Hz	4°C-1Hz	4°C-0.1Hz	20°C-10Hz	20°C-1Hz	20°C-0.1Hz	40°C-10Hz	40°C-1Hz	40°C-0.1Hz
CO_RI19.0C	17575	14120	10834	9653	6335	3779	2979	1489	668.6
	16972	13609	10403	8874	5748	3390	2556	1218	531.9
	17739	14322	11007	9414	6155	3651	2765	1345	600.1
PI_RI19.0C	15298	11104	7214	6859	3643	1655	1348	515	191.3
	15919	11710	7765	7178	3882	1801	1447	499.8	206.4
	15316	11247	7474	6872	3703	1719	1402	477.2	207.2
MO_RI19.0C	14255	10727	7711	7990	4844	2546	2205	960.8	394.7
	14992	11608	8356	7705	4735	2538	1951	833.1	342.7
	12892	10049	7320	6620	4073	2186	1924	835.1	347.1

Table D.51. Statistical Values for Dynamic Modulus Data.

Temperature - Frequency	Normality (Shapiro-Wilk Test) Prob<W	Equal Variance (Levene and Bartlett tests) Prob>F	ANOVA or Welch's ANOVA (significant difference in means) $\alpha = 0.05$
4°C-10Hz	0.7402	0.1670, 0.2861	0.0028**
4°C-1Hz	0.1841	0.3660, 0.4420	0.0007**
4°C-0.1Hz	0.0163*	0.4861, 0.6679	<0.0001**
20°C-10Hz	0.2219	0.1009, 0.2689	0.0024**
20°C-1Hz	0.1749	0.1414, 0.3728	0.0002**
20°C-0.1Hz	0.1746	0.1957, 0.4392	<0.0001**
40°C-10Hz	0.3914	0.2798, 0.2651	0.0001**
40°C-1Hz	0.3207	0.1900, 0.1118	<0.0001**
40°C-0.1Hz	0.2787	0.2080, 0.0839	<0.0001**

*Significant values based on significance level

**Significantly different means

Table D.52. Summary of Statistical Analysis Method for Dynamic Modulus.

Data	Comparison	Normality Check (Passed)	Trans. Method	Equal Variance Check (Passed)	Trans. Method	Statistical Analysis Method
Dynamic Modulus	4°C-10Hz	Yes	None	Yes	None	ANOVA, Tukey-Kramer HSD
	4°C-1Hz	Yes		Yes		
	4°C-0.1Hz	No		Yes		
	20°C-10Hz	Yes		Yes		
	20°C-1Hz	Yes		Yes		
	20°C-0.1Hz	Yes		Yes		
	40°C-10Hz	Yes		Yes		
	40°C-1Hz	Yes		Yes		
	40°C-0.1Hz	Yes		Yes		

Table D.53. Significant Differences for Dynamic Modulus Data.

Comparison	p-values (α = 0.05)								
	4°C-10Hz	4°C-1Hz	4°C-0.1Hz	20°C-10Hz	20°C-1Hz	20°C-0.1Hz	40°C-10Hz	40°C-1Hz	40°C-0.1Hz
CO19.0C vs. PI19.0C	0.033	0.0021	0.0001	0.0026	0.0002	0.0001	0.0001	0.0001	0.0001
CO19.0C vs. MO9.5C	0.0023	0.0007	0.0002	0.0079	0.0021	0.0004	0.0026	0.0016	0.0012
PI19.0C vs. MO19.0C	0.0894	0.4507	0.61	0.5077	0.0406	0.0057	0.0059	0.0049	0.0094

The phase angle results were statistically compared just as the dynamic modulus results. The phase angle results used in the statistical analysis are found in Table D.54. For the statistical analysis, the test results for normality and equal variances are shown in Table D.55. Table D.56 provides a summary of the results and the resultant statistical analysis method chosen for each of the relevant parameters. In summary, all phase angle data passed the normality check. All data for 4°C did not pass the variance check along with the data for 40°C-0.1Hz. Because of this, it was decided to use a Welch's ANOVA test to determine the significant differences. The results of the statistical analysis are shown in Table D.57 in terms of the p-values from the hypothesis test. In this table, cases where the p-value is less than a significance level of 95% are highlighted in red. For the phase angle data, CO_RI19.0C is significantly different from PI_RI19.0C. CO_RI19.0C is similar to MO_RI19.0C in five of the nine combinations, with a couple of those very close to the threshold. PI_RI19.0C is different from MO_RI19.0C as the temperature increases from 4°C.

Table D.54. Phase Angle Results for Statistical Analysis.

Mixture	4°C-10Hz	4°C-1Hz	4°C-0.1Hz	20°C-10Hz	20°C-1Hz	20°C-0.1Hz	40°C-10Hz	40°C-1Hz	40°C-0.1Hz
CO_RI19.0C	7.86	9.83	12.62	15.57	20.12	25.19	29.05	30.72	30.60
	8.20	10.13	12.94	16.45	20.98	25.89	31.04	33.66	34.10
	7.78	9.84	12.68	16.28	20.69	25.70	30.68	33.23	33.40
PI_RI19.0C	11.14	15.33	21.29	23.41	29.97	34.86	38.85	36.51	31.76
	10.88	14.78	20.22	22.93	29.31	34.33	37.76	37.72	31.66
	10.78	14.66	20.09	22.68	29.01	33.7	37.12	37.93	31.59
MO_RI19.0C	10.34	13.61	17.84	18.75	24.74	31.06	33.41	34.44	32.50
	8.64	11.58	16.10	18.27	23.72	29.06	34.32	35.14	32.31
	8.85	11.68	15.72	18.49	24.27	30.20	32.14	32.98	31.10

Table D.55. Statistical Values for Phase Angle Data.

Temperature - Frequency	Normality (Shapiro-Wilk Test) Prob<W	Equal Variance (Levene and Bartlett tests) Prob>F	ANOVA or Welch's ANOVA (significant difference in means) α = 0.05
4°C-10Hz	0.0963	0.0211*, 0.0826	0.0004**
4°C-1Hz	0.1299	0.0179*, 0.0741	0.0005**
4°C-0.1Hz	0.1987	0.0490*, 0.1294	0.0010**
20°C-10Hz	0.1206	0.4074, 0.7139	0.0002**
20°C-1Hz	0.1722	0.9743, 0.9797	<0.0001**
20°C-0.1Hz	0.2359	0.3937, 0.4476	0.0002**
40°C-10Hz	0.6081	0.8873, 0.9550	0.0022**
40°C-1Hz	0.7668	0.3124, 0.6593	0.0197**
40°C-0.1Hz	0.7644	0.0248*, 0.0153*	0.6284

*Significant values based on significance level
**Significantly different means

Table D.56. Summary of Statistical Analysis Method for Phase Angle Data.

Data	Comparison	Normality Check (Passed)	Trans. Method	Equal Variance Check (Passed)	Trans. Method	Statistical Analysis Method
Phase Angle	4°C-10Hz	Yes	None	No	None	Welch's ANOVA, Games-Howell
	4°C-1Hz	Yes		No		
	4°C-0.1Hz	Yes		No		
	20°C-10Hz	Yes		Yes		
	20°C-1Hz	Yes		Yes		
	20°C-0.1Hz	Yes		Yes		
	40°C-10Hz	Yes		Yes		
	40°C-1Hz	Yes		Yes		
	40°C-0.1Hz	Yes		No		

Table D.57. Significant Differences for Phase Angle Data.

Comparison	p-values (α = 0.05)								
	4°C-10Hz	4°C-1Hz	4°C-0.1Hz	20°C-10Hz	20°C-1Hz	20°C-0.1Hz	40°C-10Hz	40°C-1Hz	40°C-0.1Hz
CO19.0C vs. PI19.0C	0.0002	0.0006	0.0026	0.0001	0.0001	0.0002	0.0017	0.0383	0.6624
CO19.0C vs. MO9.5C	0.2211	0.1214	0.0476	0.0086	0.0018	0.0181	0.0555	0.3995	0.816
PI19.0C vs. MO19.0C	0.1533	0.0883	0.023	0.0004	0.0005	0.014	0.0116	0.0383	0.7967

Cyclic Fatigue Tests

The cyclic fatigue test data resulting in *C* vs. *S* damage curves are shown in Figure D.32 and Figure D.33. The representative S_{app} values, D^R values, and N_f vs. Cum. (1-*C*) data are shown in Figure D.34, Figure D.35, and Figure D.36 respectively. The linear viscoelastic and S-VECD fatigue properties are shown in Table D.58. For the damage curves, CO_RI19.0C has the higher *C* values throughout the plot. CO_RI19.0C has the highest S_{app} values followed by PI_RI19.0C and then MO_RI19.0C. PI_RI19.0C has the highest D^R values followed by CO_RI19.0C and then MO_RI19.0C. The Cum. (1-*C*) vs. N_f graph shows CO_RI19.0C and PI_RI19.0C are similar. The S_{app} results seem to follow that CO_RI19.0C has the highest effective binder content, a softer binder and a finer gradation even though it has the higher dynamic modulus values. The coarser gradations of MO_RI19.0C and PI_RI19.0C may be influencing the result of lower fatigue performances.

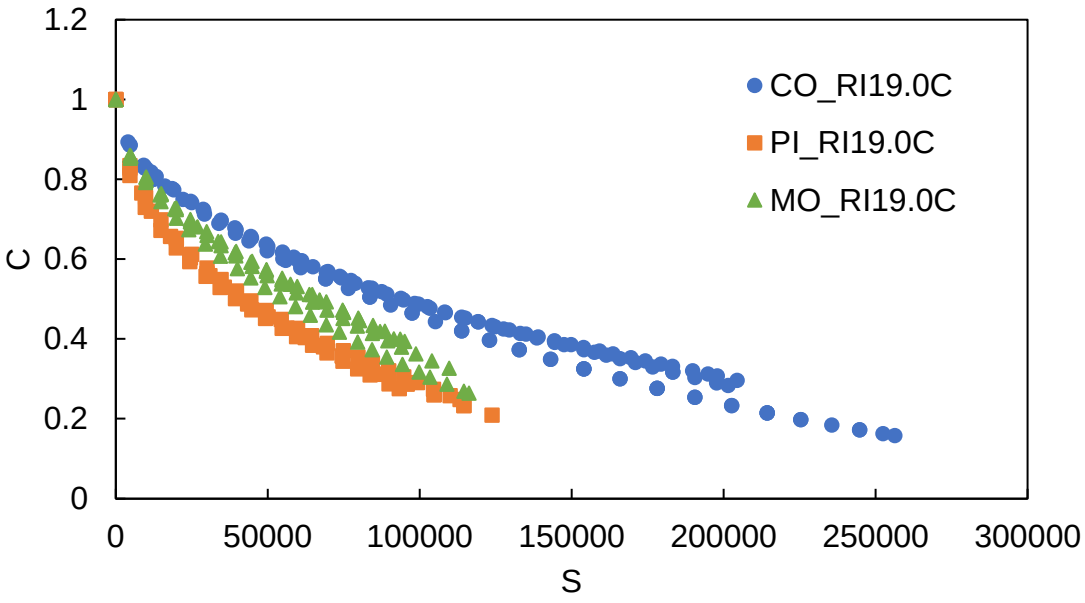

Figure D.32. *C* vs. *S* damage curves (individual specimen values).

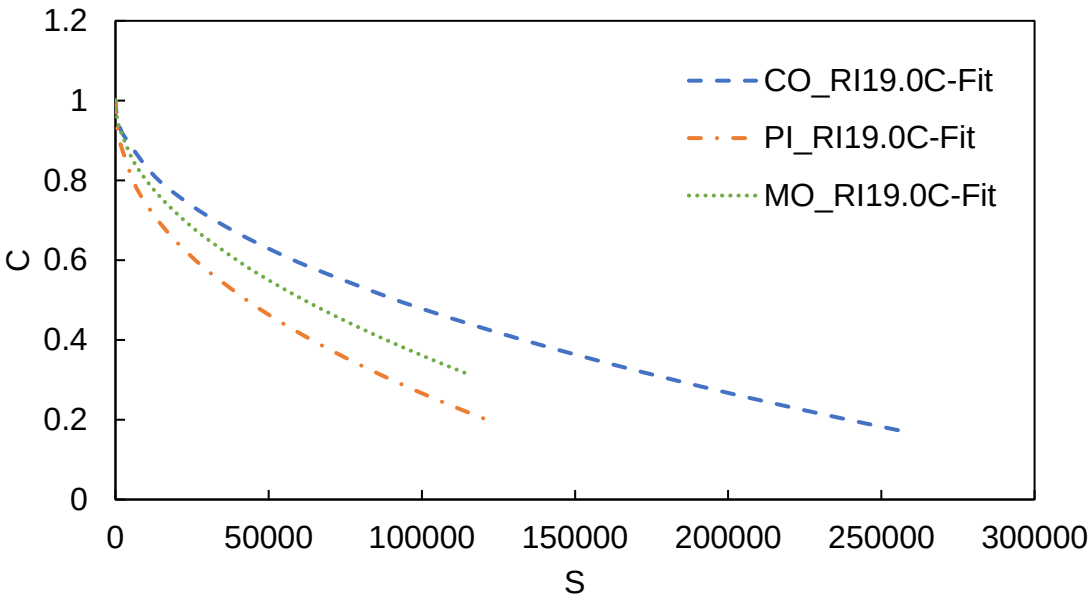

Figure D.33. *C* vs. *S* damage curves (fitted values).

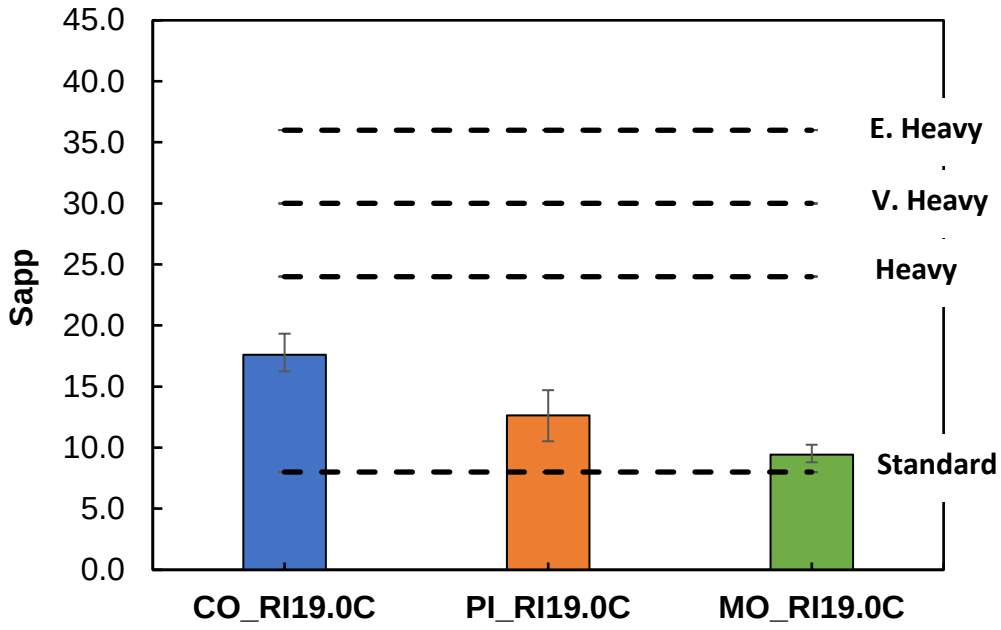

Figure D.34. Representative S_{app} values.

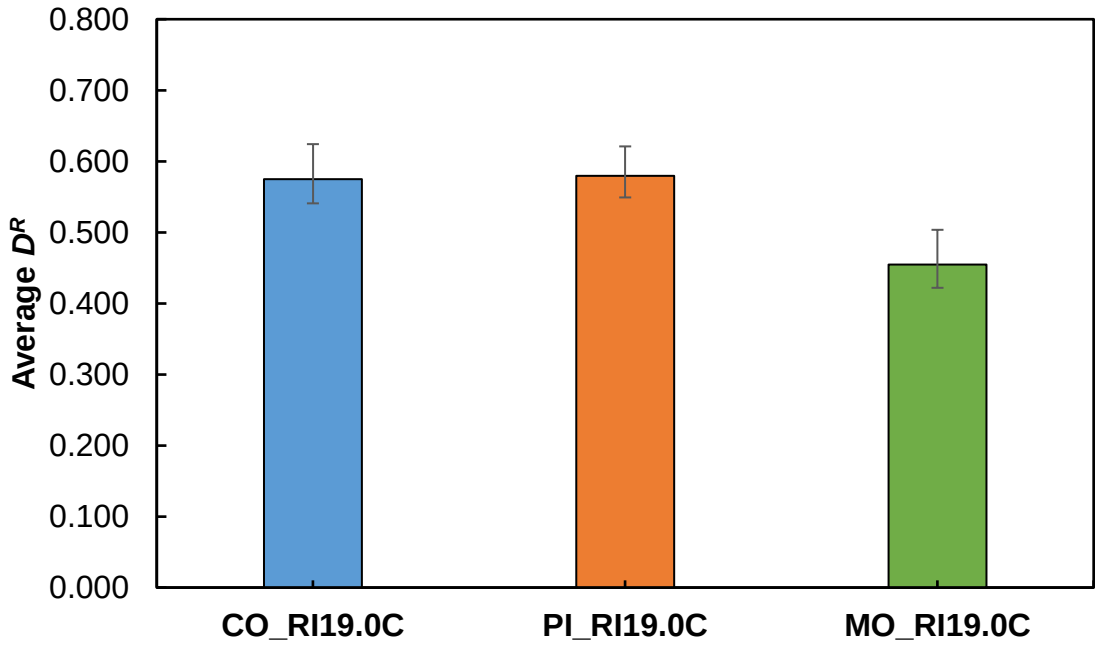

Figure D.35. Average D^R values.

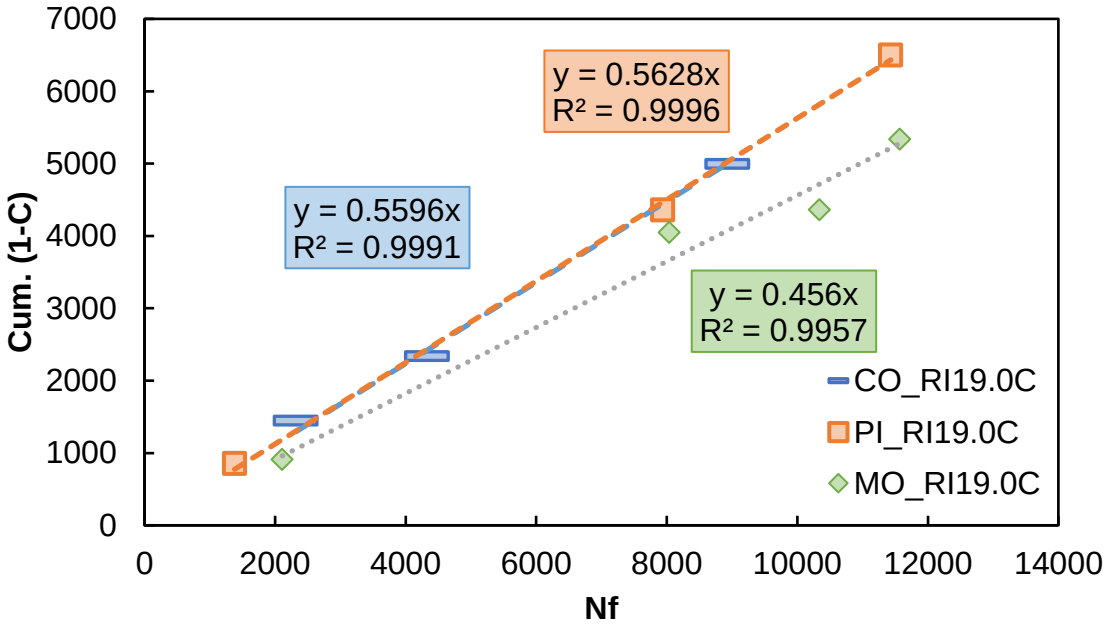

Figure D.36. Cum. (1-*C*) vs. N_f.

Table D.58. Linear Viscoelastic and FlexPAVE™ S-VECD Fatigue Properties.

Properties	CO_RI19.0C	PI_RI19.0C	MO_RI19.0C
α	3.74	3.43	3.62
C_{11}	0.0018	0.0041	0.0019
C_{12}	0.49	0.45	0.50
a_1	0.0008	0.0006	0.0005
a_2	-0.17	-0.15	-0.14
a_3	3.27	2.85	2.82

The statistical analysis for the North Carolina 19.0C intermediate mixtures includes the same parameters that were used for the statistical analysis from the other mixtures. Just as with the other two sets of mixtures, the temperature when calculating S_{app} is the same for all mixtures. The only difference in the analysis is the *C* values correspond to *S* = 20,000 and *S* = 90,000, instead of *S* = 20,000 and *S* = 120,000. This was done because the damage curves were shorter during these tests and *S* = 120,000 was not appropriate in all tests. The average *C* values targeted for these *S* values were 0.70 and 0.4. The *C* values that correspond to these two values were interpolated from the *C* vs. *S* curves characterized for each specimen from FlexMAT™. The values used in the statistical analysis for fingerprint modulus, N_f, D^R, and S_{app} are shown in Table D.59. The *C* values used in the statistical analysis are shown in Table D.60.

For the statistical analysis, the tests of normality and variance are shown in Table D.61. Table D.62 provides a summary of the results and the resultant statistical analysis method chosen for each of the relevant parameters. As mentioned in the methodology for the statistical analysis, the data was assumed normal even though the finger modulus data is flagged as non-normal. Based on the entirety of all cyclic fatigue data analyzed, it was chosen to assume equal variance with this data set and choose an ANOVA test to find differences.

The p-values that show the significant differences for the cyclic fatigue data is shown in Table D.63. This table shows the same trend as shown in the dynamic modulus data, that CO_RI19.0C is different from PI_RI19.0C and MO_RI19.0C. This shows that the D^R values for CO_RI19.0C and PI_RI19.0C are similar. The S_{app} values CO_RI19.0C are different than the other two mixtures. The S_{app} values are not flagged for PI_RI19.0C and MO_RI19.0C but are right at the significance level threshold. For the *C* vs. *S* data, this table shows that all three mixtures are different.

Table D.59. Cyclic Fatigue Results for Statistical Analysis.

Mixture	Fingerprint |E*| (MPa)	N_f	D^R	S_{app}
CO_RI19.0C	9639	8930	0.56	17.65
	10392	4330	0.54	16.25
	10671	2320	0.62	19.34
PI_RI19.0C	7894	1380	0.62	14.70
	7914	7940	0.55	10.51
	7765	11430	0.57	12.70
MO_RI19.0C	8295	2110	0.43	9.05
	8612	11570	0.46	9.85
	8195	8040	0.50	10.23
	8551	10340	0.42	8.79

Table D.60. *C* Values for Statistical Analysis.

Mixture	*C* at *S* = 20,000	*C* at *S* = 90,000
CO_RI19.0C	0.77	0.51
	0.77	0.51
	0.76	0.49
	0.77	0.50
PI_RI19.0C	0.64	0.31
	0.63	0.29
	0.65	0.32
	0.65	0.30
MO_RI19.0C	0.72	0.41
	0.72	0.39
	0.70	0.35
	0.73	0.41
	0.72	0.39

Table D.61. Statistical Values for Cyclic Fatigue Data.

Attribute	Normality (Shapiro-Wilk Test) Prob<W	Equal Variance (Levene and Bartlett tests) Prob>F	ANOVA or Welch's ANOVA (significant difference in means) α = 0.05
Fingerprint |E*|	0.0460*	0.0324*, 0.0772	<0.0001**
N_f	0.1518	0.8004, 0.8716	0.7009
D^R	0.455	0.9063, 0.9636	0.0056**
S_{app}	0.1973	0.3957, 0.2912	0.0005**
C at *S* = 20,000	0.0684	0.3494, 0.2485	<0.0001**
C at *S* = 90,000	0.1284	0.5792, 0.4195	<0.0001**

*Significant value based on significance level
**Significantly different means

Table D.62. Statistical Analysis Method for Cyclic Fatigue Data.

Attribute	Normality Check (Passed)	Trans. Method	Equal Variance Check (Passed)	Trans. Method	Statistical Analysis Method
Fingerprint |E*|	No	None	No	None	ANOVA, Tukey-Kramer HSD
N_f	Yes		Yes		
D^R	Yes		Yes		
S_{app}	Yes		Yes		
C at *S* = 20,000	Yes		Yes		
C at *S* = 90,000	Yes		Yes		

Table D.63. Significant Differences for Cyclic Fatigue Data.

Comparison	p-values (α = 0.05)					
	Fingerprint |E*| (MPa)	N_f	D^R	S_{app}	*C* at *S* = 20,000	*C* at *S* = 90,000
CO_RI19.0C vs. PI_RI19.0C	0.0001	0.8765	0.9882	0.0088	0.0001	0.0001
CO_RI19.0C vs. MO_RI19.0C	0.0003	0.678	0.0119	0.0004	0.0001	0.0001
PI_RI19.0C vs. MO_RI19.0C	0.1221	0.9401	0.0098	0.0583	0.0001	0.0001

Stress Sweep Rutting Tests

The permanent micro-strain curves for each mixture are shown in Figure D.37 and Figure D.38. The rutting strain index (RSI) values are shown in Figure D.39. For these North Carolina mixtures, the RSI values from only one location are shown because they are intermediate mixtures and the variation due to climate is almost nonexistent. Table D.64 shows the percent difference between each test.

PI_RI19.0C exhibits the highest permanent strain in both the high and low temperature tests. As shown in Table D.2, the temperatures for these SSR tests were different. CO_RI19.0C had the highest temperature, then PI_RI19.0C, and MO_RI19.0C. The difference was only one degree Celsius and two degrees Celsius, respectively for high temperature tests, but this could influence the results of these strain curves. For low temperature, CO_RI19.0C and PI_RI19.0C have the same test temperature, but MO_RI19.0C has a test temperature nine degrees Celsius lower.

For RSI, CO_RI19.0C has the best performance followed by PI_RI19.0C and MO_RI19.0C. Even though PI_RI19.0C has the largest permanent strain accumulation, MO_RI19.0C has a worse RSI value. The temperature difference in the MO_RI19.0C tests may be causing the misleading results when comparing strain curves. As discussed before, CO_RI19.0C has higher dynamic modulus values, also there is some RAS included in the mixture causing it to be stiffer, resulting in better performance. PI_RI19.0C also contains 4% RAS, which could be a reason this mixture is resulting in a better performance with respect to permanent deformation over MO_RI19.0C.

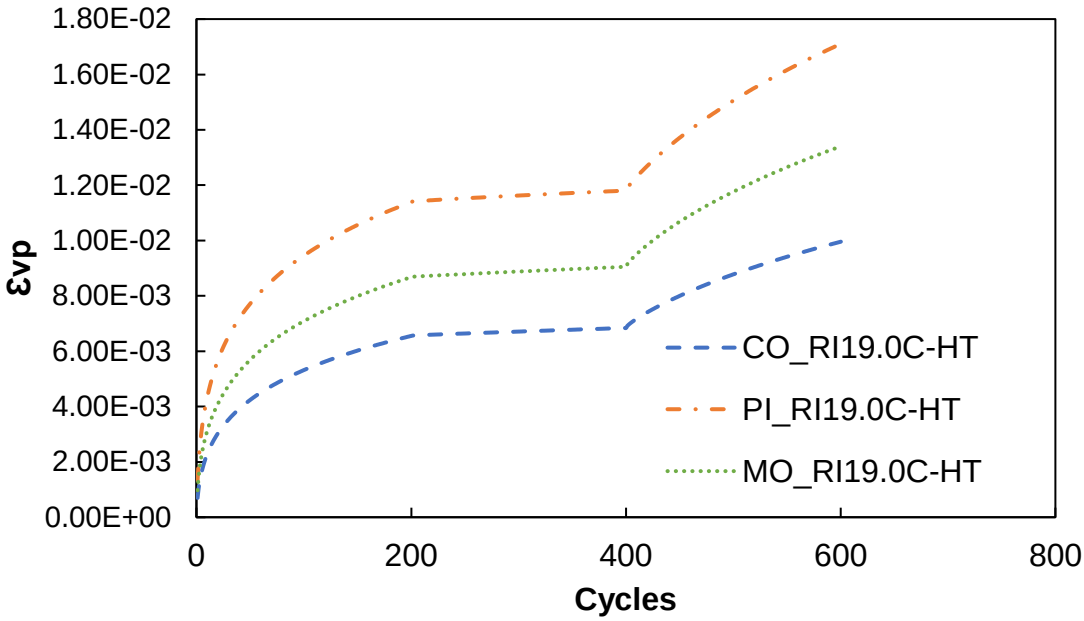

Figure D.37. Permanent micro-strain curves for high temperature tests.

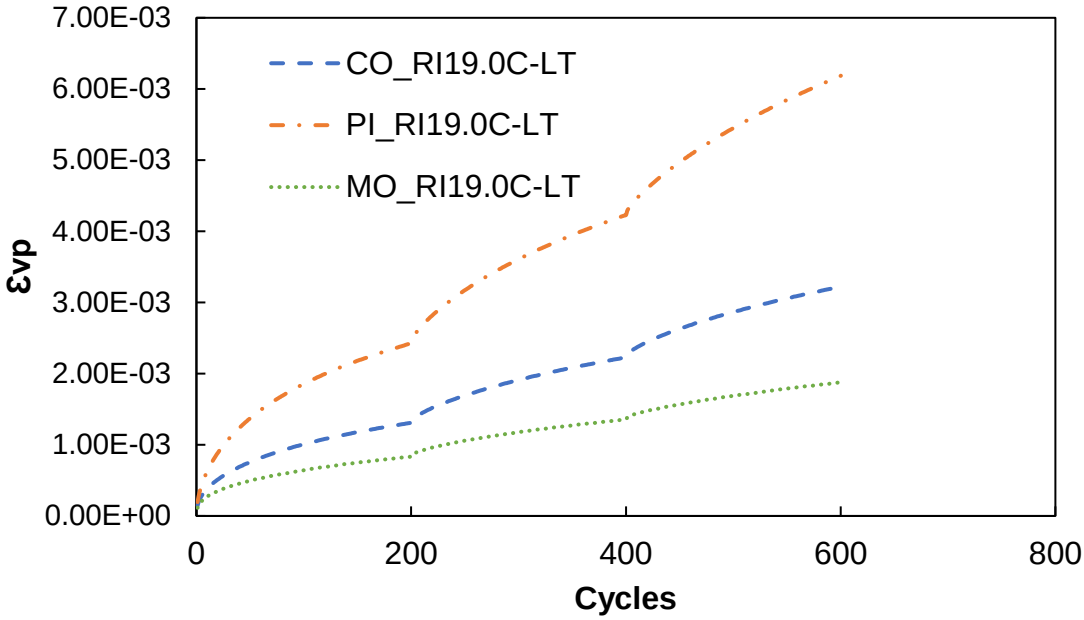

Figure D.38. Permanent micro-strain curves for low temperature tests.

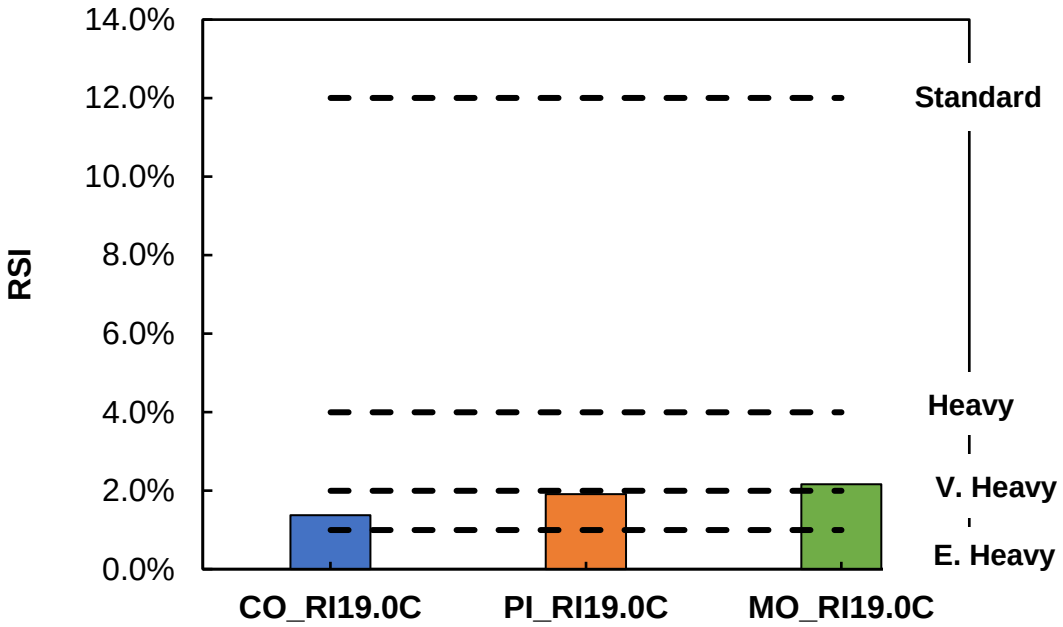

Figure D.39. Rutting strain index values (Wake Forest, NC).

Table D.64. Percent Difference in Permanent Micro-Strain for SSR Testing.

Mixture	Temperature	Percent Difference
CO_RI19.0C	HT	5.63
	LT	3.04
PI_RI19.0C	HT	3.82
	LT	5.61
MO_RI19.0C	HT	23.43
	LT	1.17

For the North Carolina mixtures, as mentioned before, the test temperatures for the SSR tests were different. Because of this, a statistical analysis of the permanent strain curves was not done. Table D.65 shows the RSI values used for the statistical analysis. There was hardly any variation from location to location for the RSI values, therefore the location with the middle RSI values was chosen for the analysis. The temperatures for calculating RSI were the same for all mixtures.

For the statistical analysis, the normal distribution checks, equal variance checks, statistical results are all shown in Table D.66. Table D.67 provides a summary of the results and the resultant statistical analysis method chosen for each of the relevant parameters.

In summary, the data for the RSI values passed the normality check and were flagged for unequal variances. As with the other North Carolina mixtures, the RSI data was flagged, therefore ANOVA and Welch's ANOVA were used to compare results.

The p-values for the SSR data that have significantly different means are shown in Table D.68. For RSI, CO_RI19.0C is significantly different than the other two mixtures. The p-values from the Games-Howell test, shown in Table D.69, show the same results, CO_RI19.0C and MO_RI19.0C are closer to the significance threshold.

Table D.65. RSI Values for SSR Tests (Wake Forest, NC).

Mixture	HT-H: LT-H	HT-H: LT-L	HT-L: LT-L	HT-L: LT-H	All temp.
CO_RI19.0C	1.44	1.52	1.30	1.25	1.37
PI_RI19.0C	1.92	1.91	1.89	1.91	1.91
MO_RI19.0C	2.51	1.82	1.83	2.52	2.16

Table D.66. Statistical Values for SSR Data.

Attribute	Normality (Shapiro-Wilk Test) Prob<W	Equal Variance (Levene and Bartlett tests) Prob>F	ANOVA, (significant difference in means) α = 0.05	Welch's ANOVA, (significant difference in means) α = 0.05
RSI (Wake Forest, NC)	0.1767	0.0017*, <0.0001*	0.0002**	0.0003**

*Significant values based on significance level
**Significantly different means

Table D.67. Summary of Statistical Analysis Method for SSR Data.

Attribute	Normality Check (Passed)	Trans. Method	Equal Variance Check (Passed)	Trans. Method	Statistical Analysis Method
RSI (Wake Forest, NC)	Yes	None	No	None	ANOVA, Welch's ANOVA

Table D.68. Significant Differences for SSR Data (ANOVA, Tukey-Kramer HSD).

Comparison	p-values (α = 0.05)
	RSI (Wake Forest, NC)
CO_RI19.0C vs. PI_RI19.0C	0.0044
CO_RI19.0C vs. MO_RI19.0C	0.0002
PI_RI19.0C vs. MO_RI19.0C	0.1625

Table D.69. Significant Differences for SSR Data (Welch's ANOVA, Games-Howell).

Comparison	p-values (α = 0.05)
	RSI (Wake Forest, NC)
CO_RI19.0C vs. PI_RI19.0C	0.0008
CO_RI19.0C vs. MO_RI19.0C	0.0115
PI_RI19.0C vs. MO_RI19.0C	0.3162

RI19.0C Analysis Summary

Table D.70 and Table D.71 show the overall significant differences for the tests' parameters. The convention for the tables is the same as it was described for the other mixtures. For dynamic

modulus, CO_RI19.0C is different than the other two mixtures. PI_RI19.0C and MO_RI19.0C are different except for at low temperatures. For phase angle data, the mixtures are different for moderate and high temperatures but PI_RI19.0C exhibits similarities to both other mixtures for low temperature. For *C* vs. *S* data, all three mixtures are different. For S_{app}, CO_RI19.0C is different from the other two mixtures. For RSI, PI_RI19.0C is similar to MO_I19.0C.

For S_{app}, all three mixtures are classified as "Standard". For RSI, CO_RI19.0C and PI_RI19.0C are classified as "Very Heavy" and MO_RI19.0C is classified as "Heavy" The traffic designation for all three mixtures, therefore, falls under "Standard" because of the fatigue performance. According to the North Carolina DOT QMS manual, there is no traffic designation, these mixtures are meant for all ESAL ranges.

Table D.70. Summary of Dynamic Modulus Test Parameters.

Mixtures	DM parameters			PA parameters		
	4°C	20°C	40°C	4°C	20°C	40°C
CO_RI19.0C	A	A	A	B	C	B
PI_RI19.0 C	B	C	C	BA	A	A
MO_RI19.0C	B	B	B	A	B	B

Table D.71. Summary of Cyclic Fatigue and Stress Sweep Rutting Test Parameters.

Mixtures	CF and SSR parameters			
	S_{app}	*C* at *S* = 20,000	*C* at *S* = 90,000	RSI (Wake Forest, NC)
CO_RI19.0C	A	A	A	B
PI_RI19.0 C	B	C	C	A
MO_RI19.0C	B	B	B	A

North Carolina RB25C Experimental Results

Dynamic Modulus Tests

The dynamic modulus results for each of the three base mixtures are shown in Figure D.40 and Figure D.41. The phase angle results from the dynamic modulus testing are shown in Figure D.42. Overall, the master curves are very close for the three tested mixtures. At lower reduced frequency values, CO_RB25C looks to be higher than PI_RB25C and MO_RB25C. However, when moving to higher reduced frequency values, MO_RB25C will change to big the mixture with the highest modulus. For the phase angles, overall, PI_RB25C and MO_RB25C are close in values and look to have the higher phase angle values when compared to CO_RB25C. By examining the information in the materials section (section 3.2.2), CO_RB25C has a lower binder content but also exhibits the highest %RBR (42%) accounting for a softer binder grade. This %RBR increases the stiffness of the mixture, thus increasing the dynamic modulus. MO_RB25C and PI_RB25C are close in terms of binder content and RBR%.

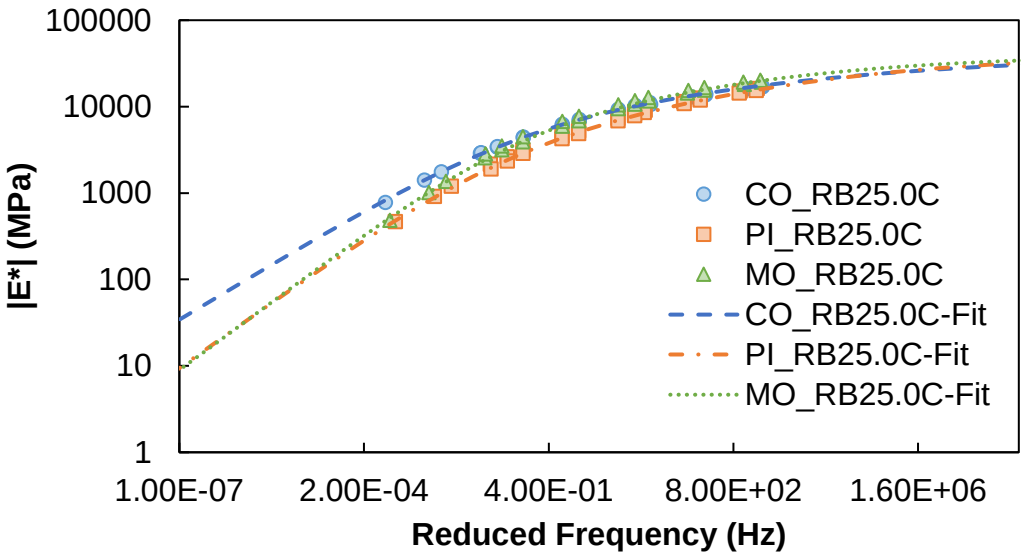

Figure D.40. Dynamic modulus results (log-log plot).

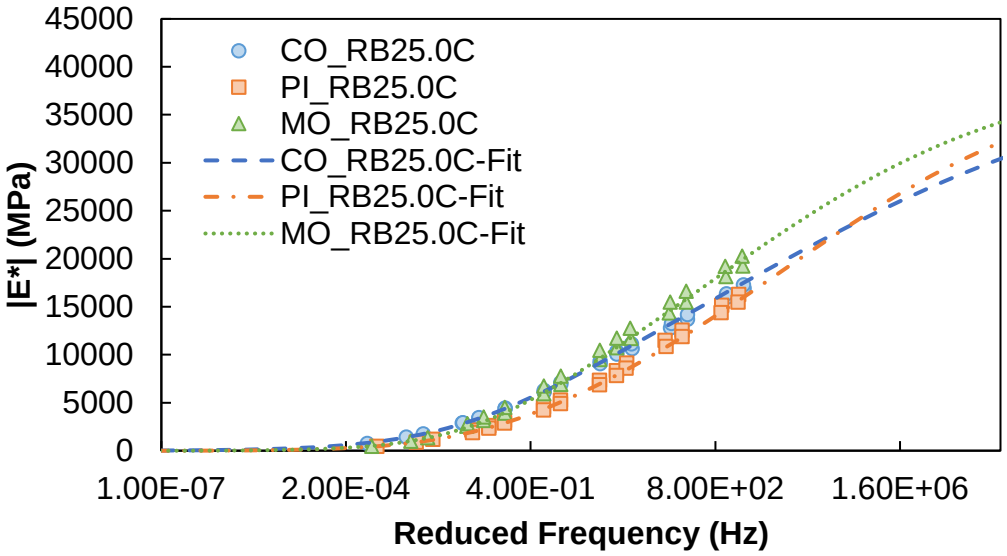

Figure D.41. Dynamic modulus results (semi-log plots).

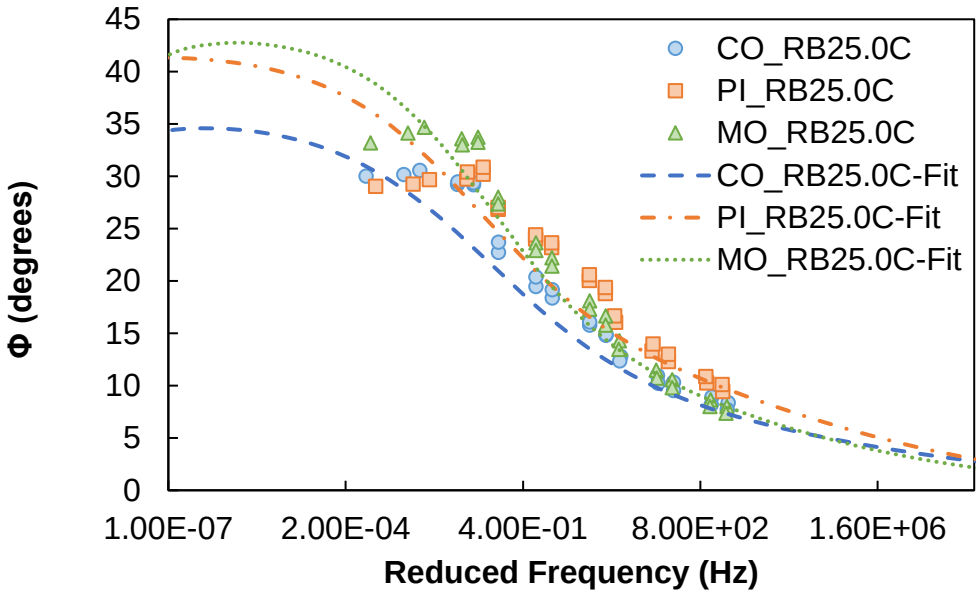

Figure D.42. Phase angle results.

The statistical analysis for the dynamic modulus results was done the exact same as in the other mixtures. The dynamic modulus values used in the statistical analysis are shown in Table D.72, Table D.73, and Table D.74. For the statistical analysis, the test results for normality and equal variances are shown in Table D.75. Table D.76 provides a summary of the results and the resultant statistical analysis method chosen for each of the relevant parameters.

In summary for the dynamic modulus data, only one combination was flagged for non-normal data. All the data passed the equal variances check except for one combination; thus, it was concluded to run an ANOVA test to find significant differences. The results of the statistical analysis are shown in Table D.77, Table D.78, and Table D.79 in terms of the p-values from the hypothesis test. In this table, cases where the p-value is less than a significance level of 95% are highlighted in red. By examining the p-values shown, all the mixtures are different at 4°C. At 20°C, CO_RB25C is statistically different than PI_RB25C and is similar to MO_RB25C. At 40°C, PI_RB25C is similar to MO_RB25C and different from CO_RB25C.

Table D.72. Dynamic Modulus Results for Statistical Analysis at 4°C.

Mixture	4°C-10Hz	4°C-5Hz	4°C-1Hz	4°C-0.5Hz	4°C-0.1Hz
CO-RB25C	16936	16024	13701	12807	10640
	17291	16364	14187	13273	11134
	18083	17170	14926	13958	11699
PI-RB25C	16281	15150	12586	11499	9149
	15505	14408	11915	10874	8611
	14827	13739	11263	10272	8116
MO-RB25C	19263	18163	15509	14365	11694
	20270	19222	16622	15493	12778
	19574	18348	15520	14284	11519

Table D.73. Dynamic Modulus Results for Statistical Analysis at 20°C.

Mixture	20°C-10Hz	20°C-5Hz	20°C-1Hz	20°C-0.5Hz	20°C-0.1Hz
CO-RB25C	10346	9362	7115	6280	4460
	10067	9094	6910	6127	4392
	10573	9495	7182	6337	4526
PI-RB25C	8357	7345	5281	4604	3148
	7854	6879	4910	4259	2887
	8174	7234	5175	4460	2961
MO-RB25C	10730	9515	6907	5962	3937
	11731	10489	7775	6760	4513
	10480	9268	6660	5729	3718

Table D.74. Dynamic Modulus Results for Statistical Analysis at 40°C.

Mixture	40°C-10Hz	40°C-5Hz	40°C-1Hz	40°C-0.5Hz	40°C-0.1Hz
CO-RB25C	3397	2898	1761	1417	778.6
	3457	2944	1812	1474	816.2
	3640	3076	1861	1480	808.1
PI-RB25C	2631	2157	1203	913.8	468.1
	2350	1908	1062	811.2	429.6
	2428	2013	1110	837.1	421.6
MO-RB25C	3179	2573	1364	1012	483.3
	3514	2837	1513	1122	543
	2919	2325	1191	863.6	403.8

Table D.75. Statistical Values for Dynamic Modulus Data.

Comparison	Normality (Shapiro-Wilk Test) Prob<W	Equal Variance (Levene and Bartlett tests) Prob>F	ANOVA or Welch's ANOVA (significant difference in means) α = 0.05
4°C-10Hz	0.819	0.8965, 0.9043	0.0005**
4°C-5Hz	0.8615	0.9752, 0.9539	0.0006**
4°C-1Hz	0.7861	0.9711, 0.9960	0.0008**
4°C-0.5Hz	0.6754	0.8733, 0.9800	0.0008**
4°C-0.1Hz	0.3573	0.7102, 0.9223	0.0010**
20°C-10Hz	0.1835	0.1109, 0.3424	0.0005**
20°C-5Hz	0.1117	0.0774, 0.2685	0.0005**
20°C-1Hz	0.1147	0.0537, 0.1600	0.0008**
20°C-0.5Hz	0.1391	0.0489*, 0.1200	0.0009**
20°C-0.1Hz	0.0673	0.0537, 0.0903	0.0010**
40°C-10Hz	0.2597	0.3964, 0.4769	0.0022**
40°C-5Hz	0.3456	0.4113, 0.4007	0.0016**
40°C-1Hz	0.1731	0.3014, 0.3083	0.0006**
40°C-0.5Hz	0.0538	0.2196, 0.2367	0.0003**
40°C-0.1Hz	0.0174*	0.2074, 0.2190	0.0001**

*Significant values based on significance level
**Significantly different means

Table D.76. Summary of Statistical Analysis Method for Dynamic Modulus.

Data	Comparison	Normality Check (Passed)	Trans. Method	Equal Variance Check (Passed)	Trans. Method	Statistical Analysis Method
Dynamic Modulus	4°C-10Hz	Yes	None	Yes	None	ANOVA, Tukey-Kramer HSD
	4°C-5Hz	Yes		Yes		
	4°C-1Hz	Yes		Yes		
	4°C-0.5Hz	Yes		Yes		
	4°C-0.1Hz	Yes		Yes		
	20°C-10Hz	Yes		Yes		
	20°C-5Hz	Yes		Yes		
	20°C-1Hz	Yes		Yes		
	20°C-0.5Hz	Yes		No		
	20°C-0.1Hz	Yes		Yes		
	40°C-10Hz	Yes		Yes		
	40°C-5Hz	Yes		Yes		
	40°C-1Hz	Yes		Yes		
	40°C-0.5Hz	Yes		Yes		
	40°C-0.1Hz	No		Yes		

Table D.77. Significant Differences for Dynamic Modulus Data at 4°C.

Levels	p-values (α = 0.05)				
	4°C-10Hz	4°C-5Hz	4°C-1Hz	4°C-0.5Hz	4°C-0.1Hz
CO_RB25C, PI_RB25C	0.0216	0.0149	0.0098	0.0069	0.0042
CO_RB25C, MO_RB25C	0.0097	0.0159	0.0488	0.0807	0.2574
PI_RB25C, MO_RB25C	0.0004	0.0005	0.0007	0.0069	0.001

Table D.78. Significant Differences for Dynamic Modulus Data at 20°C.

Levels	p-values (α = 0.05)				
	20°C-10Hz	20°C-5Hz	20°C-1Hz	20°C-0.5Hz	20°C-0.1Hz
CO_RB25C, PI_RB25C	0.002	0.0017	0.0015	0.0014	0.001
CO_RB25C, MO_RB25C	0.2371	0.4462	0.9875	0.9324	0.2038
PI_RB25C, MO_RB25C	0.0005	0.0006	0.0013	0.0019	0.0052

Table D.79. Significant Differences for Dynamic Modulus Data at 40°C.

Levels	p-values (α = 0.05)				
	40°C-10Hz	40°C-5Hz	40°C-1Hz	40°C-0.5Hz	40°C-0.1Hz
CO_RB25C, PI_RB25C	0.0021	0.0013	0.0005	0.0003	0.0001
CO_RB25C, MO_RB25C	0.2613	0.0705	0.0045	0.0013	0.0003
PI_RB25C, MO_RB25C	0.011	0.0185	0.0819	0.1633	0.5917

The phase angle results were statistically compared just as the dynamic modulus results. The phase angle results used in the statistical analysis are found in Table D.80, Table D.81, and Table D.82.

For the statistical analysis, the test results for normality and equal variances are shown in Table D.83. Table D.84 provides a summary of the results and the resultant statistical analysis method chosen for each of the relevant parameters. In summary, all phase angle data passed the normality check except for two combinations. All the data pass the variance check. Because of this, it was decided to run an ANOVA test to determine the significant differences. The results of the statistical analysis are shown in Table D.85, Table D.86, and Table D.87 in terms of the p-values from the hypothesis test. In this table, cases where the p-value is less than a significance level of 95% are highlighted in red. For the phase angle data, CO_RB25C is significantly different from PI_RB25C until reaching 40°C temperature, after which, both are similar. CO_RB25C is similar to MO_RB25C in four of the fifteen combinations. PI_RB25C is different from MO_RB25C for all the evaluated temperatures.

Table D.80. Phase Angle Results for Statistical Analysis at 4°C.

Mixture	4°C-10Hz	4°C-5Hz	4°C-1Hz	4°C-0.5Hz	4°C-0.1Hz
CO-RB25C	8.4	8.94	10.34	10.97	12.82
	7.72	8.2	9.56	10.26	12.39
	7.73	8.22	9.57	10.31	12.42
PI-RB25C	9.46	10.27	12.32	13.34	16.08
	10.14	10.89	13.02	14.01	16.69
	10.6	11.42	13.53	14.44	17.13
MO-RB25C	8.01	8.65	10.57	11.51	14.31
	7.37	8.03	9.83	10.73	13.49
	8.07	8.78	10.76	11.75	14.71

Table D.81. Phase Angle Results for Statistical Analysis at 20°C.

Mixture	20°C-10Hz	20°C-5Hz	20°C-1Hz	20°C-0.5Hz	20°C-0.1Hz
CO-RB25C	14.83	15.79	18.4	19.49	22.74
	14.92	16.11	19.17	20.39	23.73
	14.93	16.18	19.31	20.47	23.79
PI-RB25C	18.8	20.05	23.21	24.02	26.85
	19.4	20.61	23.66	24.42	27.04
	18.46	19.47	22.21	23.14	25.96
MO-RB25C	16.67	18.12	22.23	23.65	28.01
	15.81	17.31	21.44	22.94	27.39
	17.06	18.61	22.84	24.29	28.69

Table D.82. Phase Angle Results for Statistical Analysis at 40°C.

Mixture	40°C-10Hz	40°C-5Hz	40°C-1Hz	40°C-0.5Hz	40°C-0.1Hz
CO-RB25C	29.2	29.23	30.59	30.18	30.02
	29.38	29.49	30.96	30.59	30.6
	28.4	28.31	29.5	29.22	29.22
PI-RB25C	30.21	29.74	29.68	29.26	29.06
	30.89	30.44	30.19	29.67	29
	31.02	30.29	29.95	29.52	29.25
MO-RB25C	33.74	33.59	34.68	34.14	33.21
	33.27	33.02	33.92	33.28	31.91
	34.68	34.67	35.74	35.42	34.37

Table D.83. Statistical Values for Phase Angle Data.

Temperature - Frequency	**Normality (Shapiro-Wilk Test) Prob<W**	**Equal Variance (Levene and Bartlett tests) Prob>F**	**ANOVA or Welch's ANOVA (significant difference in means) α = 0.05**
4°C-10Hz	0.1187	0.7628, 0.8390	0.0016**
4°C-5Hz	0.0824	0.8729, 0.8758	0.0012**
4°C-1Hz	0.1132	0.9100, 0.9208	0.0007**
4°C-0.5Hz	0.1484	0.8348, 0.9030	0.0004**
4°C-0.1Hz	0.2923	0.4005, 0.5144	0.0002**
20°C-10Hz	0.2079	0.1074, 0.0554	0.0001**
20°C-5Hz	0.454	0.3947, 0.3939	0.0002**
20°C-1Hz	0.2022	0.7878, 0.8602	0.0006**
20°C-0.5Hz	0.071	0.9663, 0.9583	0.0006**
20°C-0.1Hz	0.3363	0.9971, 0.9865	0.0002**
40°C-10Hz	0.4418	0.6272, 0.8066	0.0001**
40°C-5Hz	0.2131	0.3990, 0.6057	0.0002**
40°C-1Hz	0.0348*	0.2620, 0.3350	0.0003**
40°C-0.5Hz	0.0320*	0.1970, 0.1958	0.0004**
40°C-0.1Hz	0.0677	0.2097, 0.0734	0.0021**

*Significant values based on significance level
**Significantly different means

Table D.84. Summary of Statistical Analysis Method for Phase Angle Data.

Data	Comparison	Normality Check (Passed)	Trans. Method	Equal Variance Check (Passed)	Trans. Method	Statistical Analysis Method
Phase Angle	4°C-10Hz	Yes	None	Yes	None	ANOVA, Tukey-Kramer HSD
	4°C-5Hz	Yes		Yes		
	4°C-1Hz	Yes		Yes		
	4°C-0.5Hz	Yes		Yes		
	4°C-0.1Hz	Yes		Yes		
	20°C-10Hz	Yes		Yes		
	20°C-5Hz	Yes		Yes		
	20°C-1Hz	Yes		Yes		
	20°C-0.5Hz	Yes		Yes		
	20°C-0.1Hz	Yes		Yes		
	40°C-10Hz	Yes		Yes		
	40°C-5Hz	Yes		Yes		
	40°C-1Hz	No		Yes		
	40°C-0.5Hz	No		Yes		
	40°C-0.1Hz	Yes		Yes		

Table D.85. Significant Differences for Phase Angle Data at 4°C.

Levels	p-values (α = 0.05)				
	4°C-10Hz	4°C-5Hz	4°C-1Hz	4°C-0.5Hz	4°C-0.1Hz
CO_RB25C, PI_RB25C	0.0032	0.0019	0.0008	0.0004	0.0001
CO_RB25C, MO_RB25C	0.9333	0.9959	0.4323	0.1924	0.0157
PI_RB25C, MO_RB25C	0.0032	0.0021	0.0022	0.0017	0.0021

Table D.86. Significant Differences for Phase Angle Data at 20°C.

Levels	p-values (α = 0.05)				
	20°C-10Hz	20°C-5Hz	20°C-1Hz	20°C-0.5Hz	20°C-0.1Hz
CO_RB25C, PI_RB25C	0.0001	0.0002	0.0007	0.0008	0.0016
CO_RB25C, MO_RB25C	0.0121	0.0078	0.0023	0.0012	0.0002
PI_RB25C, MO_RB25C	0.0018	0.007	0.3124	0.8939	0.0652

Table D.87. Significant Differences for Phase Angle Data at 40°C.

Levels	p-values (α = 0.05)				
	40°C-10Hz	40°C-5Hz	40°C-1Hz	40°C-0.5Hz	40°C-0.1Hz
CO_RB25C, PI_RB25C	0.0241	0.1497	0.7637	0.6964	0.4643
CO_RB25C, MO_RB25C	0.0001	0.0002	0.0006	0.0011	0.0071
PI_RB25C, MO_RB25C	0.0012	0.0011	0.0004	0.0006	0.0022

Cyclic Fatigue Tests

The cyclic fatigue test data resulting in *C* vs. *S* damage curves are shown in Figure D.43 and Figure D.44. The representative S_{app} values, D^R values, and N_f vs. Cum. (1-*C*) data are shown in Figure D.45, Figure D.46, and Figure D.47 respectively. The linear viscoelastic and S-VECD fatigue properties are shown in Table D.88. For the damage curves, CO_RB25C has the higher *C* values throughout the plot. PI_RB25C has the highest S_{app} and D^R values followed by CO_RB25C and then MO_RB25C. The Cum. (1-*C*) vs. N_f graph shows D^R values as the slopes for each mixture.

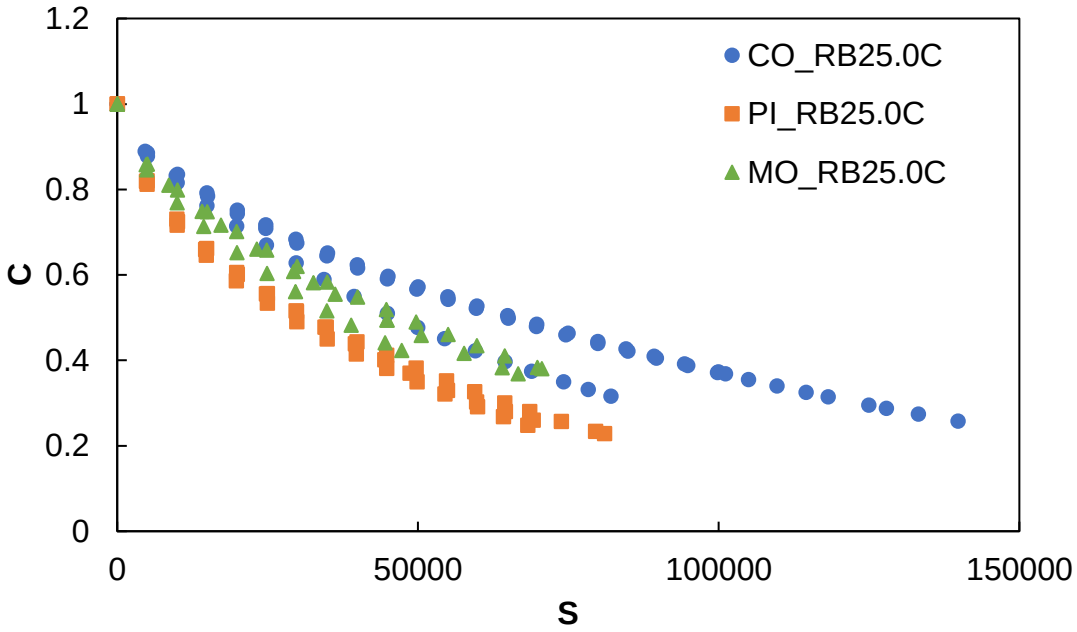

Figure D.43. *C* vs. *S* damage curves (individual specimen values).

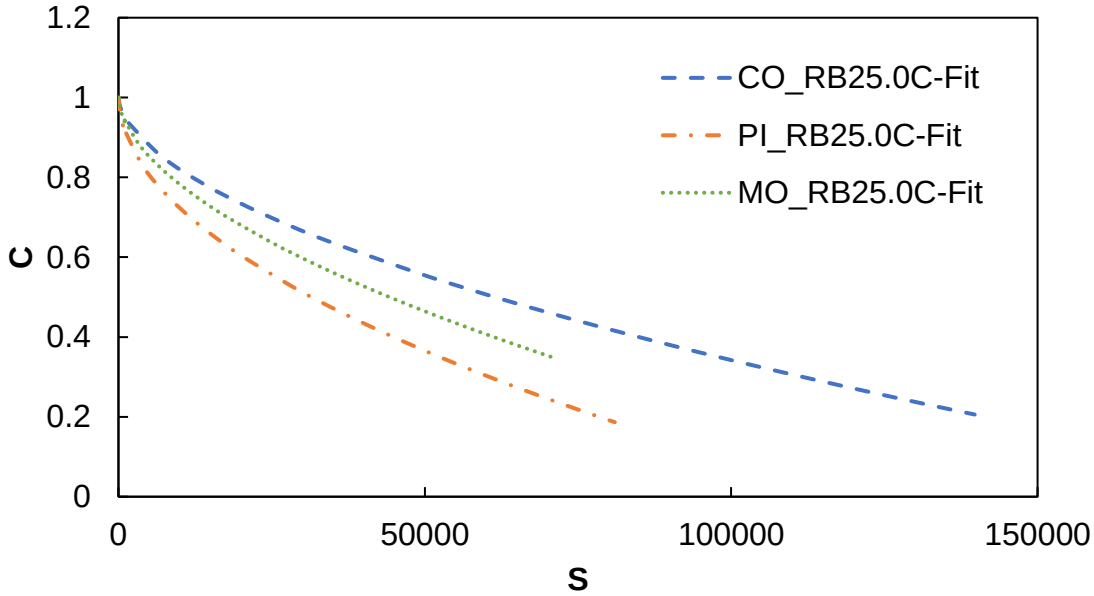

Figure D.44. *C* vs. *S* damage curves (fitted values).

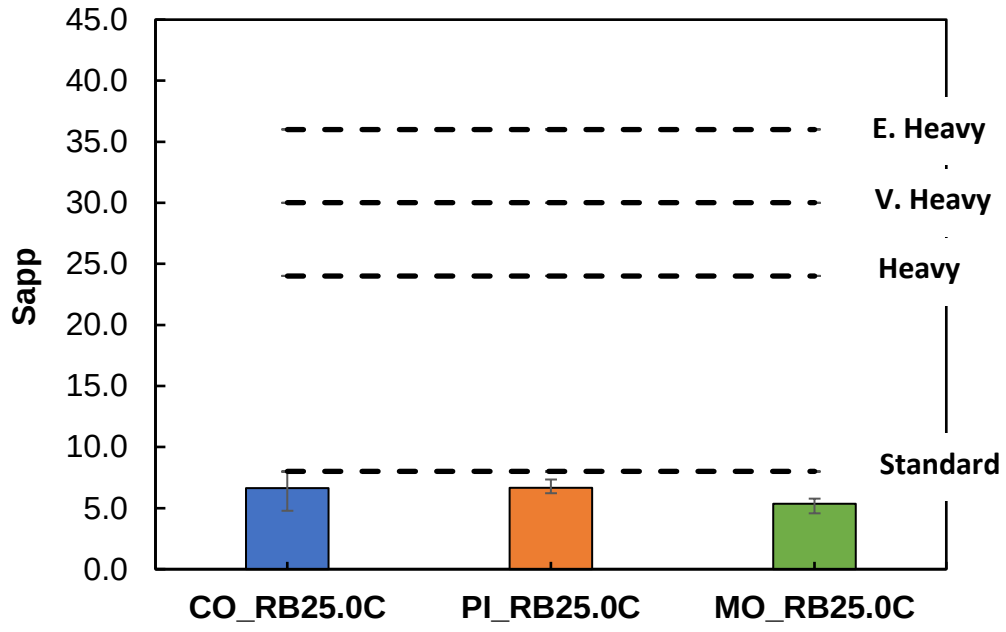

Figure D.45. Representative S_{app} values.

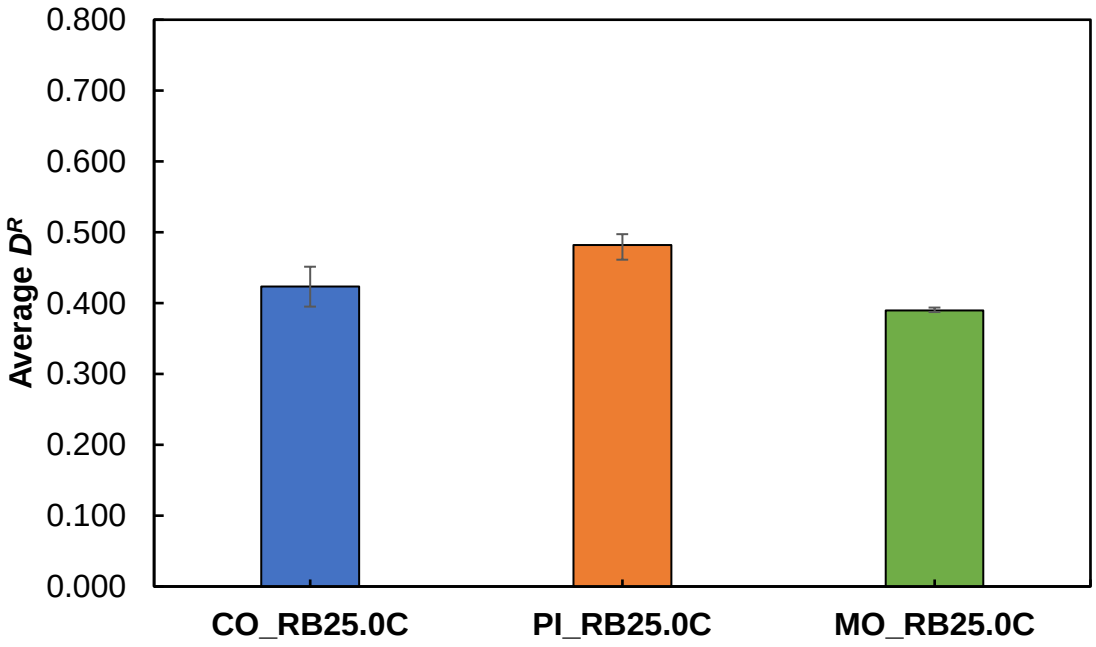

Figure D.46. Average D^R values.

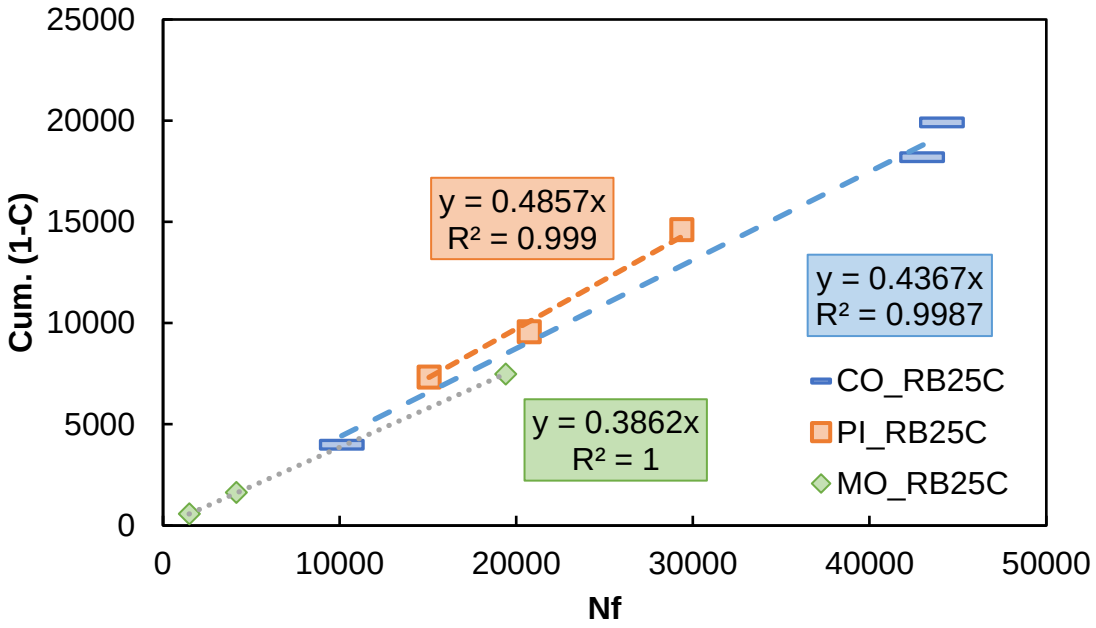

Figure D.47. Cum. (1-*C*) vs. N_f.

Table D.88. Linear viscoelastic and FlexPAVE™ S-VECD fatigue properties.

Properties	CO_RB25.0C	PI_RB25.0C	MO_RB25.0C
α	3.59	3.17	3.09
C11	0.0010	0.0024	0.0013
C12	0.56	0.52	0.56
a1	0.0005	0.0006	0.0006
a2	-0.15	-0.15	-0.15
a3	3.01	2.90	2.99

The statistical analysis for the North Carolina RB25C base mixtures includes the same parameters that were used for the statistical analysis from the other mixtures. Just as with the other two sets of mixtures, the temperature when calculating S_{app} is the same for all mixtures. The only difference in the analysis is the *C* values correspond to *S* = 20,000 and *S* = 45,000, instead of *S* = 20,000 and *S* = 120,000 or S=90,000. This was done because the damage curves were shorter during these tests and *S* = 120,000 or 90,000 was not appropriate in all tests. The average *C* values targeted for these *S* values were 0.67 and 0.48. The *C* values that correspond to these two *S* values were interpolated from the *C* vs. *S* curves characterized for each specimen from FlexMAT™. The values used in the statistical analysis for fingerprint modulus, N_f, D^R, and S_{app} are shown in Table D.89. The *C* values used in the statistical analysis are shown in Table D.90.

For the statistical analysis, the tests of normality and variance are shown in Table D.91. Table D.92 provides a summary of the results and the resultant statistical analysis method chosen for each of the relevant parameters. The data pass the normality and equal variances tests. ANOVA test is utilized to find the differences.

The p-values that show the significant differences for the cyclic fatigue data are shown in Table D.93. This table shows that CO_RB25C is different from PI_RB25C and is similar to MO_RB25C.

Also, it shows that the D^R values for CO_RB25C and MO_RB25C are similar. The S_{app} values are similar for all of the three mixtures.

Table D.89. Cyclic Fatigue Results for Statistical Analysis.

Mixture	Fingerprint |E*| (MPa)	N_f	D^R	S_{app}
CO_RB25.0C	12111	44100	0.45	7.98
	11712	42990	0.42	7.21
	11179	10130	0.40	4.77
PI_RB25.0C	9373	29370	0.50	7.34
	10006	15060	0.49	6.42
	9410	20740	0.46	6.21
MO_RB25.0C	11553	1490	0.39	5.49
	12403	19400	0.39	5.76
	11902	4160	0.39	4.59
	12111	44100	0.45	7.98

Table D.90. *C* Values for Statistical Analysis.

Mixture	*C* at *S* = 20,000	*C* at *S* = 45,000
CO_RB25.0C	0.74	0.59
	0.75	0.60
	0.71	0.51
	0.73	0.58
PI_RB25.0C	0.60	0.41
	0.58	0.38
	0.60	0.40
	0.60	0.40
MO_RB25.0C	0.69	0.49
	0.70	0.52
	0.65	0.44
	0.68	0.50

Table D.91. Statistical Values for Cyclic Fatigue Data.

Attribute	Normality (Shapiro-Wilk Test) Prob<W	Equal Variance (Levene and Bartlett tests) Prob>F	ANOVA or Welch's ANOVA (significant difference in means) α = 0.05
Fingerprint |E*|	0.1156	0.9507, 0.9400	0.0009**
N_f	0.4453	0.0973, 0.4248	0.1601
D^R	0.1234	0.2250, 0.0950	0.0034**
S_{app}	0.8418	0.1064, 0.3031	0.2848
C at *S* = 20,000	0.168	0.5514, 0.4921	<0.0001**
C at *S* = 45,000	0.2335	0.2659, 0.2173	0.0001**

*Significant value based on significance level
**Significantly different means

Table D.92. Statistical Analysis Method for Cyclic Fatigue Data.

Attribute	Normality Check (Passed)	Trans. Method	Equal Variance Check (Passed)	Trans. Method	Statistical Analysis Method
Fingerprint |E*|	Yes	None	Yes	None	ANOVA, Tukey-Kramer HSD
N_f	Yes		Yes		
D^R	Yes		Yes		
S_{app}	Yes		Yes		
C at S = 20,000	Yes		Yes		
C at S = 45,000	Yes		Yes		

Table D.93. Significant Differences for Cyclic Fatigue Data.

Comparison	p-values (α = 0.05)					
	Fingerprint |E*| (MPa)	N_f	D^R	S_{app}	C at S = 20,000	C at S = 45,000
CO_RB25C vs. PI_RB25C	0.0022	0.6057	0.0243	0.9992	0.0001	0.0001
CO_RB25C vs. MO_RB25C	0.6978	0.1418	0.1731	0.336	0.0045	0.0123
PI_RB25C vs. MO_RB25C	0.0011	0.4716	0.0029	0.3512	0.0001	0.0075

Stress Sweep Rutting Tests

The permanent micro-strain curves for each mixture are shown in Figure D.48 and Figure D.49. The rutting strain index (RSI) values are shown in Figure D.50. For these North Carolina mixtures, the RSI values from only one location are shown because they are base mixtures and the variation due to climate is almost nonexistent. Table D.94 shows the percent difference between each test.

PI_RB25C exhibits the highest permanent strain in both the high and low temperature tests. As shown in Table D.2, the temperatures for these SSR tests were different. CO_RB25C had the highest temperature, then PI_RB25C, and MO_RB25C. The difference was only one degree Celsius and two degrees Celsius, respectively for high temperature tests, but this could influence the results of these strain curves. For low temperature, CO_RB25C and PI_RB25C have the same test temperature, but MO_RB25C has a test temperature eleven degrees Celsius lower.

For RSI, CO_RB25C has the best performance followed by PI_RB25C and MO_RB25C. Even though PI_RB25C has the largest permanent strain accumulation, MO_RB25C has a worse RSI value. The temperature difference in the MO_RB25C tests may be causing the misleading results when comparing strain curves. As discussed before, CO_RB25C has higher dynamic modulus values, also there is some RAS included in the mixture causing it to be stiffer, resulting in better performance. PI_RB25C has the lowest binder content, which could be a reason this mixture is resulting in a better performance with respect to permanent deformation over MO_RB25C.

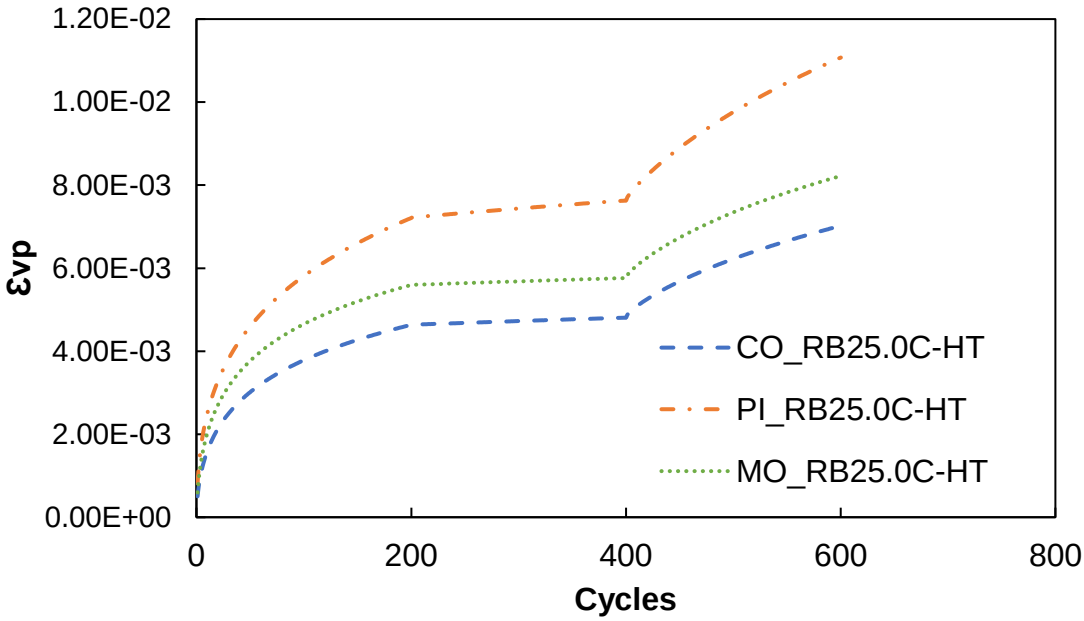

Figure D.48. Permanent micro-strain curves for high temperature tests.

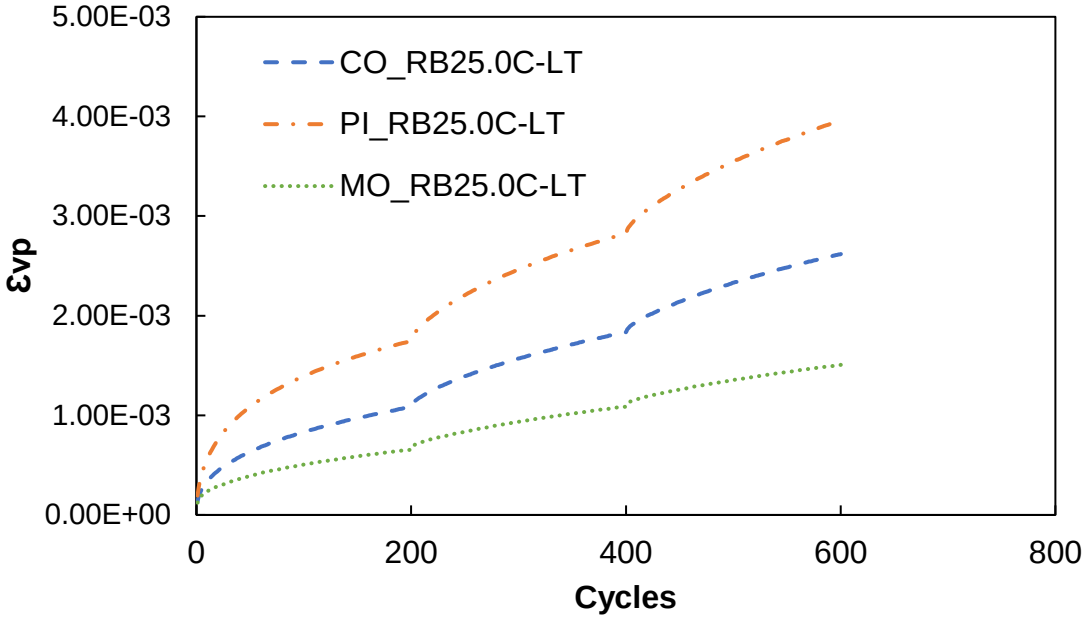

Figure D.49. Permanent micro-strain curves for low temperature tests.

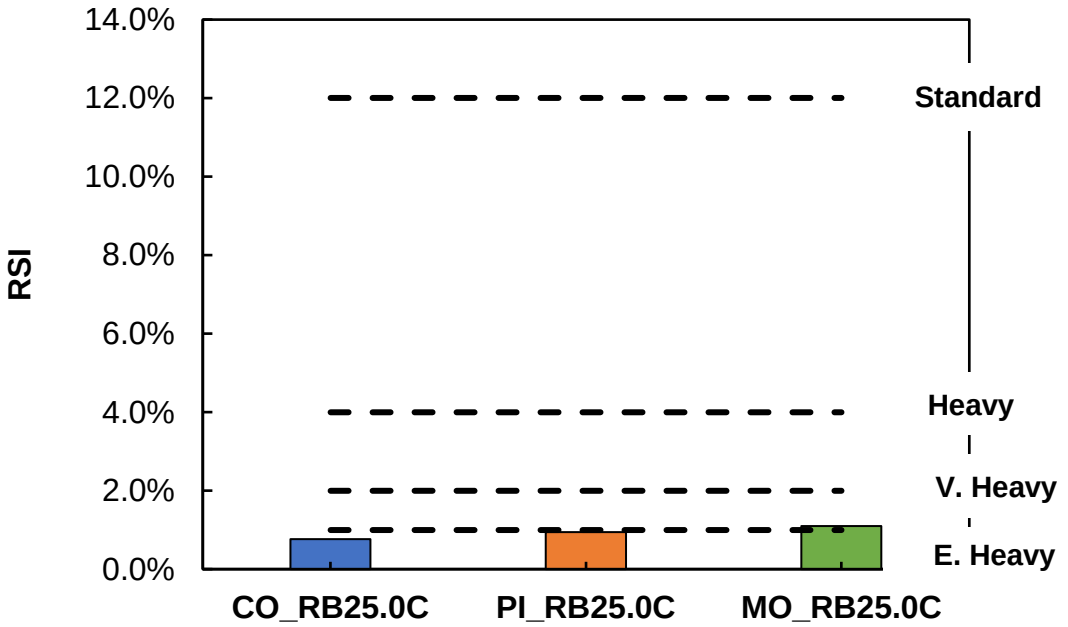

Figure D.50. Rutting strain index values (Wake Forest, NC).

Table D.94. Percent Difference in Permanent Micro-Strain for SSR Testing.

Mixture	Temperature	Percent Difference
CO_RB25C	HT	0.98
	LT	14.28
PI_RB25C	HT	27.33
	LT	23.33
MO_RB25C	HT	4.67
	LT	22.30

For the North Carolina mixtures, as mentioned before, the test temperatures for the SSR tests were different. Because of this, a statistical analysis of the permanent strain curves was not done. Table D.95 shows the RSI values used for the statistical analysis. There was hardly any variation from location to location for the RSI values, therefore the location with the middle RSI values was chosen for the analysis just as for the NC RI19.0C mixtures. The temperatures for calculating RSI were the same for all mixtures.

For the statistical analysis, the normal distribution checks, equal variance checks, statistical results are all shown in Table D.96. Table D.97 provides a summary of the results and the resultant statistical analysis method chosen for each of the relevant parameters.

In summary, the data for the RSI values failed the normality check and were flagged for unequal variances. As with the other North Carolina mixtures, the RSI data was flagged, therefore Welch's ANOVA was used to compare results.

The p-values from the Games-Howell test, shown in Table D.98 show that all the mixtures were similar in terms of rutting performance.

Table D.95. RSI Values for SSR Tests (Wake Forest, NC).

Mixture	HT-H: LT-H	HT-H: LT-L	HT-L: LT-L	HT-L: LT-H	All temp.
CO_RB25C	1.02	0.73	0.53	0.83	0.76
PI_RB25C	1.03	0.61	0.93	1.93	0.94
MO_RB25C	1.21	1.04	0.99	1.14	1.10

Table D.96. Statistical Values for SSR Data.

Attribute	Normality (Shapiro-Wilk Test) Prob<W	Equal Variance (Levene and Bartlett tests) Prob>F	Welch's ANOVA, (significant difference in means) α = 0.05
RSI (Wake Forest, NC)	0.0220*	0.1176, 0.0074*	0.2118

*Significant values based on significance level
**Significantly different means

Table D.97. Summary of Statistical Analysis Method for SSR Data.

Attribute	Normality Check (Passed)	Trans. Method	Equal Variance Check (Passed)	Trans. Method	Statistical Analysis Method
RSI (Wake Forest, NC)	No	None	No	None	ANOVA, Welch's ANOVA

Table D.98. Significant Differences for SSR Data (Welch's ANOVA, Games-Howell).

Comparison	p-values (α = 0.05) RSI (Wake Forest, NC)
CO_RB25C vs. PI_RB25C	0.2795
CO_RB25C vs. MO_RB25C	0.2635
PI_RB25C vs. MO_RB25C	0.9991

RB25C Analysis Summary

Table D.99 and Table D.100 show the overall significant differences for the tests' parameters. The convention for the tables is the same as it was described for the other mixtures. For dynamic modulus, all the mixtures are different at 4°C. CO_RB25C and MO_RB25C are similar at 20°C and PI_RB25C and MO_RB25C are similar at 40°C. For phase angle data, the mixtures are different with two of them being similar at all the temperatures. For *C* vs. *S* data, all three mixtures are different. For S_{app} and RSI, all the mixtures are similar.

For S_{app}, all three mixtures are classified as "Standard". For RSI, CO_RB25C and PI_RB25C are classified as "Extremely Heavy" and MO_RB25C is classified as "Very Heavy". The traffic designation for all three mixtures therefore falls under "Standard" because of the fatigue

performance. According to the North Carolina DOT QMS manual, there is no traffic designation, these mixtures are meant for all ESAL ranges.

Table D.99. Summary of Dynamic Modulus Test Parameters.

Mixtures	DM parameters			PA parameters		
	4°C	20°C	40°C	4°C	20°C	40°C
CO_RB25C	B	A	A	B	B	B
PI_RB25C	C	B	B	A	A	B
MO_RB25C	A	A	B	B	A	A

Table D.100. Summary of Cyclic Fatigue and Stress Sweep Rutting Test Parameters.

Mixtures	CF and SSR parameters			
	S_{app}	C at S = 20,000	C at S = 45,000	RSI (Wake Forest, NC)
CO_RB25C	A	A	A	A
PI_RB25C	A	C	C	A
MO_RB25C	A	B	B	A

APPENDIX E: SUPPLEMENTARY INFORMATION ON PAVEMENT SIMULATIONS

Performance of reference and current materials were evaluated through 216 simulations using AASHTO Pavement Design ME and 72 simulations using FlexPAVE™. The results for fatigue cracking and rut depth using Pavement ME and FlexPAVE™ are summarized in Table E.1. The performance ratios calculated based on the simulation results are summarized in Table E.2.

Table E.1. Summary of Performance Simulation Results.

Simulation #ID	Simulation Code	Pavement ME		FlexPAVE™		
		Fatigue Cracking (%)	Total Rutting (in.)	Fatigue Damage (%)	Fatigue Cracking (%)	Total Rutting (in)
1_1	1-S95B-FDA-t-Sand-PI-ref	1.66	0.46			
1_2	2-S95B-FDA-t-Silt-PI-ref	9.93	0.38	26.39	49.07	0.40
1_3	3-S95B-FDA-t-Clay-PI-ref	27.40	0.76			
1_4	4-S95B-FDA-t-Sand-MO-ref	1.61	0.44			
1_5	5-S95B-FDA-t-Silt-MO-ref	4.70	0.35	23.93	48.34	0.35
1_6	6-S95B-FDA-t-Clay-MO-ref	19.70	0.71			
1_7	7-S95B-FDA-t-Sand-CO-ref	1.49	0.38			
1_8	8-S95B-FDA-t-Silt-CO-ref	1.92	0.30	18.39	42.75	0.41
1_9	9-S95B-FDA-t-Clay-CO-ref	4.70	0.65			
1_10	10-S95B-FDA-t-Sand-PI-cur	2.21	0.59			
1_11	11-S95B-FDA-t-Silt-PI-cur	24.25	0.49	23.02	47.92	0.42
1_12	12-S95B-FDA-t-Clay-PI-cur	44.32	0.88			
1_13	13-S95B-FDA-t-Sand-MO-cur	1.57	0.51			
1_14	14-S95B-FDA-t-Silt-MO-cur	3.71	0.41	22.73	47.76	0.36
1_15	15-S95B-FDA-t-Clay-MO-cur	15.89	0.78			
1_16	16-S95B-FDA-t-Sand-CO-cur	1.48	0.39			
1_17	17-S95B-FDA-t-Silt-CO-cur	1.83	0.31	18.56	43.10	0.42
1_18	18-S95B-FDA-t-Clay-CO-cur	3.67	0.65			
2_1	19-S95B-FDA-int-Sand-PI-ref	1.48	0.40			
2_2	20-S95B-FDA-int-Silt-PI-ref	2.44	0.34	11.83	14.41	0.44
2_3	21-S95B-FDA-int-Clay-PI-ref	13.98	0.64			
2_4	22-S95B-FDA-int-Sand-MO-ref	1.47	0.38			
2_5	23-S95B-FDA-int-Silt-MO-ref	1.84	0.31	9.46	4.72	0.40
2_6	24-S95B-FDA-int-Clay-MO-ref	6.15	0.61			
2_7	25-S95B-FDA-int-Sand-CO-ref	1.45	0.33			
2_8	26-S95B-FDA-int-Silt-CO-ref	1.56	0.27	5.50	0.19	0.46
2_9	27-S95B-FDA-int-Clay-CO-ref	2.62	0.55			
2_10	28-S95B-FDA-int-Sand-PI-cur	1.93	0.54			
2_11	29-S95B-FDA-int-Silt-PI-cur	22.37	0.47	11.48	12.65	0.46
2_12	30-S95B-FDA-int-Clay-PI-cur	73.33	0.79			
2_13	31-S95B-FDA-int-Sand-MO-cur	1.49	0.46			
2_14	32-S95B-FDA-int-Silt-MO-cur	2.33	0.39	10.82	9.56	0.41

Simulation #ID	Simulation Code	Pavement ME		FlexPAVE™		
		Fatigue Cracking (%)	Total Rutting (in.)	Fatigue Damage (%)	Fatigue Cracking (%)	Total Rutting (in)
2_15	33-S95B-FDA-int-Clay-MO-cur	11.44	0.69			
2_16	34-S95B-FDA-int-Sand-CO-cur	1.46	0.34			
2_17	35-S95B-FDA-int-Silt-CO-cur	1.66	0.28	6.71	0.64	0.47
2_18	36-S95B-FDA-int-Clay-CO-cur	3.48	0.56			
2_19	37-S95C-FDA-int-Sand-PI-ref	1.48	0.45			
2_20	38-S95C-FDA-int-Silt-PI-ref	2.82	0.38	12.14	16.09	0.41
2_21	39-S95C-FDA-int-Clay-PI-ref	18.32	0.69			
2_22	40-S95C-FDA-int-Sand-MO-ref	1.47	0.42			
2_23	41-S95C-FDA-int-Silt-MO-ref	1.96	0.35	9.80	5.75	0.35
2_24	42-S95C-FDA-int-Clay-MO-ref	7.81	0.65			
2_25	43-S95C-FDA-int-Sand-CO-ref	1.45	0.35			
2_26	44-S95C-FDA-int-Silt-CO-ref	1.58	0.28	5.92	0.30	0.33
2_27	45-S95C-FDA-int-Clay-CO-ref	2.83	0.57			
2_28	46-S95C-FDA-int-Sand-PI-cur	1.80	0.50			
2_29	47-S95C-FDA-int-Silt-PI-cur	17.16	0.43	11.24	11.46	0.42
2_30	48-S95C-FDA-int-Clay-PI-cur	65.28	0.77			
2_31	49-S95C-FDA-int-Sand-MO-cur	1.47	0.38			
2_32	50-S95C-FDA-int-Silt-MO-cur	1.82	0.31	9.97	6.28	0.35
2_33	51-S95C-FDA-int-Clay-MO-cur	5.37	0.62			
2_34	52-S95C-FDA-int-Sand-CO-cur	1.46	0.33			
2_35	53-S95C-FDA-int-Silt-CO-cur	1.63	0.27	6.46	0.51	0.33
2_36	54-S95C-FDA-int-Clay-CO-cur	3.21	0.55			
3_1	55-S95C-FDA-T-Sand-PI-ref	1.45	0.35			
3_2	56-S95C-FDA-T-Silt-PI-ref	1.46	0.30	1.22	0.00	0.52
3_3	57-S95C-FDA-T-Clay-PI-ref	1.61	0.51			
3_4	58-S95C-FDA-T-Sand-MO-ref	1.45	0.32			
3_5	59-S95C-FDA-T-Silt-MO-ref	1.45	0.27	0.81	0.00	0.46
3_6	60-S95C-FDA-T-Clay-MO-ref	1.50	0.47			
3_7	61-S95C-FDA-T-Sand-CO-ref	1.45	0.26			
3_8	62-S95C-FDA-T-Silt-CO-ref	1.45	0.22	0.20	0.00	0.41
3_9	63-S95C-FDA-T-Clay-CO-ref	1.46	0.41			
3_10	64-S95C-FDA-T-Sand-PI-cur	1.45	0.38			
3_11	65-S95C-FDA-T-Silt-PI-cur	1.55	0.34	1.33	0.00	0.53
3_12	66-S95C-FDA-T-Clay-PI-cur	2.66	0.56			
3_13	67-S95C-FDA-T-Sand-MO-cur	1.45	0.29			
3_14	68-S95C-FDA-T-Silt-MO-cur	1.45	0.24	1.07	0.00	0.46
3_15	69-S95C-FDA-T-Clay-MO-cur	1.47	0.43			
3_16	70-S95C-FDA-T-Sand-CO-cur	1.45	0.25			
3_17	71-S95C-FDA-T-Silt-CO-cur	1.45	0.21	0.28	0.00	0.41
3_18	72-S95C-FDA-T-Clay-CO-cur	1.46	0.39			

Simulation #ID	Simulation Code	Pavement ME		FlexPAVE™		
		Fatigue Cracking (%)	Total Rutting (in.)	Fatigue Damage (%)	Fatigue Cracking (%)	Total Rutting (in)
4_1	73-S95B-ABC-t-Sand-PI-ref	1.46	0.59			
4_2	74-S95B-ABC-t-Silt-PI-ref	1.49	0.52	22.42	47.58	0.47
4_3	75-S95B-ABC-t-Clay-PI-ref	1.55	0.94			
4_4	76-S95B-ABC-t-Sand-MO-ref	1.47	0.58			
4_5	77-S95B-ABC-t-Silt-MO-ref	1.53	0.50	27.21	49.22	0.44
4_6	78-S95B-ABC-t-Clay-MO-ref	1.67	0.94			
4_7	79-S95B-ABC-t-Sand-CO-ref	1.45	0.51			
4_8	80-S95B-ABC-t-Silt-CO-ref	1.47	0.44	23.27	48.05	0.49
4_9	81-S95B-ABC-t-Clay-CO-ref	1.49	0.86			
4_10	82-S95B-ABC-t-Sand-PI-cur	1.46	0.73			
4_11	83-S95B-ABC-t-Silt-PI-cur	1.48	0.65	15.55	34.04	0.50
4_12	84-S95B-ABC-t-Clay-PI-cur	1.52	1.08			
4_13	85-S95B-ABC-t-Sand-MO-cur	1.46	0.67			
4_14	86-S95B-ABC-t-Silt-MO-cur	1.47	0.59	21.50	46.92	0.46
4_15	87-S95B-ABC-t-Clay-MO-cur	1.51	1.03			
4_16	88-S95B-ABC-t-Sand-CO-cur	1.45	0.53			
4_17	89-S95B-ABC-t-Silt-CO-cur	1.46	0.46	19.88	45.23	0.50
4_18	90-S95B-ABC-t-Clay-CO-cur	1.48	0.88			
5_1	91-S95B-ABC-int-Sand-PI-ref	1.78	0.49			
5_2	92-S95B-ABC-int-Silt-PI-ref	6.33	0.77	16.82	38.71	0.44
5_3	93-S95B-ABC-int-Clay-PI-ref	2.80	0.43			
5_4	94-S95B-ABC-int-Sand-MO-ref	1.77	0.47			
5_5	95-S95B-ABC-int-Silt-MO-ref	6.24	0.74	14.44	28.82	0.40
5_6	96-S95B-ABC-int-Clay-MO-ref	2.67	0.40			
5_7	97-S95B-ABC-int-Sand-CO-ref	1.54	0.40			
5_8	98-S95B-ABC-int-Silt-CO-ref	2.57	0.66	8.60	2.78	0.46
5_9	99-S95B-ABC-int-Clay-CO-ref	1.78	0.34			
5_10	100-S95B-ABC-int-Sand-PI-cur	1.72	0.68			
5_11	101-S95B-ABC-int-Silt-PI-cur	4.03	0.96	12.64	18.91	0.47
5_12	102-S95B-ABC-int-Clay-PI-cur	2.39	0.61			
5_13	103-S95B-ABC-int-Sand-MO-cur	1.59	0.58			
5_14	104-S95B-ABC-int-Silt-MO-cur	2.65	0.86	11.30	11.74	0.42
5_15	105-S95B-ABC-int-Clay-MO-cur	1.86	0.51			
5_16	106-S95B-ABC-int-Sand-CO-cur	1.46	0.42			
5_17	107-S95B-ABC-int-Silt-CO-cur	1.54	0.69	7.77	1.53	0.47
5_18	108-S95B-ABC-int-Clay-CO-cur	1.48	0.36			
5_19	109-S95C-ABC-int-Sand-PI-ref	1.47	0.54			
5_20	110-S95C-ABC-int-Silt-PI-ref	1.59	0.49	16.58	37.95	0.41
5_21	111-S95C-ABC-int-Clay-PI-ref	1.80	0.82			
5_22	112-S95C-ABC-int-Sand-MO-ref	1.47	0.49			

Simulation #ID	Simulation Code	Pavement ME		FlexPAVE™		
		Fatigue Cracking (%)	Total Rutting (in.)	Fatigue Damage (%)	Fatigue Cracking (%)	Total Rutting (in)
5_23	113-S95C-ABC-int-Silt-MO-ref	1.58	0.44	14.14	27.26	0.35
5_24	114-S95C-ABC-int-Clay-MO-ref	1.78	0.78			
5_25	115-S95C-ABC-int-Sand-CO-ref	1.46	0.40			
5_26	116-S95C-ABC-int-Silt-CO-ref	1.49	0.36	8.54	2.66	0.34
5_27	117-S95C-ABC-int-Clay-CO-ref	1.56	0.68			
5_28	118-S95C-ABC-int-Sand-PI-cur	1.56	0.60			
5_29	119-S95C-ABC-int-Silt-PI-cur	2.14	0.56	12.77	19.63	0.42
5_30	120-S95C-ABC-int-Clay-PI-cur	3.34	0.90			
5_31	121-S95C-ABC-int-Sand-MO-cur	1.49	0.45			
5_32	122-S95C-ABC-int-Silt-MO-cur	1.65	0.40	11.45	12.49	0.35
5_33	123-S95C-ABC-int-Clay-MO-cur	2.01	0.75			
5_34	124-S95C-ABC-int-Sand-CO-cur	1.45	0.39			
5_35	125-S95C-ABC-int-Silt-CO-cur	1.48	0.34	7.72	1.47	0.34
5_36	126-S95C-ABC-int-Clay-CO-cur	1.53	0.85			
6_1	127-S95C-ABC-T-Sand-PI-ref	3.34	0.64			
6_2	128-S95C-ABC-T-Silt-PI-ref	8.76	0.59	17.49	40.67	0.47
6_3	129-S95C-ABC-T-Clay-PI-ref	16.81	0.90			
6_4	130-S95C-ABC-T-Sand-MO-ref	3.30	0.59			
6_5	131-S95C-ABC-T-Silt-MO-ref	8.12	0.53	15.32	33.04	0.39
6_6	132-S95C-ABC-T-Clay-MO-ref	16.70	0.85			
6_7	133-S95C-ABC-T-Sand-CO-ref	1.80	0.46			
6_8	134-S95C-ABC-T-Silt-CO-ref	2.73	0.41	9.52	4.90	0.38
6_9	135-S95C-ABC-T-Clay-CO-ref	5.65	0.71			
6_10	136-S95C-ABC-T-Sand-PI-cur	15.41	0.74			
6_11	137-S95C-ABC-T-Silt-PI-cur	25.11	0.68	13.97	26.35	0.48
6_12	138-S95C-ABC-T-Clay-PI-cur	31.70	1.00			
6_13	139-S95C-ABC-T-Sand-MO-cur	5.12	0.53			
6_14	140-S95C-ABC-T-Silt-MO-cur	13.33	0.47	12.63	18.80	0.39
6_15	141-S95C-ABC-T-Clay-MO-cur	22.21	0.79			
6_16	142-S95C-ABC-T-Sand-CO-cur	1.73	0.44			
6_17	143-S95C-ABC-T-Silt-CO-cur	2.40	0.39	8.73	3.02	0.38
6_18	144-S95C-ABC-T-Clay-CO-cur	4.44	0.70			
7_1	145-S95B-BB-t-Sand-PI-ref	1.50	0.45			
7_2	146-S95B-BB-t-Silt-PI-ref	1.66	0.39	16.15	36.42	0.39
7_3	147-S95B-BB-t-Clay-PI-ref	2.20	0.69			
7_4	148-S95B-BB-t-Sand-MO-ref	1.49	0.43			
7_5	149-S95B-BB-t-Silt-MO-ref	1.62	0.36	13.74	25.09	0.36
7_6	150-S95B-BB-t-Clay-MO-ref	2.11	0.69			
7_7	151-S95B-BB-t-Sand-CO-ref	1.46	0.37			
7_8	152-S95B-BB-t-Silt-CO-ref	1.51	0.31	9.22	4.10	0.41

Simulation #ID	Simulation Code	Pavement ME		FlexPAVE™		
		Fatigue Cracking (%)	Total Rutting (in.)	Fatigue Damage (%)	Fatigue Cracking (%)	Total Rutting (in)
7_9	153-S95B-BB-t-Clay-CO-ref	1.69	0.60			
7_10	154-S95B-BB-t-Sand-PI-cur	1.91	0.62			
7_11	155-S95B-BB-t-Silt-PI-cur	3.74	0.55	14.02	26.62	0.41
7_12	156-S95B-BB-t-Clay-PI-cur	10.19	0.87			
7_13	157-S95B-BB-t-Sand-MO-cur	1.55	0.52			
7_14	158-S95B-BB-t-Silt-MO-cur	1.83	0.45	13.89	25.93	0.37
7_15	159-S95B-BB-t-Clay-MO-cur	2.94	0.77			
7_16	160-S95B-BB-t-Sand-CO-cur	1.48	0.38			
7_17	161-S95B-BB-t-Silt-CO-cur	1.58	0.32	10.01	6.42	0.41
7_18	162-S95B-BB-t-Clay-CO-cur	1.93	0.62			
8_1	163-S95B-BB-int-Sand-PI-ref	1.46	0.42			
8_2	164-S95B-BB-int-Silt-PI-ref	1.52	0.36	12.38	17.42	0.44
8_3	165-S95B-BB-int-Clay-PI-ref	1.78	0.64			
8_4	166-S95B-BB-int-Sand-MO-ref	1.46	0.40			
8_5	167-S95B-BB-int-Silt-MO-ref	1.51	0.34	10.07	6.64	0.40
8_6	168-S95B-BB-int-Clay-MO-ref	1.73	0.62			
8_7	169-S95B-BB-int-Sand-CO-ref	1.45	0.34			
8_8	170-S95B-BB-int-Silt-CO-ref	1.47	0.28	5.91	0.30	0.46
8_9	171-S95B-BB-int-Clay-CO-ref	1.55	0.55			
8_10	172-S95B-BB-int-Sand-PI-cur	1.61	0.58			
8_11	173-S95B-BB-int-Silt-PI-cur	2.34	0.52	11.24	11.49	0.46
8_12	174-S95B-BB-int-Clay-PI-cur	5.59	0.81			
8_13	175-S95B-BB-int-Sand-MO-cur	1.48	0.50			
8_14	176-S95B-BB-int-Silt-MO-cur	1.60	0.43	11.01	10.40	0.41
8_15	177-S95B-BB-int-Clay-MO-cur	2.16	0.72			
8_16	178-S95B-BB-int-Sand-CO-cur	1.46	0.36			
8_17	179-S95B-BB-int-Silt-CO-cur	1.50	0.30	6.31	0.45	0.46
8_18	180-S95B-BB-int-Clay-CO-cur	1.67	0.57			
8_19	181-S95C-BB-int-Sand-PI-ref	1.46	0.48			
8_20	182-S95C-BB-int-Silt-PI-ref	1.54	0.42	12.58	18.54	0.41
8_21	183-S95C-BB-int-Clay-PI-ref	1.85	0.70			
8_22	184-S95C-BB-int-Sand-MO-ref	1.46	0.44			
8_23	185-S95C-BB-int-Silt-MO-ref	1.52	0.38	10.28	7.37	0.35
8_24	186-S95C-BB-int-Clay-MO-ref	1.78	0.66			
8_25	187-S95C-BB-int-Sand-CO-ref	1.45	0.36			
8_26	188-S95C-BB-int-Silt-CO-ref	1.47	0.30	6.19	0.39	0.33
8_27	189-S95C-BB-int-Clay-CO-ref	1.56	0.57			
8_28	190-S95C-BB-int-Sand-PI-cur	1.57	0.53			
8_29	191-S95C-BB-int-Silt-PI-cur	2.13	0.47	11.12	10.90	0.41
8_30	192-S95C-BB-int-Clay-PI-cur	4.61	0.76			

Simulation #ID	Simulation Code	Pavement ME		FlexPAVE™		
		Fatigue Cracking (%)	Total Rutting (in.)	Fatigue Damage (%)	Fatigue Cracking (%)	Total Rutting (in)
8_31	193-S95C-BB-int-Sand-MO-cur	1.46	0.40			
8_32	194-S95C-BB-int-Silt-MO-cur	1.53	0.33	10.60	8.64	0.34
8_33	195-S95C-BB-int-Clay-MO-cur	1.82	0.61			
8_34	196-S95C-BB-int-Sand-CO-cur	1.45	0.35			
8_35	197-S95C-BB-int-Silt-CO-cur	1.49	0.29	6.19	0.39	0.33
8_36	198-S95C-BB-int-Clay-CO-cur	1.65	0.55			
9_1	199-S95C-BB-T-Sand-PI-ref	1.52	0.44			
9_2	200-S95C-BB-T-Silt-PI-ref	1.91	0.39	7.83	1.60	0.49
9_3	201-S95C-BB-T-Clay-PI-ref	3.95	0.62			
9_4	202-S95C-BB-T-Sand-MO-ref	1.50	0.41			
9_5	203-S95C-BB-T-Silt-MO-ref	1.77	0.35	5.84	0.28	0.42
9_6	204-S95C-BB-T-Clay-MO-ref	3.39	0.58			
9_7	205-S95C-BB-T-Sand-CO-ref	1.46	0.33			
9_8	206-S95C-BB-T-Silt-CO-ref	1.55	0.28	2.46	0.00	0.38
9_9	207-S95C-BB-T-Clay-CO-ref	2.07	0.49			
9_10	208-S95C-BB-T-Sand-PI-cur	2.07	0.49			
9_11	209-S95C-BB-T-Silt-PI-cur	5.51	0.44	7.09	0.89	0.49
9_12	210-S95C-BB-T-Clay-PI-cur	20.25	0.68			
9_13	211-S95C-BB-T-Sand-MO-cur	1.50	0.36			
9_14	212-S95C-BB-T-Silt-MO-cur	1.73	0.31	6.41	0.49	0.41
9_15	213-S95C-BB-T-Clay-MO-cur	3.03	0.53			
9_16	214-S95C-BB-T-Sand-CO-cur	1.47	0.31			
9_17	215-S95C-BB-T-Silt-CO-cur	1.63	0.26	2.46	0.00	0.38
9_18	216-S95C-BB-T-Clay-CO-cur	2.49	0.47			

Table E.2. Summary of Performance Ratios.

Simulation Code	Pavement ME			FlexPAVE			
	Fatigue Cracking	Total Rutting	Min. Ratio	Fatigue Damage	Fatigue Cracking	Total Rutting	Min. Ratio
S95B-FDA-t-Sand-PI	0.75	0.78	0.75				
S95B-FDA-t-Silt-PI	0.41	0.77	0.41	1.15	1.02	0.94	0.94
S95B-FDA-t-Clay-PI	0.62	0.87	0.62				
S95B-FDA-t-Sand-MO	1.02	0.86	0.86				
S95B-FDA-t-Silt-MO	1.27	0.84	0.84	1.05	1.01	0.97	0.97
S95B-FDA-t-Clay-MO	1.24	0.91	0.91				
S95B-FDA-t-Sand-CO	1.00	0.98	0.98				
S95B-FDA-t-Silt-CO	1.05	0.97	0.97	0.99	0.99	0.98	0.98
S95B-FDA-t-Clay-CO	1.28	0.99	0.99				
S95B-FDA-int-Sand-PI	0.76	0.74	0.74				
S95B-FDA-int-Silt-PI	0.11	0.72	0.11	1.03	1.14	0.96	0.96
S95B-FDA-int-Clay-PI	0.19	0.81	0.19				
S95B-FDA-int-Sand-MO	0.98	0.82	0.82				
S95B-FDA-int-Silt-MO	0.79	0.80	0.79	0.87	0.49	0.97	0.49
S95B-FDA-int-Clay-MO	0.54	0.88	0.54				
S95B-FDA-int-Sand-CO	1.00	0.96	0.96				
S95B-FDA-int-Silt-CO	0.94	0.96	0.94	0.82	0.30	0.99	0.30
S95B-FDA-int-Clay-CO	0.75	0.98	0.75				
S95C-FDA-int-Sand-PI	0.82	0.91	0.82				
S95C-FDA-int-Silt-PI	0.16	0.90	0.16	1.08	1.40	0.98	0.98
S95C-FDA-int-Clay-PI	0.28	0.89	0.28				
S95C-FDA-int-Sand-MO	1.00	1.11	1.00				
S95C-FDA-int-Silt-MO	1.08	1.13	1.08	0.98	0.91	1.01	0.91
S95C-FDA-int-Clay-MO	1.46	1.04	1.04				
S95C-FDA-int-Sand-CO	1.00	1.04	1.00				
S95C-FDA-int-Silt-CO	0.97	1.05	0.97	0.92	0.59	1.01	0.59
S95C-FDA-int-Clay-CO	0.88	1.04	0.88				
S95C-FDA-T-Sand-PI	1.00	0.90	0.90				
S95C-FDA-T-Silt-PI	0.94	0.89	0.89	0.92	0.58	0.99	0.58
S95C-FDA-T-Clay-PI	0.60	0.92	0.60				
S95C-FDA-T-Sand-MO	1.00	1.11	1.00				
S95C-FDA-T-Silt-MO	1.00	1.13	1.00	0.75	0.18	1.01	0.18
S95C-FDA-T-Clay-MO	1.02	1.09	1.02				
S95C-FDA-T-Sand-CO	1.00	1.05	1.00				
S95C-FDA-T-Silt-CO	1.00	1.06	1.00	0.72	0.14	1.01	0.14
S95C-FDA-T-Clay-CO	1.00	1.05	1.00				
S95B-ABC-t-Sand-PI	1.00	0.80	0.80				
S95B-ABC-t-Silt-PI	1.01	0.79	0.79	1.44	1.40	0.94	0.94
S95B-ABC-t-Clay-PI	1.02	0.87	0.87				

Simulation Code	Pavement ME			FlexPAVE			
	Fatigue Cracking	Total Rutting	Min. Ratio	Fatigue Damage	Fatigue Cracking	Total Rutting	Min. Ratio
S95B-ABC-t-Sand-MO	1.01	0.86	0.86				
S95B-ABC-t-Silt-MO	1.04	0.85	0.85	1.27	1.05	0.96	0.96
S95B-ABC-t-Clay-MO	1.11	0.91	0.91				
S95B-ABC-t-Sand-CO	1.00	0.96	0.96				
S95B-ABC-t-Silt-CO	1.00	0.96	0.96	1.17	1.06	0.97	0.97
S95B-ABC-t-Clay-CO	1.01	0.98	0.98				
S95B-ABC-int-Sand-PI	1.03	0.72	0.72				
S95B-ABC-int-Silt-PI	1.57	0.79	0.79	1.33	2.05	0.95	0.95
S95B-ABC-int-Clay-PI	1.17	0.70	0.70				
S95B-ABC-int-Sand-MO	1.11	0.81	0.81				
S95B-ABC-int-Silt-MO	2.36	0.86	0.86	1.28	2.46	0.95	0.95
S95B-ABC-int-Clay-MO	1.43	0.79	0.79				
S95B-ABC-int-Sand-CO	1.05	0.96	0.96				
S95B-ABC-int-Silt-CO	1.66	0.97	0.97	1.11	1.81	0.98	0.98
S95B-ABC-int-Clay-CO	1.20	0.95	0.95				
S95C-ABC-int-Sand-PI	0.94	0.89	0.89				
S95C-ABC-int-Silt-PI	0.74	0.88	0.74	1.30	1.93	0.96	0.96
S95C-ABC-int-Clay-PI	0.54	0.92	0.54				
S95C-ABC-int-Sand-MO	0.99	1.10	0.99				
S95C-ABC-int-Silt-MO	0.95	1.10	0.95	1.24	2.18	0.99	0.99
S95C-ABC-int-Clay-MO	0.88	1.05	0.88				
S95C-ABC-int-Sand-CO	1.00	1.04	1.00				
S95C-ABC-int-Silt-CO	1.01	1.04	1.01	1.11	1.81	0.99	0.99
S95C-ABC-int-Clay-CO	1.01	0.80	0.80				
S95C-ABC-T-Sand-PI	0.22	0.88	0.22				
S95C-ABC-T-Silt-PI	0.35	0.87	0.35	1.25	1.54	0.98	0.98
S95C-ABC-T-Clay-PI	0.53	0.90	0.53				
S95C-ABC-T-Sand-MO	0.64	1.11	0.64				
S95C-ABC-T-Silt-MO	0.61	1.12	0.61	1.21	1.76	1.00	1.00
S95C-ABC-T-Clay-MO	0.75	1.07	0.75				
S95C-ABC-T-Sand-CO	1.04	1.05	1.04				
S95C-ABC-T-Silt-CO	1.14	1.05	1.05	1.09	1.63	1.00	1.00
S95C-ABC-T-Clay-CO	1.27	1.03	1.03				
S95B-BB-t-Sand-PI	0.78	0.73	0.73				
S95B-BB-t-Silt-PI	0.44	0.71	0.44	1.15	1.37	0.95	0.95
S95B-BB-t-Clay-PI	0.22	0.80	0.22				
S95B-BB-t-Sand-MO	0.97	0.82	0.82				
S95B-BB-t-Silt-MO	0.89	0.79	0.79	0.99	0.97	0.97	0.97
S95B-BB-t-Clay-MO	0.72	0.90	0.72				
S95B-BB-t-Sand-CO	0.99	0.96	0.96				

Simulation Code	Pavement ME			FlexPAVE			
	Fatigue Cracking	Total Rutting	Min. Ratio	Fatigue Damage	Fatigue Cracking	Total Rutting	Min. Ratio
S95B-BB-t-Silt-CO	0.96	0.96	0.96	0.92	0.64	0.98	0.64
S95B-BB-t-Clay-CO	0.87	0.98	0.87				
S95B-BB-int-Sand-PI	0.91	0.73	0.73				
S95B-BB-int-Silt-PI	0.65	0.70	0.65	1.10	1.52	0.96	0.96
S95B-BB-int-Clay-PI	0.32	0.79	0.32				
S95B-BB-int-Sand-MO	0.99	0.81	0.81				
S95B-BB-int-Silt-MO	0.94	0.78	0.78	0.91	0.64	0.97	0.64
S95B-BB-int-Clay-MO	0.80	0.86	0.80				
S95B-BB-int-Sand-CO	1.00	0.96	0.96				
S95B-BB-int-Silt-CO	0.98	0.95	0.95	0.94	0.67	0.98	0.67
S95B-BB-int-Clay-CO	0.93	0.97	0.93				
S95C-BB-int-Sand-PI	0.93	0.90	0.90				
S95C-BB-int-Silt-PI	0.72	0.89	0.72	1.13	1.70	0.98	0.98
S95C-BB-int-Clay-PI	0.40	0.92	0.40				
S95C-BB-int-Sand-MO	1.00	1.11	1.00				
S95C-BB-int-Silt-MO	0.99	1.14	0.99	0.97	0.85	1.01	0.85
S95C-BB-int-Clay-MO	0.98	1.08	0.98				
S95C-BB-int-Sand-CO	1.00	1.04	1.00				
S95C-BB-int-Silt-CO	0.99	1.06	0.99	1.00	1.00	1.00	1.00
S95C-BB-int-Clay-CO	0.94	1.03	0.94				
S95C-BB-T-Sand-PI	0.73	0.90	0.73				
S95C-BB-T-Silt-PI	0.35	0.89	0.35	1.10	1.80	0.98	0.98
S95C-BB-T-Clay-PI	0.20	0.91	0.20				
S95C-BB-T-Sand-MO	1.00	1.12	1.00				
S95C-BB-T-Silt-MO	1.02	1.15	1.02	0.91	0.57	1.01	0.57
S95C-BB-T-Clay-MO	1.12	1.10	1.10				
S95C-BB-T-Sand-CO	0.99	1.05	0.99				
S95C-BB-T-Silt-CO	0.96	1.06	0.96	1.00	1.00	1.00	1.00
S95C-BB-T-Clay-CO	0.83	1.04	0.83				

APPENDIX F: SUPPLEMENTARY INFORMATION ON LONG TERM PAVEMENT PERFORMANCE PLAN

Overview

The development of new pavement design and analysis methods that rely on large amounts of field performance data has increased the need for state highway agencies to monitor and record reliable information on the behaviors of their pavements. In North Carolina, the long-term pavement performance (LTPP) database offers one source of data for this purpose. This database includes 50 total sites, 11 of which are active. Of the fifty sites, 31 are asphalt concrete pavement, one is continuously reinforced concrete pavement (CRCP), and 18 are jointed plain concrete pavement (JPCP). Table F.1 below, shows a summary of the different pavement structures incorporated into these sites. With respect to location, six of the sites are in the coastal regions (Divisions 1, 2, 3, 4, or 6), 34 are located in the piedmont region (Divisions 5, 7, 8, or 9), and 10 are located in the mountain region (Divisions 10-14).

Table F.1. Pavement Structure Summary for North Carolina Sites

Base	Asphalt Concrete	Portland Cement Concrete	PCC w/ AC Overlay (Composite)
Granular (unbound)	13	6	1
Treated (bound)	15	7	4
Granular and treated	None	4	None

The currently active LTPP sites are along I-285 northwest of Lexington (x8) and on Bryan Road (x3) in Eastern North Carolina. The sites along I-285 are part of SPS-2: “Strategic Study of Structural Factors for Rigid Pavements, New/Reconstructed JPCC pavements” and those on Bryan Road are part of SPS-8: “Study of Environmental Effects in the Absence of Heavy Loads”.

While this data is useful, it has been found to ultimately be insufficient to adequately address all the questions that the NCDOT has with respect to materials, structural performance, and ultimately design. For example, the makeup and structure of these sites makes it difficult to understand whether aggregate base pavements offer a structural advantage/disadvantage over full depth pavements. Having a set of pavements set aside for performance assessment and monitoring that exceeds what is normally done in the course of pavement management activities could have numerous benefits including calibration of existing and emerging pavement design methodologies; test beds to evaluate new evaluation technologies such as remote and high speed sensing; sites to experimentally evaluate materials and validate outcomes from laboratory based studies, and many others.

This section of the report documents how the NCDOT could instigate and populate a long-term pavement performance monitoring program in the state. Such a program would involve several critical components; 1) site selection method (both immediately and in the long-term) and layout plans, 2) data collection and cataloging information, 3) procedures to control data quality, and 4) materials sampling requirements.

Site selection and planning

A critical component to ensuring adequate information is obtained from the performance monitoring effort is to carefully consider the sites that are selected for the database. These sites could include already existing roadways, newly constructed roadways, or roadways purpose-built to study specific effects.

Factors to Consider in Site Selection

When selecting sites for the database, there are several factors that need to be considered so that the resultant data is broad enough to represent the full range of conditions in the state and thus provide a sufficient amount of data to yield usable information. These criteria include the traffic, materials, structures, and climate. Guidelines on the categorization and consideration of these factors are provided below.

Traffic

The first factor to consider for selecting a site is the amount of traffic that utilizes the roadway. The specific factors to consider are the cumulative number of trucks (structural performance assessment), total number of all vehicles (functional performance assessment), and weight distributions of the trucks using the facility. The suggested parameters for categorization in each of these factors is summarized in Table F.2 below. Consideration for data collection and monitoring of traffic at the test sites should be considered as well. Sites that are already located near traffic monitoring stations should be given serious consideration to include in the database even if they offer some redundancies in the database with respect to the other factors identified below.

Table F.2. Traffic Factors, Parameters, and Categories to Consider for Site Selection

Factor	Parameter	Categories	Rationale
Cumulative Truck Traffic	Cumulative 20-year ESALs	0-3 million 3-10 million 10-30 million > 30 million	These categories are consistent with current NCDOT AC mixture type selection procedures. The exception to this rule is the separation of traffic into 3-10 million and 10-30 million, which is done because it is believed that a range of 3-30 million ESALs would too large a range in conditions.
Cumulative Overall Traffic	20 Year ADT	80,000 or larger 40,000 or larger 20,000 or larger <20,000	Consistency with current NCDOT terminal serviceability and reliability level categories.
Weight Distributions	HWY 2008-11 ALF Cluster	Cluster 1 Cluster 2 Cluster 3 Cluster 4	HWY 2008-11 established axle load factor clusters for Pavement ME Design based on the proportions of Class 5 and Class 9 trucks as well as functional classification of the roadways.

Materials

Sites should also be selected to obtain a cross-section of materials. Table F.3 summarizes the materials to consider when selecting sites. The table does not include materials that may need to be included in pre-existing sites (I19.0B, B25.0B, S12.5D, etc.) as it should be understood that in

selecting existing sites some materials that were previously used are no longer used. One of the most important material factors to consider in selecting sites is the surface type. Site selection should reflect typical practice (unless sites are selected for purpose-built experiments) and so there will be a strong correlation between material types and traffic condition. For example, flexible pavement sites with 20-year cumulative ESALs between 3 and 30 million ESALs will also use S9.5C surface mixtures. Likewise, a subset of the pavements with high traffic levels will have S9.5D and PCC surface materials. This same correlation will also exist with respect to bound foundation layers. If the performance database will be used exclusively to examine structural phenomenon, then surface friction courses (OGAFC or UTWBC) will not need to be considered; however, if the NCDOT envisions using some sites to examine functional issues (friction, macrotexture, safety, etc.) then it is important that the database encompass these types of surfaces as well.

Table F.3. Summary of Materials

Pavement Layer	Materials
Surface	Asphalt concrete (S9.5B, S9.5C, S9.5D)
	Friction course (OGAFC, UTWBC)
	Portland cement concrete (PCC)
Bound foundation layers	Asphalt concrete (I19.0C, B25.0C)
	Permeable asphalt drainage course
	Cement treated base (CTB)
Unbound foundation layers	Aggregate base course (ABC)
Subgrade	Untreated (AASHTO types 1-7)
	Lime treated
	Cement treated

Structures

Site selection should consider three main categories; flexible, rigid, and composite. Within asphalt concrete pavement, the structure types to consider include aggregate base course pavements (ABCP), full depth asphalt pavement (FDAP), or deep strength asphalt pavement (DSAP, pavements with both an aggregate base course and an asphalt base course). Within each of these categories, consideration of pavements with and without subgrade stabilization should also be considered. The predominant concrete pavement strategy in North Carolina involves JPCP and so site selection here can focus on just JPCP. For completeness, the site selection should consider including PCC sections; however, since there currently are active LTPP sites that include rigid pavements, and since the vast majority of roadways in North Carolina are flexible, this may not need to be prioritized.

Climate

The final category for selecting a site is the climate condition. Within the LTPP categorization, all of North Carolina is within a single climate region; wet, no-freeze. However, the NCDOT recognizes three regional climate zones and sites should be selected accordingly. These three regions are the coast, piedmont, and mountains. The three regions and the NCDOT divisions associated with each region are shown in Table F.4. Strictly speaking, these three regions are not purely differentiated by climate. Other factors also differ by region including the dominant paving contractors and practices with respect to material selection (especially treatment of subgrade), soil types, and possibly quality assurance/control allowances (use of nuclear gauges, etc.).

Table F.4. North Carolina DOT Division Based on Climatic Region

	Region		
	Coastal	Piedmont	Mountain
NCDOT Division	1, 2, 3, 4, and 6	5, 7, 8, and 9	10, 11, 12, 13, 14

Selecting and Incorporating Existing Projects

Originally, it was believed that the NCDOT could start its performance database by incorporating a subset of the 31 sites that were identified and used in RP2019-20 (this project), but had not yet received rehabilitation. These sites would have known performance histories and would have been reviewed and quality checked. In addition, since they would not have been rehabilitated, they could provide valuable performance information to help the NCDOT refine the products and recommendations from RP2019-20. A summary of the sites with relevant details including construction year and approximate year of last rehabilitation are given in Table F.5. It is seen from this table that most of the sites (25 out of 33) are currently 'non-active'. That is, they have been overlaid at least once since their original construction. Of the remaining eight sites, five had *PCR* values below 60 at the last data point available when the data was pulled from the PMS database (either 2020 or 2021). Thus, it is likely that they will be overlaid soon (if they have not been already overlaid as the time of this writing). The remaining three sites have somewhat questionable reliability; one is a secondary route with an unknown construction date, one is a secondary route showing a *PCR* of 85.1, 17 years after construction, and the other site (a NC route) shows a *PCR* of 76.3 despite being 20 years old. According to the PMS database, this third site is also surfaced with a S12.5B mixture, which is no longer used in North Carolina.

Existing sites from other sources could be identified and included; however, the research team's own efforts to collect more sites and incorporate these into the calibration dataset proved limited. Thus, it is recommended that only new constructed sites be used to populate the database.

Table F.5. Summary of Candidate Sites for Including in the Initial Database.

Route ID	Construction Year	Date of Last Rehabilitation	Route ID	Construction Year	Date of Last Rehabilitation
40001125099	1999	2014	10600140065 (2)	2000	2015
40001211051	2000	2012	40001954032	1997	2017
40001412033	2002	2017	30000024013	1998	**Active**
40001933026	1999	**Active**	20000001077	2006	2018
40001452077	2004	**Active**	30000087043 (1)	1998	2016
40002705023 (1)	2006	**Active**	30000087043 (2)	1998	2014
40002705023 (2)	2006	**Active**	30000157032 (1)	2000	2015
40001546041	1999	2014	30000157032 (2)	2000	2010
40003632060 (4)	2000	2017	30000109029	2000	**Active**
40002200036	1999	2017	20000070041 (3)	2002	2010
40002433001	2000	**Active**	20000070049 (2)	1999	2010
30000054001 (1)	1999	2010	30000055092 (1)	2002	2008
30000054001 (2)	1999	2010	30000055092 (2)	2002	2010
30000054001 (3)	1999	2014	10800485060	2000	2017
40001765099	1999	**Active**	10000074078	2004	2006
10000140065	2000	2014	10600074078	2004	2012
10600140065 (1)	2000	2012			

Selecting and Incorporating New Projects

'New projects', for the purposes of this guideline, are those that are being newly constructed as part of the normal North Carolina DOT construction plan. These newly constructed projects could become part of this database and utilized for future reference. Over time, the selection criteria for including new projects should include addressing gaps in traffic levels, materials used, layer types within the structures, and climate from the existing database. Initially, sites should be selected that encompass different climate regions and where possible different traffic levels. When selecting new sites, the Materials and Tests Unit should coordinate closely with the Traffic Survey Unit to consider installing a traffic monitoring station (minimum) or a weigh in motion station (ideal). New construction sites should be carefully monitored to collect the necessary data for populating the database (production variation, as-constructed layer thicknesses, materials for testing, etc.). Thus, careful planning will be needed to identify sites with sufficient time to develop an appropriate sampling plan.

It is expected that 'New sites' would need to be continually added to the database as existing sites became inactive. As the database matures, it may also become important to distribute the sites so that the ages vary and that their conditions reflect pre-overlay and post-overlay conditions. Thus, it should expected that one to two new sites would be added every year. Likewise it would be expected that one to two sites would rotate off each year. Rotation out of the database would not necessarily occur when sites received their first overlay (10-15 years), but would definitely occur when the pavement structural life was expended and a major rehabilitation event occurred (25-40 years). A good target is to populate the database with initially would be 10 sites selected over an initial two year period. Subsequent years could add one to two sites so that by the time the first batch of sites reached the time for their first overlay (approximately 12 years), the database would contain between approximately 20 to 30 sites in total. As the sites began receiving overlays, a portion could be retained to monitor the overlay performance and a portion rotated off. In this scenario the database would continue to house between 20 and 30 sites, which would permit overall representative sampling by geographical region, traffic category, and functional class.

Selection Criteria for Purpose-Built Projects

In addition to housing traditionally engineered, constructed, and maintained sites in the database, purpose-built sites should also be considered. These sites would be similar to the specific pavement studies (SPS) projects that are incorporated into the LTPP program. The selection criteria for these purpose-built projects would be based on specific needs (validating a new design method, providing implementation support for a research project, etc.). Some examples of potential purpose-built site experiments including experimental matrices are given below. These examples are illustrative of the scope and extent that would be needed to provide statistically supported outcomes.

Strategic study of flexible pavement structural factors

A strategic study of flexible pavement structural factors might be used to provide systematic data to help calibrate design guidelines and/or provide data to support best practices. These factors could include the presence or absence of a drainage layer or feature and its location within the pavement structure, the use of varying base types, varying base thickness, and varying asphalt pavement layer thickness. Other factors to consider would be moisture, temperature, subgrade type, and location. Although North Carolina is considered a uniformly wet non-freeze state; regional variations are known to exist with respect to soils, constituent materials for asphalt concrete mixtures, and other pavement related practices. As the number of factors and levels

increase this particular experimental matrix could grow substantially. Therefore, a carefully designed experiment using established statistical practices could be followed. Given the costs associated with these experiments, the NCDOT should allocate resources to consult a statistical expert before embarking on an experiment of this magnitude. One potential experimental design that would consider structural configuration (type and thicknesses), traffic, and climate is shown in Table F.6.

Table F.6. Experimental Design for Strategic Study of Flexible Pavement Structural Factors

Site	Climate[1]			Pav. Type[2]		Subgrade[3]		Thickness[4]			Traffic[5]			
	C	P	M	A	F	S	NS	Thin	Int.	Thick	L	M	H	VH
1	X			X		X			X				X	
2	X			X		X				X	X			
3	X			X			X		X					X
4	X			X			X			X		X		
5	X				X	X				X			X	
6	X				X	X				X				X
7	X				X		X	X						X
8	X				X		X		X			X		
9		X		X		X		X			X			
10		X		X		X		X						X
11		X		X			X	X					X	
12		X		X			X			X				X
13		X			X	X		X				X		
14		X			X	X			X					X
15		X			X		X		X		X			
16		X			X		X			X	X			
17			X	X		X			X		X			
18			X	X		X			X			X		
19			X	X			X	X				X		
20			X	X			X			X			X	
21			X		X	X		X					X	
22			X		X	X				X		X		
23			X		X		X	X			X			
24			X		X		X		X				X	

[1] C = Coastal, P = Piedmont, and M = Mountains

[2] A = ABC pavement and F = Full-Depth Asphalt pavement

[3] S = stabilized subgrade and N = non-stabilized subgrade

[4] Based on design reliability relative to traffic volumes; Thin = 50% reliability, Int. = 85% reliability, Thick = 98% reliability.

[5] Based on 20-year cumulative ESALs; L = 0 to 3 million, M = 3-10 million, H = 10-30 million, and VH = > 30 million

The experimental design shown above incorporates climate region, traffic amount, pavement structure, and subgrade. As stated before, there are three climate regions in North Carolina: Coast, Piedmont, and Mountains. Four traffic levels were included in this experimental design based on the 20-year cumulative ESALs: 0 – 3 million ESALs, 3-10 million ESALs, 10-30 million ESALs, and > 30 million ESALs. Subgrade is considered as either stabilized or non-stabilized and would

be expected to vary according to climate region as well (sandy versus clay in Coast versus Piedmont for example). The pavement structure would vary as to whether it uses an aggregate base course (ABC pavement) or an asphalt base (FDA pavement) and also whether it was relatively overdesigned (designed to a 98% reliability) or underdesigned (designed to a 50% reliability). If conducted in a full factorial manner, this particular experimental matrix would require a total of 144 individual test sites. The experimental design proposed in Table F.6 represents a fractional factorial design (specifically a D-optimal design) involving a total of 24 different experiments. Theoretically, the same effects could be identified with a minimum of 16 sites; however, this design would not allow for error estimation.

Study of environmental effects in the absence of heavy loads

The purpose of an environmental effects study would be to characterize the impact of environmental factors on pavement performance. The primary objectives of this experiment could be to; 1) identify and quantify the effect of environmental factors and design on asphalt concrete pavement performance in the absence of heavy loads, 2) quantify environmental effects and develop recommendations for mitigating these effects through effective designs and materials selection, and 3) estimate the proportion of total pavement damage caused by these environmental factors. In this study, "environment" includes climatic factors (e.g., moisture, rainfall, temperature, and freeze/thaw) and subgrade type (e.g., frost-susceptible, expansive, fine-grained, coarse-grained, and soil properties such as percent of clay and silt.) As with the SPS-8 study (Chatti et al. 2005), the absence of heavy loads is defined as traffic applied to a test section that is typically less than 10,000 equivalent single axle loads a year. For this experiment, the ideal sites would have at least 100 vehicles per day and no more than 10,000 ESALs in a year. Table F.7 below shows an example of an experimental matrix that could be used for this study. As with the structural effects experiment, this experiment has been developed using a fractional factorial design and would require a minimum of 12 individual sites. The minimum number of sites would be seven, but with this design the error in resultant analysis could not be quantified (i.e., the study would be saturated).

Table F.7. Experimental Design for Study of Environmental Effects in Absence of Heavy Loads

Site	ABC Thickness		AC Thickness		Surface Type		Subgrade[1]		Climate[2]		
	6"	12"	3"	7"	S9.5B	S9.5C	S	NS	C	P	M
1	X		X		X			X			X
2	X		X			X		X	X		
3	X		X			X	X			X	
4	X			X	X		X		X		
5	X			X	X		X				X
6	X			X		X		X		X	
7		X	X		X			X	X		
8		X	X		X		X			X	
9		X	X			X	X				X
10		X		X	X			X		X	
11		X		X		X	X		X		
12		X		X		X		X			X

[1] S = stabilized subgrade and N = non-stabilized subgrade

[2] C = Coastal, P = Piedmont, and M = Mountains

The experimental matrix for this study would incorporate the three climate regions within North Carolina, the type of subgrade present (indirectly by site selection in the three regions), whether that subgrade is stabilized (lime or cement depending on subgrade properties), a single base type (dense-graded untreated granular base), two base layer thicknesses (6 and 12 in.), two asphalt layer thicknesses (3 and 7 in.), and two surface layer types (RS/S9.5B and RS/S9.5C). The choice of climate regions would encompass factors related to moisture (rainfall) and temperature. The type of subgrade can also affect the frost- and moisture-susceptibility and expansiveness of the soil. This effect coupled with the type of climate can have major effects on the pavement performance. The base type stays the same in order to best isolate the effects of the environment on the pavement performance. Having the two base layer thicknesses, as six and twelve inches, gives an overall performance with respect to pavement structure similar to the structural factors study. This effect is also considered by using two different asphalt layer thicknesses for the surface layers. By keeping the base layer static in this experimental design, the environmental effects can be examined more closely. Also, by combining the results of this study and the previous study, the structural effects and the environmental effects can be more easily decoupled and considered for design.

Study of different reclaimed binder ratios in asphalt pavements

The purpose of this study would be to characterize the impact different reclaimed binder ratios (RBR) have on asphalt pavement performance. The experiment itself would characterize the impacts that changing the RBR has on a pavement, examining the effects if RBR consists of more reclaimed asphalt pavements (RAP) than reclaimed asphalt shingles (RAS), and refining the upper limits of RBR for asphalt pavement performance. For this study, the factors that are included are the RBR, components of RBR (i.e. RAP versus RAS), and then location. Table F.8 exhibits the factors used in this study.

The region, RBR distribution, and RBR replacement are incorporated into this proposed study. Again, a fractional factorial design incorporating 24 sites is proposed, but unlike the previous sites it is proposed to incorporate some replication where a second mix design from the same region and with the same RBR replacement/distribution be included. The percentages of RBR that will be included are 10, 25, and 40 percent. The RAP and RAS percentages are 80/20 (RAP/RAS) and 50/50 to cover different relative contributions of the two recycled binder sources. The locations as mentioned in the prior studies are based on the three regions of North Carolina. Evaluating three regions is suggested since the originating material streams might differ as well as the contractor practices. In reality, it may be sufficient to select a range of contractors who are known to handle recycled materials differently. To control experimental study, locations with similar traffic, subgrade, and climate can be used so that the RBR effects on pavement can be seen instead of these factors listed above. If this selection cannot be done, the study could be combined with the other two studies above and the effects from the other factors can be eliminated, thus highlighting the effects from RBR.

Site Layout Plans

Site layout should be similar for all selections that go into the LTPP database. All test sections should be a minimum of 500 ft (152 m), preferably in the absence of curves or grade changes. If there are grade changes, these should be clearly distinguishable as cut or fill sections so if this causes defects in the section, this could be easily identified as the problem. In the LTPP program there are two types of studies: general pavement studies (GPS) and specific pavement studies

(SPS). For GPS, there is usually one test section with a 500 ft (152 m) maintenance zone on one end and a 250 ft (76 m) maintenance zone on the other end. For SPS, there are usually multiple 500 ft (152 m) test sections separated by 800 ft (244 m) transition zones. These transition zones are long enough to allow for sufficient space for changes in materials and pavement structure design during construction. The same maintenance zones are on both ends of the multiple test sections; they do not surround each individual test section in this case. Meeting these minimum requirements will reduce errors in construction and design that could affect the data collected from each individual study.

Table F.8. Experimental Design for Study of Different Reclaimed Binder Ratios in Asphalt Pavements

Site	%RBR Replacement			RBR Distribution[1]		Region			Replication with another mix?
	10%	25%	40%	80/20	50/50	C	P	M	
1,2	X			X			X		X
3	X			X		X			
4	X			X				X	
5,6	X				X		X		X
7,8	X				X	X			X
9		X		X			X		
10,11		X		X		X			X
12		X		X				X	
13		X			X		X		
14		X			X	X			
15,16		X			X			X	X
17.18			X	X			X		X
19			X	X		X			
20			X	X				X	
21			X		X		X		
22,23			X		X	X			X
24			X		X			X	

[1] First number is the proportion of the RBR replacement from RAP and the second number is the proportion of the RBR replacement from RAS

Data Collection

Traffic

Traffic data, including the number of vehicles, weights, and classification should be measured in order to properly interpret any performance that is measured at the site. This data should be collected at or near the proposed test section or site and in the same direction of travel. Historical data for the roadway should also be derived from volume counts or classification and weight studies conducted at or near the site. Figure F.1 shows a map of the current NCDOT traffic counting stations. Panel (a) shows the 103 continuous monitoring stations currently in use and panel (b) shows the annual traffic survey counting stations (ATSCS) that exist on primary roads. For the ATSCS stations there are approximately another 33,000 stations on secondary routes. Note that the traffic stations (both types) only count the total number of vehicles and do not segregate traffic by type (passenger vehicle, single unit truck, and multi-unit truck). The intent of the data collection is to measure the same traffic that crosses over the test section, therefore “near” could

be several miles on an interstate highway with widely spaced interchanges or it could be less than 1000 feet away on an arterial in a highly populated urban area. Also, data from parallel roadways or from roadways with similar volumes and similar functional classification is useful for estimating the AADT and ESALs per year for possible historical data purposes but this data does not meet the traffic data collecting requirements.

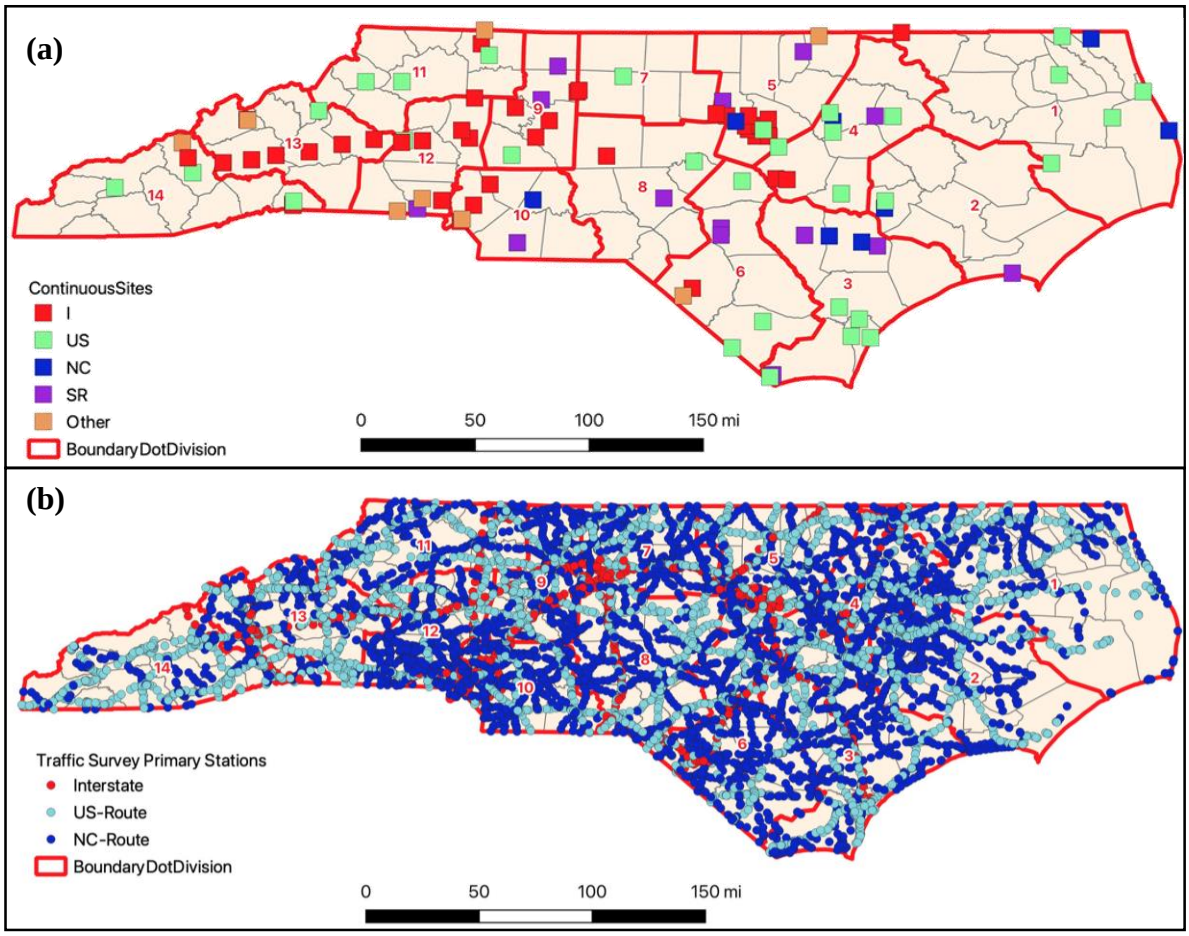

Figure F.1. Location of traffic monitoring data in North Carolina; (a) continuous monitoring stations and (b) annual traffic survey counting stations.

The traffic data collection can be done using WIM and/or AVC equipment. This equipment can be used and monitored in number of ways. The goal is to limit the expected bias and error within the data collected. As shown below in Table F.9, the best collection plan is continuous classification using WIM equipment for one week during each of the four seasons. This plan eliminates expected bias and limits expected error significantly, to be able to obtain true, trustworthy traffic data. All data should be analyzed following the standard NCDOT practice or where that is not conclusive, following the FHWA guidelines (Quinely 2010).

Table F.9. Summary of Expected Error for Selected Sampling Plans (FHWA 2001)

Sampling		Expected Bias	Expected	95%
Classification	WIM	to Annual Est.	Error (%)	CI
1 weekday	1 weekday	20	45	200
1 weekend day	1 weekend day	-50	55	50
2 weekdays	2 weekdays	20	45	100
1 week	1 week	0	30	50
1 week during each of 4 seasons	1 week during each of 4 seasons	0	30	50
1 weekday and 1 weekend day per season for 4 seasons	1 weekday and 1 weekend day per season for 4 seasons	0	35	80
Continuous	1 weekday	0	30	50
Continuous	2 weekdays	0	25	50
Continuous	1 weekday and 1 weekend day	0	25	50
Continuous	1 week	0	25	40
Continuous	1 weekday during each of 4 seasons	0	12	30
Continuous	2 weekdays during each of 4 seasons	0	10	25
Continuous	1 week during each of 4 seasons	0	8	20

Materials

Materials sampling, testing, and cataloging is needed to provide a comprehensive characterization of the pavement layer structure and layer thicknesses of the pavement materials used in each section or project. This data is also useful for obtaining necessary material parameters and mechanical properties for various design and analysis methodologies. The material sampling should be done by sampling materials according to the appropriate state or AASTHO/ASTM standards, core drilling, auguring, test pit opening, and/or nuclear density testing. This sampling would be followed by performing a combination of laboratory material characterization tests to correctly characterize the material within the pavement structure(s). To help with data collection, standard material sampling and laboratory testing protocols with data entry sheets should be developed to record the data collected in the field and the laboratory.

Before going to sites and collecting samples, a formal plan should be prepared that indicates the sections, locations of the samples, and different layers that were to be collected from each location. The location numbers and sample numbers should also be defined beforehand. Establishing a plan prior to sampling ensures a smooth process of sample collection, labeling, wrapping, and transportation of samples to labs. The labeling of the samples should include the test section ID, sample location, sample number, sample date, and field number set.

Table F.10 through Table F.12 lists the material properties that should be measured and the associated test method or methods that should be used. Many of these properties are already part of standard quality assurance and material approvals and can thus be obtained from that data by establishing appropriate reporting protocols prior the project start. For properties that vary

throughout production the central tendency (mean or median) statistics of variation should be recorded and the mean/median reported in the database. Detailed records of the variation of these properties during production should also be retained and retained in supplementary storage for easy access during analysis.

Some tests are listed as optional in Table F.10 through Table F.12 and would require additional testing and sampling of relatively large quantities of mixture (described in Table F.13). It is recommended that the as-produced mixtures be sampled, but that they be compacted and tested in the laboratory (plant-mixed, lab-compacted). The alternative, lab-mixed and lab-compacted, would create better consistency across the mixture tests (since plant production variations would not be part of the dataset); however, the purpose of these tests is to characterize the materials that are actually placed in the pavement. If sufficient space is available for storage, then it is recommended to sample both plant-produced mixtures and the component materials (aggregate/asphalt/RAP/RAS). In this case the weights of component materials needed should be approximately 20 percent higher than the quantity shown in Table F.13 to account for losses during mixing and also greater uncertainty in mixing/fabrication. In the case of the asphalt materials, sampling during production should be done after sufficient time for plant warmup so that the material sampled represents the overall quality of material produced.

Table F.10. Summary of Suggested Materials Testing Plan for Asphalt Materials

Material Type	Test Designation	NCDOT[1]	AASHTO	ASTM
Asphalt Concrete	Maximum Specific Gravity	✓	T 209	D6857
	Bulk Specific Gravity (at N_{des} during production)	✓	T 166	D6752
	Bulk Specific Gravity (as Constructed)			
	Core Examination and Thickness[3]		T 148	
	Asphalt Binder Content	✓	T 164 or T 308	
	Dynamic Modulus	✓	T 378, TP 132	
	Cyclic Fatigue[2]		TP 133, TP 107	
	SSR		TP 134	
	Flow Number[2]		T 378	
	Ideal CT[2]			D8225
	I-FIT[2]		TP 124	
	Hamburg[2]		T 324	
	APA[2]		T 340	
Asphalt Binder	Rotational Viscometer, Original		T 316	
	High Temp. Grade, Original		T 315	
	High Temp. Grade, RTFO		T 315 and T 240	
	Int. Temp. Grade, RTFO+PAV		T 315 and R 28	
	Low Temp. Grade, RTFO+PAV		T 313 and R 28	
	Dynamic Modulus Mastercurve[2]		--[3]	
	Linear Amplitude Sweep, RTFO+PAV[2]		T 391 and R 28	
	MSCR, RTFO[2]		T 350 and T 240	

[1] NCDOT test method is available

[2] Optional test

[3] Alternatively could use ground penetrating radar (GPR) measurements

Table F.11. Summary of Suggested Materials Testing Plan for RAP/RAS, Aggregates, and Portland Cement Concrete

Material Type	Test Designation	NCDOT[1]	AASHTO	ASTM
RAP/RAS	Gradation of RAP/RAS	✓	T 30	
	Gradation of RAP/RAS aggregate	✓	T 30	
	Asphalt Binder Content		T 164 or T 308	D2172 or D6307
	Specific Gravity of RAP Aggregate	✓	T 85 and T 84	C127 and C128
	Maximum Specific Gravity of RAP	✓	T 209	D6857
	Asphalt binder extraction/recovery[2]		T 319	
	High Temp. Grade, as recovered[2]		T 315	
	High Temp. Grade, RTFO[2]		T 315 and T 240	
	Int. Temp. Grade, RTFO+PAV[2]		T 315 and R 28	
	Low Temp. Grade, RTFO+PAV[2]		T 313 and R 28	
Aggregate	Gradation of Aggregate	✓	T 30	
	Specific Gravity of Coarse Aggregate	✓	T 85	C127
	Specific Gravity of Fine Aggregate	✓	T 84	C128
Portland Cement Concrete	Compressive Strength of In-Place Concrete	✓	T 22 and T 23	C1074
	Flexural Strength Test			C78
	Air Content		T 152	
	Slump		T 119M	
	Visual Examination and Length Measurement of Cores[3]		T 148	C856
	Coefficient of Thermal Expansion[2]		T 336	
	Static Modulus of In-Place Concrete[2]			C469
	Surface Resistivity[2]		T 358	
	Volumetric Shrinkage[2]			C157
	Super Air Meter[2]		TP 118	

[1] NCDOT test method is available
[2] Optional test
[3] Alternatively could use ground penetrating radar (GPR) measurements

Prior to any project a materials sampling and testing plan should be established. This plan will consist of five components;

1. The NCDOT should review the overall project site layout including any boring logs and a review of any cut/fill/embankment sections to identify areas of variation.
2. An initial plan should be formulated to ensure sufficient amounts of material are collected for the desired testing plan or the appropriate information is obtained from the contractor at the time of construction (see Table F.10).
3. The initial plan should be reviewed by the Materials and Tests unit as well as the resident engineer for the project to develop a final sampling report that identifies the locations for sampling, the material types and quantities to be sampled, and the unique sample identifiers for the materials.
4. Once the project starts, the materials should be sampled according to the applicable AASHTO or NCDOT standards. Any deviations from the sampling report should be noted and explained.

5. The materials sampled should be tested in accordance with the applicable standards either internally at the NCDOT or by a testing lab approved by the NCDOT.
6. The test data should be compiled into the appropriate format, checked for quality, and uploaded to the performance database for long-term storage and analysis.

When sampling materials, consideration should be given to both immediate testing needs and long-term storage for future testing. Thus, care should be taken in carefully cataloging the details of the materials sampled and labeling them clearly. The labels should include a unique identified tied to the project site and lot. Where possible, these labels should be identical to any existing NCDOT lot/sublot naming conventions to ease future coordination of any test results with quality assurance/quality control data. The precise naming convention to follow for a given project would be established during Step 3 above. In addition, critical information to collect and record when sampling include the date of sampling, location of sampling, quantity sampled, and the person who performed the sampling. More details on sampling requirements and expectations can be found in FHWA (1994a and 1994b).

Table F.12. Summary of Suggested Materials Testing Plan for Base and Subgrade

Material Type	Test Designation	NCDOT[1]	AASHTO	ASTM
Unbound Granular Base/ Subbase	Particle Size Analysis	✓	T 11 and T 27	
	Sieve Analysis	✓	T 11 and T 27	
	Atterberg Limits	✓	T 89 and T 90	
	Moisture-Density Relations	✓	T 180	
	Resilient Modulus		T 307	
	Classification		M 145	
	Natural Moisture Content	✓	T265	
Bound (Treated) Base/ Subbase	Type and Classification of Material and Type of Treatment		M 145	
	Compressive Strength			C39-04a[A], D2166[B]
Subgrade	Sieve Analysis	✓	T 11 and T 27	
	Hydrometer to 0.001 mm (0.04 mils)	✓	T 88	
	Atterberg Limits	✓	T 89 and T 90	
	Classification/Type of Subgrade Soils	✓	M 145	
	Moisture-Density Relations	✓	T 180	
	Resilient Modulus (@ in situ density, moisture)		T 307	
	Natural Moisture Content	✓	T 265	

[1] NCDOT test method is available
[2] Optional test

Table F.13. Summary of Sample Requirements for Material Testing

Materials	Test Method	Quantities to Sample (lb)
Asphalt Concrete	Classification	100 lb
	Dynamic Modulus (via AASHTO TP 132)[1]	60 lb
	Dynamic Modulus (via AASHTO TP 133)[1]	90 lb
	Cyclic Fatigue (via AASHTO TP 133)[1]	60 lb
	Cyclic Fatigue (via AASHTO TP 133)[1]	120 lb
	Flow Number[1]	225 lb
	SSR[1]	120 lb
	Ideal CT[2]	31.5 lb
	I-FIT[2]	31.5 lb
	Hamburg[2]	42 lb
	APA[2]	42 lb
Asphalt Binder	Full suite of characterization	1 qt
RAP/RAS	Gradation, Binder Content, and Specific Gravity	25 lb (coarse) 10 lb (fine)
	Asphalt PG Grade Determination	500 g[3]
Unbound Granular Base/Subgrade	Classification	50 lb
	Resilient Modulus	100 lb

[1] An additional 90 lbs of mixture should be sampled for AMPT tests in order to do an air void study to set compaction mass. This study would only need to be done once, e.g., if sampling for a testing program with dynamic modulus and cyclic fatigue only one air void study would be needed.

[2] An additional 31.5 lbs of mixture should be sampled for an air void study to set compaction mass. This study would only need to be done once for all tests indicated.

[3] Total mass of asphalt binder needed. The amount of RAP needed to obtain 500 grams of extracted and recovered binder will vary by stockpile. An approximate amount of RAP materials to obtain to ensure enough binder can be extracted and recovered is 25 lb.

Structure

The collection of material data described in the section above ties into the collection and characterization of various pavement structures. Test sections from different projects can be categorized together based on the pavement structure being used whether it is an asphalt (flexible) pavement or a concrete (rigid) pavement. The multiple layers within the structure can be identified prior to construction or can be characterized by material sampling as described above. Data to collect for each layer would include the layer type, requisite JMF (if applicable), as-designed thickness, and as-built thickness.

Layers should be identified according to a unique, layer specific, alphabetic or numeric code. Following the convention of the LTPP program, the natural subgrade should be numbered as '1' (or 'A') with each subsequent layer incremented by one level. With respect to the asphalt layers, it is recommended to count each unique JMF as its own layer. Consideration will need to be given to the presence (or lack) of fill layers. The LTPP data collection program, for example, considers the fill layers as the natural subgrade if their thickness is greater than 1.2 m (approximately 4 ft).

Climate

Climate data can be collected using automated weather stations (AWS), but these weather stations can be troublesome as regular maintenance is required. Without regular maintenance these weather stations become inoperable, and the collected data cannot be accepted. It is noted that in the LTPP program, AWS's were phased out due to the required maintenance and the costs that came with the maintenance.

A more efficient climate data collection method is utilizing virtual weather stations (VWS). The climate conditions can be collected from the United States National Climatic Data Center. This data can be improved and become more complete with the use of Modern Era-Retrospective Analysis for Research and Applications (MERRA) data. Test sites on various projects may not be typically located near operating weather stations, therefore extracting data from surrounding weather stations, and using a distance-weighted averaging function, virtual weather statistics can be created for each individual test section. To create a VWS up to five operating weather stations surrounding the test section should be identified. These weather stations need to meet the following criteria in the order listed:

1. Type of station, first order stations being preferred over cooperative stations, which are preferred over MERRA-2.
2. Operating weather station(s) coverage time period relative to the pavement test sections construction date.
3. Distance between the test site and operating weather station(s).
4. Elevation difference between the test site and operating weather station(s).
5. Locations of mountains (if necessary).
6. Microclimate effects.

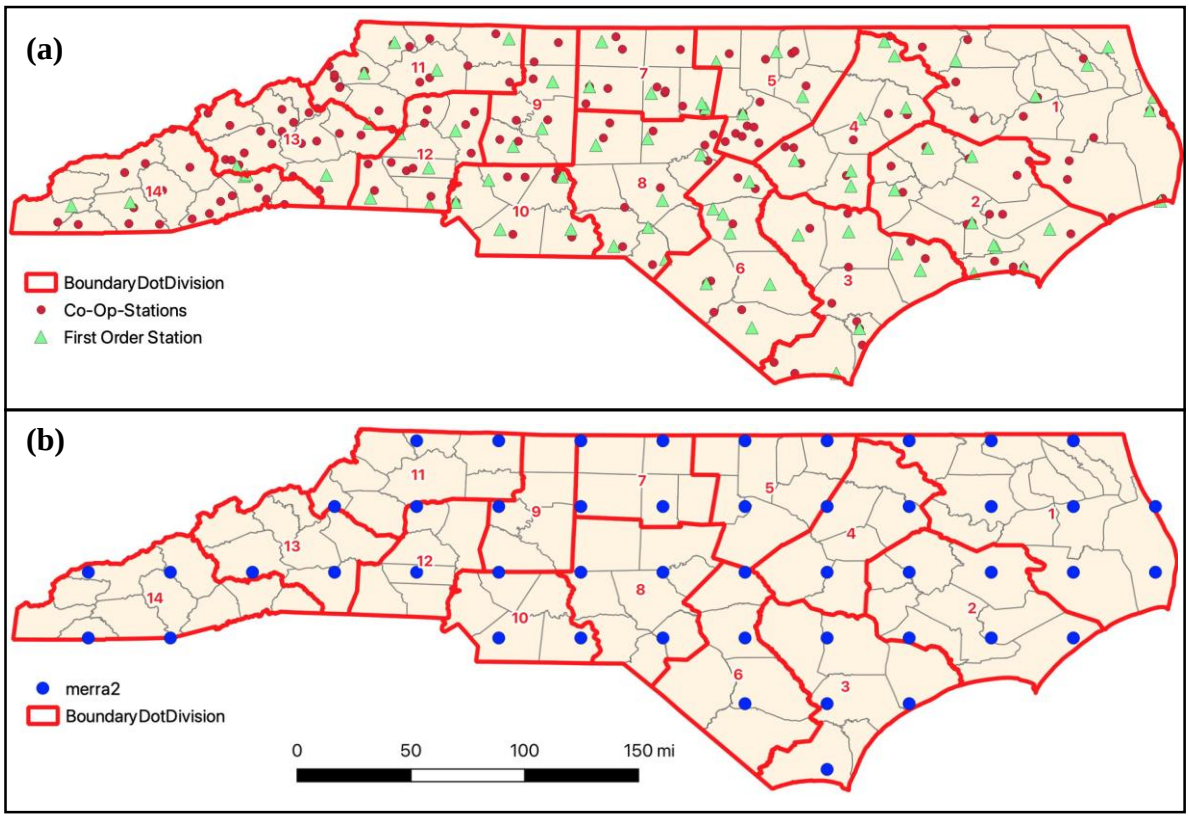

Figure F.2. Location of potential climate stations; (a) Co-Op and first order stations and (b) MERRA-2 stations

Using operating weather stations that meet the above criteria and utilizing the averaging function, climate data can be computed for each test section. Daily statistics such as temperature, rainfall, wind speed, and humidity are obtained from selected operating weather stations and subjected to range and logic checks as defined in Quality Control Manual (FHWA 2002). Only the data that

passes these QC checks should be used to compute the daily virtual weather station statistics. The aggregated summaries are also then subjected to QC checks as well. Figure F.2 shows the extent of the Co-op stations (172), first order stations (77), and MERRA-2 stations (48) in North Carolina.

Performance

Pavement performance measures should be measured regularly. At a minimum, the NCDOT should separately catalog and independently analyze the photo logs from the vendor performed automated distress survey. It is recommended that the NCDOT separately catalog and analyze the data for these study sites because vendors do periodically change and their analysis algorithms may not be entirely consistent. However, photo logs may be more consistent across the vendors. For non-primary routes where automated distress surveys are not regularly performed, it is suggested that the NCDOT add the study sites to the automated data collection efforts. Some periodic and random 'ground-truth' surveys involving lane closures and detailed assessment of the study sites is recommended, but this should only be done in a highly sampled way to validate the assessment from the photo logs. Regular surveys of this manner are likely not required nor recommended due to the disruption they may cause.

Likewise the NCDOT should conduct periodic FWD, continuous friction, and macrotexture measurements on the test sites as their resources allow. At a minimum, it is suggested that FWD measurements be taken immediately after construction and annually once the *PCR* falls below 90. For continuous friction and macrotexture these should be measured immediately after construction, and afterwards following the recommendations in RP 2020-11.

Cataloging and Analyzing Data

To facilitate data cataloging, a final set of traffic, material, structure, and climate variables would need to be identified and a formal database structure enacted. This could be done using already available platforms (Microsoft Access for example) or by purpose built software. Detailed discussions with the NCDOT IT department would be needed to identify the appropriate structure. In addition, the structure should be coordinated with the Pavement Management Section, State Maintenance Operations, and others in the Materials and Tests unit because data and resources from each would likely be cataloged in the database.

Regardless of the final structure, the data should be cataloged along six different dimensions; section information, traffic information, material properties, structural properties, climate characteristics, and performance. Table F.14 lists the minimum information that would be cataloged under each of these areas. However, the NCDOT should carefully consider all data elements currently cataloged for the LTPP program. A summary of these can be found in FHWA (1994a and 1994b). For each of these data elements or dimensions, standard reporting sheets should be developed and standardized.

Data should be stored as it is received and validated in the format appropriate for the database. In addition, the data collection forms themselves should be digitized (or digitally generated) for storage in the database or in supplementary external storage. This supplementary external storage should also house copies of any contract documents relevant to the test site, constructional quality assurance/control records, and any other information generated.

Table F.14. Data to Catalog for Each Site

Dimension	Data to Catalog
Section Information	• Site ID (unique ID for the site within the database) • Route Number • Section ID (NCDOT section ID if different from the Site ID) • Contract • County and NCDOT division • Functional class • GPS coordinates of the start and end points of the section • Direction monitored • Lane monitored (multi-lane facilities) • Number of lanes • Lane width • Shoulder width • Type of pavement (ABCP, FDAP, DSAP, JPCP)
Traffic Information	• ADT at the time of construction • ADT monitored for each year or estimated from nearby stations • Truck distributions for each year • Estimated cumulative ESALs for each year
Material Properties	• Same as those measured according to the test methods chosen from Table F.10.
Structural Properties	• Types of layers • Job Mix Formula numbers (asphalt layers) • Thickness of layers • Joint information (JPCP only) • Dowel/Tie bar information (JPCP only) • Year of original construction
Climate Characteristics	• Hourly values of temperature, precipitation, wind speed, humidity, and cloud cover.
Performance	• Yearly performance survey results (automated) • Year *IRI* results • Periodic deflection results • Photo log for site • Performance assessment in terms of key distress severity and extent • Friction/Texture (for functional performance sites) • Maintenance treatments applied including date

Data Quality Control

Since the performance data will contain numerous data inputs provided from multiple parties over several years, it is important that adequate quality control checks be enacted. The research team recommends following the guidelines from the LTPP quality control program with any collected data. In the LTPP program data quality was checked using five separate levels.

- **Level A: Initial Data Checks** - Records start at level A when they first enter the system and are set back to A when changes are made to a given record.

- **Level B: Dependency Checks** - Possible to have dependency checks, but most data inputs do not require them.
- **Level C: Minimum Data Elements** - Tables and accompanying fields that must be included in a data record are identified in this level.
- **Level D: Expanded Range Checks** - Identify an acceptable range of values for the data tables and accompanying fields from Level C.
- **Level E: Intramodular Checks** - Various specific checks that requires a procedure or action. Intramodular checks vary in each data set. If this check is not met, then an error message will be displayed

As described by the LTPP documents, these checks are performed sequentially (i.e., Level C is only performed once Level B checks are passed) and a data element is 'graded' based on the last level it passes. Some examples of checks on the inventory data, material testing data, deflection data, profile data, and other data elements are summarized in Table F.15 through Table F.25. Note that in these tables the page numbers listed refer to pages in the detailed LTPP guideline document (FHWA 2002). The exact quality control measures that need to be enacted will depend on the data elements that the NCDOT elects to include in their database.

Table F.15. Summary of QC Inventory Dataset

Level	Fields	Page[1]
A	N/A	2 – 1
B	Total of 26 checks. Examples: Age of section, aggregate composition, gradation	2 – 1
C	Age; Aggregate Composition; Gradation	2 – 4
D	Total of 25 checks. Example for Inventory Age dataset: Confirm that the ranges for the final number of lanes, number of lanes added, and original number of lanes are between 1 and 6, 1 and 2, and 1 and 6, respectively.	2 – 6
E	Total of 24 checks Example for Inventory Age dataset: Confirm that the construction date is less than or equal to the traffic open date.	2 – 11

[1] Page number in FHWA (2002)

Table F.16. Summary of QC Transverse Profile and Rutting Dataset

Level	Fields	Page[1]
A	N/A	6 – 1
B	N/A	6 – 1
C	Transverse Profile data; Rut data	6 – 1
D	Total of 7 checks. Example for Transverse Profile dataset: Confirm that the ranges for point location and X1 – X10 are between -8.0 and 307.0; and 0 and 5000 mm.	6 – 2
E	Total of 9 checks Example for Transverse profile dataset: Confirm that if device code equal to "D", then check to ensure X1 is less than X2 is less than X3 is less than X4 is less then X(1+truncated) (Pavement width/ footpad spacing).	6 – 5

[1] Page number in FHWA (2002)

Table F.17. Summary of QC Material Testing Dataset

Level	Fields	Page[1]
A	N/A	3 – 1
B	Check that all existing records in the testing sample log with matching state code, SHRP ID, construction number, and sample number are at level E	3 – 1
C	Asphalt Concrete; Aggregate; Portland Cement Concrete	3 – 1
D	Total of 97 checks. Example for Aggregate Testing dataset: Confirm that the ranges for absorption of coarse aggregate, bulk specific gravity of coarse aggregate, and field set are between 0 and 10, 2 and 4, and 1 and 10, respectively.	3 – 12
E	Total of 161 checks Example for Aggregate Testing dataset: There must be a record in the testing sample basic information with matching state code, SHRP ID, field set, location number and sample number, test date must be greater than or equal to date sampled.	3 – 64

[1] Page number in FHWA (2002)

Table F.18. Summary of QC Levels for Profile Dataset

Level	Fields	Page[1]
A	N/A	4 – 1
B	N/A	4 – 1
C	Longitudinal profile section; Elevation measurements; Texture measurements	4 – 1
D	Total of 9 checks. Example for longitudinal profile section summary: Confirm that the ranges for the center lane *IRI*, left wheel path *IRI*, right wheel path *IRI*, and MRI are all between 0.4 and 4.8 m/km.	4 – 2
E	Total of 20 checks. Example for the longitudinal profile section summary: Confirm that there must be at least one record in the 150 mm longitudinal profile elevation measurement table with matching visit number and run number.	4 – 4

[1] Page number in FHWA (2002)

Table F.19. Summary of QC Deflection Dataset

Level	Fields	Page[1]
A	N/A	5 – 1
B	N/A	5 – 1
C	Drop data; deflection data; temperature data	5 – 1
D	Total of 18 checks. Example for temperature dataset: Confirm that the ranges for the depths where measurements were taken for layer 1 and 2 are between 10 and 49 mm; and 24 and 350 mm.	5 – 4
E	Total of 49 checks Example for Temperature dataset: For each record in deflection temperature values at least one record must exist in deflection location information with matching State code, SHRP ID, and test date.	5 – 7

[1] Page number in FHWA (2002)

Table F.20. Summary of QC Levels for Surface Distress Dataset

Level	Fields	Page[1]
A	N/A	7 – 1
B	N/A	7 – 1
C	Distress surveys for AC, CRCP, JPCC, and PADIAS; Distress survey ratings	7 – 1
D	Total of 12 checks. Example for AC distress survey measurements: Confirm that after and before temperatures are between -20 and 60°C, bleeding is between 0.0 and 420.0 sq. m, and block cracking is between 0.0 and 650.0 sq. m.	7 – 11
E	Total of 38 checks. Example for AC distress survey measurements: The summation of low, moderate, and high severity levels for block cracking should be between 0.0 and 50.0 sq. m.	7 – 23

[1] Page number in FHWA (2002)

Table F.21. Summary of QC Levels for Friction Dataset

Level	Fields	Page[1]
A	N/A	8 – 1
B	N/A	8 – 1
C	Friction data	8 – 1
D	Total of 1 check. Example for Friction data: Confirm that the ranges for friction number begin and end are between 25 and 100%; and friction speed is between 35 and 55 mph.	8 – 1
E	Total of 1 check. Example for Friction data: For SHRP ID, Sate Code, and Construction Number, if the friction method is equal to 3, there must be a valid entry in friction method other.	8 – 2

[1] Page number in FHWA (2002)

Table F.22. Summary of QC Levels for Maintenance Dataset

Level	Fields	Page[1]
A	N/A	9 – 1
B	N/A	9 – 1
C	Asphalt Maintenance; General Maintenance data; Portland Cement Concrete maintenance	9 – 1
D	Total of 12 checks. Example for Portland Cement Concrete maintenance: Confirm that the ranges for air content max are between 0.0 and 12.0; and flexure strength are between 300 and 2000 psi.	9 – 2
E	Total of 14 checks. Example for Portland Cement Concrete maintenance: Confirm that air content maximum is greater than air content mean is greater than air content minimum.	9 – 4

[1] Page number in FHWA (2002)

Table F.23. Summary of QC Levels for Surface Distress Dataset

Level	Fields	Page[1]
A	N/A	10 – 1
B	N/A	10 – 1
C	Asphalt Concrete; Hot Mix RAP ; Cold Mix RAP	10 – 1
D	Total of 55 checks. Example for HMRAP rehabilitation data: Confirm that the asphalt specific gravity is between 0.930 and 1.100; and asphalt viscosity 140 is between 150 and 5000 poise.	10 – 9
E	Total of 12 checks. Example for HMRAP rehabilitation data: If recycle agent type equals to 48 then valid entry must be in recycle agent other.	10–24

[1] Page number in FHWA (2002)

Table F.24. Summary of QC Levels for Traffic Dataset

Level	Fields	Page[1]
A	N/A	11 – 1
B	N/A	11 – 1
C	Calibration data; Traffic Data	11 – 1
D	Total of 26 checks. Example for WIM calibration data: Confirm that GVW difference and single axle difference are between -5.0 and 5.0%.	11 – 3
E	Total of 33 checks. Example for WIM calibration data: If WIM calibration technique equals L, WIM calibration number of test trucks is greater than 1.	11 – 8

[1] Page number in FHWA (2002)

Table F.25. Summary of QC Levels for Climate Dataset

Level	Fields	Page[1]
A	N/A	12 – 1
B	N/A	12 – 1
C	Virtual Climate Station data; Original Climate Station data	12 – 1
D	Total of 18 checks. Example for Virtual Climate Station data: Confirm that precipitation per day is between 0.0 and 300.0 mm; and maximum monthly humidity average is between 0 and 100%	12 – 2
E	Total of 25 checks. Example for Virtual Climate Station data: If both minimum monthly humidity average and maximum monthly humidity average are null, record should be deleted.	12–5

[1] Page number in FHWA (2002)

References

Chatti, K., Bunch, N., Haider, S.W., Pulipaka, A.S., Lyles, R.W., Gilliland, D., and Desaraju, P. LTPP Data Analysis: Influence of Design and Construction Features on the Response and Performance of New Flexible and Rigid Pavements. National Cooperative Highway Research Program, NCHRP Web-Only Document 74. 2005.

Federal Highway Administration (FHWA). Specific Pavement Studies Material Sampling and Testing Requirements for Experiment SPS-2: Strategic Study of Structural Factors for Rigid Pavements. LTPP Division: HNR-40, Washington, D.C., 1994a

Federal Highway Administration (FHWA). Specific Pavement Studies Material Sampling and Testing Requirements for Experiment SPS-1: Strategic Study of Structural Factors for Flexible Pavements. LTPP Division: HNR-40, Washington, D.C., 1994b.

Federal Highway Administration (FHWA). LTPP Information Management System: IMS Quality Control Checks. Online. https://www.fhwa.dot.gov/publications/research/infrastructure/pavements/ltpp/qcm/qcm.pdf, Accessed on July 2020, 2002.

Quinely, R. WIM Data Analysts Manual. Final Report No. FHWA-IF-10-018, Federal Highway Administration, Washington, D.C., 2010.